Genetic and molecular characterization of the regulation of chloroplast protein import in *Arabidopsis thaliana*



Na Li

St Cross College

University of Oxford

A thesis submitted for the degree of

Doctor of Philosophy in Plant Sciences

Hilary 2023

Genetic and molecular characterization of the regulation of chloroplast protein import in *Arabidopsis thaliana*

Na Li

St Cross College

DPhil in Plant Sciences

Hilary 2023

Abstract

Plastids are a unique group of interconvertible organelles which are descended from prokaryotic endosymbionts. The most prototypical member of the group is undoubtedly the chloroplast, which carries out photosynthesis and many other essential biosynthetic processes. Within the course of evolution, over 90% of the retained ancestral protein-coding genes have been transferred into the nuclear genome. The encoded chloroplast-destined proteins must therefore be imported as precursor proteins from the cytosol, through the import apparatus comprising the TOC/TIC complexes. Over the last few years, a proteolytic system called the Ubiquitin-Proteasome System (UPS) has been recognized to target TOC proteins for degradation. The dynamic regulation of the import pathway enables plastids to respond to environmental and developmental cues. A recent discovery demonstrated that the ubiquitinated membrane-embedded TOC proteins can be extracted through a pathway called chloroplast-associated protein degradation (CHLORAD) before degradation by the cytosolic 26S proteasome. In CHLORAD, SP1 acts as the E3 ligase, SP2 functions as an exit channel, and the ATPase Cdc48 provides the motor force for extraction.

Cdc48 functions in a variety of cellular processes and its activity depends on a wide range of cofactors. The ubiquitin regulatory X (UBX) domain-containing proteins constitute by far the

largest family of Cdc48 cofactors. PUX10, a member of the plant UBX domain-containing protein (PUX) family, is an integral chloroplast outer membrane protein that contains a UBX domain and a ubiquitin-associated (UBA) domain that interact with Cdc48 and ubiquitin, respectively. Although *pux10* mutant *Arabidopsis thaliana* seedlings in general appeared phenotypically normal, PUX10 expression levels influenced the rapid degradation of over-accumulated TOC proteins under certain circumstances, such as senescence or abiotic stress. Thus, I propose that PUX10 is involved in the CHLORAD pathway, mediating the recruitment of Cdc48 from the cytosol to the chloroplast surface, and promoting Cdc48 binding to polyubiquitinated TOC proteins for degradation.

In a parallel genetic strategy to understand chloroplast protein import regulation, I studied a new suppressor of the *plastid protein import 1* (*ppi1*) mutation in *Arabidopsis* called *suppressor of ppi1 locus 3* (*sp3*). Preliminary characterization suggested that the *SP3* encodes the GIGANTEA protein which regulates photoperiodic flowering and negatively regulates chloroplast biogenesis. Further investigation of the functional interactions of SP3 with CHLORAD and TOC components will be required to fully understand the nature of these relationships.

Acknowledgements

Firstly, I am grateful to the Biotechnology and Biological Sciences Research Council (BBSRC) for the scholarship and research funding for my DPhil studies (grant number BB/M011224/1). I must also thank the Oxford Interdisciplinary Bioscience Doctoral Training Partnership for providing training and support over the last four and half years. I would also like to thank St Cross College for their welfare support.

I would like to express my sincere gratitude to my supervisor Professor Paul Jarvis for his guidance, discussion, and support throughout my DPhil studies.

I am grateful to the members of the Jarvis group, past and present, for the kindness and help they have given to me. I would like to offer particular thanks to Dr Qihua Ling. He has always been available to offer technical support and discussion with his great expertise, and I am hugely indebted to him for all the help he has given to me ever since I joined Jarvis's group in 2016. I would like to express my gratitude to: Yi Sun, Sreedhar Nellaepalli and Jun Fang for their discussion and advice; Robert Sowden, Sabri Ali, Samuel Watson, Simon Thomson and Zhe (Luke) Ji for their help and friendship; John Baker for photographing plants for the project.

I would also like to thank my dear friend, Huaidong Du, for her sustained encouragement and support, especially during COVID-19 pandemic.

This work would not have been possible without the ceaseless support from my family, especially my mum.

Dedication

For my sons: Zihan (王梓涵), an intelligent little boy with incredible diligence and determination; Zixuan (王梓萱), a smart little boy with a big warm heart.

Statement of authorship

The following people made contributions to the work presented in this thesis:

Zara Lewis	Cloning the CDSs of the 12 *PUX* genes into the Gateway donor vector pDONR201 (related to Figure 2.1).
Alistair Haslam and Dr Saumya Awasthi	Conducting the EMS mutagenesis and screen for the *sp3* project. (Table 4.1)
Alistair Haslam	Conducting preliminary genetic analyses for the *sp3* project (Table 4.1)
Dr Binquan Huang	Conducting further screening for the *sp3* project, new *sp1* and *sp2* alleles screen, backcrossing *sp3* into *ppi1* and preparing genomic DNAs for NGS for the *sp3* project (Table 4.1 and 4.2).
Dr Sabri Ali	Conducting the SHOREmap analysis for the *sp3* project (Table 4.3)
Dr Errin Johnson	Processing *Arabidopsis* leaf samples for TEM (related to Figure 3.7 and 4.11).

The following works had been completed by the author of this thesis before this DPhil study:

Single mutant genotyping: *pux10-1* and *pux10-4*; most T-DNA insertion mutants of *SP3* candidate genes (Figure 2.6 and Table 4.4).

Genetic crossing and genotyping: *pux10-1 ppi1* and *pux10-1 tic110*; most of double mutants of *ppi1* and T-DNA insertion mutants of *SP3* candidate genes (except *At1g22770*) (Figure 3.5A and Table 4.4).

Transgenic materials: PUX10-OX; Cdc48-DN *pux10-1*; Cdc48-WT PUX10-OX (Figure 2.7).

Plasmid constructs: all the constructs used for BiFC assays; all the constructs used for subcellular localization analysis of 12 PUX proteins; p2GW7-PUX10-HA; constructs based on binary vectors for Agrobacterium-mediated transformation of *Arabidopsis* using the floral dipping method.

Confocal imaging: the subcellular localization analyses of 12 PUX proteins; most of the BiFC analyses (Figure 2.1, 2.8B, 3.1, 3.3A).

Abbreviations

A

AAA+	ATPase associated with various cellular activities
ABA	abscisic acid
APC/C	Anaphase Promoting Complex/Cyclosome
APS	ammonium persulfate
At	*Arabidopsis thaliana*
ATP	adenosine triphosphate
AtpB	ATP synthase subunit beta

B

Bcl-2	B cell lymphoma 2
BAG	(Bcl-2)-associated athanogene
BiFC	bimolecular fluorescence complementation
BSA	bovine serum albumin

C

CAB	light-harvesting chlorophyll a/b-binding protein
CDS	coding sequence
Cdc48	cell division cycle 48
CDKA1	cyclin-dependent kinase A-1
cDNA	complementary DNA
CFP	Cyan Fluorescent Protein
CHIP	C-terminus of Hsc70-interacting protein

CHLORAD	chloroplast associated protein degradation
CIA2	chloroplast import apparatus 2
cia5	*chloroplast protein import apparatus 5*
Clp	caseinolytic protease
CO	CONSTANS
Co-IP	co-immunoprecipitation
CRL	cullin-RING ligase
C. *reinhardtii*	*Chlamydomonas reinhardtii*
Cryo-EM	cryogenic electron microscopy

D

dCAPS	derived cleaved amplified polymorphic sequences
Da	Dalton
DEK5	defective kernel 5
Der1	Derlin-1
Dfm1	derlin-like family member protein 1
DMF	*N,N*'-dimethylforamide
DMSO	dimethyl sulfoxide
DNA	deoxyribonucleic acid
dNTPs	deoxyribonucleoside triphosphates
Doa10	degradation of alpha 10
DTT	dithiothreitol
DUB	de-ubiquitinating isopeptidases

E

E1	ubiquitin-activating enzyme
E2	ubiquitin-conjugating enzyme
E3	ubiquitin ligase
ECL	enhanced chemiluminescence
EDTA	ethylenediaminetetraacetic acid
EGAD	endosome and Golgi associated degradation
EGTA	ethylene glycol tetraacetic acid
eIF4E1	Eukaryotic translation initiation factor 4E-1
ELF4	EARLY FLOWERING 4
EMS	ethyl methane sulphonate
ER	endoplasmic reticulum
ERAD	ER-associated protein degradation

F

FAF2	FAS-Associated Factor
FKBP73	FK506 binding protein 73
fts1	*Ferrochelatase two suppressor 1*
FtsH	filamentation temperature-sensitive H
Fzo1	fuzzy onions 1

G

GA	gibberellic acid
gDNA	genomic DNA
GFP	green fluorescent protein
GI	GIGANTEA

Glk	gloden2-like
gp78	glycoprotein 78
GTP	guanosine triphosphate
GUN1	genomes uncoupled 1

H

HECT	homologous to the E6-AP carboxyl terminus
HMG-CoA	3-hydroxy-3-methyl-glutaryl-coenzyme A
Hrd1	HMG-CoA reductase degradation 1
HOP	Hsp70/Hsp90 organizing protein
HRP	horse-radish peroxidase
HS	heat stress
Hsc70-4	heat shock protein cognate 70-4
Hsp70	heat shock protein 70
Hsp90	heat shock protein 90
Hsp90C	chloroplast heat shock protein 90
Hsp93	heat shock protein 93
Hsp100	heat shock protein 100

I

IEM	inner envelope membrane
IMS	intermembrane space
INMAD	inner nuclear membrane associated degradation
IP	immunoprecipitation

K

kDa	kilodalton
KOC1	regulatory kinase at the outer chloroplast membrane 1

L

LB	lysogeny broth
LDs	lipid droplets
LDAD	lipid droplet associated degradation
LOV	light, oxygen or voltage sensing

M

MAD	mitochondria-associated protein degradation
mar1	*modifier of altered response to gravity 1*
MCS	Multiple-cloning site
MDa	megadalton
MES	2-(*N*-morpholino) ethanesulfonic acid
mRNA	messenger RNA
MS	Murashige and Skoog medium

N

NASC	Nottingham Arabidopsis Stock Centre
NGS	next generation sequencing
Npl4	nuclear protein localization 4

O

OD	optical density
OEM	outer envelope membrane
OEP	outer membrane protein

OEP80	outer membrane protein of 80 kDa
OMP85	outer membrane protein of 85 kDa
OTU1	ovarian tumour 1
OX	overexpression

P

p35S	CaMV35S promoter
pPUX10	PUX10 promoter
PCR	polymerase chain reaction
PEB	protein extraction buffer
PEG	polyethylene glycol
PEX	peroxin
PIC	protease inhibitor cocktail
PNGase	peptide N-glycanase
ppi1	*plastid protein import 1*
ppi2	*plastid protein import 2*
ppi3	*plastid protein import 3*
ppi4	*plastid protein import 4*
POTRA	Polypeptide transport-associated
pre-mRNA	precursor messenger RNA
preprotein	precursor protein
PUB	PNGase/UBA or UBX containing proteins
PUL	PLAP, Ufd3p, Lub1p
PUX	plant UBX domain-containing protein

PUX10-OX	PUX10 overexpression

R

RbcL	Ribulose-1,5-bisphosphate carboxylase/oxygenase large subunit
RbcS	Ribulose-1,5-bisphosphate carboxylase/oxygenase small subunit
RFP	red fluorescent protein
RING	really interesting new gene
RNA	ribonucleic acid
ROS	reactive oxygen species
rRNA	ribosomal RNA
RT	reverse transcription
RT-PCR	reverse transcription polymerase chain reaction

S

SAP5	stress-associated protein5
SDS	Sodium dodecyl sulphate
SDS-PAGE	Sodium dodecyl sulphate-polyacrylamide gel electrophoresis
SEM	standard error of the mean
SFR2	sensitive to freezing 2
SNAPs	single nucleotide polymorphisms
26SP	26 proteasome
SP1	suppressor of *ppi1* locus 1

SP1-OX	SP1 overexpression
SP2	suppressor of *ppi1* locus 2
SP3	suppressor of *ppi1* locus 3
SPL1	SP1-like 1
SPL2	SP1-like 2
SPP	stromal processing peptidase
SUMO	small ubiquitin-like modifier protein
SVIP	small VCP-inhibiting protein

T

TAIR	The Arabidopsis information resource
TAG	triacylglycerols
TBE	Tris/borate/EDTA
TBS	Tris-buffered saline
TBS-T	Tris-buffered saline with Tween 20
T-DNA	transfer DNA
TE	Tris/EDTA buffer
TEM	Transmission electron microscopy
TEMED	Tetramethylethylenediamine
TGS	Tris/Glycine/SDS
TIC	Translocon at the inner envelope membrane of the Chloroplasts
TM	transmembrane
TOC	Translocon at the outer envelope membrane of the

	Chloroplasts
TOM	translocon of the outer mitochondria membrane
TPR	tetratricopeptide repeat
tRNA	transfer RNA
TT3.1	thermo-tolerance 3.1
TT3.2	thermo-tolerance 3.2

U

UAS	ubiquitin-associating
Ub	ubiquitin
UBA	ubiquitin-associated
UBL	ubiquitin-like
UBX	ubiquitin regulatory X
UBXL	UBX-like
Ufd1	ubiquitin fusion degradation 1
UIM	ubiquitin-interacting motif
UPL	The HECT ubiquitin-protein ligase
UPS	ubiquitin-proteasome system
UTR	untranslated region

V

v/v	v$olume\ (mL)$/v$olume\ (mL)$
VBM	VCP-binding motif
VCP	valosin containing protein
VIM	VCP interacting motif

Vms1	VCP mitochondrial stress-responsive 1

W

WT	wild type
w/v	weight (g)/volume (ml)

Y

YFP	yellow fluorescent protein

Z

ZTL	ZEITLUPE

Table of Contents

Abstract i

Acknowledgements iii

Statement of authorship iv

Abbreviations vi

Chapter 1 1

1 General introduction 2

1.1 Plastids – diversity and evolutionary origins 2

1.1.1 The diversity of plastids 2

1.1.2 Where did plastids originate? 2

1.2 Chloroplast protein import 3

1.2.1 Transit peptides 4

1.2.2 Preprotein trafficking in the cytosolic 5

1.2.3 The TOC-TIC complexes 6

1.2.3.1 The TOC complex 7

1.2.3.1.1 Toc159 8

1.2.3.1.2 Toc34 10

1.2.3.1.3 Toc75 11

1.2.3.2 The TIC complex 13

1.2.3.2.1 The conventional model of the TIC complex 14

1.2.3.2.2 The 1-MDa TIC complex 16

1.3 The regulation of the TOC complex 18

1.3.1 The ubiquitin-proteasome system (UPS) 18

1.3.2 The E3 ubiquitin ligases 19

1.3.3 The UPS and organelle biogenesis 21

1.3.4 Chloroplast-Associated Protein Degradation 25

1.3.4.1 SP1 25
1.3.4.2 SP2 26
1.3.4.3 Cdc48 27
1.3.4.4 CHLORAD 28
1.3.4.5 Beyond CHLORAD 29
1.3.5 Cdc48 and its cofactors 30
1.3.5.1 Cdc48 structure and cellular functions 30
1.3.5.2 Categories of Cdc48 cofactors 31
1.3.5.3 The Cdc48-Npl4-Ufd1 complex 32
1.4 Project rationale 33
1.4.1 Investigating the participation of PUX proteins in CHLORAD 33
1.4.2 Identification of new regulators of chloroplast protein import 35
1.4.3 Thesis aims and structure 36
Chapter 2 39
Results 1 39
2 Identification of a cofactor of Cdc48 in chloroplasts 40
2.1 Abstract 40
2.2 Introduction 41
2.3 Results 42
2.3.1 Subcellular localization screening of PUX proteins in *Arabidopsis* 42
2.3.2 Further localization and topology analysis of the PUX10 protein 44
2.3.3 Identification of *pux10* mutant and *PUX10* overexpression lines 46
2.3.4 PUX10 can recruit Cdc48 to chloroplast envelope membranes 48
2.3.5 PUX10 interacts with Cdc48 via its UBX domain 49
2.3.6 PUX10 interacts with ubiquitin via its UBA domain 50
2.4 Discussion 51
2.5 Tables and figures 56

Chapter 3 ..... **74**

Results 2 ..... **74**

3 Functional analysis of the PUX10 in chloroplast associated protein degradation **75**

3.1 Abstract **75**

3.2 Introduction **76**

3.3 Results **77**

3.3.1 Physical interactions of PUX10 with SP1 and SP2 77

3.3.2 PUX10 physically interacts with TOC proteins 79

3.3.3 The *pux10-1* mutation moderately suppresses the *ppi1* phenotype 81

3.3.4 The *pux10-1* mutation partially blocks the phenotypic effects of *SP1* overexpression in the *ppi1* background 82

3.3.5 Analysis of the role of PUX10 in the SP1-dependent regulation of leaf senescence 84

3.4 Discussion **85**

3.5 Figures **91**

Chapter 4 ..... **105**

Results 3 ..... **105**

4 A forward genetic screen for new suppressors of the *ppi1* mutation **106**

4.1 Abstract **106**

4.2 Introduction **107**

4.3 Result **108**

4.3.1 Forward genetic screen for the *suppressor* of *ppi1 locus 3* 108

4.3.2 Generation of the *sp3* mutant mapping population and genomic sequence datasets 110

4.3.3 Identification of candidate loci for *sp3* by using SHOREmap analysis 110

4.3.4 Identification of the causative locus for carrying the *sp3* mutation 111

4.3.5 Assessing the relationship of *sp3* to chloroplast biogenesis 115
4.3.6 Analysing the subcellular localization of SP3/GI 115
4.4 Discussion 116
4.5 Tables and figures 124
Chapter 5 147
5 General discussion 148
5.1 Summary of key findings 148
5.2 Critical appraisal of the role of PUX10 in CHLORAD pathway 151
5.2.1 PUX10 is a chloroplast-localized scaffold protein that recruits Cdc48 to ubiquitinated TOC proteins 151
5.2.2 PUX10 promotes the rapid turnover of TOC components. 153
5.2.3 Functionally redundant cofactors of Cdc48 in CHLORAD 154
5.2.4 A working model of PUX10 in CHLORAD Pathway 156
5.3 A new *suppressor* of the *ppi1* mutation 158
5.4 Concluding remarks and perspectives 160
Chapter 6 161
6 Materials and methods 162
6.1 Plant materials 162
6.2 Plant growth conditions 162
6.2.1 Plants grown on soil 163
6.2.2 Plants grown on medium 163
6.3 Plant physiological studies 164
6.3.1 Crossing of *Arabidopsis* plants 164
6.3.2 Floral dipping transformation of *Arabidopsis* plants 165
6.3.3 Chlorophyll measurements 166
6.3.3.1 DMF extraction and spectrophotometer 166
6.3.3.2 SPAD meter 167

6.3.4 Senescence 167
6.4 Plant DNA and RNA related works 168
6.4.1 DNA extraction from *Arabidopsis* leaf tissue 168
6.4.2 Polymerase Chain Reactions (PCR) 168
6.4.3 Agarose gel electrophoresis 169
6.4.4 Genotyping of T-DNA insertion mutants 169
6.4.5 Genotyping by dCAPS 170
6.4.6 RNA extraction from *Arabidopsis* leaf tissue 170
6.4.7 First-strand cDNA synthesis 171
6.4.8 Semi-quantitative RT-PCR 171
6.5 Bacterial work and molecular cloning 171
6.5.1 Preparation of lysogeny broth (LB) medium 171
6.5.2 *E. coli* transformation and plasmid DNA extraction 172
6.5.3 Blue-white screening 173
6.5.4 Preparation of competent *Agrobacterium* cells 173
6.5.5 *Agrobacterium* freeze-thaw transformation 174
6.5.6 Cloning using Gateway system 174
6.5.7 Cloning using restriction enzyme digest and ligation method 175
6.5.8 Constructs generated for this study 176
6.6 Protein analysis 176
6.6.1 Total protein extraction from *Arabidopsis* plants 176
6.6.2 Protein quantification by Bradford assay 177
6.6.3 Preparation of SDS-PAGE gel 177
6.6.4 SDS-PAGE 178
6.6.5 Coomassie staining 179
6.6.6 Western blotting 179
6.7 Chloroplast-related assays 180

6.7.1 Chloroplast isolation 180
6.7.2 Alkaline treatment of chloroplasts 183
6.7.3 Chloroplast "dual protease" protection assay 184
6.8 Protoplast transient expression and immunoprecipitation 186
6.8.1 Protoplasts isolation from *Arabidopsis* plants 186
6.8.2 Protoplast transfection 187
6.8.3 co-immunoprecipitation (co-IP) 187
6.8.4 Subcellular localization and BiFC experiments 189
6.9 Microscopy 189
6.9.1 Confocal microscopy 189
6.9.2 Transmission electron microscopy 190
6.9.2.1 Leaf sample fixation 190
6.9.2.2 Leaf sample dehydration 192
6.9.2.3 Epoxy resin infiltration 192
6.9.2.4 Leaf sample embedding, sectioning and staining 193
6.9.2.5 Imaging 193
6.10 Forward genetic screen 194
6.10.1 Mutagenesis 194
6.10.2 M2 screening 195
6.10.3 Genomic DNA preparation for NGS 196
6.10.4 Mapping by sequencing 196
6.11 Tables 197
Bibliography 203

Chapter 1

General introduction

1 General introduction

1.1 Plastids – diversity and evolutionary origins

1.1.1 The diversity of plastids

Plastids are a group of functionally diverse organelles widely distributed throughout plants, algae and a range of other eukaryotic organisms (Jarvis & Lopez-Juez, 2013). The most archetypal plastid is undoubtedly the chloroplast, which carries out photosynthesis and many other essential biosynthetic processes. Other typical members of the plastid family include proplastids-undifferentiated plastids existing in meristems that can differentiate into other types of plastids; etioplasts-the progenitors of chloroplasts that develop in darkness and rapidly differentiate into chloroplasts upon exposure to light; chromoplasts-the plastids containing carotenoid pigments which confer colour to flowers and fruits; amyloplasts-the plastids specialised for starch storage.

Plastids change their morphology dynamically in response to developmental status and environmental cues, and such conversion plays an important role in plant development (Rolland et al., 2012). For instance, proplastids are undifferentiated plastids found in the meristematic cells of shoots and roots. During leaf development, proplastids differentiate into etioplasts in dark grown seedlings, and etioplasts can then rapidly differentiate into chloroplasts when exposed to light (Jarvis & Lopez-Juez, 2013; Lopez-Juez & Pyke, 2005). In addition, chloroplasts can redifferentiate into chromoplasts with high carotenoid content to give flowers and fruits their colours (Sadali et al., 2019), and into gerontoplasts through disassembly during senescence (Biswal et al., 2012). Moreover, amyloplasts, which are packed with starch granules and found in roots and storage tissues, can turn into chloroplasts; this is for instance observed when potato tubers are exposed to light and turn green (Anstis & Northcot, 1973).

1.1.2 Where did plastids originate?

Today, the widely accepted hypothesis to explain this question is endosymbiosis (Keeling, 2010; Reyes-Prieto et al., 2007). The notion of endosymbiosis was first proposed by Konstantin

Mereschkowski in 1905 when he observed the symbiotic relationship between fungi and algae. The term "endosymbiosis" refers to the phenomenon of an organism living within another organism. In 1923, Ivan Wallin used this theory to explain the origin of mitochondria in eukaryotes. However, not until the 1960s did Lynn Margulis propose that both mitochondria and plastids originate from an endosymbiotic event (Martin et al., 2012).

Plastids arose when a unicellular heterotrophic protist engulfed a free-living photosynthetic cyanobacterium, and retained it, around 1.5 billion years ago (Shih & Matzke, 2013; Sibbald & Archibald, 2020). The endosymbiont was then reduced to a functional organelle bounded with two membranes and was transmitted vertically to subsequent generations (Timmis et al., 2004). The endosymbiont's genome has undergone substantial reduction during evolution. For instance, only ~150 genes are retained in the contemporary chloroplast (Leister, 2003). What accounts for the retention of this small subset of genes in chloroplast? The colocation for redox regulation of gene expression hypothesis argues that there is a selective advantage of genome retention in chloroplasts: rapid compensatory expression effects are needed to respond to alterations in the redox state and composition of the photosynthetic electron transport chain, to preserve their function and protect plants from damage (Allen, 2015; Barbrook et al., 2006).

1.2 Chloroplast protein import

Over the course of evolution, the plastid genome has been largely reduced, and most of the protein-coding sequences have been transferred to the host nuclear genome or lost. The ~150 remaining plastidic genes encode proteins which function as part of the photosynthetic or genetic systems. For instance, in *Arabidopsis thaliana*, plastid DNA encodes 54 core plastid proteins that are involved primarily in photosynthesis and 31 proteins that mediate plastid DNA expression. In addition, 45 genes encode rRNAs or tRNAs. In order to maintain similar level of metabolic complexity in a modern plastid as existed in the ancestral cyanobacteria, thousands of nucleus-coded proteins must be targeted "back" to the plastid after translation in the cytosol (Nakai, 2018; Paila et al., 2015; Sjuts et al., 2017).

Research into plastid protein import has predominantly focused on the chloroplast, due to its high abundance and essential functions in conducting photosynthesis and many other important metabolic processes and biosynthesis. For chloroplasts, over 90% of the 3000 organellar proteins are encoded in the nucleus and translated on cytosolic ribosomes, and eventually imported into the organelle via membrane-bound machinery.

1.2.1 Transit peptides

Most chloroplast proteins are produced as precursors in the cytosol, bearing a cleavable amino-terminal targeting sequence called a transit peptide. Transit peptides engage cytosolic sorting factors and the translocation machinery in the envelope membranes, and therefore play a crucial role in mediating the correct localization of chloroplast-destined proteins, in most cases. Following import, the transit peptides are rapidly removed by the stromal processing peptidase (SPP) (Kessler & Schnell, 2009; Li & Chiu, 2010; Soll & Schleiff, 2004).

Chloroplast transit peptides were first reported by Blair & Ellis (1973), based on the finding that pea chloroplasts can synthesize only a small proportion of their constituent proteins (Blair & Ellis, 1973). They presumed that the remaining proteins are synthesized outside of chloroplast on cytosolic ribosomes, and suggested therefore that nucleus-encoded, chloroplast destined proteins share a common "site" which directs their subcellular localization. This theory soon gained support with the finding in the green alga *Chlamydomonas reinhardtii* that a larger, 20 kDa Rubisco small subunit (RbcS) precursor can be processed to a smaller, 15 kDa mature form via the action of a specific endopeptidase; this was subsequently proved to be SPP, a stroma-resident metalloprotease which is responsible for removing transit peptides from precursors upon their import into the organelle (Richter & Lamppa, 1999; Vandervere et al., 1995). Towards the end of the 1970s, the transit peptide theory obtained mainstream acceptance following the successful *in vitro* reconstitution of RbcS precursor import into chloroplasts by two independent research groups. In each case, the import of the precursor occurred in parallel with its proteolytic processing (Chua & Schmidt, 1978; Dobberstein et al., 1977).

Because significant mistargeting of chloroplast precursor proteins (preproteins) would likely cause cytotoxicity problems, it is reasonable to expect that the chloroplast transit peptides should share well-defined primary structural motifs to guarantee the efficiency and specificity of preprotein targeting. However, after analyzing a large set of transit peptides, it was demonstrated that transit peptides can vary in size from 13 to 146 amino acids and lack conserved sequence features (Bruce, 2001; Kessler & Schnell, 2009; Li & Teng, 2013a). Their most obvious conserved properties appear to be the enrichment of hydroxylated residues (serine and threonine in particular) and a lack of acidic residues, which confer on transit peptide an overall positive charge. In fact, it has been proposed that transit peptides might be intrinsically disordered, forming "perfect random coils", and that this is important for the recruitment of cytosolic chaperones at the early stage of the import pathway (Vonheijne & Nishikawa, 1991). However, it has also been argued that transit peptides may adopt helical conformation only upon contact with the outer envelope membrane (Bruce, 1998; Endo et al., 1992; Krimm et al., 1999; Wienk et al., 1999).

Overall, the highly variable amino acid composition in chloroplast transit peptide may reflect diverse interacting domains for cytosolic chaperones, chloroplast envelope membrane components, and stromal chaperones and sorting factors, or even for different plastid forms.

1.2.2 Preprotein trafficking in the cytosolic

Following translation on cytosolic ribosomes, chloroplast-targeted preproteins need to navigate to the outer envelope membrane of the chloroplast. During this process, soluble, cytosolic factors act to facilitate the migration of the preproteins, maintaining their import-competent conformation, preventing their premature interaction with other proteins, and providing an increased fidelity of targeting to the chloroplast. Statistical algorithms indicated that >75% of plastid transit peptides have high-affinity binding sites for molecular chaperones of the heat shock protein 70 kDa (Hsp70) family, and physical interactions between the two have been demonstrated in *vitro* and in *vivo* (Rial et al., 2000; Zhang & Glaser, 2002). However, the

functional significance of Hsp70 binding by transit peptides has come under debate, because its disruption does not have an effect on protein translocation *in vitro* (Rial et al., 2006; Rial et al., 2003). Additionally, the cytosolic heat shock protein cognate 70-4 (Hsc70-4) interacts with the E3 ligase, carboxy terminus of Hsc70-interacting protein (CHIP), to mediate plastid preprotein degradation to prevent cytosolic precursor accumulation (Lee et al., 2009). This finding indicated that Hsp70 proteins not only support the migration of preproteins, but also act to promote their degradation.

In addition, some proproteins were shown to associate with cytosolic heat shock protein 90 kDa (Hsp90). Hsp90 has been proposed to cochaperone FK506 binding protein 73 (FKBP73) and Hsp70/Hsp90 organizing protein (HOP) through repetitive tetratricopeptide repeat (TPR) domains to deliver the preproteins to the chloroplast surface, by an interaction between the TPR domain of Toc64 and preprotein-Hsp90 complexes (Fellerer et al., 2011; Panigrahi et al., 2013). However, such a delivery to Toc64 seems not necessary since Toc64 is not essential in *Arabidopsis* or Moss *Physcomitrium patens* as shown by mutant studies (Aronsson et al., 2007; Hofmann & Theg, 2005).

Other evidence suggested that some transit peptides contain a motif that is specifically recognized by a member of the 14-3-3 class of regulatory proteins. Furthermore, it has also been reported that 14-3-3 proteins interact with Hsp70 and other factors, possibly forming a "guidance complex", which increases the efficiency of chloroplast protein import in *vitro* (May & Soll, 2000). However, the "guidance complex" hypothesis is still contentious because point mutations within the 14-3-3 biding motif of transit peptides of several chloroplast preproteins did not cause obvious import defects (Nakrieko et al., 2004).

1.2.3 The TOC-TIC complexes

Although there is yet to be a clear consensus on the regulation of preprotein targeting in the cytosol, the import of preproteins through the translocon at the outer envelope membrane of chloroplast (TOC) and the translocon at the inner envelope membrane of chloroplast (TIC), has

been very well characterized (Jarvis & Lopez-Juez, 2013; Nakai, 2018; Richardson & Schnell, 2020). The preprotein initially interacts with the chloroplast via its transit peptide at the TOC complex, and then later it passes through the TIC complex. Upon the emergence into the stroma, the transit peptide is removed by SPP, as noted earlier, allowing the mature protein to adopt its final conformation or be routed to its destination via internal sorting pathways (Inoue et al., 2013). Transit peptide mediated translocation through the TOC-TIC complexed has been known as the canonical protein import pathway (Shi & Theg, 2013). However, there do exist several non-canonical protein import pathways, and as much as 10% of chloroplast proteins have been estimated to import via such routes (Baslam et al., 2016; Jarvis, 2004; Jarvis & Lopez-Juez, 2013).

The TOC and TIC complexes each comprise multiple proteins, with the core components identified for the first time in the 1990s through various biochemical analyses of isolated pea chloroplasts (Jarvis, 2008). The TOC and TIC function cooperatively to engage and import chloroplast-targeted preproteins. In 2022, the first cryogenic electron microscopy (Cryo-EM) structures of TOC-TIC supercomplexes from *C. reinhardtii* were reported simultaneously by two research groups, revealed their composition and architectural arrangement, and potential pathways for chloroplast preprotein translocation (Jin et al., 2022; Liu et al., 2023). The so-far characterized components of the two complexes from *Arabidopsis* will be discussed in detail next, especially the TOC complex which is most closely linked to this research project.

1.2.3.1 The TOC complex

The TOC complex resides in the chloroplast outer envelope membrane (OEM) and mediates the initial recognition of the transit peptides of preproteins for their translocation across the membrane. The core TOC components are the β-barrel protein Toc75 and two types of GTPases, Toc159 and Toc34 – all named in accordance with their molecular weights in kilodaltons. The three components have distinct roles within the plastid protein import process. Toc159 and Toc34 function as preprotein receptors, while Toc75 forms a transmembrane channel. The transit peptides of preproteins are recognised by Toc34 and Toc159, via their GTPase domains

that extend into the cytosol, and then threaded through the channel formed by the large, membrane-spanning β-barrel domain of Toc75 (Jarvis, 2008).

The stoichiometry and molecular weight of the Toc34:Toc75:Toc159 core complex is still debatable. It has been proposed to be arranged with component ratios of 3:3:1 or 4-5:4:1, and with a complex mass of ~500 kDa or 800-1000 kDa, respectively (Kikuchi et al., 2006; Schleiff et al., 2003). The difference between these two proposals might be due to the application of different experimental approaches, or other reasons such as the instability of Toc159, a potential superdimer formed by two TOC core complexes, or even the association of unidentified proteins to the complex (Kikuchi et al., 2006; Schleiff et al., 2003).

It has been proposed that there exist at least two types of the TOC complex for importing different client preproteins: one with preference for abundant photosynthetic preproteins, and another that favours non-photosynthetic preproteins, such as house-keeping proteins (Ivanova et al., 2004; Jarvis & Lopez-Juez, 2013; Kubis et al., 2004). The TOC receptor proteins have been revealed as fundamental determinants of such a client specificity (Ling et al., 2019; Ling et al., 2012; Zufferey et al., 2017).

1.2.3.1.1 Toc159

In *Arabidopsis*, Toc159-type subunits are encoded by four genes: *TOC159*, *TOC132*, *TOC120* and *TOC90* (Kubis et al., 2004). The Toc159 protein has a complicated structure. It contains three domains, including a large acidic domain (known as the "A" domain) at the N-terminus and a central GTPase domain (known as the "G" domain), both of which are cytosolic, as well as a large C-terminal membrane-anchoring domain (known as the "M" domain) (Bolter et al., 1998; Chen et al., 2000; Hirsch et al., 1994; Leipe et al., 2002; Smith et al., 2004). The three domains are present in all homologues but Toc90, which lacks an A domain. The A domain is frequently cleaved by unknown proteolytic activity, and in fact Toc159 was initially described as an 86 kDa protein (so-called Toc86) (Kessler et al., 1994; Perry & Keegstra, 1994). Considering its extreme instability, the biological significance of the A domain has remained elusive. The full-length

Toc159 has been observed to import preproteins more efficiently compared with the variant with a cleaved A domain, suggesting that the A domain plays a role in the import of preproteins (Bolter et al., 1998). Phosphoproteomic analysis demonstrated that the A domain is hyperphosphorylated, while biochemical analysis suggested that the A domain may help to define substrate selectivity (Agne et al., 2010; Inoue et al., 2010). The recent discovery of regulatory kinase at the outer chloroplast membrane 1 (KOC1) provided evidence supporting the functional significance of Toc159 phosphorylation (Zufferey et al., 2017). KOC1 phosphorylated the A domain of Toc159 in *vitro*, and an *Arabidopsis koc1* mutant showed diminished preprotein import efficiency. However, the phenotype of the *Arabidopsis* Toc159 knockout mutant, *plastid protein import 2* (*ppi2*), can be entirely complemented by a truncated protein lacking the A domain (Agne et al., 2010; Agne et al., 2009; Lee et al., 2003). The M domain is strikingly atypical due to it lacking an apparent hydrophobic region. However, both *in vivo* and *in vitro* assays and complementation experiments have demonstrated that the M-domain is the minimal domain required for efficient protein import (Chen et al., 2000; Lee et al., 2003). In addition, a proteoliposome reconstitution study demonstrated that Toc75 was required for the integration of the M domain into the membrane, and both Toc75 and the M domain of Toc159 cooperated during the preprotein translocation across the outer membrane, suggesting that Toc159 is proximal to the Toc75 pore (Lee et al., 2003; Wallas et al., 2003). Recent structural prediction by AlphaFold revealed the M domain to adopt a β-barrel structure (Jumper et al., 2021; Sun & Jarvis, 2023). Additionally, the recently characterized Cryo-EM structures of TOC-TIC supercomplexes from *Chlamydomonas* suggested that the M domain forms a hybrid barrel with Toc75 (Jin et al., 2022; Liu et al., 2023).

Toc159 is considered as the predominant isoform of the Toc159 family in *Arabidopsis*; homozygous knockout mutants (termed as *ppi2*) show a severe, albino phenotype due to the disrupted chloroplast development and cannot survive to adulthood (Bauer et al., 2000; Kubis et al., 2004). *TOC159* is strongly expressed in young, photosynthetic tissues, and the protein is required for the import of photosynthetic proteins.

A phylogenetic analysis divided the Toc159 family into distinct subtypes, one containing Toc159 and the other containing Toc132 and Toc120 (Kubis et al., 2004). Unlike *TOC159*, *TOC132* and *TOC120* show a uniformly low-level expression pattern and are relatively prominent in nonphotosynthetic tissues. *Arabidopsis* Toc132 and Toc120 single mutants show a weakly chlorotic phenotype and no defective phenotype at all, respectively, though the double mutants exhibit a severe albino phenotype, indicating high functional redundancy between the two genes. The overexpression of *TOC132* cannot recover the defect of *ppi2* plants, indicating the divergent functions of Toc159 and Toc132 (Ivanova et al., 2004; Kubis et al., 2004).

Toc90 is a small and structurally distinctive member of Toc159 family. Toc90 shows the lowest sequence identity to the other three proteins with the A domain being completely truncated. Interestingly, *TOC90* is expressed at a uniformly high level throughout development, suggesting that Toc90 may hold unique substrate specificity (Kubis et al., 2004). Although the knockout mutant of *TOC90* (known as *ppi4*) does not show visible phenotypic defect, the *ppi4 ppi2* double mutant shows an enhanced albino phenotype compared to the *ppi2* single mutant (Hiltbrunner et al., 2004). In addition, the overexpression of *TOC90* can partially rescue the phenotype of the *ppi2* mutant with respect to chlorophyll content and protein import efficiency, indicating some degree of functional redundancy with Toc159 (Infanger et al., 2011).

1.2.3.1.2 Toc34

Like Toc159, Toc34 is also a GTPase receptor but it has a simpler structure (Kessler et al., 1994). There are two isoforms of Toc34 present in *Arabidopsis*, Toc33 and Toc34. Both share a similar structure, comprising a very short transmembrane helix at the C-terminus anchoring the protein in the outer membrane, and a cytosolic GTPase domain (Constan et al., 2004). The most significant divergence between the two is at their C-terminal ends.

In general, Toc33 is the major isoform in *Arabidopsis*, and the Toc33 loss-of-function mutant, *ppi1*, displays a small and chlorotic phenotype with a strikingly reduced chlorophyll level, and significant defects in chloroplast ultrastructure and protein import efficiency (Jarvis et al., 1998;

Kubis et al., 2003). Although Toc33 shares a similar protein structure to Toc34, their gene expression profiles are rather different. *TOC33* shows a higher expression level than *TOC34*, and is particularly expressed in rapidly growing, photosynthetic tissues (Gutensohn et al., 2000; Kubis et al., 2003).

TOC34 displays relatively uniform expression throughout development, and a relatively higher level of expression in roots. The Toc34 knockout mutant, *ppi3*, shows no obvious phenotypic defects in aerial tissues, but it does display perturbed root development, which is consistent with its expression pattern (Gutensohn et al., 2000; Kubis et al., 2003). The lack of defective phenotypes in the aerial tissues in *ppi3* mutant may result from the functional compensation by the highly related protein Toc33.

Based on the mutant phenotypes, it has been proposed that Toc33 is more responsible for the import of precursors of the photosynthetic apparatus, whereas Toc34 is more involved in the import of non-photosynthetic preproteins (Kubis et al., 2003). However, such preference is not absolute. The genetic evidence indicates that the two genes are collectively essential for chloroplast function. The *ppi1* phenotype can be complemented by the overexpression of the *TOC34* gene, and the double knockout mutant of the two genes displays embryonic lethality (Constan et al., 2004; Hust & Gutensohn, 2006; Jarvis et al., 1998).

1.2.3.1.3 Toc75

Toc75 is capable of binding with transit peptides and conducting the transport of preproteins by forming the channel of the TOC complex (Hinnah et al., 1997; Hinnah et al., 2002; Schnell et al., 1994; Tranel et al., 1995). Toc75 belongs to the conserved outer membrane protein of 85 kDa (Omp85) protein superfamily (Hsu & Inoue, 2009; O'Neil et al., 2017). The members of the Omp85 family are widely found in the outer membranes of Gram-negative bacteria, and in mitochondria and chloroplasts in eukaryotes which reflects the endosymbiotic origin of these organelles (Gentle et al., 2005). The domain architecture of Toc75 contains an N-terminal domain with three POTRA (polypeptide transport associated) repeats that localizes to the

intermembrane space (IMS), and a C-terminal membrane-embedded β-barrel domain that contains 16 transmembrane β-strands. While the β-barrel domain of Toc75 forms the membrane-spanning pore of the TOC complex, the POTRA domain may be responsible for binding preproteins or cofactors, performing chaperone-like activities to prevent misfolding or aggregation as the preprotein passes the IMS (Ertel et al., 2005; O'Neil et al., 2017). Additionally, in the chloroplast outer envelope membrane there is another Omp85-related protein called outer envelope protein of 80 kDa (OEP80). OEP80 is a paralogue of Toc75, and phylogenetic analysis indicated that OEP80 and Toc75 diverged from a common ancestor early in the evolution of plastids. Despite their structural similarity, OEP80 is not thought to be part of TOC complex (Day et al., 2014; Eckart et al., 2002; Hsu & Inoue, 2009; Inoue & Potter, 2004). Unlike Toc75 that can self-insert into the OEM via a bipartite targeting signal (Tranel et al., 1995; Tranel & Keegstra, 1996), OEP80 enters the chloroplast through the TOC complex regardless of the presence of a transit peptide (Day et al., 2019; Gross et al., 2021). The molecular function of OEP80 remains elusive, though the studies on the null mutants of *TOC75* and *OEP80* indicated both proteins are essential for viability during embryogenesis but perform distinct functions (Hsu et al., 2008; Patel et al., 2008; Topel et al., 2012). Intriguingly, the studies using *Arabidopsis* Toc75 and OEP80 RNAi lines provided *in vivo* support for the hypothesis that OEP80 is important for the biogenesis of β-barrel proteins (Toc75 in this case) (Huang et al., 2011).

Recently the TOC-TIC supercomplex was isolated from *Chlamydomonas* and the structure of the supercomplex was determined through Cryo-EM. According to these structures, instead of forming a β-barrel alone, Toc75 form a hybrid β-barrel pore together with the M domain of a member of the Toc159 family (Toc90 or Toc120), while Toc34 binds to the peripheral region of Toc75 (Jin et al., 2022; Liu et al., 2023). The hybrid β-barrel may account for the flexibility of the chloroplast import system for importing wide variety of preproteins including even quite large domains (Ganesan et al., 2018; Ganesan & Theg, 2019). It is reasonable to assume that Toc75 may similarly form a hybrid channel with Toc159 family members in the outer envelope membrane of higher plant chloroplasts.

The *Arabidopsis* genome contains three Toc75-related genes: *TOC75-I*, *TOC75-III* and *TOC75-IV*, although *TOC75-I* is a pseudogene – its sequence contains a series of nonsense, frameshift, and splice-junction mutations and it is not obviously expressed in any tissue (Baldwin et al., 2005). *TOC75-III* encodes the major isoform; it is highly expressed and strongly regulated, particularly within young and rapidly expanding tissues. Toc75-III is essential for plant viability; null mutation of *TOC75-III* causes embryo lethality, reflecting the importance of the protein import channel of the TOC complex, even during embryogenesis (Baldwin et al., 2005; Hust & Gutensohn, 2006). However, the *toc75-III* missense allele (termed *toc75-III-3* / *mar1* (modifier of altered response to gravity 1)), enabled studies on the role of Toc75-III in chloroplast biogenesis (Stanga et al., 2009). The *toc75-III-3* mutant is chlorotic due to a reduced chlorophyll content, defective chloroplast ultrastructure, and a reduction of protein import efficiency, demonstrating the functional importance of Toc75 to chloroplast biogenesis (Huang et al., 2011). By contrast, *TOC75-IV* is expressed at a much lower level with a more uniform expression profile than *TOC75-III*. Homozygous *TOC75-IV* knockout mutants show no obvious mutant phenotypes under standard growth conditions. However, *toc75-IV* mutants do display less efficient de-etiolation than wild type, which suggests that Toc75-IV may play some role during growth in the dark (Baldwin et al., 2005).

1.2.3.2 The TIC complex

The TIC complex locates in the chloroplast inner envelope membrane (IEM) and translocates the preproteins through the IEM. Unlike the well-characterized TOC complex, the exact membership of the TIC complex is still not entirely resolved. Many putative TIC components have been identified and studied; however, no consensus model of TIC composition has yet been agreed, and many basic questions remain contentious, such as the identity of the TIC pore.

Overall, the proteins which were mostly recently discussed to be associated with the TIC complex are Tic20, Tic56, Tic100 and Tic214/Ycf1, although several other proteins, including Tic21, Tic22, Tic32, Tic40, Tic55, Tic62, Tic110 and Tic236, have also been described as components of the TIC complex (Chen et al., 2018; Jarvis, 2008; Kikuchi et al., 2013). Most

recently, a new 12-kDa protein named Tic12 in *Arabidopsis* was reported to be an essential component of the TIC complex (Zhao et al., 2022).

Due to the controversies within the field, this section will be subdivided into two parts. First, the 'conventional' model and its components will be presented, followed by a brief discussion about the new 1-MDa complex model proposed by Professor Masato Nakai's group.

1.2.3.2.1 The conventional model of the TIC complex

The originally identified components of the TIC import machinery include Tic110, Tic40, Tic20 and Tic21, along with other associated molecular chaperones such as Tic22 in the IMS (Kouranov et al., 1998; Kouranov & Schnell, 1997; Kovacheva et al., 2005) and Tic236 which was proposed to link the TOC and TIC complexes (Chen et al., 2018).

Tic110 was the first to be identified and it is a major component of the chloroplast envelope (Lubeck et al., 1996; Schnell et al., 1994; Wu et al., 1994). Tic110 is an integral protein of the IEM containing two membrane spanning α-helices and a large, hydrophilic stromal extension, though the conflicting reports exist concerning the topology of Tic110 (Inaba et al., 2003; Jackson et al., 1998). It has been proposed to form the membrane-spanning pore of the TIC complex (Heins et al., 2002). However, further study on the crystal structure of various fragments of Tic110 indicated that its structure is not optimal for channel function, but more likely acts as a scaffold for recruiting stromal chaperones to translocating preproteins (Tsai et al., 2013). Tic110 has been proved to physically interact with the heat shock protein 100 (Hsp100)-type chaperone Hsp93/ClpC to perform a preprotein quality control role at the stromal side of the inner membrane (Flores-Perez et al., 2016; Flores-Perez & Jarvis, 2013; Rial & Ceccarelli, 2005). However, Tic110 was absent in the Cryo-EM structure of the TOC-TIC supercomplex from *C. reinhardtii*, which suggests that Tic110 may fucntion downstream of the core TOC-TIC complex, or that there are fundamental differences between plants and algae in this regard (Jin et al., 2022; Liu et al., 2023).

Tic40 has only a single N-terminal transmembrane domain, and a large stromal extension (Chou et al., 2003; Stahl et al., 1999). The stromal region comprises a series of TPR domains which are known for promoting protein-protein interactions. This structure implies that Tic40 might act as a scaffold for chaperones recruitment (Bedard et al., 2007). Furter studies indicated that Tic40 forms a complex with Tic110 and Hsp93 (Chou et al., 2003; Kovacheva et al., 2005; Stahl et al., 1999).

Tic20 is an integral membrane component of the IEM containing four transmembrane α-helices (Chen et al., 2002). Tic20 has been proposed to be the major TIC complex channel protein based on its structure (Kikuchi et al., 2013; Kouranov et al., 1998). A proteoliposome reconstitution study demonstrated that Tic20 can form a cation selective channel independent of Tic110 (Kovacs-Bogdan et al., 2011). In addition, preprotein import experiments indicated that Tic20 is physically associated with translocating preproteins (Kikuchi et al., 2009). The recently revealed Cryo-EM structures of the TOC-TIC complex from *C. reinhardtii* revealed that Tic20 forms a core component of the TIC complex (Jin et al., 2022; Liu et al., 2023).

Despite structural similarity, Tic21 is not closely related to Tic20. The *Arabidopsis* Tic21 knockout mutant *chloroplast protein import apparatus 5* (*cia5*) shows an albino phenotype as well as defective chloroplast protein import, indicating a role in protein import (Teng et al., 2006). Conversely, another study argued that Tic21 is critical for maintaining the cellular metal homeostasis instead of the chloroplast protein import (Duy et al., 2007). Interestingly, Tic21 was later proposed to be peripherally associated with a large complex containing Tic20 (Kikuchi et al., 2009). However, whether or not Tic21 is involved directly in the preprotein translocation remains inconclusive.

Tic22 is one of the first proteins to be molecularly localized to the IMS, and it shows a peripheral association with the outer face of the IEM. Precursor binding and crosslinking assays demonstrated that Tic22 can physically interact with preproteins (Kouranov et al., 1998; Kouranov & Schnell, 1997). The association of Tic22 with outer and inner translocon components, as well as shared structural characteristics with other chaperones, implies a

function as a chaperone facilitating preprotein transit across the IMS (Glaser et al., 2012; Paila et al., 2016; Rudolf et al., 2013; Tripp et al., 2012).

Tic236 is a recently discovered component of the chloroplast import machinery in *Arabidopsis* (Chen et al., 2018). Tic236 is anchored in the IEM where it associates with Tic20, while the large C-terminus protrudes into the IMS to directly bind to the POTRA domain of Toc75. The protein is therefore proposed to function as a physical link between the TOC and TIC translocons. *Arabidopsis* Tic236 knockout mutations are embryonically lethal, while knockdown mutants show reduced chloroplast protein import but no change in the abundance of TOC proteins as well as outer membrane insertion, which is consistent with the proposed TOC-TIC bridging function during chloroplast protein import. Additionally, Tic236 was recently identified as the suppressor of crumpled leaf (CRL), a chloroplast outer membrane protein which plays a crucial role in plastid division. Defective plastid division in both *crl* and Tic236 knockdown mutants implied that the CRL-Tic236 module is crucial for plastid division (Asano et al., 2004; Fang et al., 2022). It is worthwhile to mention that the Tic236 homologues in other plant species have been proposed to have different functions (Matsushima et al., 2014; Zhang et al., 2019a).

Collectively, the mutants of above-mentioned TIC components display defective chloroplast biogenesis varying in severity from chlorotic to albino, and, in some cases, to embryonically lethal, indicating their functional importance for chloroplast function (Chen et al., 2018; Chou et al., 2003; Hirabayashi et al., 2011; Inaba et al., 2005; Kasmati et al., 2013; Kasmati et al., 2011; Rudolf et al., 2013).

1.2.3.2.2 The 1-MDa TIC complex

In 2013, Professor Masato Nakai's group captured a 1-MDa complex from *Arabidopsis* through an immunoprecipitation experiment using protein A - tagged Tic20 (Kikuchi et al., 2013). The 1-MDa complex contains Tic20, Tic56, Tic100 and Tic214 (also known as Ycf1) but is lacking both Tic110 and Tic40, while Tic21 shows only weak interaction. In *vitro* preprotein import experiments suggested that all four TIC proteins could physically associate with preproteins in the same way as well-established TOC components such as Toc159, Toc75 and Toc33.

Conversely, no specific association of Tic110 or Tic40 with the 1MDa complex was observed in the *in vitro* import assays, though both proteins have long been proposed to play central roles in the preprotein translocation across the IEM. Based on these observations, this group argued that Tic110 and Tic40 are not core component of the TIC complex; instead, the intrinsic IEM protein Tic20, containing four transmembrane helices, was proposed to form a channel complex with three additional constituents, Tic214, Tic100 and Tic56 (Kikuchi et al., 2013; Nakai, 2018). In addition, Professor Masato Nakai's group recently identified a small protein, Tic12, to be an additional component of the 1-MDa TIC complex (Zhao et al., 2022).

In *Arabidopsis*, null mutants of Tic100 and Tic56 displayed albino phenotypes with disturbed chloroplast development (Kohler et al., 2015; Lopez-Juez et al., 1998; Loudya et al., 2022). Intriguingly, Tic214 is encoded by a chloroplast gene ycf1 which is essential for plant viability, and no Tic214 mutant could hence be obtained (Drescher et al., 2000).

This 1-MDa TIC complex was later reported to be conserved in the green algae *Chlamydomonas* (Ramundo et al., 2020). And, as already noted, in 2022, two research groups simultaneously reported the Cryo-EM structure of a TOC-TIC supercomplex from *Chlamydomonas*. The five TIC components belonging to the 1-MDa TIC complex – Tic214, Tic100, Tic56, Tic20 and Tic12 – were identified in the purified TOC-TIC supercomplex.

However, the 1-MDa TIC complex also received challenges. For instance, the Tic214 homologues are highly variable or even absent in grasses (de Vries et al., 2015). Further experiments demonstrated that protein import could occur in the absence of Ycf1 (Bolter & Soll, 2017). Additionally, Tic100 and Tic56 are also lacking in the Poaceae family, and the full-length version of Tic56 is dispensable in *Arabidopsis* (Kohler et al., 2016; Schafer et al., 2019). Thus, it is possible that the TIC complex is greatly divergent in the grasses (Jarvis & Lopez-Juez, 2013; Paila et al., 2015). Moreover, Tic20 was proposed to form the inner membrane channel in the 1-MDa model, but Tic20 shows much lower abundance compared to Tic110 (Kovacs-Bogdan et al., 2011; Vojta et al., 2004).

In *Arabidopsis*, Tic20-I is the major isoform, and Tic20-I mutation shows a severe albino phenotype with defective chloroplast biogenesis. However, double *tic20-I tic20-IV* knockout mutants are embryo-lethal, indicating that Tic20-IV may show partial functional redundancy with Tic20-I (Hirabayashi et al., 2011; Kasmati et al., 2011). Thus, there might be additional TIC complexes in plants that act in the absence of, or in parallel to, the 1-MDa TIC complex (Nakai, 2018; Thomson et al., 2020).

1.3 The regulation of the TOC complex

As mentioned previously, plastids display a high morphological and functional diversity; different types of plastids can interconvert during certain development stages or under particular environment conditions. Considering that different plastids have diverse proteomes, the components of the TOC complexes, acting at the onset of the import pathway, will need to be altered to assist the import of the specifically required proteins. In the last decade, high-throughput comparative proteomic analysis has indeed supported this view, that proteins are differentially accumulated in accordance with the remodeling of metabolism and even internal membrane systems during plastid transitions (Barsan et al., 2012; Reiland et al., 2011; Zhang et al., 2010). How might the TOC complexes be regulated to enable such differences? Previous studies indicated that plastid protein turnover is regulated through three different pathways. Plastid intrinsic proteases supervise the quality control of individual organelle proteins (Adam & Clarke, 2002). Autophagy is another proteolytic system which mainly contributes to nutrient recycling and typically processes many proteins at once (Li & Vierstra, 2012). The major breakthrough to the regulation of plastid protein import was the identification of the ubiquitin-proteasome system as an important protein turnover pathway in plastids, acting on OEM proteins (Ling et al., 2019; Ling et al., 2012).

1.3.1 The ubiquitin-proteasome system (UPS)

The UPS is a major proteolytic system in eukaryotes for removing most abnormal polypeptides and short-lived cellular regulators, through degradation by the cytosolic 26S proteasome, and it

allows cells to respond rapidly to intracellular signals and different environmental conditions. It is therefore essential for maintaining protein homeostasis in eukaryotic cells (Komander & Rape, 2012; Vierstra, 2009). Degradation of a protein via the UPS involves two discrete and successive steps: tagging of the substrate protein by the covalent attachment of multiple ubiquitin molecules, which is termed ubiquitination; and the subsequent degradation of the tagged protein by the 26S proteasome, a large (2.5 MDa) and highly conserved proteolytic complex.

Ubiquitination is a refined post-translational modification in which an 8.6 kDa ubiquitin protein is attached to a substrate protein through a cascade of three important enzymes: E1 (ubiquitin-activating enzyme), E2 (ubiquitin-conjugating enzyme) and E3 (ubiquitin ligase). First, an E1 activates the ubiquitin by forming a thioester bond in an ATP-dependent reaction. The activated ubiquitin is then transferred to an E2. Finally, an E3 catalyses the transfer of ubiquitin from the E2 to the substrate (Vierstra, 2009). A ubiquitin is eventually conjugated to the substrate protein via an isopeptide bond formed between the last amino acid of ubiquitin (glycine 76) and a lysine residue (typically) in the substrate protein. Ubiquitin has seven lysine residues and can itself be ubiquitinated, enabling the formation of a polyubiquitin chain on the substrate, a process which may be assisted by ubiquitin chain elongation factors, or E4 enzymes (Hoppe, 2005). Lysine 48 (K48) and lysine-63 (K63) linked chains have been well-characterized. Diverse substrate-ubiquitin structures are crucial for targeting proteins to different fates. For example, K48-linked polyubiquitin chains target proteins for 26S-proteasomal degradation, whereas K63-linked polyubiquitin chains are associated with a range of cellular activities including autophagy, DNA repair, endocytic trafficking, and translation. Upon degradation, the ubiquitin moieties are removed from substrates by de-ubiquitinating isopeptidase (DUB) enzymes (Amerik & Hochstrasser, 2004).

1.3.2 The E3 ubiquitin ligases

The substrate specificity of ubiquitination is mainly determined by the E3 ligases, which is reflected in their dominance in number compared to E2 and E1 enzymes. Although there are

only two E1 and ~40 E2 genes, there are ~1400 E3 ligase genes in *Arabidopsis thaliana* (Ling & Jarvis, 2015a). Diversity of the latter is spread over four classes, of which three comprise a single protein with a distinctive domain; these are HECT (Homologous to the E6-AP Carboxyl Terminus), RING (Really Interesting New Gene), and U-box type E3 ligases. Another category is composed of a protein complex and these are called Cullin-RING Ligases (CRLs) (Vierstra, 2009).

The HECT E3 ligases are in general relatively large proteins, of more than 100 kDa. They have a distinct ubiquitination mechanism by forming a thioester intermediate with the ubiquitin via a cysteine residue in the HECT domain before transferring ubiquitin to the substrate (Downes et al., 2003; Huibregtse et al., 1995). In *Arabidopsis*, there are seven HECT E3 ligases named UPL1 to UPL-7. Although they show less diversity compared to other plant E3 ligases, HECT E3 ligases have not yet been extensively studied. Previous research demonstrated that UPL3 plays a critical role in controlling endoreduplication cycles in trichomes and gibberellic-acid 3 signalling (Downes et al., 2003); UPL5 is involved in regulating leaf senescence (Miao & Zentgraf, 2010).

The RING E3s are the most abundant type of ubiquitin ligases. For instance, there are nearly 500 different RING proteins in *Arabidopsis* (Stone et al., 2005). The RING domain was originally identified in a protein encoded by the *Really Interesting New Gene* (RING) in 1991 by Paul S. Freemont and colleagues (Freemont et al., 1991). The domain comprises 40-60 amino acids and its conserved cysteine and histidine residues coordinate the binding of two Zn^{2+}. The RING domain is responsible for binding the ubiquitin-charged E2 and stimulating discharge of its ubiquitin cargo. Based on the nature of the metal ligand residues coordinating the zinc ions and the number of amino acids between them, eight types of RING domains have been classified. Of those, the RING-H2 and RING-HC constitute the majority of the categories (Borden, 2000; Stone et al., 2005). The large number of potential RING proteins suggests their important role in protein regulation. A multitude of studies conducted over the recent decade have documented the key roles of the RING-type E3s in various plant developmental processes, including seed

germination, auxin signalling, photomorphogenesis, secretory pathway, response to abiotic stress, and plastid development (Chen & Hellmann, 2013; Ling et al., 2012).

The U-box E3s are RING-like ubiquitin ligases containing a modified RING domain that binds the E2-ubiquitin intermediate without employing Zn^{2+} coordination, and they are widely distributed in eukaryotic organisms. While yeast and humans contain 2 and 21 U-box E3 genes, respectively, they form major protein families in plants with, for example, 64 and 77 members annotated in *Arabidopsis* and rice, respectively (Azevedo et al., 2001; Wiborg et al., 2008; Zeng et al., 2008). Increased numbers of U-box proteins in higher plants might indicate their diverse roles in plants, which is indeed supported by recent research on their functions in biotic and abiotic stress responses, seed germination, and flowering-time regulation (Bergler & Hoth, 2011; Li et al., 2012; Salt et al., 2011; Seo et al., 2012; Shen et al., 2007b; Shen et al., 2007a; Yan et al., 2003).

The CRLs possess the greatest diversity among plants E3 ligases, and exhibit enormous plasticity in substrate specificity. The CRLs are assembled on a cullin scaffold onto which binds a RING-Box 1 (RBX1) at its N terminus, providing a docking platform for ubiquitin-charged E2, and an adaptor protein and a substrate receptor (responsible for substrate specificity) at its C terminus. Four major CRL families are known in plants that contains either a cullin protein (CUL1, CUL3 or CUL4) or a Cullin-like protein APC2, and these are named SCF, BTB, DWD and APC/C based on their founding member, respectively (Hua & Vierstra, 2011).

1.3.3 The UPS and organelle biogenesis

Because the UPS is located in the cytosol, cytosolically located misfolded proteins can be easily targeted for degradation via the UPS (Kim et al., 2017). However, not all UPS targets are so readily accessible to the proteasome in the cytosol. Membrane-bound proteins or proteins inside certain organelles may also be degraded by the UPS, but this requires specific systems for both their ubiquitination and retrotranslocation, to transport the target protein into the cytosol. One representative example is endoplasmic reticulum (ER)-associated protein degradation (ERAD).

This is a system to facilitate the degradation of ER luminal misfolded proteins (ERAD-L) and ER membrane-bounded proteins that are misfolded in their luminal (ERAD-M) or cytosolic (ERAD-C) domains. There are at least two predominant protein complexes that operate in ERAD; the degradation of alpha 10 (Doa10) complex that is responsible for the ubiquitination of membrane proteins with misfolded cytosolic domains, and the HMG-CoA reductase degradation 1 (Hrd1) complex that can target substrates with misfolded domains in the lumen or membrane of the ER. In both cases, a membrane bound E3 ligase (Doa10 or Hrd1) can recognize a misfolded substrate, which is ubiquitinated and then extracted from the ER. It is noteworthy that the extensive membrane spans of both Doa10 and Hrd1 enable them to potentially form a retrotranslocation channel during the extraction of ubiquitinated proteins (Ruggiano et al., 2014; Wu & Rapoport, 2018). However, the retrotranslocation activity of Hrd1 is seemingly to only critical in ERAD-L. For ERAD-M, a Derlin-like family member protein 1 (Dfm1) was proved to serve as a retrotranslocon for the extraction of integral membrane substrates from the ER (Neal et al., 2018).

The extraction step is an energy-consuming process which is assisted by motive power from cell division cycle 48 (Cdc48), also known as p97 or valosin-containing protein (VCP), a conserved eukaryotic ATPase located in the cytosol (Ruggiano et al., 2014). The interaction of Cdc48 with ubiquitinated substrates is mediated by a heterodimer of adaptor proteins, termed ubiquitin fusion degradation 1 (Ufd1) and nuclear protein localization 4 (Npl4); and this complex is sometimes referred to as the Cdc48-Npl4-Ufd1 complex (Braun et al., 2002).

Analogous systems of protein extraction and degradation via the UPS have been identified in a number of other organelles and compartments, and these include mitochondria associated degradation (MAD) (Taylor & Rutter, 2011), lipid droplet associated degradation (LDAD) (Deruyffelaere et al., 2018; Kretzschmar et al., 2018), inner nuclear membrane associated degradation (INMAD) (Foresti et al., 2014), and endosome and Golgi associated degradation (EGAD) (Schmidt et al., 2019).

As noted earlier, the cytosolic chaperone Hsc70-4 binds to the transit peptide of preprotein and recruit the preprotein to HSC70-interacting protein (CHIP), a cytosolic E3 ligase for ubiquitination and degradation. The Hsc70-4 and CHIP was greatly induced in the *Arabidopsis* Toc159 mutant *ppi2*, which had a severely defective protein import into chloroplasts (Lee et al., 2009). The initial connection discovered between the UPS and chloroplast biogenesis was provided by analyses of *Arabidopsis* C-terminus of CHIP E3 ligase, that targets chloroplast preproteins that have failed to import and which may accumulate in the cytosol. The degradation of the precursors of caseinolytic protease (Clp) and filamentation temperature-sensitive H (FtsH) was found to be mediated by the CHIP E3 ligase (Shen et al., 2007b; Shen et al., 2007a). Related to this, it was found that a direct interaction between the 26S proteasome and a transit peptide of precursor is essential for the degradation of unimported chloroplast preproteins (Sako et al., 2014). In addition, B cell lymphoma 2 (Bcl-2)-associated athanogene (BAG) protein is a considerably conserved protein in animals and plants. BAG proteins directly interact with Hsc70 via the common conserved BAG domains. Plant BAG proteins play crucial roles in various biological processes such as autophagy, abiotic stress response and plant immunity. Interestingly, the *Arabidopsis* Bcl2-associated athanogene 1 (AtBAG1) was identified as a cofactor in Hsc70-mediated unimported preprotein degradation (Lee et al., 2016).

Besides CHIP, the wheat stress-associated protein5 (SAP5), a cytosolic E3 ligase, was discovered to interact with chloroplast heat shock protein 90 (Hsp90C) precursors to mediate their degradation (Zhang et al., 2019b). Hsp90C is a member of the Hsp90 family of molecular chaperones located in the plastid of higher plants and green algae. Hsp90C and TIC complex function cooperatively to drive translocation of preproteins into chloroplasts (Inoue et al., 2013).

Intriguingly, chloroplast preprotein degradation via a novel endosome-to-vacuole pathway was recently unveiled in rice. Upon heat stress the plasma membrane–localized ubiquitin E3 ligase thermo-tolerance 3.1 (TT3.1) is relocated to endosomes where it ubiquitinates the preprotein of chloroplast thermo-tolerance 3.2 (TT3.2); the latter is subsequently delivered to endosomes for vacuolar degradation, protecting chloroplasts from heat stress damage (Zhang et al., 2022a).

Furthermore, the UPS targeted proteolytic events in cytosol controlling chloroplast biogenesis was also found to occur during early plant development. Seed germination is repressed by DELLA (Asp-Glu-Leu-Leu-Ala) proteins through the UPS-dependent regulation of developmental signals (Xue et al., 2022). Conversely, the hormone gibberellic acid (GA) inhibits DELLA factor accumulation by triggering the ubiquitination and subsequent degradation of DELLA proteins by the 26S proteasome to enable germination and, in turn, chloroplast biogenesis. Under low GA conditions, DELLA proteins directly interact with the cytosolic precursor of Toc159, to promote its degradation by the UPS (Shanmugabalaji et al., 2018).

The UPS-dependent regulation of chloroplast preproteins also occurs at a transcriptional level, in the nucleus (Martin et al., 2016; Ruckle et al., 2007; Tang et al., 2016; Tokumaru et al., 2017). For instance, GOLDEN2-LIKE (GLK) transcription factors are essential for normal chloroplast development by upregulating genes related to light harvesting and chlorophyll synthesis (Chen et al., 2016). *Arabidopsis* transcription factor golden2-like 1 (GLK1), which is known to activate the expression of photosynthesis-related genes during chloroplast biogenesis, is subject to UPS-dependent degradation (Tokumaru et al., 2017). Additionally, Cul4 E3 ligase mediated ubiquitination and degradation of golden2-like 2 (GLK2) transcription factor by 26S proteasome in tomato plays an important role in the regulation of chloroplast development and pigment metabolism (Tang et al., 2016). The expression of *Glk1* is regulated by genomes uncoupled 1 (GUN1) via plastid-to-nucleus retrograde signaling to coordinate plastid protein import and nuclear gene expression in response to the developmental state of the organelle (Kakizaki et al., 2009). However, the posttranslational regulation of Glk1 through UPS seems to be performed in a GUN1-independent manner in response to plastid signals. Taken together, these findings indicate that multiple mechanisms have been evolved in plastids to ensure adequate nuclear encoded plastid proteins import and normal chloroplast (Tokumaru et al., 2017).

1.3.4 Chloroplast-Associated Protein Degradation

1.3.4.1 SP1

The first evidence for direct UPS action on chloroplast-resident proteins came from the identification of suppressor of *ppi1* locus 1 (SP1) through a forward genetic for second-site suppressors of the chlorotic phenotype of the Toc33 mutant *ppi1* (Ling et al., 2012). As mentioned earlier, *ppi1* has a distinctive pale-yellow phenotype and reduced ability to import photosynthetic proteins into chloroplasts. The *sp1* mutation was found to partially suppress the *ppi1* phenotype with increased chloroplast protein import, resulting the better developed chloroplast and a greener plant.

The *SP1* locus encodes a RING-type E3 ligase that localizes in the chloroplast OEM. The SP1 protein is small and has a relatively simple architecture, comprising two transmembrane domains, a C-terminal RING domain projecting into the cytosol that is responsible for the ubiquitination of substrates, and an intermembrane space domain that is important for interaction with target proteins. The SP1 protein was shown to regulate chloroplast biogenesis by targeting the components of the TOC machinery for proteasomal degradation. The *sp1* mutations therefore suppress the *ppi1* phenotype by recovering the TOC protein abundance, promoting protein import and chloroplast biogenesis. Conversely, SP1 overexpression depletes TOC proteins and enhances (accentuates) the phenotype of *ppi1*. Moreover, the regulation by SP1 of the turnover of TOC proteins is important for plastid type interconversion events. It enables regulation of the composition of TOC complexes, modifying protein import preferences, thus leading to organelle proteome changes and eventually developmental transitions (Ling et al., 2012; Ling et al., 2021). It was reported that SP1 is also present in other organelles such as the mitochondria and peroxisomes, and involved in the regulation of the peroxisome protein import machinery (Pan et al., 2018; Pan et al., 2016). However, such proposals have been challenged and were unprovable through further investigation (Ling et al., 2017).

Further work on the functions of SP1 revealed that SP1 is also important for abiotic stress tolerance in plants. It does this by depleting the chloroplast protein import apparatus, thus limiting the import of photosynthetic proteins to suppress photosynthesis, and thereby reducing reactive oxygen species (ROS) accumulation during stress (Ling & Jarvis, 2015b).

It is worthwhile to mention that two homologues of SP1 were identified in *Arabidopsis*: SP1-like1 (SPL1) and SP1-like2 (SPL2). Both SPL1 and SPL2 are topologically similar to SP1 and reside in the chloroplast envelope (Ling et al., 2012). Though some studies claimed that the two homologues were also present in other organelles, such as peroxisomes and mitochondria, even nucleus, such discrepancies remain greatly contentious (Gao et al., 2015; Pan et al., 2018; Pan et al., 2016). In very recent research, it was proved that both SPL1 and SPL2 are bona fide components of the CHLORAD system through a series of genetic and biochemical analyses. SPL1, lacking E3 ligase activity, functions as a negative regulator of SP1; conversely, SPL2, the more distantly related SP1 homologue, shares functional redundancy with SP1 (Mohd Ali et al., 2023). This conclusion concerning SPL2 was also supported by analyses conducted in tomato. It was revealed that both SP1 and SPL2 were involved in the chloroplast-to-chromoplast transition during fruit ripening in tomato. Knockdown of *SP1*, or *SPL2* delayed tomato fruit ripening, whereas the overexpression of *SP1* accelerated ripening. Biochemical analysis suggested that such a control on plastids transition during fruit ripening was closely linked to the reorganization of TOC machinery and subsequent plastid proteomic changes caused by the manipulation of *SP1* or *SPL2* (Ling et al., 2021).

1.3.4.2 SP2

After SP1-mediated ubiquitination, the polyubiquitinated TOC proteins need to be removed from the OEM before degradation by the cytosolic 26S proteasome. However, SP1 does not have the extensive transmembrane spans necessary to form a retrotranslocon, unlike Hrd1 and Doa10 which mediate retrotranslocation of ER membrane or lumen proteins. Instead, a separate protein, SP2, was identified to act as a retrotranslocation channel. Like *sp1*, *sp2* was identified in an *Arabidopsis* mutant screen for suppressors of the mutant *ppi1* (Ling et al., 2019).

SP2 is an Omp85-type β-barrel protein located in the chloroplast OEM. The *sp2* mutations can suppress the phenotype of *ppi1* with respect to chlorosis, chloroplast development, and chloroplast protein import efficiency. Like SP1, SP2 can also directly interact with the TOC proteins. The *sp2* mutations are hence highly similar to the *sp1* mutations, indicating that both proteins might function in the same proteolytic pathway. Genetic analysis confirmed this hypothesis since the *sp1 sp2 ppi1* triple mutant displays no phenotypic additivity (with respect to plant greening) relative to the *sp1 ppi1* and *sp2 ppi1* double mutants. In addition, the effect of SP1 overexpression is abrogated by the *sp2* mutation. Moreover, whereas the single overexpression of SP1 or SP2 has no obvious phenotypic consequence in the wild-type background, the simultaneous overexpression of both genes induces severe chlorosis linked to defective chloroplast development. This evidence strongly supports the notion that SP1 and SP2 function together (Ling et al., 2019).

Like other members of Omp85 superfamily, such as Toc75 and OEP80, SP2 has been proved to have the capacity to form a membrane channel (Hsueh et al., 2017).

1.3.4.3 Cdc48

SP1 and SP2 can physically interact to form a complex on the OEM, with SP1 mediating ubiquitination of the TOC components and SP2 forming a channel for translocating ubiquitinated TOC proteins to the cytosol. However, there is still one more question remained. Since the eradication of TOC components from OEM requires energy input, which protein provides motive force for such extraction?

To answer this question, the ERAD system, a well-characterized pathway mediating the degradation of misfolded or redundant ER proteins, must be mentioned here. As described earlier, the ERAD system has been extensively studied in yeast and mammals due to its relevance in human diseases. Though the understanding of ERAD in plants is not as comprehensive, substantial progress has been made over the past decade, revealing the functions of ERAD in stress responses and plant development (Chen et al., 2020). In yeast, there are at least two

predominant protein complexes that operate in ERAD, dependant on where the misfolded protein is located. In both cases, a membrane bound E3 ligase (Doa10 or Hrd1) plays an essential role in the recognition and ubiquitination of the misfolded substrate. Moreover, as already noted, the extensive membrane spans of both Doa10 and Hrd1 can potentially form a retrotranslocation channel during the extraction of ubiquitinated protein. Such extraction is assisted by motive power provided by the Cdc48 ATPase (Ruggiano et al., 2014).

To investigate if this is the case for the extraction of ubiquitinated TOC proteins from chloroplasts, a co-immunoprecipitation experiment followed by mass spectrometry was applied, to seek similar regulators. Cdc48A, the major isoform of Cdc48 in *Arabidopsis*, was thus identified by its interaction with Toc33 (Ling et al., 2019).

Cdc48 is an essential component in *Arabidopsis*, and knockout mutants of Cdc48 are embryo lethal making functional studies difficult. However, plants with inducible overexpression of a dominant-negative form of Cdc48 (Cdc48-DN) show chlorosis and over-accumulation of TOC proteins, revealing similarities with the *sp1* and *sp2* mutations. Besides Toc33, Cdc48 was proved to physically interact with Toc159 at the chloroplast envelope. Together, these data indicated that Cdc48 is also involved in TOC protein degradation (Ling et al., 2019).

1.3.4.4 CHLORAD

Genetic analysis demonstrated that SP2 and Cdc48 act together in the same proteolytic pathway as SP1. Meanwhile, physical interaction studies indicated that the three components can form a complex at the surface of the chloroplast. This proteolytic system involving SP1, SP2 and Cdc48 was termed chloroplast-associated protein degradation (CHLORAD), and is an analogous system to ERAD (Ling et al., 2019).

Though CHLORAD system was originally proposed for eradicating TOC proteins that mediate chloroplast protein import, many internal chloroplast proteins were recently proved to be targeted by CHLORAD (Li et al., 2022; Sun et al., 2022). Thus, a broader role of CHLORAD in

chloroplast biogenesis was unveiled, though some important questions still require further investigation; for instance, how, when, and where are intra-chloroplast protein ubiquitinated?

1.3.4.5 Beyond CHLORAD

The identification of the CHLORAD system was a major breakthrough for chloroplast biogenesis research in the past decade. The CHLORAD pathway influences plastid development and functions by interacting with TOC proteins to modify protein import and degradation. It was demonstrated to participate in plant stress tolerance and fruit ripening (Ling & Jarvis, 2015b; Ling et al., 2021). Interestingly, recent research indicated that the SUMOylation system also participates in the regulation of TOC proteins (Accossato et al., 2020; Watson et al., 2021). Additionally, SUMOylation was found to facilitate chloroplast protein import under heat stress (HS) (Zheng et al., 2022a).

SUMOylation is an essential post-translational modification in eukaryotic cells, which conjugates small ubiquitin-like modifier (SUMO), a ubiquitin-like protein, to target proteins. Like ubiquitination, SUMOylation is also catalysed by an enzyme cascade, including an E1 activating enzyme complex, an E2 conjugating enzyme, and an E3 ligase (Benlloch & Lois, 2018; Han et al., 2021; Roy & Sadanandom, 2021). SUMOylation is a well-known and conserved response strategy under environmental stress (Kurepa et al., 2003; Rytz et al., 2018), whereas our current knowledge on SUMO functions in chloroplast biogenesis is at a nascent stage.

In 2010, a high-throughput screen for SUMO substrates in *Arabidopsis* suggested that Toc159 might be a SUMO substrate (Elrouby & Coupland, 2010). Later it was shown that SUMOylation partially stabilizes Toc159 under a low GA conditions during early development (Accossato et al., 2020). Furthermore, through a comprehensive genetic and biochemical analysis, it was revealed that SUMO system component mutations can suppress the chlorotic phenotype of *ppi1*; in addition, it was revealed that the TOC proteins physically interact with key SUMO system proteins and are likely SUMOylated. This work shed light on a direct functional link between the SUMO system and the chloroplast import apparatus and highlighted the complexity of the

regulation of the TOC complex (Watson et al., 2021). Although SUMOylation and ubiquitination are largely independent from each other, there is accumulating evidence for crosstalk between the pathways (Bergink & Jentsch, 2009; Geoffroy & Hay, 2009; Perry et al., 2008; Ramachandran et al., 2015; Rott et al., 2017). However, the precise nature of the interplay between the two systems in the regulation of chloroplast protein import needs further investigation.

1.3.5 Cdc48 and its cofactors

1.3.5.1 Cdc48 structure and cellular functions

Cdc48 is a member of the AAA (ATPase Associated with diverse cellular Activities) protein family. It contains a substrate and cofactor interacting N-terminal domain and two tandem ATPase domains, D1 and D2. Cdc48 hexamerizes into a double-ring structure with a central pore formed by the D1 and D2 ATPase domains. Assembly of the hexameric Cdc48 complex relies on the D1 domain, whereas during the ATP hydrolysis which energizes Cdc48 to perform mechanical functions the bulk of activity is exerted by the D2 domain (Xia et al., 2016). Conformational change induced by ATP hydrolysis creates a motor force through movement of the rings and N domain, allowing the extraction and denaturation of bound substrates through the centre pore (Bodnar & Rapoport, 2017).

Cdc48 is an evolutionally conserved protein that plays an essential regulatory function in a broad array of cellular processes (Begue et al., 2017; Hanzelmann & Schindelin, 2017). In plants, Cdc48 is particularly critical when rapid cellular changes are needed, such as during reproduction, germination, growth, differentiation, and immune responses (Park et al., 2008; Rosnoblet et al., 2017). As a molecular chaperone, Cdc48 segregates polyubiquitinated proteins from complexes or membranes, and the substrate proteins are then degraded by the proteosome. In some cases, such as chromatin-associated processes, substrates may instead by recycled (Franz et al., 2016).

1.3.5.2 Categories of Cdc48 cofactors

Although Cdc48 is involved in various cellular processes, it exhibits hardly any substrate specificity on its own. The functional versatility of Cdc48 relies on a large number of cofactors recruiting it to different cellular pathways, of which more than 30 are currently known across plants, yeast and mammals (Buchberger et al., 2015; Hanzelmann & Schindelin, 2017).

The cofactors can be broadly grouped into three major classes based on their functions and domains: substrate-recruiting cofactors, substrate-processing cofactors, and regulatory cofactors. Prominent examples of the substrate-recruiting cofactors are the ubiquitin-associated and ubiquitin regulatory X (UBA-UBX) proteins, and the Npl4/Ufd1 heterodimer. The substrate-processing cofactors consist of ubiquitin ligases, deubiquitinase (DUB) enzymes, and peptide N-glycanase (PNGase). The regulatory cofactors are responsible for the recycle of Cdc48 hexamers, or post-translational modifications like acetylation, phosphorylation, SUMOylation, and ubiquitination (Hanzelmann & Schindelin, 2017). The majority of the cofactors bind to the N-terminal domain of Cdc48 via domains such as UBX (ubiquitin regulatory X) and UBXL (UBX-like), or motifs such as VBM (VCP-binding motif), VIM (VCP interacting motif), and the SHP box (Hanzelmann & Schindelin, 2017). A small number of the cofactors bind to the C-terminal tail of Cdc48 (Allen et al., 2006; Zhao et al., 2007).

The UBX domain consists of a ubiquitin-like β-Grasp fold and is the most common Cdc48 binding motif. UBX proteins can be subdivided into two families: UBX-only proteins, and UBA-UBX proteins which also contain a UBA (ubiquitin-associated) domain that can interact with ubiquitinated substrates. All 13 UBX domain-containing proteins that have been identified in mammals have been demonstrated to bind Cdc48, further confirming the UBX domain as a general Cdc48 interaction motif (Kloppsteck et al., 2012).

The UBXL domain adopts a structure similar to the UBX domain (though the two share a low degree of sequence identity) and binds in a similar position with respect to Cdc48. It is found in

a few DUB enzymes, as well as Npl4 in which it is also known as the ubiquitin fold domain (UBD) (Bruderer et al., 2004; Kim et al., 2014).

Both the VIM motif and VBM motif adopt an α-helical conformation comprised of positively charged residues. The VIM motif was originally identified in the mammalian ERAD ubiquitin ligase gp78 (Ballar et al., 2006), and then subsequently in SVIP (small VCP-inhibiting protein), a membrane-anchored negative regulator of ERAD (Ballar et al., 2007). It was also found in Vms1 (VCP mitochondrial stress-responsive 1), the substrate binding protein in MAD (Heo et al., 2013). The typical protein containing a VBM motif is the E3 ligase Hrd1, a protein involved in protein retrotranslocation during ERAD (Liu et al., 2013).

The SHP binding motif has been identified in several UBX proteins as an additional binding element and notably in Ufd1, the latter typically forming a stable heterodimer with the UBXL protein NPL4. The SHP motif binds to a different site of the Cdc48 N-domain than the other N-domain interaction motifs (Hanzelmann & Schindelin, 2017; Le et al., 2016).

Lastly, the structurally unrelated PUB (PNGase/UBA or UBX containing proteins) and PUL (PLAP, Ufd3p, and Lub1p) domains are currently the only known domains that interact with the unstructured C-terminus of Cdc48 (Allen et al., 2006; Qiu et al., 2010). The direct interactions between the PUB/PUL domains and Cdc48 is regulated by post-translational modifications (Li et al., 2008; Zhao et al., 2007).

Whereas the Cdc48 cofactors are extensively understood in yeast and mammals, their identification and characterization in plants has been rather sporadic.

1.3.5.3 The Cdc48-Npl4-Ufd1 complex

The heterodimeric Npl4-Ufd1 complex is the cofactor that participates in many ubiquitin-dependent Cdc48-driven processes, particularly ERAD (Ye et al., 2003). Substrate initially binds to Ufd1-Npl4 via its attached polyubiquitin chain, and then moves through the pore of the Cdc48 ATPase rings and is thereby unfolded. In MAD, Npl4 also acts as the cofactor of Cdc48, coordinating with another protein called Vms1 (Heo et al., 2010). The *Arabidopsis* genome

encodes two homologues of Npl4 and four of Ufd1 (Liu & Li, 2014); however, the functions of them are largely uncharacterized in plants. It was reported that Cdc48 physically associates with its heterodimeric cofactor Ufd1-Npl4 to regulate centromere disassembly in pollen vegetative cells (Merai et al., 2014). In 2020, the Cdc48-Npl4-Ufd1 complex was shown to be involved in the inner nuclear membrane protein degradation in *Arabidopsis* (Huang et al., 2020). Most recently, the function of the Cdc48-Npl4-Ufd1 complex in the degradation of internal chloroplast proteins, namely RbcL and AtpB, two plastid genome-encoded proteins, was unveiled (Li et al., 2022).

1.4 Project rationale

1.4.1 Investigating the participation of PUX proteins in CHLORAD

The Cdc48 chaperone is an essential component of CHLORAD providing motive force for substrate protein retrotranslocation. However, as a cytosolic protein, how is Cdc48 recruited to the chloroplast OEM to function in CHLORAD? The family UBX domain containing proteins constitute by far the largest family of Cdc48 cofactors (Schuberth & Buchberger, 2008). I hence propose that one or more UBX proteins is responsible for recruiting Cdc48 to CHLORAD.

The UBX proteins are a large, evolutionarily conserved family. They normally contain a UBX domain at the C terminus for binding with Cdc48, as well as a UBA domain at the N terminus for ubiquitin binding. In *Saccharomyces cerevisiae* there are seven proteins containing the UBX domain, namely Shp1 (also known as Ubx1) and Ubx2 to Ubx7 (Schuberth et al., 2004). Among them, the Ubx2 protein has been well studied, and it has been shown that Ubx2 mediates interaction of the Cdc48 complex with the ER membrane-bound ERAD ubiquitin ligases Hrd1 and Doa10 (Neuber et al., 2005; Schuberth & Buchberger, 2005; Schuberth et al., 2004). The Ubx2 protein is located in the ER membrane, and it binds with Cdc48 via its UBX domain, while its additional UBA domain functions in substrate recruitment as a ubiquitin-binding element. Recent studies have discovered that the Cdc48-Ubx2 complex regulates the ubiquitination of a mitochondrial outer membrane protein Fzo1 for proteasomal degradation to ensure the proper

fusion events of mitochondrial membranes (Nahar et al., 2020). In addition, a specific pool of Ubx2 was identified to bind to the translocase of the mitochondria outer membrane (TOM) complex to recruit Cdc48 for clearance of trapped precursor proteins from the TOM channel (Martensson et al., 2019).

In *Arabidopsis*, there are 16 plant UBX-domain containing proteins, known as PUX proteins (Liu & Li, 2014). PUX proteins are a very heterozygous family, being extensively variable in length and having various combinations of interaction domains and motifs. The only common feature is the C-terminal UBX domain (Zhang et al., 2022b; Zhang et al., 2021). Unlike their counterparts in animals and fungi, the structures and biological roles of PUX proteins have been subjected to only limited analyses, as summarized below, and thus remain largely undeciphered.

The PUX1 protein regulates Cdc48 activity by promoting the disassembly of the active hexamer, and hence inhibits its ATPase activity. *Arabidopsis pux1* mutant plants displayed accelerated growth of roots, which was related to the elevated cell division and expansion (Banchenko et al., 2019; Park et al., 2007; Rancour et al., 2004). The nucleus-localized PUX7 protein was proved to physically interact with both Cdc48 and ubiquitin. However, a lack of obvious developmental defects in corresponding mutants indicated that PUX7 might act redundantly with other members of the PUX family (Gallois et al., 2013). Interestingly, PUX7 and three other PUX proteins, PUX8, PUX9 and PUX13, contain one or more distinct ubiquitin-interacting motif (UIM) sequences which target them to autophagosomes, where they mediate the clearance of inactive Cdc48 (Marshall et al., 2019). The nucleoskeleton-associated PUX3, PUX4 and PUX5 proteins interact with Cdc48 to negatively regulate inner nuclear membrane protein degradation in plants (Huang et al., 2020). Recent works have demonstrated that PUX10 is involved in the degradation of lipid droplet proteins in lipid-rich plant tissues (Deruyffelaere et al., 2018; Kretzschmar et al., 2018).

The involvement of PUX proteins in CHLORAD by acting as cofactors for Cdc48 has not yet been illuminated (Figure 1.1). I therefore aimed to explore this idea, using genetics, molecular biology, and biochemistry.

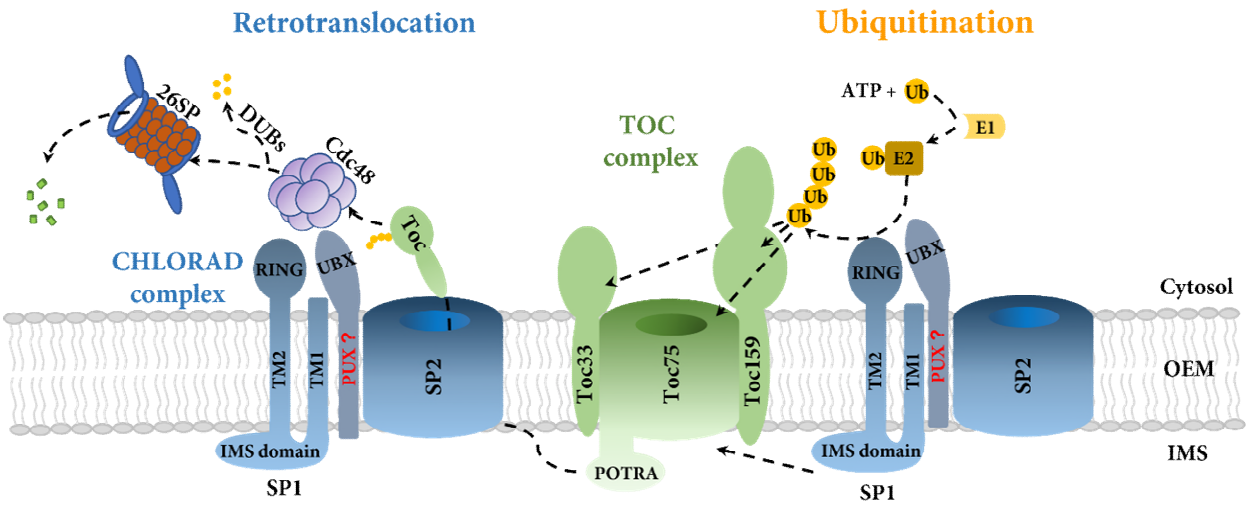


Figure 1.1. Does PUX protein involve in the CHLORAD pathway? TOC proteins are marked with a polyubiquitin by E2 ubiquitin conjugating and SP1 E3 ligase enzyme. Once dislocated into cytosol, ubiquitins are cleaved from TOC proteins by yet unknown deubiquitinases before TOCs are degraded by the 26S proteasome. *Arabidopsis* TOC proteins are shown and labelled by convention according to their molecular weight in kilodaltons. Abbreviations: POTRA domain, polypeptide transport-associated domain; RING, really interesting new gene; TM, transmembrane; PUX, plant UBX domain-containing protein; UBX, ubiquitin regulatory X; Ub, ubiquitin; OEM, outer envelope membrane; IMS, intermembrane space; SP1, suppressor of *ppi1* locus 1; SP2, suppressor of *ppi1* locus 2; Cdc48, cell division cycle protein 48; DUBs, deubiquitinases; 26SP, 26S proteasome; CHLORAD, chloroplast-associated protein degradation.

1.4.2 Identification of new regulators of chloroplast protein import

ERAD has been extensively studied in yeast and mammals, and >170 components have been characterized (Christianson et al., 2012). In contrast, our understanding of CHLORAD is not yet comprehensive. Although SP1-dependent UPS activity has been proved to play a crucial role in chloroplast biogenesis and stress tolerance (Ling et al., 2019; Ling et al., 2012; Ling & Jarvis, 2015b), new components of this regulatory machinery still need to be identified. Additionally, besides the SP1-mediated chloroplast protein degradation pathway, it is certain that SP1-independent regulatory pathways also operate in chloroplasts. For instance, DELLA-dependent

Toc159 degradation by the UPS is an SP1-independent regulatory mechanism responsible for controlling chloroplast biogenesis in early plant development (Shanmugabalaji et al., 2018).

To investigate the likelihood that there are yet many unknown CHLORAD components, a larger-scale genetic screen for suppressors of the *ppi1* mutation was conducted in the group, to identify new *sp* mutations. I aimed to analyse these new mutants, which show greener phenotypes than *ppi1* similar to *sp1 ppi1* and *sp2 ppi1*, to afford fresh insights into the role of the UPS in chloroplast regulation.

1.4.3 Thesis aims and structure

This thesis has two aims, which related directly to the two strands of my research project, both of which aimed to elucidate the regulation of chloroplast protein import: (1) The central purpose of my project was to determine whether any of the PUX proteins function in CHLORAD, and if so what the nature of these functions are and to what extent they are essential. The extensive research into UBX protein families in other eukaryotic organisms was greatly beneficial, allowing me to make hypotheses about the potential molecular characteristics of PUX proteins. However, it is also possible that distinct protein properties and functions may have been acquired by PUX proteins during evolution. (2) Alongside the PUX work, I also conducted an analysis of candidate causative genes (which were identified prior to this project) for the new *suppressor of ppi1 locus 3* (*sp3*) mutant, which came from a previous mutant screen for new *sp* mutants. A series of approaches were undertaken to achieve the aims of the thesis, involving genetics, molecular and cellular biology, protein biochemistry, and microscopy.

Chapter 2 describes how, given the presumed requirement for a cofactor to recruit Cdc48 to the chloroplast surface, the localization of all 16 PUX proteins in *Arabidopsis* was analysed, with the aim of identifying the chloroplast membrane located PUX proteins. Once PUX10 was confirmed to be the only PUX protein located in chloroplast, topology analysis of the PUX protein was performed to provide essential information for understanding its biological functions. A series of transgenic *Arabidopsis* plants expressing truncated PUX10 variants were subsequently produced

and analysed. To assess the influence of PUX10 on Cdc48 cellular distribution, various transgenic plants were produced for subcellular fractionation analysis. The interactions of PUX10 with Cdc48 and ubiquitin via its UBX and UBA domain, respectively, were assessed using bimolecular complementation and co-immunoprecipitation assays.

Chapter 3 presents a more advanced analysis of the functional links of PUX10 with CHLORAD and TOC proteins, using genetic and biochemical approaches. *Arabidopsis pux10* mutants and PUX10 overexpression lines were firstly characterized. Then, a series of genetic experiments involving crosses into *toc* mutant backgrounds was conducted, to determine whether there are genetic interactions between PUX10 and TOC components. The resulting double mutants and transgenic plants were phenotypically characterized with respect to chlorosis, chloroplast development, and TOC protein abundance. A possible link between PUX10 and SP1 was also investigated genetically through crosses. Physical interactions between PUX10 and CHLORAD components, as well as TOC proteins, were subsequently analysed, which was crucial for the establishment of functional linkages. Lastly, the potential physiological importance of PUX10 in chloroplast biogenesis was investigated.

Chapter 4 builds on the foundations of a previous mutant screen to identify new regulators of chloroplast protein import. A new suppressor mutant with a greener phenotype than *ppi1*, similar to *sp1 ppi1* and *sp2 ppi1*, had been identified and named *suppressor* of *ppi1 locus 3* (*sp3*). Moreover, genomic DNA sequencing and SHOREmap analysis had revealed single nucleotide polymorphisms in eight genes on *Arabidopsis* chromosome 1, identifying them as likely candidates for the gene responsible for the *sp3 ppi1* suppressor phenotype. For each of these candidate genes, respective T-DNA insertion mutants were obtained and characterized, and crossed into the *ppi1* background. The phenotypes of the resulting double mutants were compared to *ppi1*, to confirm the identity of the *sp3* causative gene. Once the identification of *sp3* had been concluded, preliminary functional characterization experiments were conducted.

Both aims of this thesis can conceivably lead to significant advances in our understanding of CHLORAD, and of protein import regulation during plastid biogenesis.

Chapter 2

Results 1

Identification of a cofactor of Cdc48 in chloroplasts

2 Identification of a cofactor of Cdc48 in chloroplasts

2.1 Abstract

Thousands of nucleus-encoded proteins are imported into chloroplasts via two cooperating translocons at the outer (TOC) and inner (TIC) chloroplast envelope membranes. The import process is tightly regulated throughout development and in response to specific environmental cues. Over the past decade, the chloroplast-associated protein degradation (CHLORAD) pathway was revealed to play a crucial role in the turnover of TOC components.

One of the key components of CHLORAD, Cdc48, is an exceptionally versatile protein, and its substrate specificity depends on cofactors, of which the UBX domain proteins constitute the largest family. The *Arabidopsis* genome contains 16 UBX-containing proteins that are collectively called the plant UBX domain (PUX) protein family. Some of these have been investigated, and the identified functions provide an indication for the ways through which PUX protein can control Cdc48.

To determine whether PUX proteins are involved in CHLORAD, the subcellular localization of PUX proteins was firstly screened by confocal microscopy. PUX10 was identified as the only PUX protein located in chloroplasts, with a pattern indicating envelope localization. Protein topology analysis of PUX10 was conducted to facilitate following functional analyses, and this revealed that the protein is located in the outer envelope membrane with its UBX and ubiquitin-associated (UBA) domains both projecting towards cytosol. Biochemical analyses revealed that PUX10 controls the partitioning of Cdc48 to the chloroplasts, and that its UBX and UBA domains bind to Cdc48 and ubiquitin, respectively. In addition, a series of *pux10* mutants and transgenic plants overexpressing *PUX10* were characterized, and subsequently crossed into TOC mutant backgrounds, to investigate the genetic link between PUX10 and chloroplast protein import. Collectively, the results presented in this chapter identify PUX10 as a key Cdc48 cofactor in chloroplasts, and provide evidence that PUX10 can efficiently recruit cytosolic Cdc48 to the

chloroplast surface and, most likely, to ubiquitinated TOC proteins. However, surprisingly, no significant phenotypic suppression of TOC mutants upon *pux10* mutation could be observed.

2.2 Introduction

It is well-known that most chloroplast proteins (>90%) are synthesized in the cytosol and imported into chloroplasts post-translationally. An intricate mechanism has evolved for mediating such intracellular protein translocation, to maintain the proper development and functioning of chloroplasts. Although there are a few pathways for the targeting of nucleus-encoded chloroplastic proteins, the TOC-TIC pathway is the major route (Jarvis & Lopez-Juez, 2013; Paila et al., 2015). As the gateway of chloroplast protein import, the importance of the TOC complex is evident, and hence has received extensive studies. Among these, the identification of CHLORAD, a ubiquitin-dependent proteolytic system, is a pioneering work that provided elucidation of the regulation of TOC complex (Ling et al., 2019; Ling et al., 2012). As the provider of motive force, Cdc48 is undoubtedly an important component of CHLORAD.

Cdc48 is one of the most abundant proteins in eukaryotic cells, and it plays essential regulatory functions in a broad array of cellular processes. However, the targeting and activity of Cdc48 largely depends on its cofactors which allow it to function in a myriad of cellular pathways (Baek et al., 2013). Most of the cofactors possess conserved Cdc48-binding motifs such as UBX, UBXL, SHP, VBM, VIM and PUB. Many of these cofactors are not essential for cell growth and survival, indicating potential functional redundancies among them. The UBX domain-containing proteins constitute by far the largest family of Cdc48 cofactors (Zhang et al., 2021). The UBX domain comprises about 80 amino acid residues and displays high structural similarity with ubiquitin. The UBX proteins are involved in substrate recruitment to Cdc48 and in the temporal and spatial regulation of its activity. For instance, proteins with a UBA/UBX domain architecture, like yeast Shp1 and Ubx2 and the mammalian proteins FAF1 and SAKS1, are able to bind ubiquitinated substrates with their N-terminal UBA domain while interacting with Cdc48/p97 via their C-terminal UBX domain (McNeill et al., 2004; Schuberth et al., 2004; Song et al., 2005).

The PUX proteins define a family of plant proteins that possesses a conserved UBX domain, which mediates direct interaction with Cdc48. Emerging knowledge on the structure and function of PUX proteins provides an indication of the functional links between PUX proteins and Cdc48. Several members serve as canonical adaptors to recruit Cdc48 to specific organelles (Deruyffelaere et al., 2018; Gallois et al., 2013; Huang et al., 2020; Kretzschmar et al., 2018), while others are involved in regulating the activity of Cdc48 (Marshall et al., 2019; Park et al., 2007; Rancour et al., 2004). Among the 16 PUX proteins in *Arabidopsis,* PUX10 is the only protein containing membrane-anchoring hydrophobic regions. Previous studies suggested that PUX10 is a lipid droplet (LD)-anchored scaffolding protein to mediate the degradation of ubiquitinated oleosins via recruiting Cdc48 to LDs during seed germination (Deruyffelaere et al., 2018; Kretzschmar et al., 2018). Intriguingly, PUX10 was dramatically relocated to chloroplasts during seed maturation (Deruyffelaere et al., 2018).

In this chapter, such chloroplast localization of PUX10 was confirmed by both protoplast transient expression and stable transformation of a PUX10-YFP fusion protein. Furthermore, bimolecular fluorescence complementation (BiFC) experiments clearly demonstrated the interaction of PUX10 with Cdc48, as well as TOC proteins, at the chloroplast outer envelope membrane (OEM). Based on these and other observations, the hypothesis that PUX10 serves as an anchor for targeting the cytosolic Cdc48 to the chloroplasts for the turnover of TOC proteins was proposed.

2.3 Results

2.3.1 Subcellular localization screening of PUX proteins in *Arabidopsis*

The *Arabidopsis* genome encodes a family of 16 plant UBX domain (PUX) protein genes (Table 2.1). Among these, *PUX14*, *PUX15* and *PUX16* are pseudogenes based on the previous report (Gallois et al., 2013). In addition, no orthologues of *PUX14*, *PUX15* or *PUX16* could be identified in fungi or animals, which further supported the notion that these three are pseudogenes (Zhang et al., 2022b). Therefore, they were not investigated in this screening. Additionally, after

analysing the coding sequence of *PUX6* in *Arabidopsis*, the first 63 bp in the predicted first intron was found to be part of the first exon. A stop codon was hence introduced into the first exon, which resulted in a premature protein. Such a premature protein was proved to be unfunctional since no YFP signal was detected when the construct bearing full-length coding sequence of *PUX6* fused with YFP was transiently expressed in protoplasts (Figure 2.1). Moreover, similar to *PUX14*, *PUX15* and *PUX16*, there are no orthologues of *PUX6* in fungi or animals (Zhang et al., 2022b). Thus, it was concluded that *PUX6* is also a pseudogene.

To further understand the functional mechanism of Cdc48 action in CHLORAD, I used yellow fluorescent protein (YFP) fusions of PUXs to assess for possible chloroplast membrane localization that would be consistent with a role in facilitating the tethering of cytosolic Cdc48 to the chloroplast membrane during ubiquitinated TOC protein extraction. The individual coding sequences (CDSs) of *PUX* genes were cloned into the p2GWY7 vector bearing a 35S promoter and sequence encoding a YFP tag. The resulting constructs were used to transfect protoplasts isolated from ~3-week-old *Arabidopsis* plants, which were then visualised under confocal microscopy (Figure 2.1). Of those constructs for which clear fluorescence signals were detected, most displayed patterns consistent with localization in compartments other than the chloroplasts (e.g., cytosol, nucleus, endomembrane system, or mitochondria).

Most significantly, PUX10 (At4g10790) was the only protein that showed distinct localization in the chloroplast envelope membranes. To rule out the possibility of mislocalization caused by the transient overexpression of *PUX10*, stable transgenic lines expressing *PUX10-YFP* under both native and *35S* promoters were generated, and the localization of PUX10-YFP was viewed under confocal microscopy (Figure 2.2 A and B). Similar results were obtained, indicating that neither the expression system nor the expression level of *PUX10* had effect on the predominant subcellular localization of PUX10.

In the transient assays, PUX10 also showed some cytosolic localization, albeit to a much weaker extent than the chloroplast localization. To further investigate whether PUX10 is associated with

other organelles, the same PUX10-YFP construct was transiently overexpressed in protoplasts isolated from the reporter lines of various subcellular compartments, including the ER, mitochondria, and Golgi, and possible colocalization was assessed under confocal microscopy. Though no association of PUX10 with mitochondria and Golgi was observed, PUX10 possibly localized to the ER (Figure 2.3). Previous studies also suggested a weak ER localization of PUX10 upon expression under its native promoter (Deruyffelaere et al., 2018; Kretzschmar et al., 2018). However, it cannot be ruled out that such ER localization is an artefact caused by the tagging approach employed. Overall, PUX10 displayed pronounced and clear localization to the chloroplast envelopes in *Arabidopsis* leaves.

2.3.2 Further localization and topology analysis of the PUX10 protein

The PUX10 protein has two predicted transmembrane (TM) spans, an N-terminal UBA domain, and a C-terminal UBX domain (Figure 2.4 A). Firstly, to investigate whether the two predicted TMs are responsible for the chloroplast localization of PUX10, a truncated *PUX10* CDS lacking the coding region of the TMs (ΔTM1/2) fused with YFP was transiently expressed in isolated protoplasts. Confocal visualization then clearly indicated that the truncated PUX10 was located in the cytosol, which proved that the chloroplast membrane localization of PUX10 was dependent on the TMs (Figure 2.4 B). Next, transgenic plants overexpressing various truncated *PUX10* transcripts were also generated. These lacked sequences coding for one or both of the key functional domains (ΔUBA, ΔUBX or ΔUBX/UBA) or both of the TM domains (ΔTM1/2). Confocal analysis of these transgenic plants indicated that the TM domains solely contribute to the chloroplast localization of PUX10 (Figure 2.4 C). Collectively, these results demonstrated that the TMs are responsible for anchoring the PUX10 protein in the chloroplast envelope membrane.

To investigate the topology of PUX10, I generated transgenic plants expressing a FLAG-PUX10-YFP constructs, with the fusion of FLAG and YFP tags to the N- and C-termini of PUX10, respectively. The transgenic plants were characterized by immunoblotting. First, alkaline

extraction in conjunction with immunoblotting was applied to determine whether the PUX10 is a peripheral or an integral membrane protein. Chloroplasts were isolated from the transgenic plants and then treated with 100 mM Na_2CO_3 (pH 11.5), to remove non-integrated proteins from the membranes. Membrane pellet and soluble fractions were then recovered and analysed alongside a total chloroplast sample by immunoblotting using anti-GFP. Almost all the FLAG-PUX10-YFP protein was found in the membrane pellet fraction, but not in the soluble fraction, indicating that PUX10 is indeed an integral chloroplast membrane protein. Coomassie staining (bottom) for the Rubisco large subunit (LSU) and light-harvesting chlorophyll a/b-binding protein (CAB) confirmed the efficiency of the fractionation procedure (Figure 2.5 A).

There are two membrane-anchoring domains in PUX10 as predicted by both ARAMEMNON (http://aramemnon.uni-koeln.de/) and CCTOP (http://cctop.enzim.ttk.mta.hu), as shown in Figure 2.4 A, though some other software predicted only one transmembrane domain in PUX10. The PUX10 displays a domain architecture highly similar to that of Ubx2 (the homologue of PUX10 in yeast), which has an N-terminal UBA domain, a C-terminal UBX domain, and a double hydrophobic transmembrane region close to N-terminus (Neuber et al., 2005). Thus, it was assumed that the PUX10 topology is such that both UBA and UBX domains face the cytosol, for accessing ubiquitinated substrates and Cdc48, respectively, similar to the functional mechanism of Ubx2 in yeast (Deruyffelaere et al., 2018; Kretzschmar et al., 2018). However, such a topological arrangement of PUX10 has not previously been confirmed experimentally. To address this question, a 'dual protease' protection assay using thermolysin and trypsin proteases was employed (Figure 2.5 B). Thermolysin is a 34.6 kDa extracellular metalloendopeptidase. Thermolysin cannot significantly penetrate beyond the OEM, which allows it to digest specifically OEM proteins that are exposed to the cytosol without causing any major damage to the integrity of the chloroplast (Cline et al., 1984). Trypsin is a small 23.5 kDa protein of the serine protease S1 family. Unlike thermolysin, trypsin can partially disrupt the integrity of the OEM and thus gain access to the intermembrane space (IMS) where it can digest regions of

OEM proteins or IEM proteins that extend into the IMS (Chou et al., 2003; Sveshnikova et al., 2000).

Chloroplasts were isolated from the above transgenic plants, and then either mock treated or treated with thermolysin or trypsin (the former with or without Triton X-100 detergent treatment, to disrupt the chloroplast membranes as a control). After quenching the protease reactions, all samples were analysed by immunoblotting using anti-FLAG or -GFP. The full-length FLAG-PUX10-YFP fusion protein (~80 kDa) was detected in the mock treatment without applying either thermolysin or trypsin. However, both the N-terminus and C-terminus of PUX10 showed strong sensitivity to thermolysin, indicating that PUX10 was located in the OEM with both termini facing the cytosol. Complete degradation of PUX10 by trypsin further supported this conclusion. The OEM proteins Toc159 and Toc33, which have large cytosolic domains, served as controls to ensure that the thermolysin protease treatment was functioning correctly. Toc75, which is deeply embedded in the OEM, and the IEM proteins Tic110 and Tic40 were employed as controls for the efficiency of trypsin treatment (Figure 2.5 B). All together, these results provided direct evidence for the existence of two transmembrane spans in the N-terminal hydrophobic region of PUX10; and for the cytosolic orientation of both the UBX and UBA domains, ensuring their accessibility to Cdc48 and ubiquitinated substrates, respectively (Figure 2.5 C and D).

2.3.3 Identification of *pux10* mutant and *PUX10* overexpression lines

To further understand the function of *PUX10* in *Arabidopsis*, two T-DNA insertion mutants were obtained from Nottingham Arabidopsis Stock Centre (NASC): *pux10-1* (SAIL-1187-B06) and *pux10-4* (WiscDslox424B8). The *pux10-1* mutant has been characterized before in a different study (Deruyffelaere et al., 2018; Kretzschmar et al., 2018), but the *pux10-4* mutant has not previously been studied. Two different alleles of *pux10*, *pux10-2* and *pux10-3*, have been described before by other research groups (Deruyffelaere et al., 2018; Kretzschmar et al., 2018), but not used in this study. Unlike *pux10-2* and *pux10-3* which either has a T-DNA insertion in

the promoter region of *PUX10* or is in Wassilewskija (Ws) other than Columbia (Col-0) genetic background (Deruyffelaere et al., 2018; Kretzschmar et al., 2018), the *pux10-1* and *pux10-4* mutants contain T-DNA insertions in the first and fourth exons of *PUX10*, respectively, confirmed by sequencing (Figure 2.6 A). Additionally, the *pux10-1* and *pux10-4* mutants are in Col-0 genetic background, which means that the following *pux10*-involved genetic interaction analysis will be more straightforward since all other *Arabidopsis* materials used in this study are in Col-0 background.

First, I analysed *PUX10* expression by RT-PCR in the mutant backgrounds. As expected, RT-PCR amplification using primers on either side of the T-DNA insertion site occurred for wild type (Col-0) but not for *pux10-1* or *pux10-4* mutants (Figure 2.6 B). Although amplification of *PUX10* transcripts occurred in the mutant backgrounds when the primers were located downstream (RT-2F/RT-2R for *pux10-1*) or upstream (RT-1F/RT-1R for *pux10-4*) of the T-DNA insertion site, such truncated *PUX10* transcripts are very unlikely to be functional. Based on these results, both *pux10-1* and *pux10-4* were considered to be null mutants of *PUX10*. There was no significant phenotypical difference between the mutants and wild-type plants (Figure 2.6 C). Since both *pux10* mutants are phenotypically identical, the data presented hereafter are only for *pux10-1* as a representative allele.

Though the *pux10* knockout mutants showed no obvious phenotypic differences compared to wild-type plants, transgenic plants overexpressing full-length *PUX10* CDS (named as 35S: *PUX10* here or PUX10-OX in the following chapter) were severely dwarfed (Figure 2.7 A). In addition to the plants overexpressing intact *PUX10*, lines overexpressing truncated *PUX10* CDS forms were also generated, and these displayed different phenotypes. The 35S: $PUX10^{\Delta UBX}$ (UBX domain deleted), 35S: $PUX10^{\Delta UBX/UBA}$ (both UBX and UBA deleted), and 35S: $PUX10^{\Delta TM1/2}$ (both TMs deleted) transgenic lines all displayed similar phenotypes to wild type. However, the same dwarfism as that seen for full-length *PUX10* CDS overexpression was observed in the 35S: $PUX10^{\Delta UBA}$ (UBA domain deleted) transgenic plants (Figure 2.7 A).

These phenotypic differences implied that overexpression of *PUX10* can have a dominant-negative effect on plant growth, and that both the UBX and TM domains of PUX10 are essential for this effect to be mediated.

2.3.4 PUX10 can recruit Cdc48 to chloroplast envelope membranes

Given that UBX is a Cdc48-binding domain, and that Cdc48 has a wide spectrum of activity in various organelles, one can hypothesize that the dwarfism observed in both 35S: *PUX10* and 35S: *PUX10*$^{\Delta UBA}$ overexpression plants was due to greatly disrupted subcellular distribution of Cdc48 due to the overexpression of these UBX domain proteins. It is noteworthy that no dwarfism was observed in ΔTM1/2 transgenic plants, which implies that the overexpression of this cytosolic UBX domain protein does not similarly disrupt the distribution of Cdc48. The specific overaccumulation of Cdc48 on chloroplasts via the UBX domain of PUX10 (or its specific depletion from the cytosol or other compartments as a consequence) might be responsible for the developmental aberrancy shown in these transgenic plants.

To address this hypothesis, I made use of estradiol-inducible Cdc48-WT-FLAG and Cdc48-DN-FLAG constructs (Ling et al., 2019). These were introduced into PUX10-OX and *pux10* backgrounds, respectively, via genetic crossings. The Cdc48-WT protein has a transient and/or unstable association with chloroplasts, whereas the Cdc48-DN protein is a dominant-negative mutant with stabilized substrate binding that results in more stable association with chloroplasts. Chloroplasts were isolated from the resulting transgenic plants, and analysed by immunoblotting using anti-FLAG antibody, to assess the extent of chloroplast association of Cdc48. I observed that the weaker chloroplast-localized signal for Cdc48-WT-FLAG was significantly enhanced in the PUX10-OX background, whereas the strong chloroplast-localized signal for Cdc48-DN-FLAG was conversely reduced in the *pux10* knockout background. This result indicated that the abundance of PUX10 had a significant influence on the accumulation of Cdc48 at chloroplasts (Figure 2.7 B and C).

2.3.5 PUX10 interacts with Cdc48 via its UBX domain

The UBX domain is a close structural homologue of ubiquitin, and it functions as a general Cdc48-binding motif. As mentioned previously, proteins containing UBX domains have been proved to recruit Cdc48 to specific subcellular loci or organelles via UBX domain. To further investigate whether this is the case for PUX10, a bimolecular fluorescence complementation (BiFC) assay was first employed. BiFC is a method that uses the reconstitution of YFP fluorescence to validate protein interactions (Kerppola, 2008). In general, each target protein is fused to either N- or C-terminal fragments of YFP, and the two generated constructs are then introduced into protoplasts simultaneously for transient expression. If there is an interaction between the proteins of interest, the two complementary, non-fluorescent fragments of YFP are brought into proximity with each other, enabling the formation of a functional fluorophore. Thus, a fluorescent signal can be visualized under a confocal microscope. Such BiFC experiments can be used to assess for both the presence and subcellular localization of protein-protein interactions.

The full-length *PUX10* CDS and the ΔUBX (PUX10 UBX domain deleted) sequences were cloned into the pSAT4(A)-cEYFP-N1 vector, while the *Cdc48* CDS was cloned into pSAT4(A)-nEYFP-N1 vector (Citovsky et al., 2006). The resulting constructs encoding the complementary nEYFP and cEYFP fragments, respectively, were co-transfected in pairs into *Arabidopsis* protoplasts. Meanwhile, as a control, I also transfected protoplasts solely with a construct carrying the *Cdc48* CDS fused to the full-length *YFP* CDS. Subsequent confocal microscopy indicated that the Cdc48-YFP protein, expressed alone, was located exclusively in the cytosol (Figure 2.8 A). In the BiFC analysis, several key observations were made. Firstly, significant fluorescence signals were observed when the Cdc48 and full-length PUX10 fusions were co-expressed, indicating that the two proteins interact physically. Secondly, these BiFC signals were localized to the chloroplast envelope membrane, supporting the view that PUX10 mediates the relocalization of Cdc48 to the chloroplast surface. Lastly, the detected interaction depended on

the UBX domain of PUX10, since the BiFC signals were significantly reduced when ΔUBX was employed instead of the intact PUX10 protein (Figure 2.8 B and C).

To corroborate the finding of the BiFC assay, co-immunoprecipitation (co-IP) experiments were performed. co-IP is a popular and robust technique to investigate physiological interactions between proteins *in vivo* by using antibodies against a target protein to indirectly capture proteins that are bound to the target protein (Lin & Lai, 2017). To validate the interaction between PUX10 and Cdc48, I used a construct encoding HA epitope-tagged Cdc48 (Cdc48-HA), co-transfected into protoplasts with another construct encoding YFP fused to either full-length PUX10 or PUX10 lacking UBX domain (PUX10-YFP or ΔUBX-YFP) sequence. Here, PUX10-YFP and ΔUBX-YFP were used as the bait proteins immunoprecipitated with anti-YFP beads. As expected, the results clearly indicated physical interaction between full-length PUX10 and Cdc48. Meanwhile, the interaction with Cdc48 was significantly disrupted when ΔUBX was analysed, which is highly consistent with the observations from the BiFC assays (Figure 2.8 D).

Taken together, these results demonstrated that PUX10 is capable of binding Cdc48 to recruit it to the chloroplast envelope membrane through its UBX domain.

2.3.6 PUX10 interacts with ubiquitin via its UBA domain

Excluding the four pseudogenes (PUX6, PUX14, PUX15 and PUX16), among the 12 functional PUX proteins only half possess an N-terminal UBA domain, and PUX10 is one of them. The UBA domain is among the most common ubiquitin-binding domains, and it non-covalently interacts with ubiquitin that is covalently linked to other proteins through ubiquitination. The UBA domain has a common sequence motif of approximately 45 amino acid residues (Husnjak & Dikic, 2012). To assess the interaction between PUX10 and ubiquitin, co-IP assays were carried out. Constructs encoding FLAG epitope-tagged ubiquitin (FLAG-Ub) and YFP-tagged PUX10 or PUX10 lacking UBA domain (PUX10-YFP or ΔUBA-YFP) were co-transfected into protoplasts. As an experimental control, I also transfected protoplasts solely with FLAG-Ub. Anti-GFP beads were used to pull down YFP fusion proteins, and the samples were probed with

anti-FLAG antibody to detect ubiquitin. Singly expressed FLAG-Ub showed no signals in the precipitated samples, indicating specificity. However, a strong interaction was detected between full-length PUX10 and ubiquitin, and such an interaction was abrogated when PUX10 lacking UBA domain was used in the assay (Figure 2.9). Ubiquitin has seven lysine residues so that it can itself be ubiquitinated to form a polyubiquitin chain, and so the smearing detected here after immunoblotting was indicative of polyubiquitination events.

2.4 Discussion

Studies from different research groups have demonstrated the involvement of PUX proteins in recruiting Cdc48 to specific subcellular locales, or in regulating the activity of Cdc48 in *Arabidopsis thaliana* (Deruyffelaere et al., 2018; Gallois et al., 2013; Huang et al., 2020; Kretzschmar et al., 2018; Marshall et al., 2019; Park et al., 2007; Rancour et al., 2004). Among the characterized PUX proteins, PUX10 was recently identified as functioning as an LD-localized Cdc48 adaptor protein that regulates the degradation of LD proteins during seed germination. Intriguingly, the localization of PUX10 was swiftly changed from LDs to chloroplasts during seed maturation, suggesting that PUX10 delivers multifunctional roles in a phase-specific manner during plant development (Deruyffelaere et al., 2018).

This chapter, and the main strand of my major DPhil project, focused on the elucidation of PUX protein action in chloroplasts. To begin this study, I carried out a general subcellular localization screening of all 12 functional PUX proteins for chloroplast association using a protoplast transient expression system. As a result, the PUX10 protein was found to be the only PUX protein specifically associated with chloroplasts. Additionally, the analysis of different stable transgenic lines yielded similar results. This distinct association of PUX10 with chloroplasts provided the foundation for this project (Figure 2.1 and 2.2).

A highly hydrophobic transmembrane region (residues 107-132) within the central region of the PUX10 protein was predicted via various software (Figure 2.4 A). The alkaline extraction assay

and the transient expression of a truncated protein applied here demonstrated that, indeed, PUX10 is not a peripheral membrane protein but an integral chloroplast membrane protein, and this hydrophobic region is essential for the targeting of PUX10 to chloroplasts (Figure 2.4 B-C and Figure 2.5 A). PUX10 was recently found to be anchored to the membrane of LDs via the hydrophobic region in *Arabidopsis*. LDs are special organelles consisting of a phospholipid membrane monolayer surrounding a neutral lipids core, mostly composed of triacylglycerols (TAGs) (Walther & Farese, 2012). Lipid droplets are predominantly found in seeds, are abundant in pollen grains and pollen tubes, and are present in other plant cells in small amounts (Chapman et al., 2012). Recent studies demonstrated that PUX10 is involved in the degradation of structural LD proteins, which was critical for the post-germinative mobilization of neutral lipids during seed and pollen grain germination (Deruyffelaere et al., 2018; Kretzschmar et al., 2018).

Interestingly, PUX10 was shown to relocalize to chloroplasts soon after seed embryogenesis (Deruyffelaere et al., 2018), though whether such a relocalization event was accomplished via endomembrane system after germination, or de novo synthesis remain unknown. My studies showed that PUX10 is predominantly localized to chloroplasts in *Arabidopsis* leaves, though a minor association with the ER was also observed (Figure 2.3). Such partitioning between organelles was observed for the homologues of PUX10 in yeast and mammals, Ubx2 and FAS-Associated Factor 2 (FAF2, also known as Ubxd8), respectively. Ubx2 was first characterized to be a transmembrane protein localized to the ER and involved in the targeted clearance of aberrant and misfolded proteins in ERAD (Schuberth & Buchberger, 2005). Later studies further demonstrated that Ubx2 is redistributed to LDs next to the ER at certain growth phases and plays an important role in maintaining LD homeostasis (Wang & Lee, 2012). Intriguingly, the function of Ubx2 was recently expanded to mitochondria where it recruited Cdc48 to TOM (translocase of the outer mitochondrial membrane) complex for removal of clogged precursor proteins from the TOM channel (Martensson et al., 2019). Thus, Ubx2 was shown to be a very dynamic protein, and the employment of Ubx2 in multiple subcellular compartments for quality

control purposes suggested that such protein-processing pathways may require coregulation. The FAF2 protein, a close homologue of Ubx2 in mammals, is similarly involved in regulation of protein degradation in multiple compartments (the ER, LDs, and mitochondria), implying a functional conservation of this property (Mueller et al., 2008; Wang & Lee, 2012; Zheng et al., 2022). Although PUX10 did not localize to mitochondria, its association with LDs, ER, and chloroplasts – an organelle specific to photosynthetic organisms - further supported the notion that this multilocation property is conserved for this group of proteins (Figure 2.2 and 2.3). Given the lack of evidence for PUX10 participating in ER- associated protein quality control, further investigation will be needed in this regard.

Chloroplast envelope membranes act as barriers and scaffolds between the stroma and cytoplasm, which is believed to have important functions during chloroplast biogenesis. Consequently, proteins within chloroplast envelope membranes must adopt appropriate orientations to communicate with their respective interacting partners. To understand the cellular function of PUX10, it was therefore crucial to know how the protein is organized with respect to the membrane in which it resides. Here a 'dual protease' protection assay using thermolysin and trypsin was applied, to address the membrane topology of PUX10. The accessibility of both UBA and UBX domains to thermolysin indicated the cytosolic orientation of both domains (Figure 2.5 B to D). This assay provided direct evidence for the proposed membrane topology of PUX10, which was the foundation for the following functional analysis of PUX10 in *Arabidopsis*.

In agreement with the notion that it is a conserved Cdc48 cofactor, the PUX10 protein showed high efficiency in recruiting cytosolic Cdc48 to the chloroplast envelope (Figure 2.7 B), and the UBX domain of PUX10 was clearly essential for the full delivery of such subcellular location of Cdc48 (Figure 2.8). However, a weak association of Cdc48 to PUX10 and chloroplasts was still observed when a truncated PUX10 protein lacking the UBX domain was co-expressed with Cdc48 (Figure 2.8). A possible explanation for this is that the truncated PUX10 formed homodimers with native PUX10 through its UBA domains. Such dimerization was

demonstrated in previous studies in yeast (Sasaki et al., 2005). To address this hypothesis, it would have been interesting to use the *pux10* null mutant as a background for such assays.

Of 12 functional PUX proteins, six contain a UBA domain and are therefore termed UBA–UBX proteins; these are: PUX5, PUX7, PUX8, PUX9, PUX13 and PUX10. Such UBA–UBX proteins function in post-ubiquitination steps by tethering both the ubiquitinated substrate, via the UBA domain, and Cdc48, via the UBX domain, to promote the processing of the ubiquitinated substrate by Cdc48 and its subsequent degradation. Here, co-IP assays indicated that PUX10 can indeed interact with ubiquitin via its UBA domain (Figure 2.9), suggesting that it operates in a way that is typical for such proteins. What might the roles of the other PUX proteins be? While UBA domains are commonly found in proteins involved in ubiquitin-proteasome pathways, UBA domains also exist in proteins not ostensibly linked to any ubiquitination pathway (Bertolaet et al., 2001). Moreover, UBA domains have varying affinities for the distinct types of ubiquitin chain linkages that exist (Raasi et al., 2005). Additionally, in yeast and mammals, dimerization was found to occur via the UBA protein, including between different members of the UBA protein family (Bertolaet et al., 2001; Sasaki et al., 2005). Such diverse properties of UBA domains may contribute to different functions and interactions amongst the PUX proteins. Thus, the UBA domains in PUX10 and its homologues, and in the other PUX proteins, likely play an important role in defining their roles in protein homeostasis in various subcellular compartments.

Arabidopsis pux10 null mutants displayed no obvious phenotypic differences from wild-type plants (Figure 2.6). This was unsurprising since neither *sp1* nor *sp2* mutants display any obvious visible defects under normal conditions (Ling et al., 2019; Ling et al., 2012). Moreover, the single homozygous mutants of some characterized *PUX* genes were fertile and phenotypically indistinguishable from the wild type under normal growth conditions (Gallois et al., 2013; Marshall et al., 2019; Rancour et al., 2004), implying the possibility of functional redundancy. An example of such redundancy is provided by PUX7, PUX8, PUX9 and PUX13, which physically

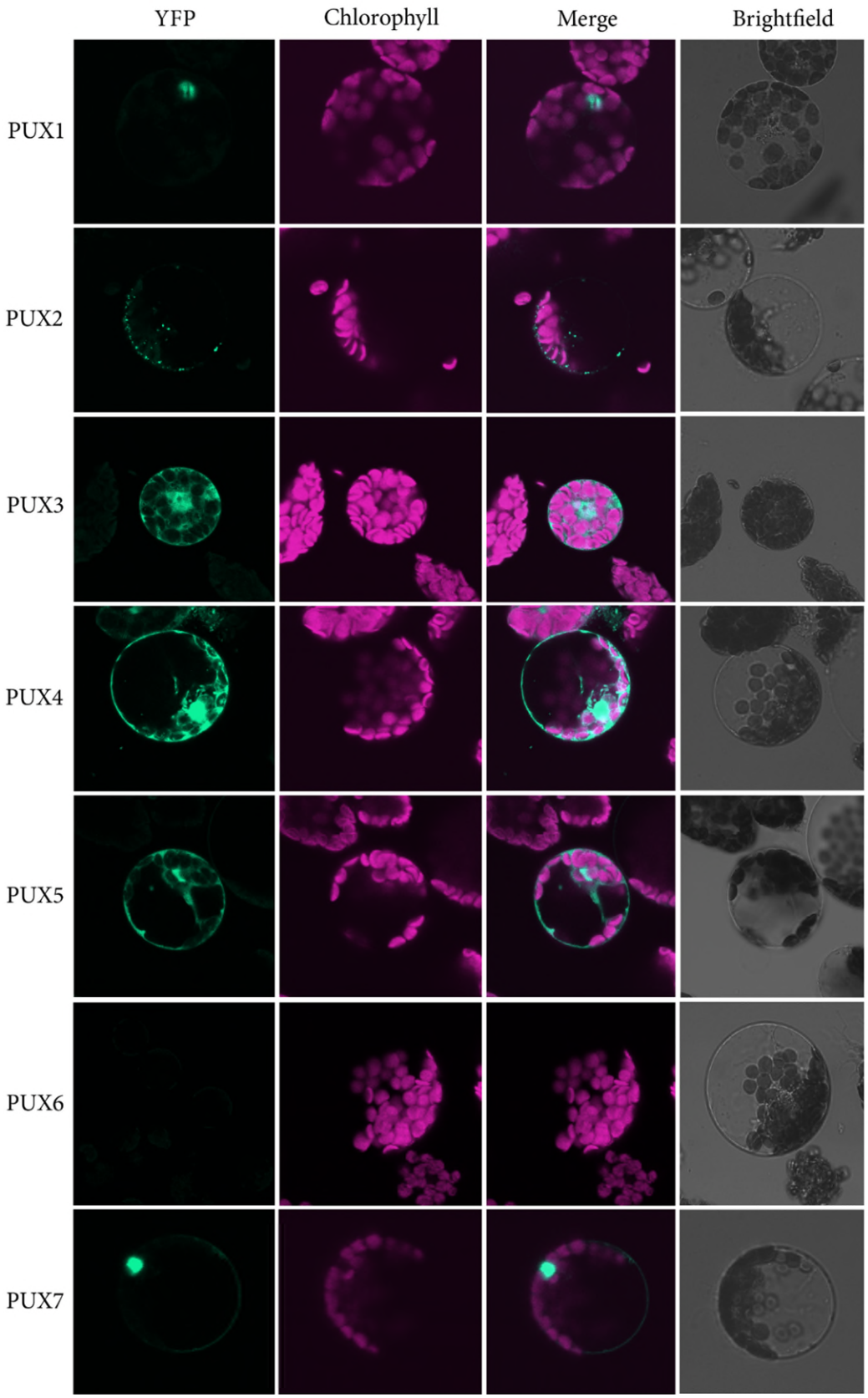
interact with the ubiquitin-fold protein ATG8 through their ubiquitin-interacting motif (UIM)-like sequences to recruit non-functional Cdc48 for autophagic clearance. The quadruple-mutant genotype lacking all four PUX proteins more effectively blocked the turnover of Cdc48 than any triple-mutant combination (Marshall et al., 2019). Similar combined action was also observed in the PUX3/4/5 subgroup in regulating inner nuclear membrane (INM) protein degradation (Huang et al., 2020). Moreover, in LD-associated protein degradation (LDAD), the *pux10* mutation considerably reduced but did not completely abrogate the degradation of structural LD proteins, indicating that PUX10 plays an important but not indispensable role in the LDAD pathway (Deruyffelaere et al., 2018; Kretzschmar et al., 2018). Such functional redundancy was also observed for Ubx2, the homologue of PUX10 in yeast (Schuberth et al., 2004).

Taken together, the results described in this chapter clearly identify PUX10, a plant UBX domain-containing protein, as a chloroplast cofactor for Cdc48, one of the key components of the CHLORAD system. The characteristic protein domain structure of PUX10 define its role as a chloroplast membrane-anchored scaffold protein for recruiting Cdc48 to ubiquitinated substrates of the CHLORAD pathway. It is hence reasonable to propose that PUX10 is a new component of the CHLORAD apparatus. As the CHLORAD pathway directly regulates the turnover of TOC proteins, detailed investigation of the physical interactions between PUX10 and the TOC complex, as well as other CHLORAD components, will be presented in the next chapter. Additionally, a series of genetic experiments designed to unveil the functional link between PUX10 and chloroplast protein import will be described.

2.5 Tables and figures

Table 2.1. A list of known/predicted *PUX* genes in *Arabidopsis*

Protein name	Gene Name	Accession number	Reference/information
Plant UBX domain-containing protein 1	*PUX1*	At3g27310	(Park et al., 2007; Rancour et al., 2004)
Plant UBX domain-containing protein 2	*PUX2*	At2g01650	(Rancour et al., 2004)
Plant UBX domain-containing protein 3	*PUX3*	At4g22150	(Huang et al., 2020)
Plant UBX domain-containing protein 4	*PUX4*	At4g04210	(Huang et al., 2020)
Plant UBX domain-containing protein 5	*PUX5*	At4g15410	(Huang et al., 2020)
Plant UBX domain-containing protein 6	*PUX6*	At3g21660	Pseudogene
Plant UBX domain-containing protein 7	*PUX7*	At1g14570	(Gallois et al., 2013; Marshall et al., 2019)
Plant UBX domain-containing protein 8	*PUX8*	At4g11740	(Marshall et al., 2019)
Plant UBX domain-containing protein 9	*PUX9*	At4g00752	(Marshall et al., 2019)
Plant UBX domain-containing protein 10	*PUX10*	At4g10790	(Deruyffelaere et al., 2018; Kretzschmar et al., 2018)
Plant UBX domain-containing protein 11	*PUX11*	At2g43210	
Plant UBX domain-containing protein 12	*PUX12*	At3g23605	
Plant UBX domain-containing protein 13	*PUX13*	At4g23040	(Marshall et al., 2019)
Plant UBX domain-containing protein 14	*PUX14*	At4g14250	Pseudogene
Plant UBX domain-containing protein 15	*PUX15*	At1g59550	Pseudogene
Plant UBX domain-containing protein 16	*PUX16*	At4g14245	Pseudogene


YFP
Chlorophyll
Merge
Brightfield
PUX1
PUX2
PUX3
PUX4
PUX5
PUX6
PUX7

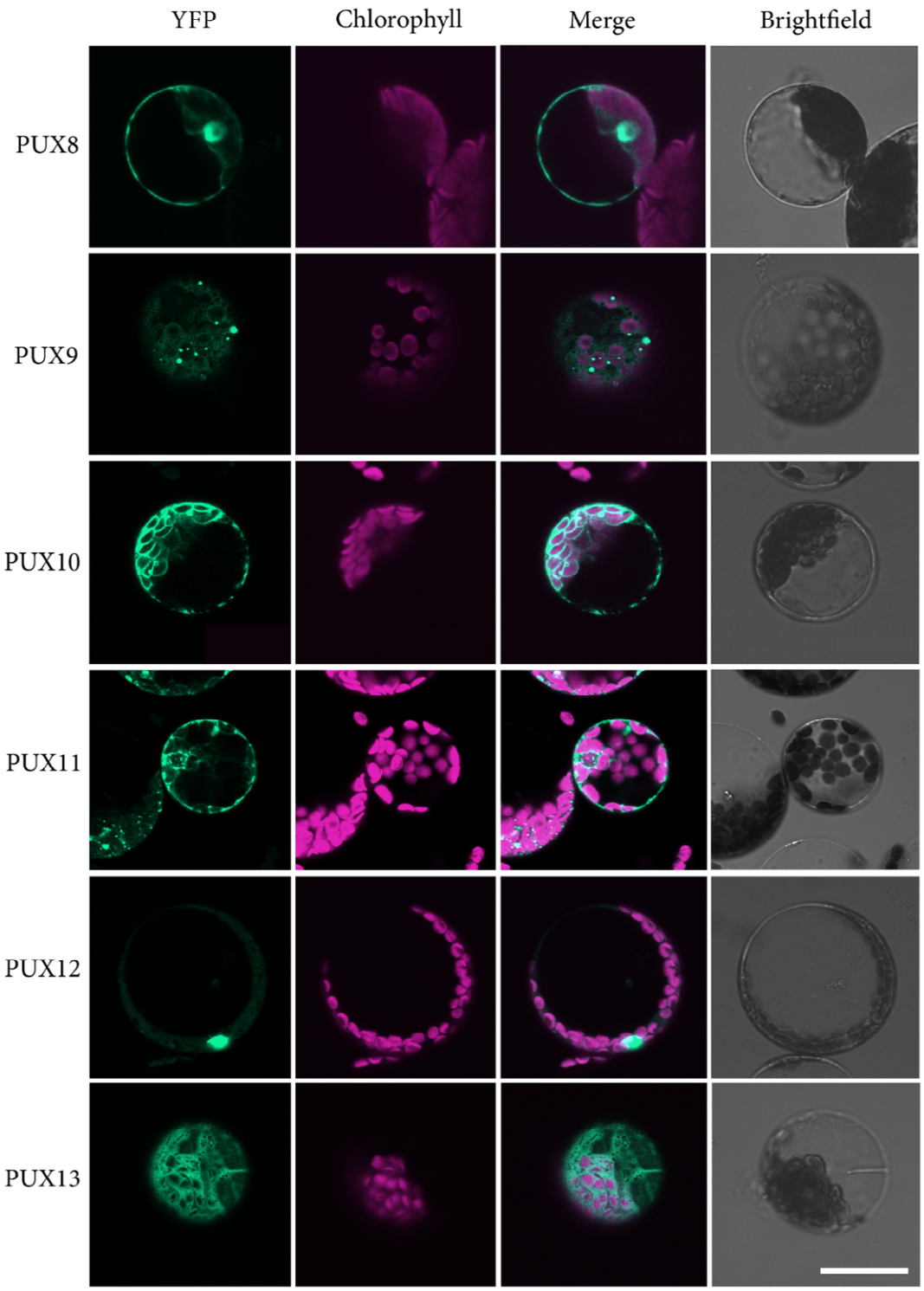


Figure 2.1. Subcellular localization analysis of *Arabidopsis* PUX proteins by confocal microscopy. *Arabidopsis* protoplasts transiently expressing the YFP-tagged PUX proteins under the control of cauliflower mosaic virus (CaMV) *35S* promoter were analysed by confocal

microscopy. Representative protoplasts are presented. In each case, YFP fluorescence, chlorophyll autofluorescence, merged YFP and chlorophyll fluorescence, and brightfield images are shown. Identical microscope settings were employed to record all the images. Bar = 20 μm.

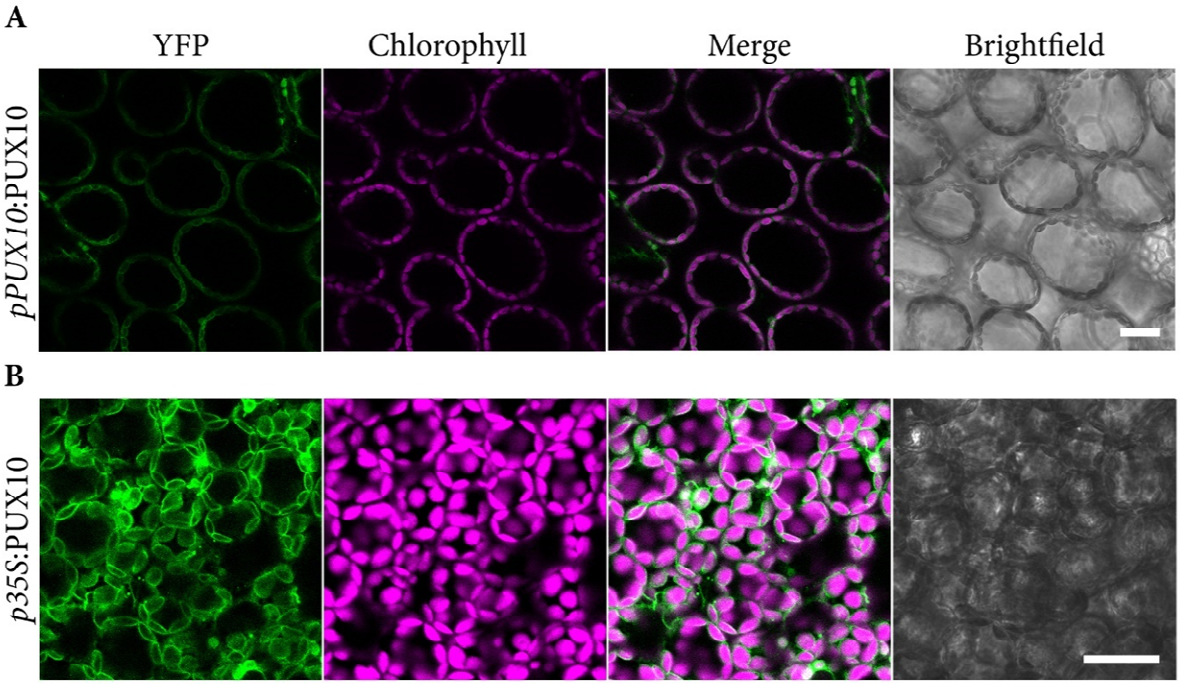


Figure 2.2. Localization of PUX10 in chloroplasts in transgenic plants. Constructs encoding PUX10-YFP driven by the native *PUX10* promoter (**A**) or the CaMV *35S* promoter (**B**) were used to stably transform *Arabidopsis* plants. Rosette leaves taken from 28-day-old T1 plants were mounted in perfluorodecalin and palisade parenchyma cells were visualized by confocal microscopy. In each case, YFP fluorescence, chlorophyll autofluorescence, merged YFP and chlorophyll fluorescence, and brightfield images are shown. Similar localization of the YFP signals was observed in 5 to 10 independent T1 transgenic plants. Identical microscope settings other than magnification were employed to record all the images. Bars = 20 μm.

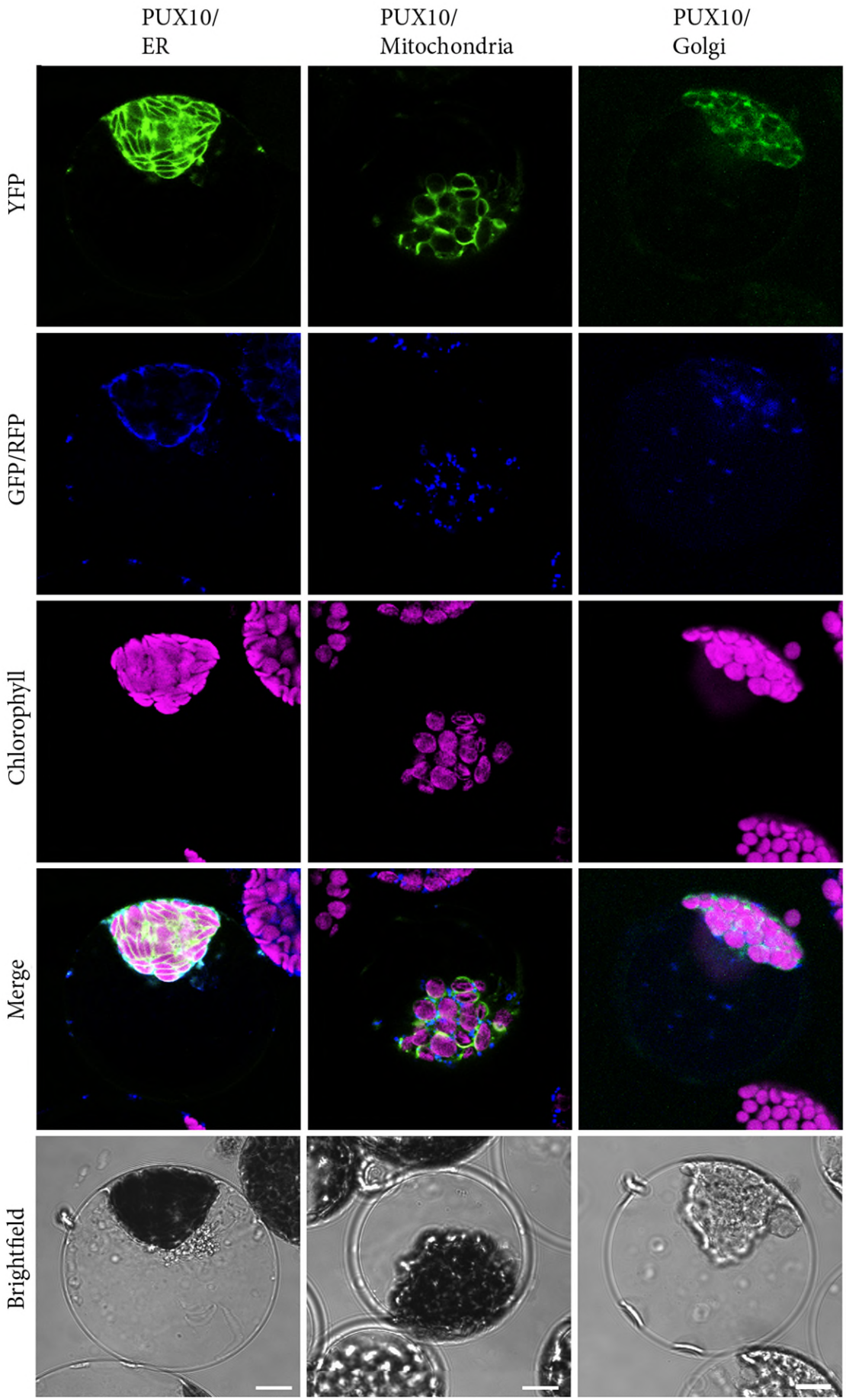

PUX10/
ER
PUX10/
Mitochondria
PUX10/
Golgi
YFP
GFP/RFP
Chlorophyll
Merge
Brightfield

Figure 2.3. The potential localization of PUX10 in other subcellular compartments. The PUX10-YFP construct from Figure 2.1 (driven by the *35S* promoter) was used to transform protoplasts isolated from *Arabidopsis* lines carrying genetically-encoded organelle markers for the ER, mitochondria and Golgi, for transient expression analysis. The fluorescence signals were visualized by confocal microscopy. Both the ER and mitochondria were marked by GFP, while Golgi was marked by RFP. In each case, YFP and GFP/RFP fluorescence, chlorophyll autofluorescence, merged YFP/GFP/RFP and chlorophyll fluorescence, and bright-field images are shown. Similar localization of the fluorescence signals was observed in 5 to 8 independent protoplasts. Identical microscope settings were employed to record all the images. Bar = 10 μm.

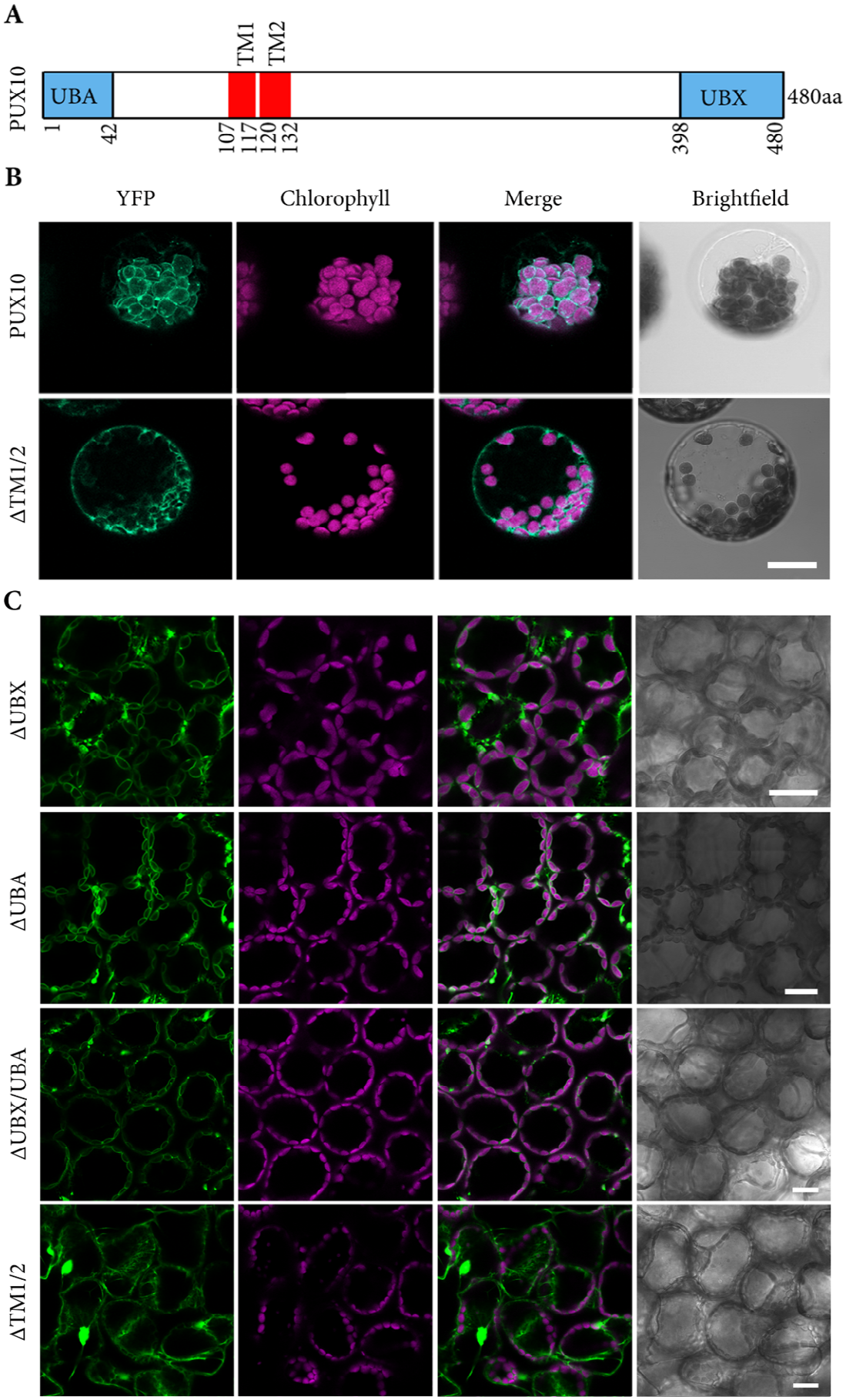

A
PUX10
UBA
TM1
TM2
UBX
480aa
1
42
107
117
120
132
398
480
B
YFP
Chlorophyll
Merge
Brightfield
PUX10
ΔTM1/2
C
ΔUBX
ΔUBA
ΔUBX/UBA
ΔTM1/2

Figure 2.4. The hydrophobic region of PUX10 is essential for PUX10 localization to chloroplasts. (**A**) A protein domain map for PUX10 showing its UBA, potential transmembrane (TM), and UBX domains. (**B**) *Arabidopsis* protoplasts transiently expressed different YFP-tagged PUX10 variants (under the control of the *35S* promoter) were analysed by confocal microscopy. Representative protoplasts are presented. In each case, YFP fluorescence, chlorophyll autofluorescence, merged YFP and chlorophyll fluorescence, and brightfield images are shown. Identical microscope settings were employed to record all the images. Localization of PUX10-YFP to the chloroplast envelope (top) depended on the transmembrane domains, as revealed by a double TM deletion mutant (bottom). Bar = 20 μm. (**C**) Constructs encoding different variants of PUX10 lacking the indicated domains (under the control of the *35S* promoter) were used to stably transform *Arabidopsis* plants. Rosetta leaves taken from 28-day-old T1 plants were mounted in perfluorodecalin and mesophyll cells were visualized by confocal microscopy. In each case, YFP fluorescence, chlorophyll autofluorescence, merged YFP and chlorophyll fluorescence, and bright-field images are shown. Similar localization of the YFP signals was observed in 5 to 10 independent T1 transgenic plants. ΔUBA: UBA domain deleted; ΔUBX: UBX domain deleted; ΔUBX/UBA: both UBX and UBA deleted; ΔTM1/2: both TMs deleted. Identical microscope settings other than magnification were employed to record all the images. Bars = 20 μm.

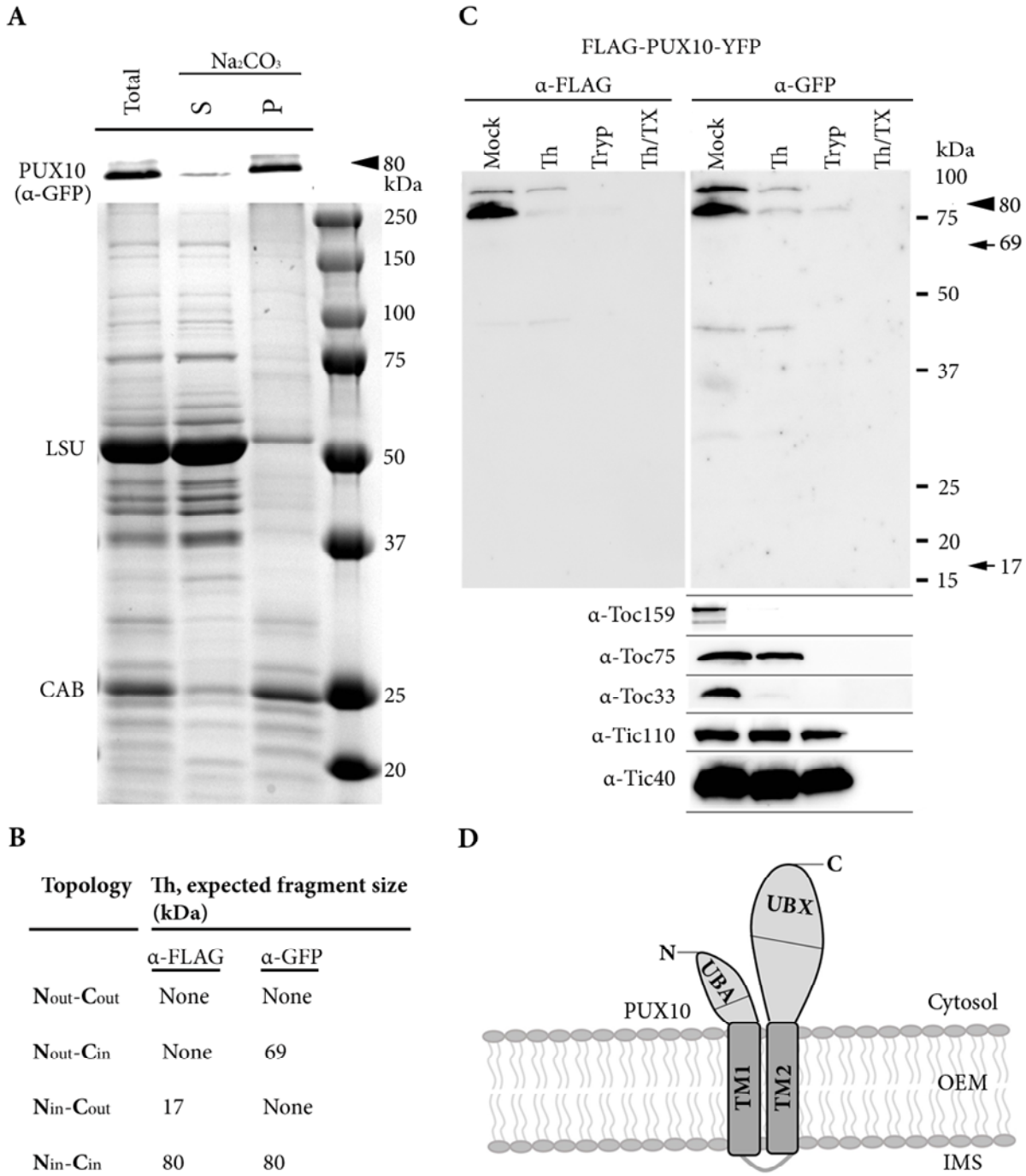


Figure 2.5. Topological analysis of the PUX10 protein. (A) Chloroplasts isolated from transgenic plants overexpressing PUX10-YFP were fractionated into membrane pellet (P) and soluble supernatant (S) fractions after high-pH (Na_2CO_3) washing. The samples were analysed by anti-GFP immunoblotting to detect the PUX10-YFP protein (top), and by Coomassie staining (bottom). Endogenous marker proteins (Rubisco large subunit, LSU; chlorophyll a/b binding

protein, CAB) partitioned as expected. The arrowhead indicates the size of full-length FLAG-PUX10-YFP fusion protein (80 kDa). Positions of molecular weight standards (size in kDa) are shown at right. (**B**) Four possible topologies of the PUX10 protein based on the number of TM domains predicted by different software. The expected size of fragment for each possible topology after the thermolysin treatment were presented. (**C**) The *PUX10* CDS was fused with sequences encoding an N-terminal FLAG tag and a C-terminal YFP tag, and cloned downstream of the *35S* promoter; the resulting *FLAG-PUX10-YFP* construct was used for stable *Arabidopsis* plant transformation. The topology of PUX10 was analysed by isolating chloroplasts from such transgenic plants and subjecting them to treatment using thermolysin (Th), trypsin (Tryp), thermolysin plus Triton X-100 (Th/TX), or buffer lacking protease (Mock). Immunoblotting using the antibodies against the FLAG and YFP tags was conducted to assess the protease accessibility of the protein termini. The arrowhead indicates the size of full-length FLAG-PUX10-YFP fusion protein (80 kDa); the arrows indicate the sizes of predicted fragments after protease treatments if alternative topologies of PUX10 are present as shown in (**B**). Immunoblot analysis of five endogenous markers proteins (TOC and TIC components) confirmed the efficiency of the protease treatments. Positions of molecular weight standards (size in kDa) are shown at right. Three biological replicates were conducted. α-FLAG, anti-FLAG; α-GFP, anti-GFP. **(D)** Schematic drawing showing the topology of PUX10 according to the protease treatment results. UBA, ubiquitin-associated; UBX, ubiquitin regulatory X; OEM, outer envelope membrane; IMS, intermembrane space.

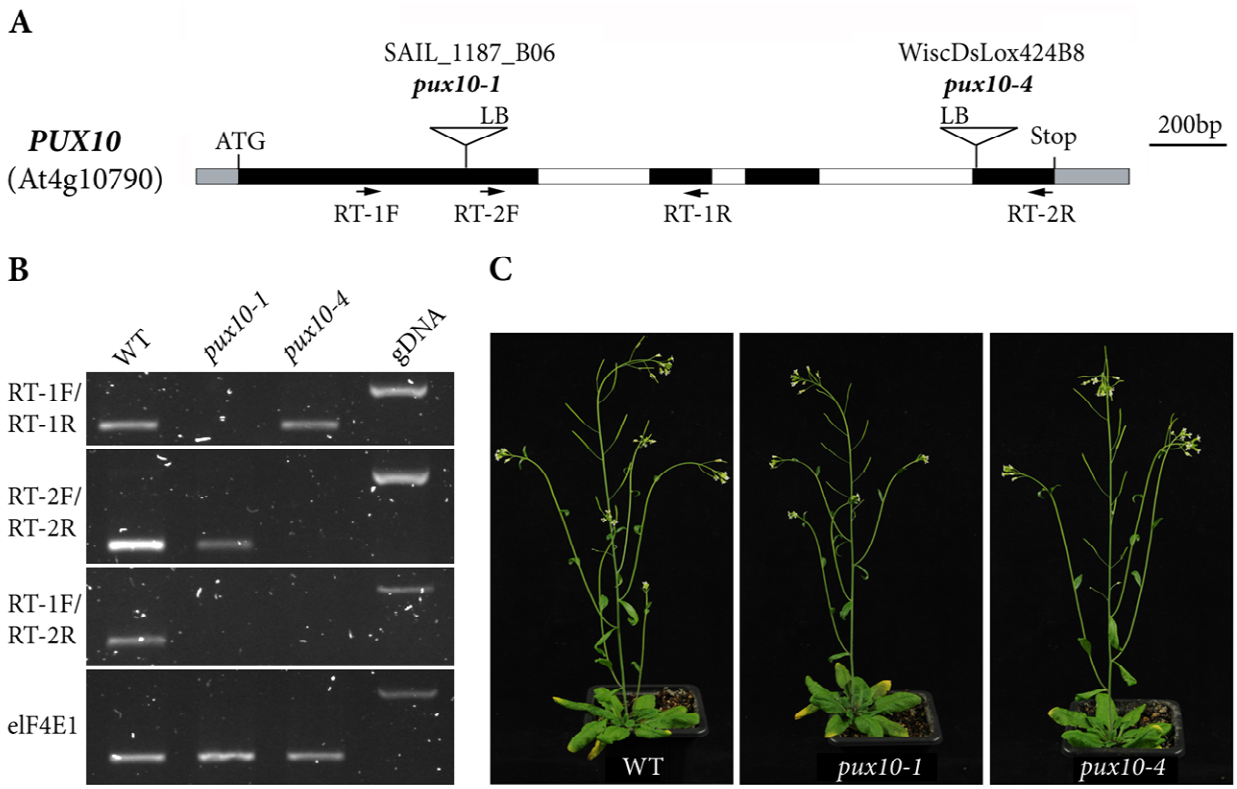


Figure 2.6. Molecular characterization of two *pux10* T-DNA insertion mutants. (A) Schematic representation of the *Arabidopsis PUX10* genomic locus (At4g10790), annotated with the positions of the *pux10* T-DNA insertion mutations. The positions of PCR primers used in (**B**) are also indicated, with arrows. Black boxes = exons; interconnecting white boxes = introns; grey boxes = untranslated regions; LB = left border sequences of the SAIL and Wisconsin T-DNA insertions. ATG = translation initiation codon; Stop = translation termination codon. (**B**) Analysis of *PUX10* mRNA expression by RT-PCR. The accumulation of *PUX10* mRNA in the *pux10* mutants and a corresponding wild-type control was analysed by RT-PCR analysis of 3-week-old seedlings using the indicated primers (primer positions are marked in (**A**), and their sequences are listed in Table 6.1). The *eIF4E1* gene was similarly analysed as a control for sample normalization. Wild-type genomic DNA (gDNA) was analysed as a positive control, and to rule out possible DNA contamination of the samples. (**C**) Phenotypic analysis of wild-type, *pux10-1* and *pux10-4 Arabidopsis* plants. The plants were grown under standard growth conditions on

soil for 6 weeks before photography. Representative individuals are shown. Similar camera settings were employed to record all the images; all images are at the same magnification.

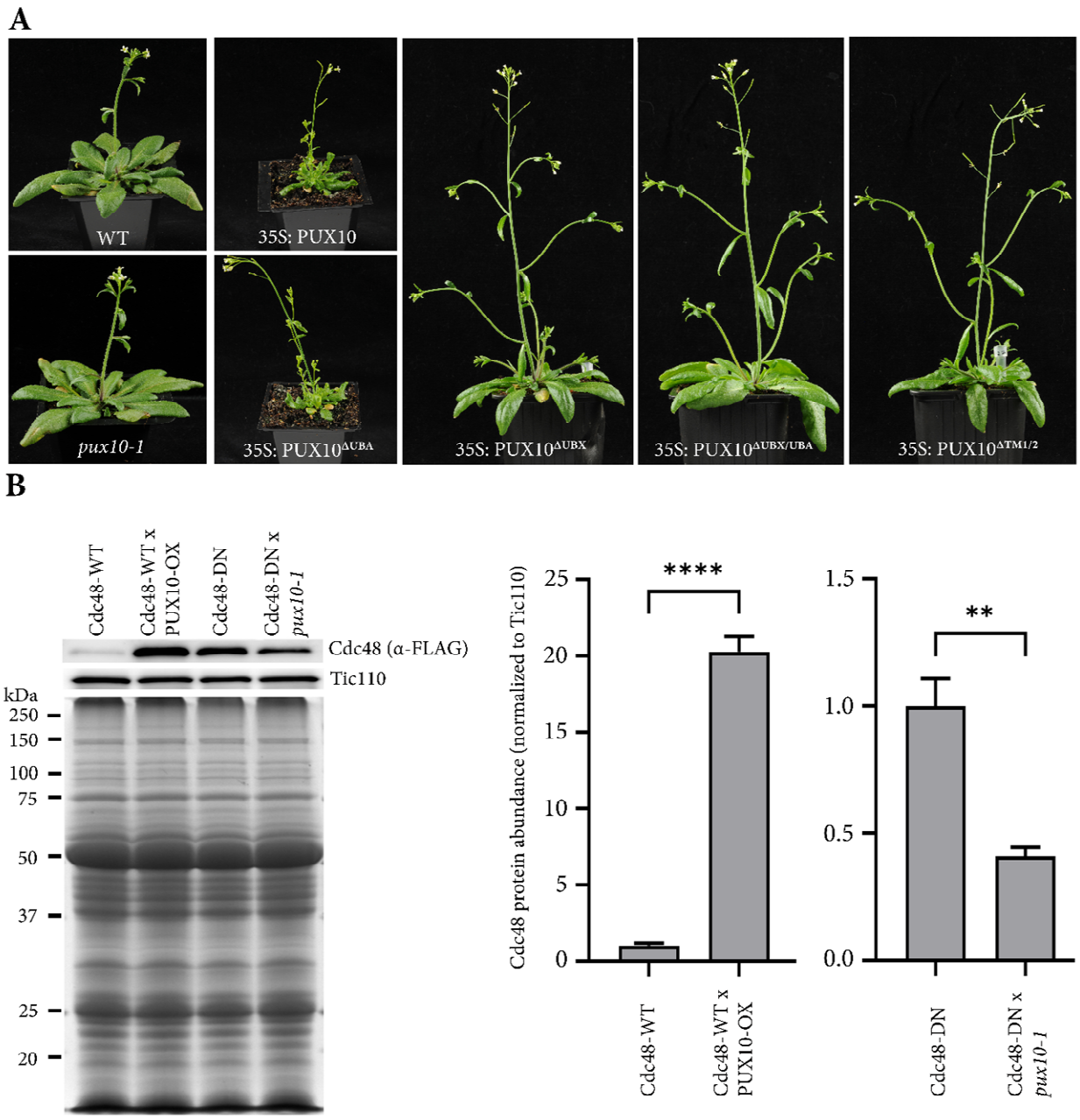


Figure 2.7. The abundance of PUX10 has a significant influence on the subcellular localization of Cdc48. (**A**) Phenotypic analysis of wild-type, *pux10-1* and transgenic *Arabidopsis* plants, the latter overexpressing various forms of the PUX10 protein under the control of the *35S* promoter. The WT and plants were grown under standard conditions before photography, and representative individuals are shown. Similar camera settings were employed to record all the images; all images are at the same magnification. The both *pux10* alleles were phenotypically identical, and so only *pux10-1* is presented here as a representative allele. The WT and *pux10-1*

plants were 5 weeks old, and all the overexpression/35S lines were 6 weeks old. Abbreviations: ΔUBA: PUX10 UBA domain deleted; ΔUBX: PUX10 UBX domain deleted; ΔUBX/UBA: PUX10 both UBX and UBA deleted; ΔTM1/2: PUX10 both TMs deleted. (**B**) The extent of localization of Cdc48 to chloroplasts is associated with the expression level of *PUX10*. Chloroplats isolated from plants expressing different FLAG-tagged Cdc48 variants (eithe WT or DN) in different genetic backgrounds (either PUX10-OX or *pux10-1*) were analysed by immunoblotting. Anti-FLAG antibody was used to detect Cdc48, while Tic110 was analysed as an endogenous loading control. An equivalent Coomassie-stained gel was prepared to show equal loading of the samples. Positions of molecular weight standards (size in kDa) are shown at left. Cdc48-DN showed significantly enhanced chloroplast association relative to Cdc48-WT, which showed weak chloroplast association, consistent with published data (Ling et al., 2019). The abundance of chloroplast-associated Cdc48 in the PUX10-OX (left) or *pux10-1* (right) backgrounds was assessed by quantifying the corresponding bands. Bands of interest from three independent experiments similar to the one shown here were quantified. Values shown are means (n=3) with error bars indicating SEM. Asterisks above the columns indicate the significance of differences (Student's *t*-test: $^{****}P < 0.0001$; $^{**}P < 0.005$). Tic110 was used as a normalization control for the quantification. α-FLAG, anti-FLAG.

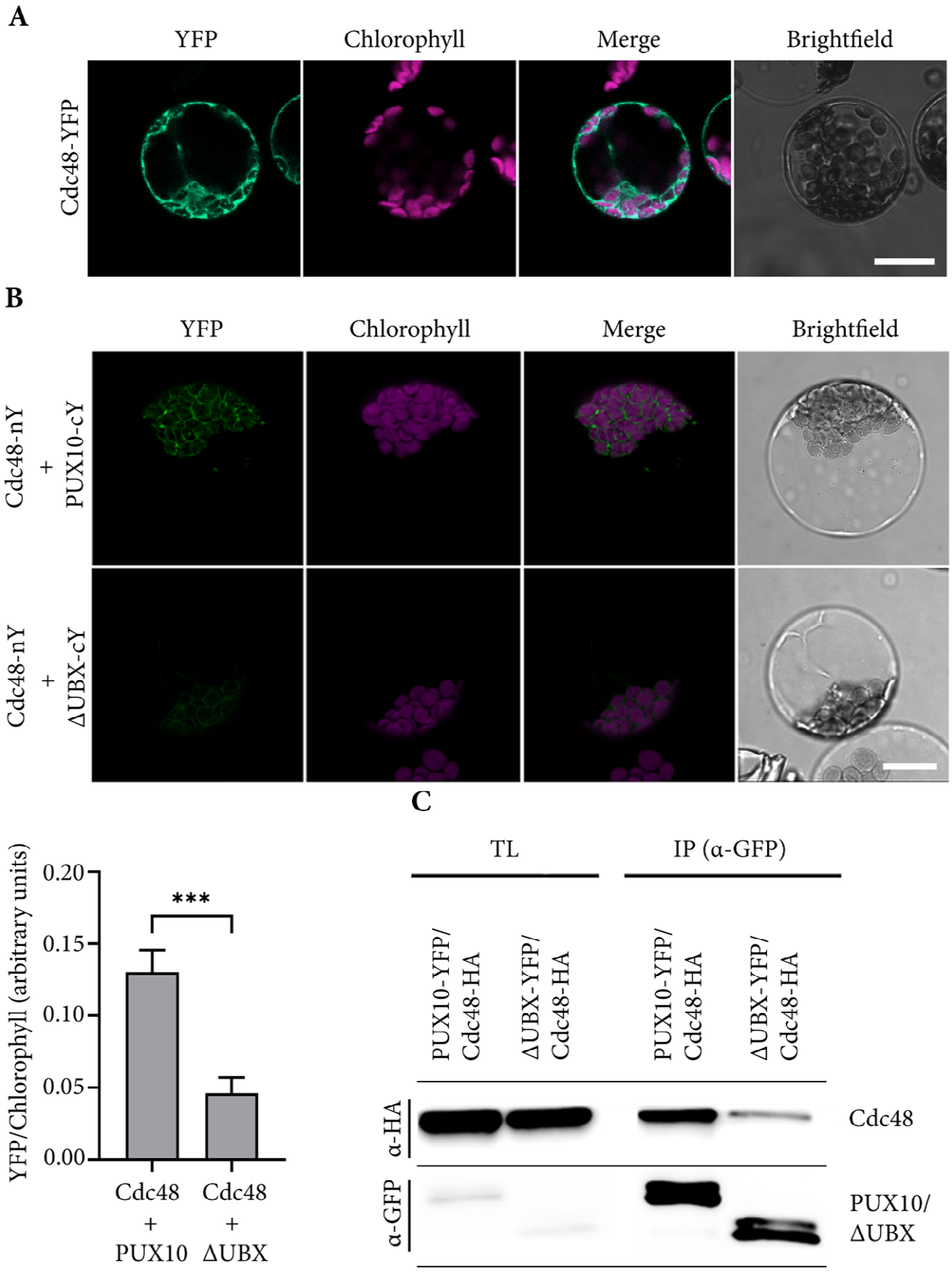

A
YFP
Chlorophyll
Merge
Brightfield
Cdc48-YFP
B
YFP
Chlorophyll
Merge
Brightfield
Cdc48-nY + PUX10-cY
Cdc48-nY + ΔUBX-cY
C
YFP/Chlorophyll (arbitrary units)
0.20
0.15
0.10
0.05
0.00
***
Cdc48 + PUX10
Cdc48 + ΔUBX
TL
IP (α-GFP)
PUX10-YFP/ Cdc48-HA
ΔUBX-YFP/ Cdc48-HA
PUX10-YFP/ Cdc48-HA
ΔUBX-YFP/ Cdc48-HA
α-HA
α-GFP
Cdc48
PUX10/ ΔUBX

Figure 2.8. PUX10 interacts with Cdc48 at the chloroplast surface via its UBX domain. (**A**) *Arabidopsis* protoplasts transiently expressing a Cdc48-YFP construct were analysed by confocal microscopy. A representative protoplast is presented. YFP fluorescence, chlorophyll autofluorescence, merged YFP and chlorophyll fluorescence, and bright-field images are shown. Identical microscope settings were employed to record all the images. Bar = 20 μm. **(B)** BiFC analysis of the interaction between Cdc48 and PUX10 was performed by studying *Arabidopsis* protoplasts co-expressing the proteins fused to complementary N-terminal (nY) and C-terminal (cY) fragments of the YFP protein, respectively. The protoplasts were visualized by confocal microscopy, and the representative images show typical results for the combination of Cdc48-nY with either PUX10-cY (top), or ΔUBX-cY (bottom). The exposure times and gain settings were identical in all images. For each protoplast, YFP fluorescence, chlorophyll autofluorescence, merged YFP and chlorophyll fluorescence, and bright-field images are shown. Bar = 20 μm. Relative intensities of the BiFC signals were quantified and normalized with respect to chlorophyll autofluorescence. Values shown are means (n=10) with error bars indicating SEM. Asterisks above the columns indicate the significance of differences (Student's *t*-test: $^{***}P < 0.0001$). (**C**) *Arabidopsis* protoplasts transiently co-expressing YFP-tagged PUX10 or ΔUBX (as shown in **B**), with HA-tagged Cdc48 were solubilised and subjected to anti-GFP Co-IP analysis. Anti-YFP immunoblot analysis was used to verify the enrichment of the PUX10-YFP or ΔUBX-YFP proteins, while anti-HA analysis was used to detect co-purification of Cdc48. Two biological replicates were conducted. Abbreviations: TL, total lysate; IP, immunoprecipitation; α-HA, anti-HA; α-GFP, anti-GFP.

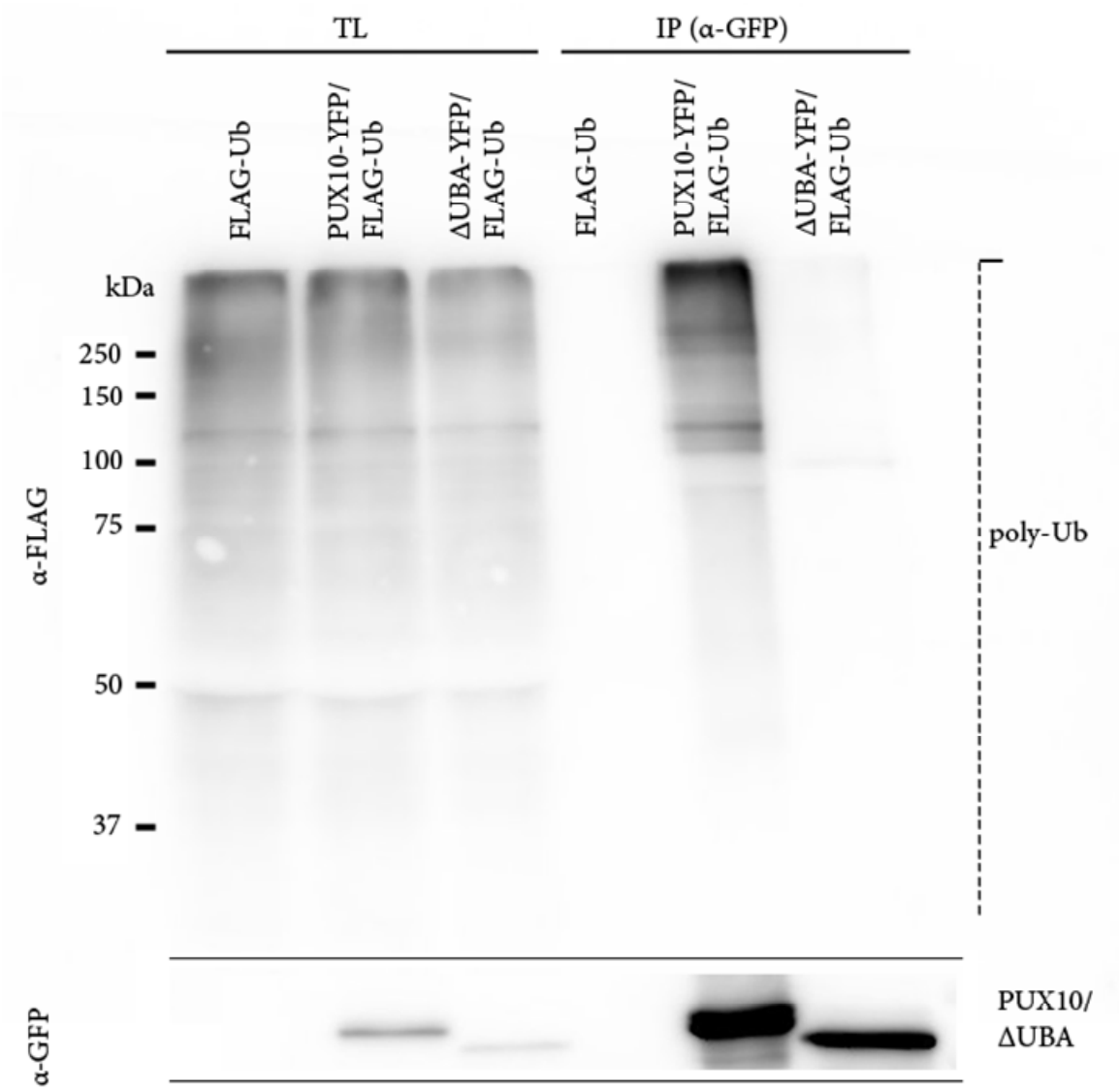


Figure 2.9. PUX10 interacts with ubiquitin via its UBA domain. *Arabidopsis* protoplasts transiently expressing FLAG-tagged ubiquitin (FLAG-Ub) solely, or co-expressing FLAG-Ub with YFP-tagged PUX10 or ΔUBA (PUX10 UBA domain deleted), were solubilized and subjected to Co-IP analysis. Anti-GFP immunoblot analysis was used to verify the enrichment of the PUX10-YFP or ΔUBA-YFP proteins, while anti-FLAG analysis was used to detect co-purification of (poly)ubiquitin. Positions of molecular weight standards (size in kDa) are shown at left. Two biological replicates were conducted. Abbreviations: TL, total lysate; IP, immunoprecipitation; poly-Ub, polyubiquitin; α-FLAG, anti-FLAG; α-GFP, anti-GFP.

Chapter 3

Results 2

Functional analysis of PUX10 in chloroplast associated protein degradation

3 Functional analysis of the PUX10 in chloroplast associated protein degradation

3.1 Abstract

The three key components of the CHLORAD pathway, SP1, SP2 and Cdc48, cooperatively targets the TOC apparatus for proteolysis in *Arabidopsis*. The experiments described in the previous chapter demonstrated that PUX10, a chloroplast outer envelope membrane anchored protein, effectively recruits the cytosolic Cdc48 to the chloroplast surface via its UBX domain, and also interacts with ubiquitin via its UBA domain. To further investigate the functional link between PUX10 and chloroplast protein import, a series of genetic, biochemical, and physiological experiments were carried out. This provided information on whether PUX10 physically interacts with SP1, SP2 and TOC proteins, and whether PUX10 regulates the turnover of the TOC machinery. Protein-protein interaction assays, based on BiFC and co-IP, indicated that PUX10 can physically interact with SP1 and SP2 and TOC proteins. Moreover, the *pux10-1* mutation was found to moderately suppress the *ppi1* phenotype in *Arabidopsis* plants, since *pux10-1 ppi1* double-mutant plants were larger and greener than *ppi1*. Such phenotypic suppression was linked to the substantial recovery of TOC protein levels in *pux10-1 ppi1* plants relative to *ppi1*. As demonstrated in previous studies, the *sp1* mutation greatly suppresses the *ppi1* phenotype, whereas, conversely, the overexpression of *SP1* (SP1-OX) accentuates the phenotype of *ppi1* mutants producing smaller and paler leaves with significantly reduced abundance of TOC proteins. Intriguingly, when the *pux10-1* mutant was crossed with SP1-OX *ppi1*, the resulting *pux10-1* SP1-OX *ppi1* plants appeared larger and greener than the SP1-OX *ppi1* progenitor plants; and this effect of the *pux10* mutation was linked to obvious increases in leaf chlorophyll content and TOC protein abundance. Furthermore, transmission electron microscopy analysis demonstrated that the *pux10-1* SP1-OX *ppi1* plants have improved chloroplast ultrastructural organization relative to SP1-OX *ppi1* plants, indicating that the

phenotypic suppression is linked to changes in the size and development of chloroplasts. Additionally, previous work showed that *SP1* overexpression accelerates the leaf senescence, while *sp1* mutations have an opposite effect. When *pux10-1* was crossed with the plants overexpressing *SP1*, the resulting *pux10-1* SP1-OX plants exhibited attenuated leaf senescence compared to SP1-OX plants, indicating that PUX10 is involved in this aspect of SP1 function. Taken together, these results support a model in which that PUX10 physically interacts with CHLORAD components and TOC proteins, recruiting Cdc48 to ubiquitinated TOC proteins to promote their rapid degradation; and in which PUX10 is required for SP1-dependent physiological processes. Nonetheless, there seems to be a degree of functional redundancy between PUX10 and unidentified proteins in such processes, as they were not completely blocked upon loss of PUX10.

3.2 Introduction

The first characterized component of CHLORAD was the E3 ligase SP1. The identification and characterization of SP1 unveiled for the first time the ubiquitin-dependent post-translational regulation of the chloroplast protein import machinery. SP1 has two transmembrane domains, a C-terminal, cytosol-facing RING domain, and an intermembrane space domain connecting the two transmembrane domains (Ling et al., 2012). Unlike its counterparts in ERAD, SP1 is unable to form a retrotranslocation channel for the extraction of ubiquitinated substrate proteins into the cytosol because it lacks the necessary number of membrane spans; this leads to the requirement for SP2. The SP2 is a member of the Omp85 superfamily of β-barrel proteins, containing 16 predicted transmembrane β-strands, and is deeply embedded in chloroplast OEM; and it has been proved to act as a translocon for the retrotranslocation of ubiquitinated TOC proteins (Ling et al., 2019).

Analysis of *sp1* mutant and *SP1* overexpressor *Arabidopsis* plants showed that *SP1* expression levels correlate inversely with the abundance of TOC proteins; and this resulted in the phenotypic suppression or enhancement of the *ppi1* mutant, respectively. Furthermore, SP1 was

proved to play an important role in the reconfiguration of TOC machinery during certain developmental phases in which plastids convert from one form to another, via the facilitation of organellar proteome changes. For instance, concerning de-etiolation and leaf senescence, *sp1* mutant plants displayed delayed plastid transition processes, whereas *SP1* overexpressor plants displayed an acceleration of such processes (Ling et al., 2012).

In the previous chapter, protein-protein interaction experiments clearly demonstrated the physical interactions between PUX10 and Cdc48, as well as ubiquitin, and led to the conclusion that PUX10 can effectively recruit cytosolic Cdc48 to the surface of the chloroplast via its UBX domain. However, whether PUX10 functions in CHLORAD cannot yet be determined; and if so, what the nature of the function is and to what extent it is essential.

Here, given the functional links of Cdc48 with SP1, SP2 and TOC proteins, a series of genetic, biochemical and physiological experiments was carried out to investigate the interactions between PUX10 and CHLORAD and the TOC complex, and to investigate the role of PUX10 in the regulation of TOC protein degradation by CHLORAD. In particular, the involvement of PUX10 in the SP1-dependent regulation of TOC protein turnover was studied.

3.3 Results

3.3.1 Physical interactions of PUX10 with SP1 and SP2

Cdc48 was previously shown to form a complex with SP1 and SP2 at the surface of the chloroplast, enabling ubiquitin-dependent degradation of TOC proteins by the 26S proteasome in the cytosol (Ling et al., 2019). Therefore, here, the first series of experiments sought to determine whether PUX10 also physically associates with SP1 and SP2.

First, BiFC assays were employed to assess for physically interactions between PUX10 and SP1. To implement the BiFC assay, the full-length *PUX10* CDS was cloned into the vector pSAT4(A)-cEYFP-N1 which appends the C-terminal fragment of YFP, while sequences encoding SP1 or the negative control proteins, sensitive to freezing 2 (SFR2) and cyclin-dependent kinase A-1

(CDKA1), were cloned into the complementary vector pSAT4(A)-nEYFP-N1 which appends the N-terminal fragment of YFP. The resulting constructs encoding the complementary nEYFP and cEYFP fragments, were transiently co-expressed in pairs in protoplasts isolated from wild-type *Arabidopsis* rosette leaves, and any reconstituted YFP signals were visualized by a confocal microscopy. In this way, PUX10 was found to physically interact with SP1 at the chloroplast envelope membrane, whereas neither of the negative control (the chloroplast membrane protein SFR2 and the cytosolic protein CDKA1) showed appreciable interaction with PUX10 (Figure 3.1).

To corroborate the results from the BiFC experiments, and validate the interaction between PUX10 and SP1, co-IP experiments were subsequently performed. The *PUX10* CDS was cloned into a modified p2GWY7 that appends a YFP tag to the C-terminus of its insert. The other two constructs employed here, encoding SP1-Myc and YFP-HA, were previously generated by other lab members (Ling et al., 2019). For co-IP analysis, the *PUX10-YFP* construct combined with the *SP1-Myc* construct, or the *PUX10-YFP* construct alone, was transiently expressed in protoplasts isolated from wild-type *Arabidopsis* rosette leaves. In parallel, the *YFP-HA* construct was also co-expressed with *SP1-Myc* in protoplasts, to serve as a negative control. The transfected cells were solubilized and subjected to immunoprecipitation with anti-Myc beads (Figure 3.2 A). As expected, only PUX10-YFP (not YFP-HA) was found to coprecipitate with SP1-Myc, indicating a specific interaction between PUX10 and SP1.

Given that SP2 is deeply embedded into OEM via the multimembrane spanning structure and lacks accessible cytosolically exposed domain, BiFC was judged to be an unfeasible method for analysing its interaction with PUX10. Therefore, co-IP assays were employed to assess the interaction between PUX10 and SP2. The *PUX10* CDS was cloned into p2GWY7, a vector that appends a YFP tag to the C-terminus of its insert. A construct encoding SP2-Myc was generated by previous lab members (Ling et al., 2019). The *PUX10-YFP* and *SP2-Myc* constructs were introduced into protoplasts simultaneously for transient expression. In parallel, the two

constructs were also transfected into protoplasts singly, in control experiments. Anti-GFP beads were used to pull down the YFP fusion protein, and the samples were probed with anti-Myc antibody to detect SP2 protein. The immunoblotting clearly demonstrated a strong interaction between PUX10 and SP2 (Figure 3.2 B).

In addition, to begin to investigate whether PUX10 may regulate the TOC apparatus in similar fashion to SP1 and SP2, the samples generated above were also analysed using antibodies against TOC and TIC components in further immunoblotting analyses. The results showed that all three TOC proteins (Toc159, Toc75 and Toc33) has co-precipitated with PUX10, whereas no association was detected between PUX10 and Tic40. This indicated specific TOC complex interactions for the PUX10 protein (Figure 3.2 B)

Collectively, the essentially identical results from the BiFC and co-IP experiments demonstrated the strong association of PUX10 with CHLORAD components and TOC proteins.

3.3.2 PUX10 physically interacts with TOC proteins

The co-IP analysis described above revealed interactions of PUX10 with Toc159, Toc75 and Toc33 (Figure 3.2 B). To complement these results with spatial information, the interactions between PUX10 and TOC proteins were assessed in subcellular context by performing further BiFC experiments. The full-length *PUX10* CDS was cloned into the pSAT4(A)-nEYFP-N1 vector which appends the N-terminal fragment of YFP, while the sequences encoding Toc159, Toc33 and the negative control protein CDKA1 were cloned into the complementary vector pSAT4-cEYFP-N1 which appends the C-terminal fragment of YFP. The resulting constructs were transiently expressed in complementary pairs in protoplasts, and the YFP signals were subsequently visualized by confocal microscopy (Figure 3.3 A). As expected, PUX10 was found to physically interact with both Toc159 and Toc33 at the chloroplast envelope. However, no appreciable interaction was observed for the negative control protein CDKA1, indicating that the detected interactions between PUX10 and TOC proteins were specific.

To investigate whether PUX10 may also regulate different forms of the TOC apparatus, Toc132 and Toc34 (which are the minor isoforms of Toc159 and Toc33, respectively, in *Arabidopsis*) were also analysed. The *Toc132* and *Toc34* CDS fragments were cloned into the pSAT4-cEYFP-N1 vector and then resulting constructs were co-transfected with PUX10-nYFP into protoplasts for BiFC analysis. Like the major isoforms, both Toc132 and Toc34 showed strong interaction with PUX10 at the chloroplast envelope (Figure 3.3 B).

Besides its defining C-terminal UBX domain, PUX10 possesses an N-terminal UBA domain. Such UBA domains are a ubiquitin-binding domains that mediate interaction between proteins and their ubiquitinated substrates. In the previous chapter, PUX10 was shown to interact with ubiquitin via its N-terminal UBA domain. Given that TOC proteins are ubiquitinated by SP1 before being targeted to the cytosolic 26S proteosome for degradation, it was hypothesized that the UBA domain of PUX10 is important for the interaction between PUX10 and TOC proteins. This possibility was investigated by co-IP analysis, using Toc33 as a representative TOC protein. Full-length *PUX10* and *ΔUBA* (PUX10 UBA domain deleted) encoding sequences were cloned into p2GWY7, a vector that appends a YFP tag to the C-terminus of its insert. The *Toc33-HA* construct used here was generated by previous lab members (Ling et al., 2019). This *Toc33-HA* construct was co-transfected, together with either the *PUX10-YFP* or the *ΔUBA-YFP* construct, into protoplasts isolated from wild-type *Arabidopsis* rosette leaves; and, as a negative control, *Toc33-HA* was also transfected in isolation. Anti-GFP beads were used to pull down the YFP fusion proteins, and the samples were probed using anti-HA and anti-ubiquitin antibodies to detect (polyubiquitinated) Toc33 (Figure 3.4). The results clearly indicated a strong association between PUX10 and polyubiquitinated Toc33 as well as unmodified Toc33. Significantly, these interactions were lost when ΔUBA was analysed, indicating that the associations were dependent on the UBA domain of PUX10. It is likely that the unmodified Toc33 protein copurified with PUX10 in this analysis by virtue of it being in a complex with other proteins that were ubiquitinated.

Taken together, these results demonstrated that PUX10 is capable of interacting with polyubiquitinated TOC proteins through its UBA domain.

3.3.3 The *pux10-1* mutation moderately suppresses the *ppi1* phenotype

As described in the previous chapter, the *pux10-1* mutant bears a T-DNA insertion in the first exon and consequently displays a complete abrogation of the expression of *PUX10*. Under standard growth conditions, *pux10-1* null mutant plants display no obvious phenotypic defects (in this regard, *pux10* is similar to *sp1* and s*p2*) (Ling et al., 2019; Ling et al., 2012), whereas the plants overexpressing *PUX10* are severely dwarfed. Given the dramatically altered subcellular distribution of Cdc48 when *PUX10* is overexpressed (Figure 2.7 B), such dwarfism is likely a side effect due to the unbalanced cellular distribution of Cdc48 rather than a specific effect of PUX10 function. Thus, *PUX10-OX* transgenic plants were excluded from the following genetic analysis.

The physical interaction of PUX10 with TOC proteins suggested a functional link between PUX10 and TOC components. To further investigate this hypothesis, the *pux10-1* mutation was introduced into the *ppi1* (a *TOC33* knockout mutant) single mutant background (and, as a control, the tic110/+ mutant background). The resulting *pux10-1 ppi1* double-mutant plants displayed a moderate increase in chlorophyll content and leaf size relative to single-mutant *ppi1* control plants (Figure 3.5 A and B). In contrast, *pux10-1 tic110*/+ double-mutant control plants displayed no phenotypic differences from *tic110*/+ single-mutant plants, which exhibit mild chlorosis, at any stage, indicating that the effect on *ppi1* was specific; note that the *tic110* genotype was analysed in the heterozygous state, since in the homozygous state it is lethal (Kovacheva et al., 2005).

To investigate the basis for this *ppi1* suppression effect, total protein extracts were prepared from wild-type, *ppi1* and *pux10-1 ppi1* plants, and the abundance of TOC proteins in the samples was compared by immunoblotting. Significantly, all tested TOC proteins were substantially recovered in the *pux10-1 ppi1* double mutant plants, relative to *ppi1*, whereas the inner envelope

membrane proteins, Tic40 and Tic110, were largely unaffected by the *pux10* mutation (Figure 3.5 C and D). These changes in TOC proteins abundance were not attributable to pretranslational events because TOC transcript levels were comparable in the different genotypes (Figure 3.5 E). Thus, the *ppi1* suppression mediated by *pux10*, much like that mediated by *sp1* and *sp2* as described previously (Ling et al., 2019; Ling et al., 2012), is linked to partially restored TOC protein accumulation.

3.3.4 The *pux10-1* mutation partially blocks the phenotypic effects of *SP1* overexpression in the *ppi1* background

Having identified a physical interaction between PUX10 with SP1, I next investigated a possible functional link between PUX10 and SP1. It is well known that the *sp1* mutation significantly suppresses the *ppi1* phenotype to produce bigger and greener plants that have increased abundance of TOC proteins and chlorophyll and improved chloroplast ultrastructural organization. Conversely, *SP1* overexpression greatly enhances the chlorosis of *ppi1*, by increasing the ubiquitination of the residual TOC proteins to signal their proteasomal degradation, resulting in the severe depletion of TOC proteins, reduced chlorophyll concentration, and smaller and paler plants (Ling et al., 2012). Given that Cdc48 is important for the degradation of ubiquitinated TOC proteins (Ling et al., 2019), and that PUX10 is a cofactor that recruits Cdc48 to the chloroplast OEM (as shown in the previous chapter), it is reasonable to hypothesize that PUX10 is required for the effective removal of TOC proteins when *SP1* was overexpressed in the *ppi1* mutant. If this is indeed the case, then the *pux10* mutation should block, or reduce the severe phenotypic effects of SP1-OX on *ppi1* plants.

To test this hypothesis, the *pux10-1* mutation was crossed into the SP1-OX *ppi1* background, and triple homozygous *pux10-1* SP1-OX *ppi1* plants were identified via genotyping and RT-PCR (Figure 3.6 A and B). As expected, SP1-OX *ppi1* plants were much smaller and more chlorotic than were *ppi1*. Most interestingly, and in accordance with the above hypothesis, the *pux10-1* SP1-OX *ppi1* plants were much greener and larger than SP1-OX *ppi1* plants, although they were

not completely recovered to the level of *ppi1* single-mutant plants (Figures 3.6 A and 3.7 A). Chlorophyll concentration was significantly increased in *pux10-1* SP1-OX *ppi1* plants relative to SP1-OX *ppi1* plants, though it was still considerably less than that in *ppi1* (Figure 3.7 B); this was consistent with the visible difference between the *pux10-1* SP1-OX *ppi1* and *ppi1* plants.

To determine whether the suppression of chlorosis observed in *pux10-1* SP1-OX *ppi1* plants was linked to effects on chloroplast biogenesis, the organelles in *ppi1*, SP1-OX *ppi1*, and *pux10-1* SP1-OX *ppi1* plants were analysed by transmission electron microscopy (TEM). Leaf samples for analysis were taken from plants that had been grown on soil under standard growth conditions. The TEM analysis demonstrated that *pux10-1* SP1-OX *ppi1* plants possess chloroplasts of increased size and improved ultrastructure compared to SP1-OX *ppi1* plants (Figure 3.7 C). Quantitative analysis revealed a clear increase in chloroplast cross-sectional area in *pux10-1* SP1-OX *ppi1* relative to SP1-OX *ppi1* (Figure 3.7 D). Moreover, there was an increased number of thylakoid lamellae per granal stack, and an increased number of interconnections between granal stacks, in *pux10-1* SP1-OX *ppi1* chloroplasts relative to SP1-OX *ppi1* chloroplasts (Figure 3.7 E). However, the overall development of chloroplasts in *pux10-1* SP1-OX *ppi1* was still less than that in *ppi1*, which again was consistent with the visible difference between the *pux10-1* SP1-OX *ppi1* and *ppi1* plants.

In SP1-OX *ppi1* plants, the phenotypic enhancement effects relative to *ppi1* is related to the reduced abundance of TOC proteins (Ling et al., 2012). To test whether the suppression effect observed in *pux10-1* SP1-OX *ppi1* plants is linked to increased TOC protein abundance, total proteins extracts prepared from *ppi1*, SP1-OX *ppi1* and *pux10-1* SP1-OX *ppi1* plants were analysed by immunoblotting. This analysis revealed significant increases in TOC protein abundance in *pux10-1* SP1-OX *ppi1*, relative to SP1-OX *ppi1,* although TOC levels were not fully stored to those seen in *ppi1* (Figure 3.8 A and B). In line with previous observation concerning the *sp1 ppi1* mutant (Ling et al., 2012), there were no significant differences in the levels of TIC

components in any of the genotypes analysed here, indicating that the effects of PUX10, like those of SP1, are specifically related to changes in the abundance of TOC components.

3.3.5 Analysis of the role of PUX10 in the SP1-dependent regulation of leaf senescence

Plastids are interconvertible organelles which undergo developmental transitions from one form to another via proteome organelle changes, and such proteome changes are directly linked to reorganization of the TOC machinery (Jarvis & Lopez-Juez, 2013). The expression level of *SP1* was previously shown to influence the rate of interconversion of different plastid types (Ling et al., 2012; Ling et al., 2021). For instance, the *sp1* mutant showed delayed leaf senescence, whereas SP1 overexpressors showed accelerated senescence. This indicates that SP1 plays a critical role in the progression of plastid interconversions; under the regulation of SP1, TOC complex can be rearranged to better enable the import of those proteins required to bring about plastid proteome changes.

To determine whether PUX10 plays a role in the SP1-dependent regulation of TOC complexes during plastid interconversions, the *pux10-1* mutation was crossed into the SP1-OX background. In the resulting *pux10-1* SP1-OX plants, PCR-based genotyping was used to confirm the presence of the *pux10* mutation, while RT-PCR was employed to confirm the overexpression of *SP1* (data not shown). Then, the *pux10-1* SP1-OX plants were subjected to leaf senescence analysis, along with wild-type, *sp1* and SP1-OX control plants. Selected leaves of similar sizes from 4-week-old plants of each genotype were covered with aluminium foil to promote darkness-induced senescence (Ling et al., 2012; Schelbert et al., 2009), and the plants were left to grow for a further five days under standard growth conditions. Finally, the maximum photochemical efficiency of photosystem II (F_v/F_m) was determined by measuring chlorophyll fluorescence using an imaging device (Ling et al., 2012).

In line with previously published results, the *sp1* mutant showed retarded leaf senescence, as judged by reduced visible yellowing and a smaller decline in F_v/F_m; whereas SP1-OX leaves showed accelerated senescence, relative to wild type (Figure 3.9). Interestingly, the *pux10-1* SP1-OX leaves showed a significant reduction in senescence compared to SP1-OX leaves, based on both visual assessment of the material and measurements of the F_v/F_m parameter. Therefore, these data imply that PUX10 is required for the reorganization of TOC complexes mediated by SP1 during an important developmental transition (Figurer 3.9). The results provide a clear indication of the physiological importance of PUX10.

3.4 Discussion

The previous chapter described a series of experiments that demonstrated the physical interaction of the chloroplast OEM protein PUX10 with Cdc48 and ubiquitin, via its UBX and UBA domains, respectively. Since UBX proteins are well known to have functions in the UPS, it is reasonable to hypothesize that PUX10 plays a role in the regulation of chloroplast protein import by participating in the CHLORAD pathway. In this chapter, this hypothesis was explored through protein-protein interaction experiments as well as genetic and biochemical studies.

In the CHLORAD system, SP1, a RING-type E3 ligase, mediates the ubiquitination of TOC proteins, while SP2 and Cdc48 cooperate to bring about the extraction ("retrotranslocation") of ubiquitinated TOC proteins from the OEM to the cytosol (Ling et al., 2019). The BiFC and co-IP experiments presented here clearly demonstrated that PUX10 physically interacts with SP1 and SP2 (Figures 3.1 and 3.2), in addition to Cdc48, suggesting that PUX10 may be part of a CHLORAD complex that recruits Cdc48 to the chloroplast surface for the dislocation of ubiquitinated TOC proteins from the OEM. Recently published studies showed that PUX10 is also a lipid droplet (LD)-localized scaffold protein for recruiting Cdc48 to LDs for the degradation of LD proteins during seed germination and pollen tube growth (Deruyffelaere et al., 2018; Kretzschmar et al., 2018). Such a Cdc48 recruiting role was also described for Ubx2, the homologue of PUX10 in yeast. In fact, the ER membrane protein Ubx2 has long been established

as a key component of ERAD, wherein it mediates interaction of the Cdc48 complex (Cdc48-Npl4) with the ER membrane-bound ubiquitin ligases Hrd1 and Doa10, as well as ERAD substrates (Neuber et al., 2005; Schuberth & Buchberger, 2005).

One of the reasons that Cdc48 is able to perform such a diversity of cellular roles is that it possesses many adaptor proteins or cofactors that can modify its functions. The Ufd1-Npl4 heterodimer is one of the most important cofactors of Cdc48, and it participates in many Cdc48-dependent processes, including ERAD (Ye et al., 2001). Although the structures and functions of the Ufd1-Npl4 heterodimer had been well characterized in yeast and other species, the functions of the two are largely uncharacterized in plants (Huang et al., 2020; Li et al., 2022). Interestingly, preliminary protein interaction analyses conducted by another lab member indicated that both Ufd1 and Npl4 interact with PUX10 at the chloroplast OEM in *Arabidopsis* (Thomson et al., unpublished data). This provides further support for the notion that PUX10 is associated with the CHLORAD complex for the degradation of TOC proteins.

Based on these observations, the possibilities of direct interactions between PUX10 and TOC proteins was also investigated, and confirmed, using both BiFC and IP analysis (Figures 3.2 and 3.3). As noted, in CHLORAD, Cdc48 drives the extraction of ubiquitinated TOC proteins from the chloroplast OEM into the cytosol for degradation. Further co-IP analysis described in this chapter clearly demonstrated that PUX10 interacts with ubiquitinated Toc33 via its UBA domain (Figure 3.4). This indicated that PUX10 can potentially act as a bridge between the cytosolic Cdc48 and the ubiquitinated TOC proteins in the chloroplast OEM, to promote the retrotranslocation of ubiquitinated TOC proteins from the chloroplast membrane.

The physical interaction between PUX10 and TOC proteins implied a potential functional link between PUX10 and chloroplast protein import, and so this possibility was investigated genetically. Significantly, the *pux10* mutation was found to moderately suppress the pale phenotype of *ppi1*, and the phenotypic suppression observed in the double-mutant *pux10-1 ppi1* plants was linked to the increases in TOC protein abundance (Figure 3.5). This parallels very closely the suppression of *ppi1* mediated by the *sp1* and *sp2* mutations (Ling et al., 2019; Ling et

al., 2012). Based on a recent report, PUX10 plays an important role during seed germination by promoting the dislocation of ubiquitinated LD proteins; but then as soon as seed maturation is started, the localization of PUX10 changed from LDs to chloroplasts (Deruyffelaere et al., 2018), indicating that PUX10 may function in chloroplasts during the early development of mature plants. The genetic analysis presented here confirmed that PUX10 is involved in chloroplast functions in mature plants. More specifically, it is involved in the regulation of TOC functions during the development of rosette leaves, and such regulation is critical for optimizing the import of the proteins specifically required by rapidly developing chloroplasts. However, the phenotypic suppression of *ppi1* by the *pux10* mutation was not as strong as that delivered by the *sp1* or *sp2* mutations, indicating that there may be functional redundancy between PUX10 and so far unknown proteins, or that PUX10 is only strictly required in specific situations.

Functional redundancy appears to be a rather conserved phenomenon regarding the cofactors for recruiting Cdc48 to organelle membranes. For example, in addition to PUX10, other Cdc48-recruitment factors were suggested to exist in LDs for LD-associated protein degradation in *Arabidopsis* (Deruyffelaere et al., 2018; Kretzschmar et al., 2018). Similar functional redundancy was reported for Ubx2 and Cdc48 in yeast ERAD (Neuber et al., 2005). Moreover, Dfm1, a Der1-like ER membrane protein, was found to be capable of recruiting Cdc48 to the ER membrane in the absence of Ubx2: the reduction in membrane-bound Cdc48 was more pronounced when both Ubx2 and Dfm1 were absent, compared to the absence of Ubx2 alone (Stolz et al., 2010). Interestingly, AtDerlin-1 (AtDer1), the homologue of Dfm1 in *Arabidopsis*, may be active in chloroplasts based on the prediction by ARAMEMNON (http://aramemnon.uni-koeln.de/), though the significance of this prediction has not been confirmed experimentally. Besides their well-known function in ERAD in eukaryotes (Schekman, 2004), Derlin proteins are also found to localize to endosomes and function in the degradation of misfolded transmembrane proteins at the plasma membrane and/or in endosomes in *Caenorhabditis elegans* and mouse macrophages (Schaheen et al., 2009). Therefore, it is possible that AtDer1 also has multi-localization in plant cells. A careful subcellular localization analysis of AtDer1 would therefore be very illuminating

regarding its functions in *Arabidopsis*, and might begin to shed light on the nature of possible PUX10 redundancies.

In the mammalian systems, besides the putative Ubx2 orthologue, other UBX and non-UBX proteins were found to contribute to the recruitment of p97/Cdc48 to the ER membrane in ERAD (Liang et al., 2006; McNeill et al., 2004; Ye et al., 2004). Thus, it seems quite plausible that some unknown chloroplast membrane-bound proteins share functionally redundancy with PUX10 during the regulated degradation of TOC proteins. Of the 12 functional PUX proteins in *Arabidopsis*, besides PUX10, PUX5, PUX7, PUX8, PUX9 and PUX13 are proteins that also contain ubiquitin-binding UBA domains (Zhang et al., 2022b). Except for PUX7, PUX5, PUX8, PUX9 and PUX13 all showed cytosolic localization (Figure 2.1). Though these proteins lack hydrophobic transmembrane domains, it is possible that they also function in the degradation of TOC proteins by bridging Cdc48 and ubiquitinated TOC components, through the UBX and UBA domains, respectively. In principle, this function would not require the bridge to be an integral membrane protein. Further biochemical and genetic analyses will be needed to address such possibilities.

Another type of ubiquitin binding domain is the zinc finger (ZnF) domain (Alam et al., 2004; Lee et al., 2006; Reyes-Turcu et al., 2006). One typical example is the Npl4 protein that acts as a substrate-recruiting cofactor of Cdc48 by forming a heterodimer with Ufd1, known as the Cdc48-Npl4-Ufd1 complex, in ubiquitin-dependent protein translocation processes (Bodnar et al., 2018). Interestingly, the homologues of Npl4 in *Arabidopsis* contain ubiquitin regulatory X-like (UBXL) domains, which can interact with Cdc48, but not ZnF domains. Instead, Ufd1C (At4g15420), a variant Ufd1 homologue in *Arabidopsis*, contains a C-terminal zinc finger domain. Data from protein interaction analyses indicated that Ufd1C interacts with Npl4, Cdc48, CHLORAD components, and TOC proteins (Thomson et al., unpublished data). Therefore, it is plausible that Ufd1C recruits Cdc48-Npl4-Ufd1 complexes to the chloroplast surface by interacting with ubiquitinated TOC proteins via its ZnF domain. In addition, PUX2 is the only

PUX protein that is predicted to have a ZnF domain, though the significance of this prediction has not been confirmed experimentally (Zhang et al., 2022b).

Aside from PUX10, PUX11 is the only PUX protein containing a membrane-anchoring hydrophobic sequence, which in this case is in the long C-terminal tail (Zhang et al., 2022b). Unlike PUX10, PUX11 possesses a typical C-terminal UBX domain but no UBA domain; instead, a ubiquitin-associating (UAS) domain in PUX11 might help to recruit ubiquitinated substrates indirectly (Lim et al., 2009). Though the functions of Ubx6/Ubx7, homologues of PUX11 in yeast, remain elusive, the mammalian homologue, Erasin (UBXD2), is an integral ER membrane protein and functions in ERAD (Liang et al., 2006). The subcellular localization analysis presented here showed that PUX11 was predominantly localized in the cytosol, but a marginal/partial localization to the chloroplasts could not be completely excluded (Figure 2.1). Thus, further characterization will be needed to assess the potential involvement of PUX11 in the regulation of chloroplast protein import.

As the core component of CHLORAD system, the E3 ubiquitin ligase SP1 labels TOC proteins with ubiquitin for degradation by the cytosolic 26S proteasome. Consequently, SP1 plays a crucial role in plastid type transitions, chloroplast development, and abiotic stress tolerance (Ling et al., 2012; Ling & Jarvis, 2015b; Ling et al., 2021). The *sp1* mutation significantly suppresses the phenotype of *ppi1*, whereas *SP1* overexpression has the converse effect (Ling et al., 2012). The physical interaction between PUX10 and SP1 suggested a functional link between PUX10 and SP1-dependent proteolytic pathways. Indeed, when the *pux10-1* mutation was introduced into the SP1-OX *ppi1* background, the resulting *pux10-1* SP1-OX *ppi1* plants were larger and greener than SP1-OX *ppi1* plants and exhibited improved chloroplast ultrastructure (Figure 3.7), clearly indicating a genetic and functional link between PUX10 and SP1. It was previously shown that the paler and smaller phenotype of SP1-OX *ppi1* plants, relative to *ppi1*, is linked to decreased TOC protein abundance and, hence, reduced protein import capacity (Ling et al., 2012). Here, the significantly increased TOC protein abundance seen in the *pux10-1* SP1-OX *ppi1* plants confirmed that PUX10 is required for the efficient action of SP1 in mediating

TOC protein degradation (Figure 3.8). Moreover, while *SP1* overexpression is found to enhance leaf senescence by accelerating the plastid transition processes (Ling et al., 2012), the reduced senescence seen in *pux10-1* SP1-OX leaves indicated that PUX10 also helps to enable such developmental functions of SP1 (Figure 3.9). It is worth mentioning that in both cases, though, the *pux10* mutation only partially blocked the phenotypic effects of *SP1* overexpression, indicating again the possibility that unknown proteins with functional redundancy to PUX10 are also involved in the degradation of ubiquitinated TOC proteins.

In summary, the results in this chapter, together with those in the previous chapter, show that PUX10 is a new component of the CHLORAD machinery for the degradation of chloroplast TOC proteins by the UPS. The UBA domain of PUX10 recognizes SP1-ubiquitinated TOC proteins, while its UBX domain recruits cytosolic Cdc48 to chloroplast surface, such that it is adjacent to its substrates. Interestingly, this bridging role of PUX10 seems not to be indispensable during chloroplast development, but as discussed this could be due to functional redundancy. Nonetheless, the suppressing effect of the *pux10* mutation on the effects of SP1-OX clearly indicate that PUX10 improves the efficiency of CHLORAD, which it does by coordinating the ubiquitination and retrotranslocation activities necessary for the rapid turnover of TOC proteins.

3.5 Figures

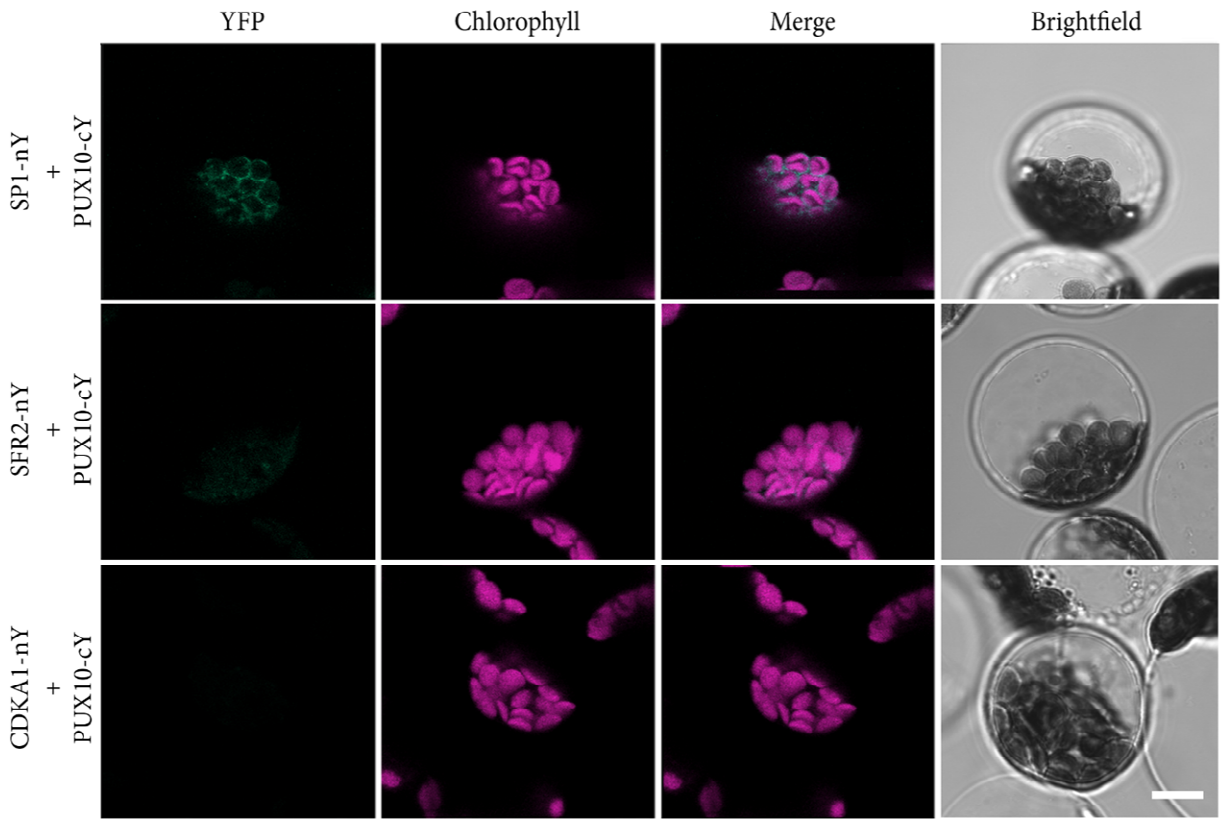


Figure 3.1. PUX10 interacts with SP1 at the chloroplast envelope membrane in BiFC assays. *Arabidopsis* protoplasts transiently co-expressing the SP1 and PUX10 proteins fused to complementary N-terminal (nY) and C-terminal (cY) fragments of the YFP protein, respectively, were analysed by confocal microscopy. In parallel, SFR2 was used as a chloroplast-localized negative control, while CDKA1 was used as a cytosol-localized negative control, instead of SP1. A representative protoplast is presented in each case. For each protoplast, YFP fluorescence, chlorophyll autofluorescence, merged YFP and chlorophyll fluorescence, and brightfield images are shown. The exposure times and gain settings used were identical in each case. Bar = 10 μm.

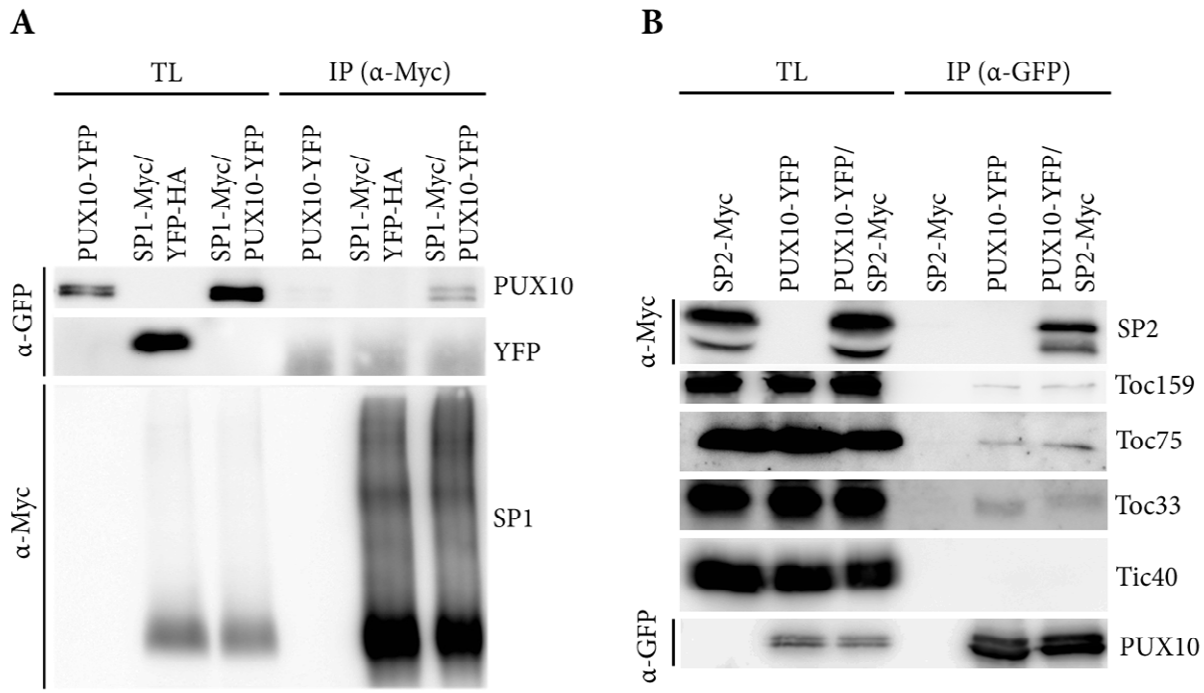


Figure 3.2. PUX10 physically interacts with SP1, SP2 and TOC protein in co-immunoprecipitation assays. (A) Co-IP analysis of the interaction between PUX10 and SP1. *Arabidopsis* protoplasts expressing YFP-tagged PUX10 (PUX10-YFP) solely, or co-expressing Myc-tagged SP1 (SP1-Myc) with either HA-tagged YFP (YFP-HA), or PUX10-YFP, were solubilized and subjected to anti-Myc IP analysis. Anti-Myc tag immunoblot analysis was used to verify the enrichment of the SP1-Myc protein, while anti-GFP analysis was used to detect co-purification of PUX10 and YFP-HA. Three biological replicates were conducted. **(B)** Co-IP analysis of the interaction between PUX10 and SP2. *Arabidopsis* protoplasts expressing either Myc-tagged SP2 (SP2-Myc) or PUX10-YFP solely, or co-expressing SP2-Myc and PUX10-YFP, were solubilized and subjected to anti-GFP IP analysis. Anti-GFP tag immunoblot analysis was used to verify the enrichment of the PUX10-YFP proteins, while anti-Myc analysis was used to detect co-purification of SP2. Further immunoblot analysis using antibodies against key TOC components were used to detect co-purification of endogenous TOC protein, while similar analysis of Tic40 provided a negative control to confirm the specificity of the detected interactions. Two biological replicates were conducted. Abbreviations: TL, total lysate; IP, immunoprecipitation; α-Myc, anti-Myc; α-GFP, anti-GFP.

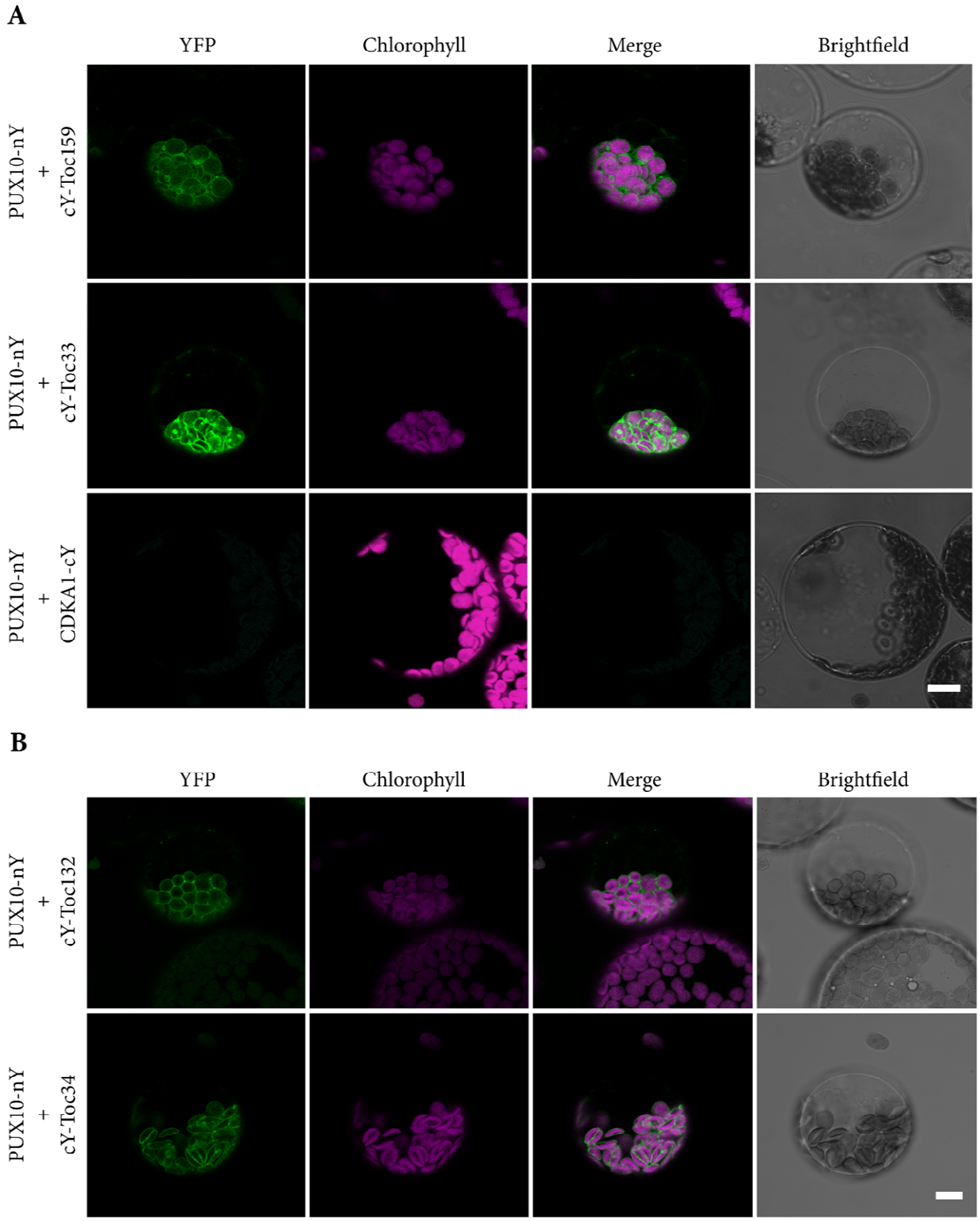


Figure 3.3. PUX10 interacts with TOC proteins at the chloroplast envelope membrane in BiFC assays. (A) Analysis of interactions with the main TOC protein isoforms, Toc159 or Toc33. *Arabidopsis* protoplasts transiently co-expressing PUX10 and either Toc159 or Toc33 fused to

complementary N-terminal (nY) and C-terminal (cY) fragments of the YFP protein, respectively, were analysed by confocal microscopy. In parallel, CDKA1 was used as a cytosol-localized negative control, instead of the TOC components. A representative protoplast is presented in each case. For each protoplast, YFP fluorescence, chlorophyll autofluorescence, merged YFP and chlorophyll fluorescence, and brightfield images are shown. The exposure times and gain settings were identical in each case. Bar = 10 μm. **(B)** Analysis of interactions with the minor TOC protein isoforms, Toc132 or Toc34. The analysis was performed as in (**A**). Here, again, a representative protoplast is presented, and the exposure times and gain settings were identical in each case. Bar = 10 μm.

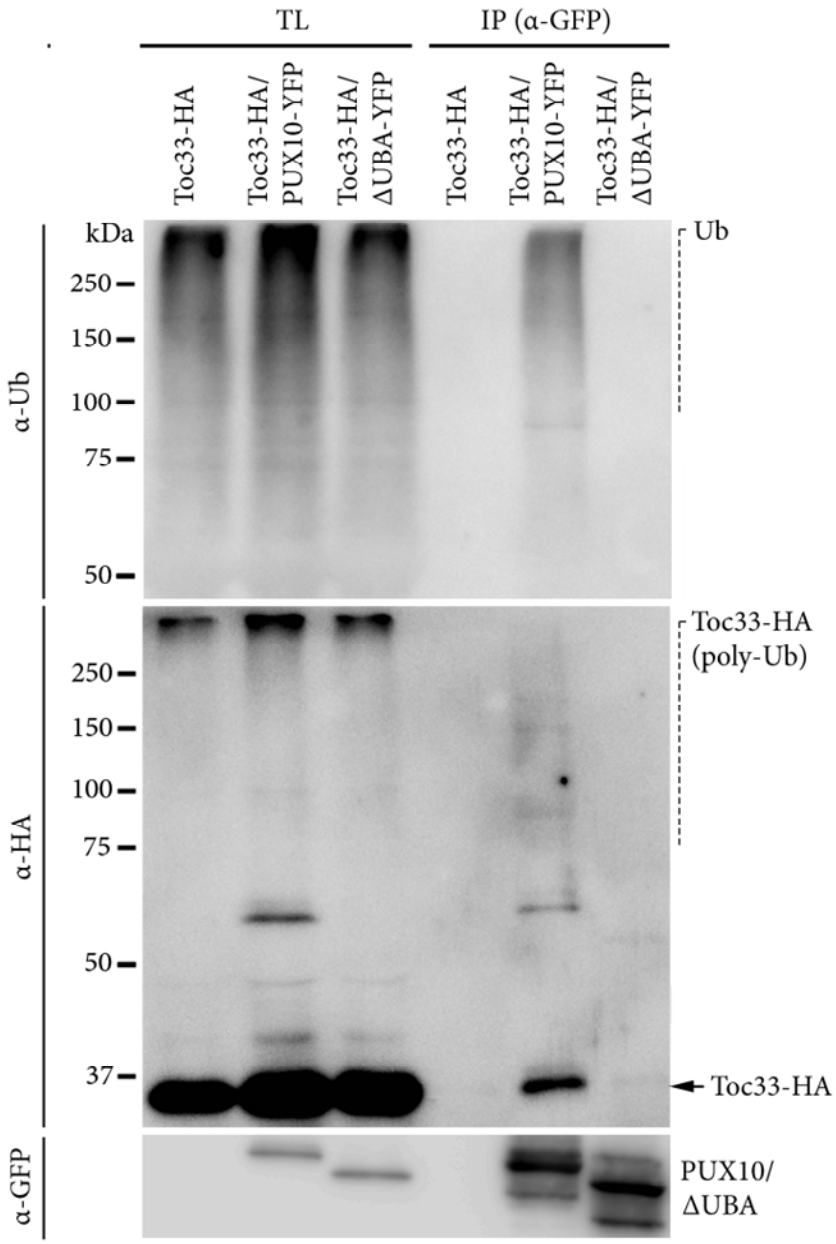


Figure 3.4. PUX10 interacts with ubiquitinated Toc33 in co-immunoprecipitation assays. *Arabidopsis* protoplasts expressing HA-tagged Toc33 (Toc33-HA) solely, or co-expressing Toc33-HA with YFP-tagged PUX10 (PUX10-YFP) or PUX10 lacking the UBA domain (ΔUBA-YFP), were solubilized and subjected to anti-GFP IP analysis. Anti-GFP immunoblot analysis was used to verify the enrichment of the PUX10-YFP or ΔUBA-YFP proteins, while anti-HA analysis was used to detect co-purification of Toc33; both unmodified (see arrow) and high molecular weight modified forms of Toc33-HA were detected. Parallel analysis of the samples by

anti-ubiquitin immunoblotting provided evidence that the high molecular weight species were polyubiquitinated Toc33. Positions of molecular weight standards (size in kDa) are shown at left. Three biological replicates were conducted. Abbreviations: TL, total lysate; IP, immunoprecipitation; α-GFP, anti-GFP; α-HA, anti-HA; α-Ub, anti-ubiquitin; Ub, ubiquitin; poly-Ub, polyubiquitin.

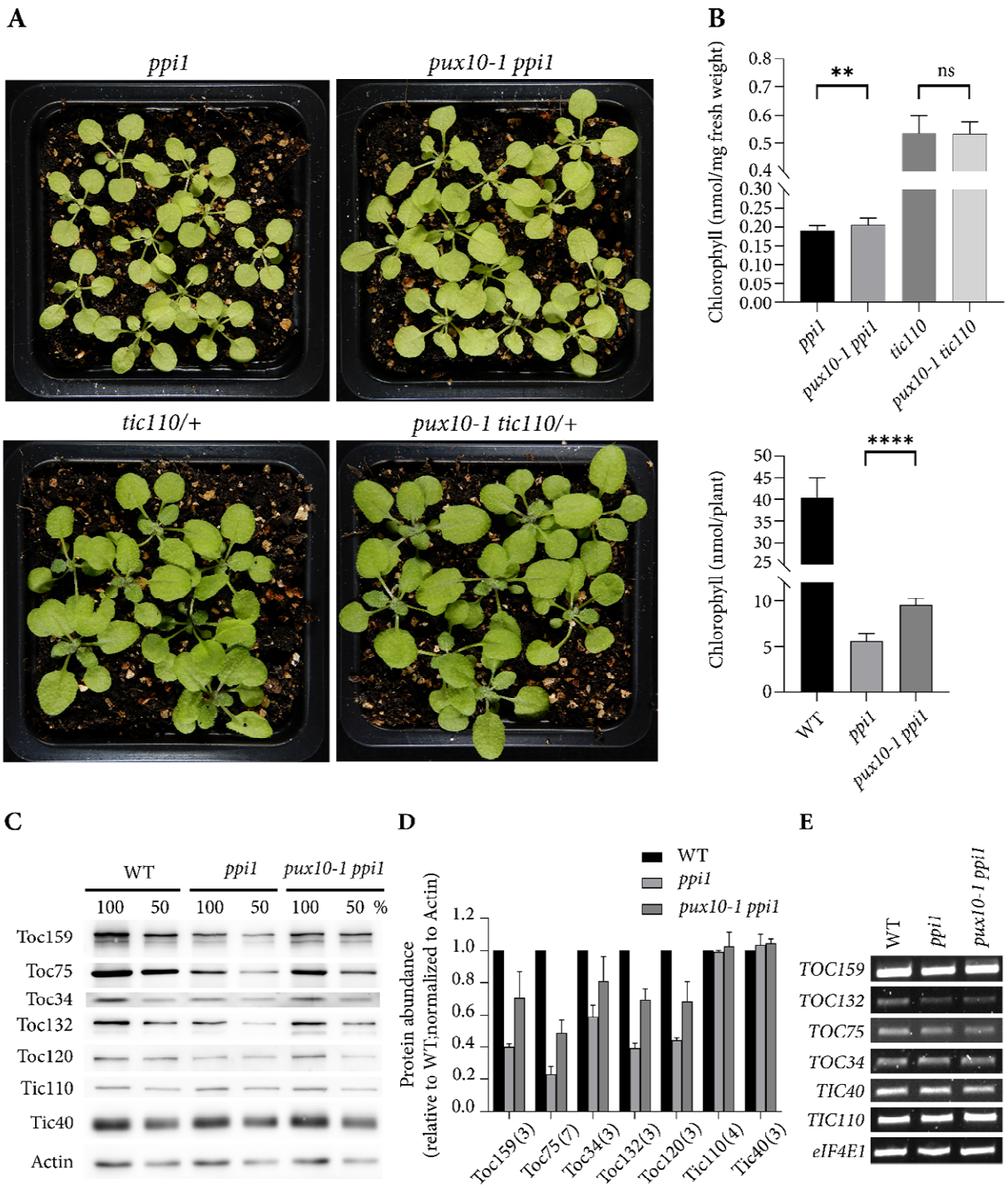


Figure 3.5. The *pux10-1* mutation suppresses the phenotype of *ppi1*. **(A)** Visible appearance of the *pux10-1 ppi1* double mutant plants, and of appreciate control plants including the *pux10-1 tic110*/+ double mutant; the *tic110* genotype was analysed in the heterozygous state, since in the homozygous state it is lethal (Kovacheva et al., 2005). Plants were grown on soil under standard

growth conditions for 3 weeks before photography. Representative plants are shown. (**B**) Quantification of chlorophyll concentration in the *pux10-1 ppi1* double-mutant and control plants. Measurements were taken on the day of photography in (**A**). First, the leaves were analysed using a Konica-Minolta SPAD-502 meter (top), and the meter values were converted to chlorophyll per fresh weight values using a verified calibration equation; values shown are means (n=30) with error bars indicating SEM. In addition, chlorophyll in the aerial tissues of the plants was extracted in organic solvent and quantified using a spectrophotometer (bottom), and converted to chlorophyll per plant values using a published equation; values shown are means (n=5) with error bars indicating SEM. Asterisks above the columns indicate the significance of differences (Student's *t*-test: $^{****}P < 0.0001$; $^{**}P < 0.005$; ns, not significant). (**C**) Immunoblot analysis of TOC and TIC protein levels in wild-type, *ppi1* and *pux10-1 ppi1* plants. Total protein samples extracted from 4-week-old seedlings of each genotype were analysed using antibodies against the indicated proteins. Two different loadings of each sample (100% and 50%) were analysed. Actin was used as a loading control. Representative blot images are shown. (**D**) Quantification of the immunoblot data presented in (**C**), and of other similar datasets. The bands were quantified, and the data for each protein were normalized to corresponding data for Actin; the data are presented as ratios relative to the wild-type value for each protein. The number of biological replicates for each protein is indicated in bracket. Values shown are means with error bars indicating SEM. (**E**) Analysis of the mRNA expression of important translocon component genes in wild-type, *ppi1* and *pux10-1 ppi1* plants. Total RNA isolated from 20-day-old plants of the indicated genotypes was analysed by RT-PCR using gene-specific primers for *TOC159*, *TOC132*, *TOC75*, *TOC34*, *TIC40*, *TIC110* and the reference gene *eIF4E1*. Amplifications employed a limited number of cycles to avoid saturation, and products were analysed by agarose gel electrophoresis.

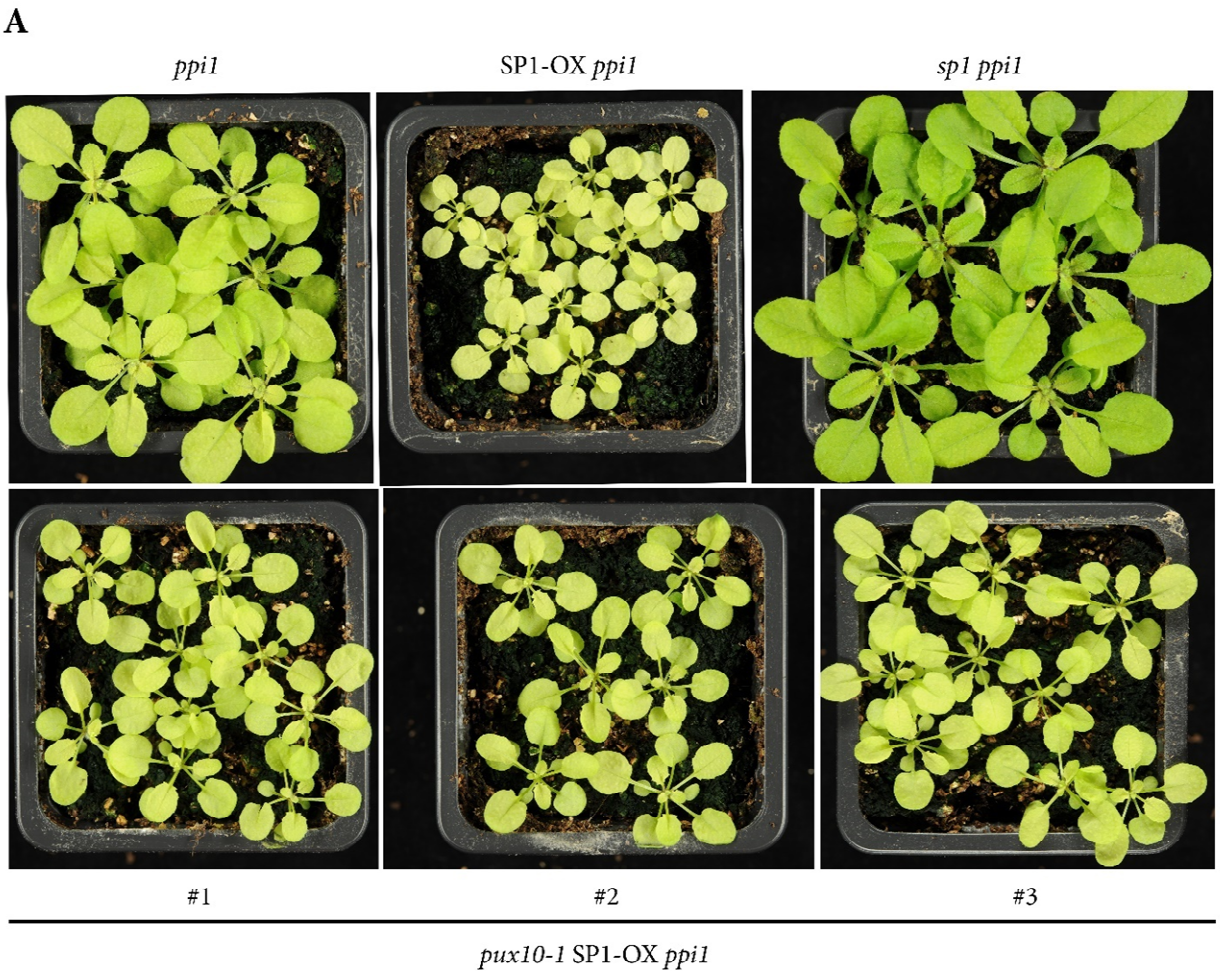


Figure 3.6. The *pux10-1* mutation suppresses the phenotype of SP1-OX *ppi1*. **(A)** The *pux10-1* mutant was crossed to an SP1-OX *ppi1* transgenic line, and F2 individuals showing a greener phenotype than SP1-OX *ppi1* controls were carried forward for genotyping and further analysis. Plants from three representative *pux10-1* SP1-OX *ppi1* F3 lines are presented. Plants were grown

on soil under standard growth conditions for 4 weeks before photography. (**B**) Analysis by RT-PCR of the overexpression of *SP1* in the selected F3 lines shown in (**A**). Total RNA samples isolated from 2-week-old plants were analysed by RT-PCR using gene-specific primers for *SP1* and the reference gene *eIF4E1*. SP1-OX *ppi1* was similarly analysed as a positive control, while *ppi1* and *sp1 ppi1* were analysed as negative controls. Amplifications employed a limited number of cycles to avoid saturation, and products were analysed by agarose gel electrophoresis.

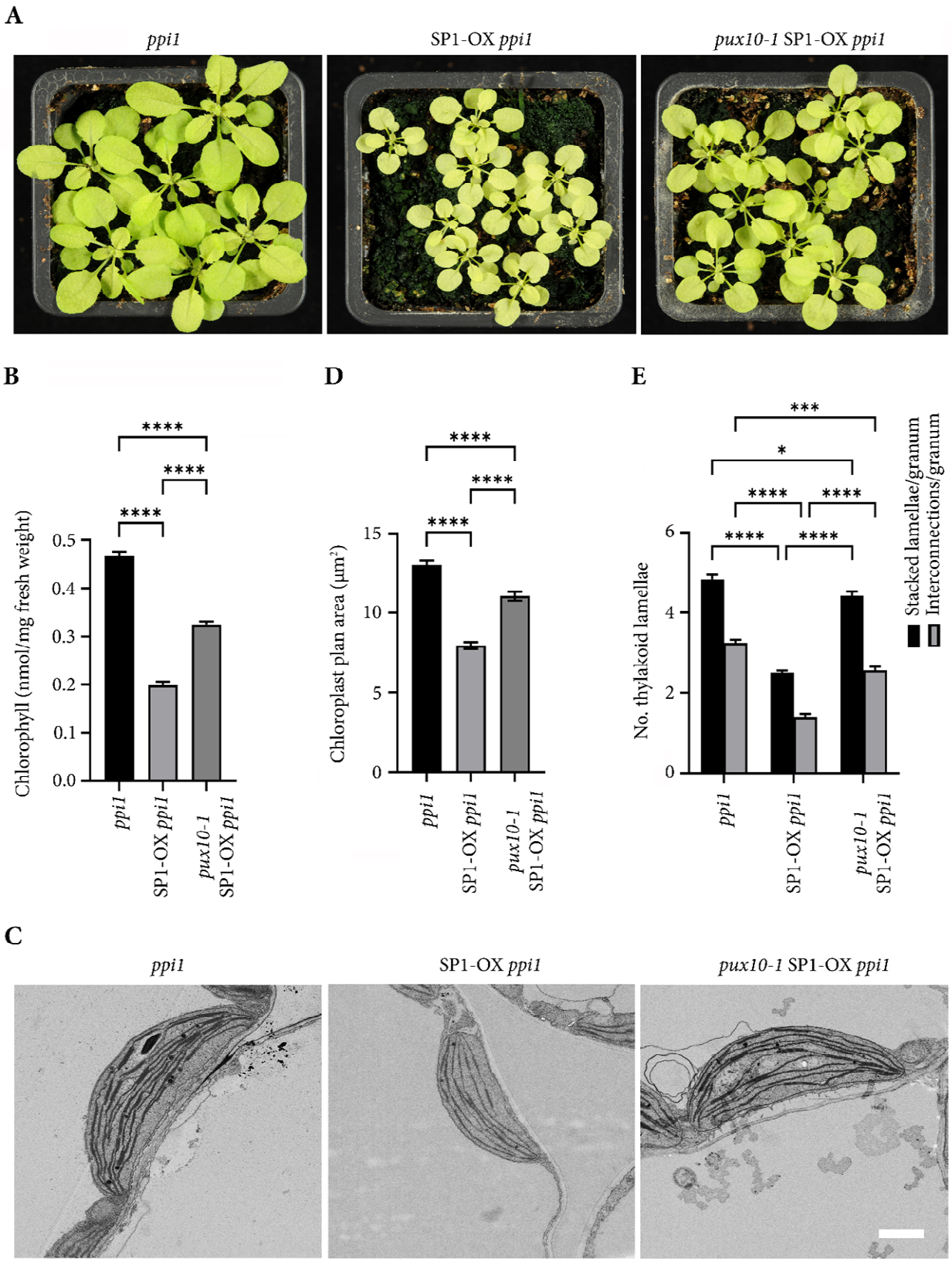

A
ppi1
SP1-OX ppi1
pux10-1 SP1-OX ppi1
B
Chlorophyll (nmol/mg fresh weight)
0.5
0.4
0.3
0.2
0.1
0.0
****
****
****
ppi1
SP1-OX ppi1
pux10-1 SP1-OX ppi1
D
Chloroplast plan area (µm²)
15
10
5
0
****
****
****
ppi1
SP1-OX ppi1
pux10-1 SP1-OX ppi1
E
No. thylakoid lamellae
6
4
2
0
***
*
****
****
****
****
Stacked lamellae/granum
Interconnections/granum
ppi1
SP1-OX ppi1
pux10-1 SP1-OX ppi1
C
ppi1
SP1-OX ppi1
pux10-1 SP1-OX ppi1

Figure 3.7. The *pux10-1* mutation partially blocks the effects of *SP1* overexpression. (A) Visible appearance of the *pux10-1* SP1-OX *ppi1* triple homozygous plants and appreciate control plants. Plants were grown on soil under standard growth conditions for 4 weeks before photography. Representative plants are shown. (**B**) Quantification of chlorophyll concentration in similar 4-week-old plants using a Konica Minolta SPAD-502 meter. Meter values were converted to chlorophyll per fresh weight values using an established equation. Values shown are means (n =30) with error bars indicating SEM. (**C**) Ultrastructure of rosette leaf chloroplasts in 4-week-old plants. Samples were analysed by transmission electron microscopy, and typical organelles are shown. Scale bar = 1 μm. Quantitative analysis of the presented electron micrographs and of other similar micrographs, is shown in (**D**) and (**E**). (**D**) Quantification of chloroplast cross-sectional area. The data are based on measurements of 60 chloroplasts per genotype. Values shown are means with error bars indicating SEM. (**E**) Quantification of thylakoid development. The number of lamellae per granal stack, and the number of membrane interconnections per granal stack, was determined for each genotype. The data are based on the measurements of 80 chloroplasts (for lamellae per granum), or 50 chloroplasts (for interconnection per granum) per genotype. Values shown are means with error bars indicating SEM.

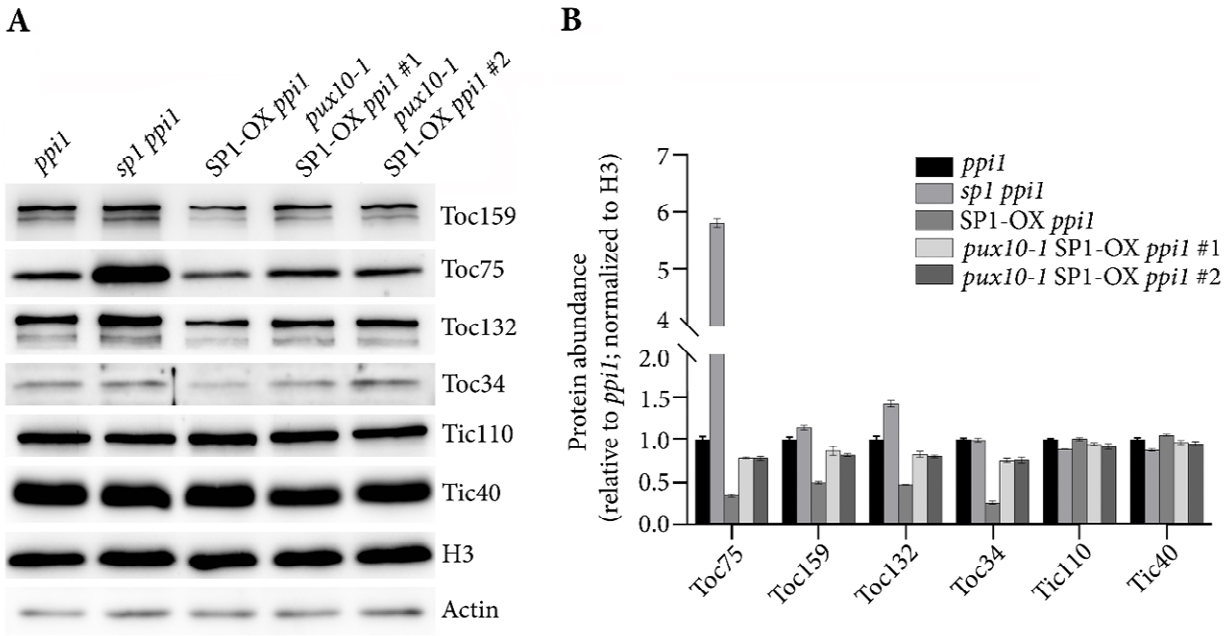


Figure 3.8. **The suppression effect of *pux10-1* mutation in SP1-OX *ppi1* plants is linked to increased TOC protein abundance.** **(A)** Total protein samples extracted from leaves of 4-week-old plants of the indicated genotypes were analysed by immunoblotting using the indicated antibodies. Equal amounts of the different samples were loaded. Actin and histone H3 were used as loading controls. Representative blot images are shown. **(B)** Quantification of the immunoblot data presented in (**A**), and of other similar datasets. The bands were quantified, and the data for each protein were normalized to corresponding data for H3; the data are presented as ratios to the *ppi1* value for each protein. The data reflect three biological replicates. Values shown are means (n = 3) with error bars indicating SEM.

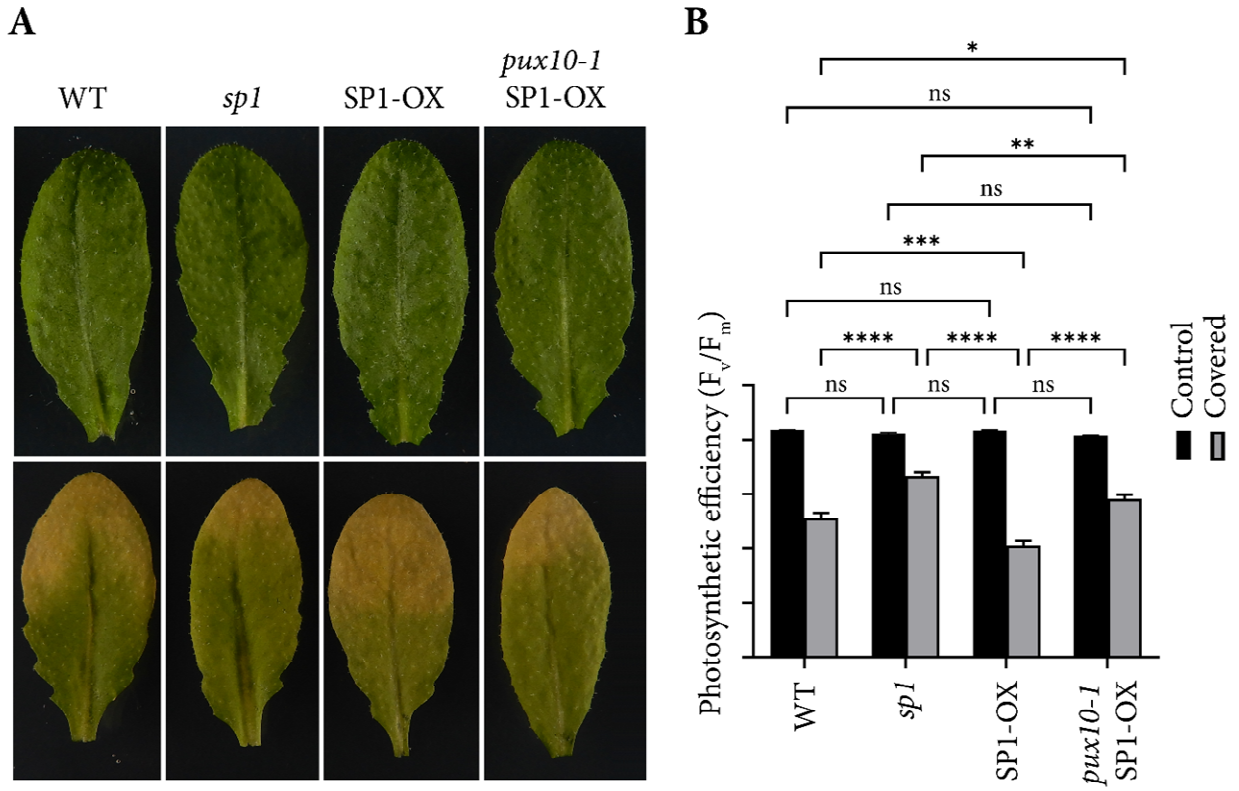


Figure 3.9. PUX10 is required for the SP1-dependent dark-induced leaf senescence. (A) Attached leaves of 4-week-old plants of the indicated genotypes were left uncovered (top; control) or were covered with aluminium foil (bottom; covered), and the plants were kept under standard growth conditions for 5 days before leaf detachment and photography. A representative leaf from each genotype for each condition is shown. (**B**) Maximum photochemical efficiency of photosystem II (F_v/F_m) was measured for leaves similar to those presented in (**A**) using a CF Imager to estimate the extent of senescence. The data were derived from 8 leaves per genotype (for control, uncovered), and 10 leaves per genotype (for senescence, covered). Values shown are means with error bars indicating SEM. The asterisk above the columns indicates the significance of difference (Student's *t*-test: $^{****}P < 0.0001$).

Chapter 4

Results 3

A forward genetic screen for new suppressors of the *ppi1* mutation

4 A forward genetic screen for new suppressors of the *ppi1* mutation

4.1 Abstract

Forward genetics is a phenotype-driven approach for determining the genetic basis responsible for a particular function. The identification of both *SP1* (suppressor of *ppi1* locus 1) and *SP2* (suppressor of *ppi1* locus 2), two key components of the CHLORAD machinery regulating the turnover of chloroplast TOC proteins, was achieved through such a genetic screen: the pale *TOC33* knockout mutant *ppi1* was mutagenized with EMS and plants displaying synthetic recovery phenotypes were isolated and characterized as the suppressors of *ppi1*. Given the importance and complexity of the regulatory mechanisms governing TOC complexes, this forward screen was repeated on a larger scale in the group, prior to this doctoral study, to seek new second-site suppressors of *ppi1*. Around 20,000 *Arabidopsis ppi1* seeds were subjected to EMS mutagenesis, and 64 mutant lines which displayed a greener phenotype than the *ppi1* progenitor were isolated. Of these, a total of 19 mutants were further selected and subjected to secondary screening for potential mutations in either *SP1* or *SP2*. This led to the identification of two new *sp1* alleles and five new *sp2* alleles, and to the discovery of *suppressor of ppi1 locus 3* (*sp3*), which contained no mutations in either *SP1* or *SP2*. Next generation sequencing (NGS) was then applied to map the causative genetic lesions in the genome of *sp3* plants. The following SHOREmap analysis identified eight candidate genes on chromosome 1 bearing various types of mutation. Based on the gene expression and genetic complementation analysis, *SP3* was identified as the gene encoding GIGANTEA, which is a key nucleus-localized regulator of photoperiodic flowering in *Arabidopsis*. The *sp3 ppi1* plants appeared greener but not larger than the *ppi1* progenitor plants; this effect of the *sp3* mutation was linked to obvious increases in leaf chlorophyll content and chloroplast ultrastructure. Although the exact molecular mechanism of

SP3 action in chloroplast development has not yet been characterized, the work presented in this chapter provides a solid foundation for future functional analysis.

4.2 Introduction

As the gateway for thousands of preproteins entering the chloroplast, the TOC complex is crucial for chloroplast development. The need to adapt to changes in developmental and environmental conditions implies that chloroplast protein import is regulated, and indeed such regulation can take place in the cytosol or at the chloroplast envelope. In the past decade, a forward genetic screening approach was applied in the group to search for the suppressors of *ppi1*, the *TOC33* knockout mutant, leading to the identification of two chloroplast membrane-bound proteins, SP1 and SP2. Genetic and biochemical analyses demonstrated that SP1 and SP2, together with the cytosolic ATPase Cdc48, act together to form a complex on the surface of chloroplast that regulates the degradation of TOC proteins. This proteolytic system was termed chloroplast-associated protein degradation (CHLORAD). Identification of the CHLORAD complex pioneeringly shed light on the regulation of the TOC complex (Ling et al., 2019; Ling et al., 2012). Follow-up studies indicated that SP1-mediated remodeling of the TOC complex contributes to organellar proteome changes not only during plant development but also during plant stress responses (Ling & Jarvis, 2015b; Ling et al., 2021). Intriguingly, the discovery of SP1-independent Toc159 degradation via DELLA proteins under low GA in early plant development implied further complexity of the regulation of the TOC complex (Shanmugabalaji et al., 2018).

Suppressor screen is a powerful way to uncover more information about a known gene or mutation, including the identification of other interacting components in a pathway. The functional suppressors act through mechanisms that will likely shed light on the process or gene of interest. To further explore the regulation of plastid protein import, a new, larger forward genetic screen for suppressors of *Arabidopsis ppi1* was conducted in the group, in similar fashion to that which led to the identification of SP1 and SP2. The aim was to search for new factors that are involved in the regulation of chloroplast protein import. The mutagen used was ethyl

methanesulfonate (EMS), an alkylating agent that randomly generates chemical modifications of nucleotides throughout the plant genome, mainly C-to-T changes resulting in C/G to T/A substitutions (Maple & Moller, 2007). As a result, such chemical mutagenesis can be used not only to search for loss-of-function mutants, but also to understand the roles of specific amino acid residues with regard to protein function by generating missense mutations.

Following EMS mutagenesis, a new mutant showing phenotypic suppression of *ppi1* similar to *sp1* and *sp2* was selected and named *suppressor* of *ppi1 locus 3* (*sp3*). The *sp3* mutant was then backcrossed to the *ppi1* single mutant, and the resulting F2 plants were phenotyped. Pooled genomic DNA was extracted from the F2 plants displaying *sp3 ppi1* phenotypes, as well as from the *ppi1* progenitor plants, and these samples were subjected to NGS to determine the order of nucleotides in the entire genome of each group of individuals. The sequenced genomes were subsequently investigated using SHOREmap analysis (Schneeberger et al., 2009) to identify the loci possessing single-nucleotide polymorphisms (SNPs) between the *sp3 ppi1* and *ppi1* genotypes that were heavily skewed (>90%) away from the *ppi1* progenitor genotype, implying linkage to the *sp3* mutant phenotype.

Prior to this doctoral study, a cluster of SNPs showing very strong linkage to the suppressor phenotype of *sp3* was observed on chromosome 1, and the causal mutation for *sp3* was therefore likely to be on this chromosome. However, the exact causative locus for *sp3* had not yet been identified and characterized. During this doctoral study, the identity of the *sp3* locus was confirmed through a series of gene expression and genetic complementation analyses, and an initial functional characterization of SP3 was conducted.

4.3 Result

4.3.1 Forward genetic screen for the *suppressor* of *ppi1 locus 3*

An estimated 20,000 *Arabidopsis ppi1* seeds were subjected to EMS mutagenesis in accordance with a published protocol (Salinas & Sánchez-Serrano, 2006). To aid the following screen, all of

the EMS-mutagenized M1 seeds were sown out in 100 separate batches, roughly divided into two groups, A and B, each containing 50 batches; each batch contained approximately 200 seeds grown in half-sized trays (15.5 x 21 x 5.5 cm). The M1 plants were grown in a greenhouse under standard growth conditions to maturity, and pooled M2 seeds were harvested from each batch. The batches of pooled M2 seeds were then grown *in vitro* on MS medium and systemically screened for plants that appeared greener than *ppi1* (in other words, those with mutations that suppressed the *ppi1* phenotype). These potential suppressor plants were then transferred to soil for growth to maturity for M3 seeds. Those greener plants that have developmental defects were not carried forward for further analysis and were discarded. In total, 195 putative new suppressor mutants were identified: 112 from group A, and 83 from group B.

Of the 112 putative new suppressor mutants from group A, 67 were screened (~60% completed); among these, 22 mutant lines failed to germinate, and 29 lines were identified as greener than *ppi1*. Of the 83 putative new suppressor mutants from group B, all were screened; among these, 35 lines were identified as greener than *ppi1*. Thus, in total, 64 lines were identified to be greener than *ppi1* from both groups (Table 4.1). Given that *sp1* or *sp2* mutations can significantly suppress the chlorosis of *ppi1* plants, 19 out of 64 mutant lines displaying distinctly greener or bigger leaves relative to *ppi1* plants in the M3 generation were selected, and the CDSs of both *SP1* and *SP2* were amplified by PCR from each mutant line and subjected to Sanger sequencing. Of these 19 lines, 17 contained mutations in the CDS of either *SP1* or *SP2*, revealing the identification of two new *sp1* mutant alleles and five new *sp2* mutant alleles (Table 4.2). Two mutant lines, 47B-3 and 28B-2, contained no mutations in either *SP1* or SP2 (Table 4.2). It was worth noting that though the new *sp1* and *sp2* mutant alleles contained different mutations within the genes compared to the previously published *sp1* and *sp2* mutant alleles, they displayed similar phenotypic suppression of the *ppi1* mutation, producing greener and larger leaves with increased chlorophyll content relative to *ppi1* single-mutant plants (Figure 4.1 and 4.2). These observations indicated that the relevant areas within the *SP1* and *SP2* sequences are crucial for function.

In the end, given that the 47B-3 displayed a more distinct phenotype than 28B-2, it was selected as a putative mutant of interest and renamed as *sp3* (*suppressor* of *ppi1 locus 3*). The double-mutant *sp3 ppi1* plants were greener than *ppi1* plants, although they were not completely recovered to the level of *sp1 ppi1* plants (Figure 4.3). It is worth noting that the leaf sizes of *sp3 ppi1* plants were similar to those of *ppi1* plants (Figure 4.3). In addition, 28B-2 remains an interesting *ppi1* suppressor mutant line for future analysis.

4.3.2 Generation of the *sp3* mutant mapping population and genomic sequence datasets

The mapping of the *sp3* mutation in the *ppi1* background was done by NGS combined with computational analysis using the software package SHOREmap v3.6 (Schneeberger et al., 2009; Sun & Schneeberger, 2015). Such a mapping-by-sequencing analysis requires whole-genome sequencing information from an isogenic mapping population as well as the non-mutagenized progenitor.

The isogenic mapping population for *sp3* mutant was obtained by backcrossing the *sp3 ppi1* mutant to the progenitor *ppi1* mutant, followed by selfing of the F1 hybrid to produce F2 seed. In the F_2 generation, leaves of 240 individual plants clearly exhibiting the *sp3 ppi1* phenotype were pooled for genomic DNA extraction. Meanwhile, pooled genomic DNA was also extracted from the plants of *ppi1*, the non-mutagenized progenitor. The generation of the *sp3* mutant mapping population was conducted by Dr Binquan Huang, a previous lab member. The pooled genomic DNA samples from both the mutant mapping population and *ppi1* were sent for NGS at the Wellcome Centre for Human Genomics, Oxford, and genomic sequence datasets were generated.

4.3.3 Identification of candidate loci for *sp3* by using SHOREmap analysis

The computational tool, SHOREmap was applied to the NGS data to identify candidate *sp3* loci that possess SNPs between the mutant mapping population and the progenitor with a heavy

skew (>90%) away from the progenitor, implying a linkage to the *sp3* mutant phenotype. The generation of SHOREmap data was completed by Dr Sabri Ali, a previous lab member.

The SHOREmap analysis identified a cluster of SNPs showing strong linkage to the suppressor phenotype on chromosome 1. Further analysis revealed that eight genes are directly affected by these mutations, with the remainder of the SNPs lying in intronic and intergenic regions (Figure 4.4 and Table 4.3). The mutations in these eight candidate genes displayed allele frequency ranging from 0.84 to 0.94 in the mapping population (Table 4.3); it is likely that these values were less than 1.0 owing to some inaccuracies in the phenotyping of the plants for the mapping population. The mutations in *At1g18740*, *At1g19600* and *At1g25400* each caused an amino acid substitution; however, the amino acid properties were not dramatically changed. The mutations in *At1g20360* and *At1g20430* each affected a single nucleotide (G>A) in the 3' untranslated region (UTR), while that in *At1g20890* affected a single nucleotide (G>A) in the 5' UTR; although mutations in the UTRs can cause problems in gene expression, these are less likely to be loss-of-function mutations. Interestingly, splice site mutations were found in both *At1g20540* and *At1g22770*. A splice site mutation is a genetic mutation in a gene sequence that occurs at the boundary of an exon and an intron (i.e., a splice site) at which splicing takes place during the processing of precursor messenger RNA into mature messenger RNA. Such changes can disrupt RNA splicing resulting in the loss of exons or the inclusion of introns and an altered protein-coding sequence. Therefore, *At1g20540* and *At1g22770* were considered the most likely candidates to be the causative *sp3* locus.

4.3.4 Identification of the causative locus for carrying the *sp3* mutation

To help narrow down the list of *sp3* candidate loci, I firstly used semi-quantitative RT-PCR to compare the expression of seven of the eight candidate genes in *ppi1* single-mutant plants and *sp3 ppi1* double-mutant plants originating from the mutant screen (Figure 4.5). One of these seven candidates, *At1g20360*, could not be amplified in *sp3 ppi1* or *ppi1* using various pairs of primers. Of the others, only the expression of *At1g20540* was significantly reduced in *sp3 ppi1*

plants compared to *ppi1* plants, and the results for this gene showed a multiple banding pattern in *sp3 ppi1* plants consistent with a splicing defect (Figure 4.5). The transcript level of candidate gene *At1g22770* in *sp3 ppi1* plants was not analysed at this stage because the distinct phenotype of *sp3 ppi1* plants, including numerous rosette leaves and significantly delayed flowering, implied functional deficiency of the protein encoded by *At1g22770* as has been reported previously (Kim et al., 2012).

To aid identification of the candidate gene which was indeed responsible for the suppressor phenotype of *sp3 ppi1*, T-DNA insertion mutants for all eight candidate genes were subsequently obtained from NASC (Nottingham Arabidopsis Stock Centre), and genotyped using gene-specific primers (Table 4.4). Surprisingly, two of the three T-DNA lines for *At1g20430* (SALK_103090 and SALK_107587) and the single line for *At1g25400* (SALK_093560) were found to not contain the expected T-DNA insertions, indicating that most likely the wrong seeds had been provided. In addition, no homozygous mutant could be identified for the third T-DNA line for *At1g20430* (SALK_051176), or the single T-DNA line for *At1g20890* (SALK_043518), even though around 60 individual plants were genotyped in each case, indicating the possibility of embryo lethality of the homozygous mutant genotypes. Homozygous T-DNA insertion mutants were confirmed by genotyping for all of the remaining five candidate genes (Table 4.4).

The homozygous T-DNA insertion mutants of the candidate genes were subsequently crossed into *ppi1* background for the production of double mutants. In most cases, the identification of homozygous double mutants was confirmed by genotyping in the F2 and F3 generation using gene-specific primers (Table 4.4).

The resulting double mutants were roughly divided into two groups (Table 4.4). The first group contained *at1g18740 ppi1*, *at1g20360 ppi1*, and *at1g19600 ppi1* in which the single nucleotide mutation occurred in the 3' UTR or caused an amino acid substitution in the encoded protein. In these cases, no significant phenotypic differences were observed between *ppi1* plants and the

double-mutant plants (Figure 4.6). Therefore, the single nucleotide mutations in these three genes were deemed very unlikely to be causative of the phenotypic suppression in *sp3 ppi1*.

Given that the *At1g20540* and *At1g22770* alleles identified in the forward genetic screen were both splice site mutations, which are quite likely to affect gene function, both *at1g20540 ppi1* and *at1g22770 ppi1* were assigned to the second group. The *At1g20540* gene encodes a WD40 repeat-like superfamily protein. Such WD40 repeat proteins have been described as functioning in the CUL4-DDB1 E3 ligase complex as the substrate adaptor component (Biedermann & Hellmann, 2011). However, homozygous *at1g20540 ppi1* mutants arising from the forward genetic screen showed no phenotypic differences from *ppi1* plants following backcrossing and the segregation away of the other candidates mutations (images not included here). Moreover, both T-DNA insertion alleles of *At1g20540* showed no phenotypic suppression of *ppi1*, implying that *At1g20540* was unlikely to be the causal gene of the *sp3* phenotype (Figure 4.7).

Also assigned to the second group was the *At1g22770* gene. This gene encodes the GIGANTEA (GI) protein, which is a plant-specific nuclear protein and plays multiple roles throughout plant development including circadian clock control, flowering time regulation and stress tolerance (Mishra & Panigrahi, 2015). The most distinct phenotype of *gi* mutants is significantly delayed flowering time and numerous rosette leaves. Such phenotypes were also observed in the *gi* mutant identified in the forward genetic screen, which bears a splice site mutation, following backcrossing and the segregation away of the other candidates mutations (images not included here). Two further mutants were obtained from NASC. The first, *gi-1,* generated from X-rays mutation, contains a five-nucleotide deletion in exon 11 (4327-4331 of the genomic sequence) which results in a *GI* coding sequence with premature stop codon (Fowler et al., 1999). The second, GABI_829D10, carries a T-DNA insertion in exon 9 (Figure 4.8 A). GABI_829D10 was named *gi-12* in this study after consideration of the names of published *gi* alleles. Intriguingly, both alleles showed phenotypic suppression of *ppi1*: the *gi-1 ppi1* and *gi-12 ppi1* double-mutant plants were greener than *ppi1* plants and exhibited increased chlorophyll content (Figure 4.8 B).

Notably, the different alleles of *gi* suppressed *ppi1* to varying extents. The *gi-12 ppi1* plants were greener than *gi-1 ppi1* plants and contained a higher amount of chlorophyll (Figure 4.8 B). Interestingly, although the *gi ppi1* double-mutant plants were greener than *ppi1* plants, there was no visible difference in leaf size between the double mutants and *ppi1* single mutants; this is unlike the situation with *sp1 ppi1* plants, where the enhanced greening is accompanied by increased leaf size (Ling et al., 2012). The suppression of *ppi1* mediated by *gi* was considerably weaker than that delivered by *sp1* in relation to leaf chlorophyll content (Figure 4.9).

On the basis of these results, the allelic variant of *gi* identified in the forward genetic screen here was named *gi-13*. As noted earlier, the *gi-13* mutation is a single nucleotide substitution at the splice site between the fourth intron and the fifth exon which can potentially disrupt RNA splicing resulting an altered protein-coding sequence (Figure 4.8 A). The *gi-13 ppi1* double mutant presented here was derived from a double backcrossing of the original EMS mutant. Since multiple mutations occur in plants subjected to EMS mutagenesis, typically 3-4 sequential backcrosses of a new mutant to its progenitor line are necessary to ensure the elimination of most background mutations unrelated to the phenotype of interest. Therefore, the phenotype of the *gi-13 ppi1* mutant needs to be confirmed after further backcrossing to the *ppi1* background. To do this, given that only a single nucleotide substitution is present in the mutant, the presence of the *gi-13* mutation may be followed by using a Derived Cleaved Amplified Polymorphic Sequences (dCAPS) marker (Neff et al., 1998), as was done in generating the preliminary backcrossed line described here. Such dCAPS markers are a widely used approach for the detection of single nucleotide polymorphisms. The principle is that the mutation introduces or destroys a restriction enzyme recognition site in a PCR amplicon generated by using primers that contain one or more mismatches to the template DNA. The PCR product is subjected to restriction enzyme digestion and the presence or absence of the SNP is determined by scoring the resulting restriction pattern. Plants confirmed as being homozygous *gi-13 ppi1* double mutant using this dCAPS method showed a greener phenotype which was reflected in their chlorophyll contents, when compared to the *ppi1* single-mutant plants (Figure 4.10 A).

Thus, all three mutant alleles of *At1g22770/GI,* obtained either from NASC or from the original *ppi1* suppressor screen, appeared to suppress the phenotype of *ppi1*. This provided strong evidence that mutation of *At1g22770/GI* can suppress the *ppi1* mutation**.**

Taken together, these data allow us to provisionally identify *SP3* as *At1g22770/GI*.

4.3.5 Assessing the relationship of *sp3* to chloroplast biogenesis

To determine whether the suppression of chlorosis observed in *gi ppi1* plants was linked to effects on chloroplast biogenesis, the organelles in wild-type, *ppi1*, *gi-1 ppi1*, and *gi-12 ppi1* plants were analysed by TEM. Leaf samples for analysis were taken from plants that had been grown on soil under standard growth conditions. The TEM analysis demonstrated that *gi ppi1* plants possess chloroplasts of similar size to those in *ppi1* plants, but with improved ultrastructure compared to *ppi1* plants (Figure 4.11 A). Quantitative analysis revealed no significant difference in chloroplast cross-sectional area in both *gi ppi1* double mutants relative to *ppi1* (Figure 4.11 B). This was not necessarily surprising since the *gi ppi1* plants displayed no difference in leaf size compared to *ppi1* plants. However, there was an increased number of thylakoid lamellae per granal stack, and an increased number of interconnections between granal stacks, in both *gi ppi1* double-mutant chloroplasts relative to *ppi1* chloroplasts (Figure 4.11 C). However, the overall development of chloroplasts in *gi ppi1* was still less than that in wild type, which was consistent with the visible difference between the *sp3 ppi1* and wild-type plants.

4.3.6 Analysing the subcellular localization of SP3/GI

To begin to understand the functional mechanism whereby SP3/GI affects chloroplast biogenesis, I used yellow fluorescent protein (YFP) fusion of SP3/GI to assess the subcellular localization of the protein. The coding sequence (CDS) of *SP3/GI* gene (encoding an open reading frame of 1173 amino acids) was cloned into the p2GWY7 vector bearing a 35S promoter and sequence encoding a YFP tag. The resulting construct was used to transfect protoplasts isolated from wild-type *Arabidopsis* rosette leaves, and YFP signals were visualized by a confocal microscopy

(Figure 4.12). The SP3/GI protein was found to distribute in the nucleus and the punctate spots of SP2/GI-YFP fluorescence were observed when transiently expressed in this way (Figure 4.12). Previous studies indicated that the punctate type of GI localization implies the formation of nuclear bodies (Kim et al., 2013a).

4.4 Discussion

Suppressor screens provide a powerful way to uncover more information about a known gene or mutation, as well as to identify other interacting components in a pathway. A suppressor screen starts simply with a known mutant and then identifies second-site mutations that suppress the original mutant phenotype. One classical example is the *ppi1* (a *TOC33* knockout mutant) suppressor screen carried out in the last decade by the Jarvis lab. In this screen, *ppi1* seeds were mutagenized with EMS and the resulting M2 population was screened for the suppression of the *ppi1* chlorotic phenotype; Such suppressors possessed greener and bigger leaves. From this screen, two genes, *SP1* and *SP2*, were identified. The characterization of SP1 and SP2 brought pioneering breakthroughs concerning the regulation of plastid protein import, which is crucial for plastid biogenesis.

Following the identification of *SP1* and *SP2* through the initial *ppi1* suppressor screen (which was based on just ~7,000 M1 individuals), a second, much larger mutant screen for *ppi1* suppressors (of ~20,000 M1 individuals) was carried out using the same methods. This second screen led to the identification of *suppressor* of *ppi1 locus 3* (*sp3*), which was the main focus of this chapter. Inevitably, several of the new mutants displaying robust phenotypic suppression of *ppi1* contained mutations in either *SP1* or *SP2* rather than in novel genes. These mutants were identified via Sanger sequencing and were excluded from the following steps. In total, two new alleles of *sp1* and five new alleles of *sp2* were identified from this screen (Table 4.2).

The new *sp1-5* mutant contains a G to A nucleotide substitution in the coding region of the intermembrane space domain of SP1 (SP1ims). This mutation introduces a premature stop

codon into *SP1ims* coding sequence, resulting in a greatly shortened SP1 protein (98 amino acids instead of 343 amino acids for the full-length protein). Such a truncated SP1 protein would undoubtedly be dysfunctional. The new *sp1-4* mutant contains a G to A nucleotide substitution, and intriguingly this also lies in the *SP1ims* region. The s*p1-4* mutation causes a glycine to glutamic acid substitution (G165E), which is a non-conservative substitution and therefore quite likely to affect protein function (Figure 4.1). Both new alleles of *sp1* display suppression phenotypes that are highly consistent to those of previously identified *sp1* alleles, which are null alleles (Ling et al., 2012). This suggests that the single amino acid change in the new *sp1-4* causes a severe effect on SP1 protein function. The SP1 protein is an integral chloroplast OEM protein with two transmembrane spans that separate the protein into two major parts: a cytosolic RING domain and the IMS domain. While the RING domain interacts with cytosolic UPS components, such as E2 ubiquitin conjugating enzyme, in order to mediate ubiquitination of TOC proteins, the IMS domain has been shown to mediate interaction with TOC components (Ling & Jarvis, 2015a). Because of their small size with the shortest side chain, glycine residues can adopt a wide range of conformations that are rarely seen with other amino acids. Glycine thus plays a structurally very important role. Consequently, glycine residues at specific positions in the sequences of proteins are often evolutionarily conserved in order to maintain the overall architecture (Branden & Tooze, 1999). Thus, the glycine residues in the SP1ims domain are conceivably very important for SP1's role in recognizing TOC proteins, and their substitution could cause binding affinity changes and defective protein interactions. It was previously reported that a single glycine substitution to the polyglycine region in the transit peptide of Pea Toc75 leads to its mistargeting (Baldwin & Inoue, 2006), which provides support for the notion that glycine residues can be important for protein-protein interactions involving the TOC machinery in the OEM.

For the new alleles of *sp2*, new *sp2-5* carries a six-nucleotide deletion which results in the loss of two amino acids from the N-terminus of SP2 ahead of the first transmembrane span (Table 4.2). This deletion clearly has a weaker influence on SP2 function, based on the paler phenotype of

sp2-5 compared to other *sp2* alleles in *ppi1* background. In contrast, the other four new *sp2* alleles all display strong suppression on the phenotype of *ppi1* (Figure 4.2). Each of these four alleles contains a single amino acid substitution, as follows: glycine to aspartic acid (G105D) in new *sp2-6*, aspartic acid to asparagine (D296N) in new *sp2-7*, histidine to tyrosine (H148Y) in new *sp2-8*, and arginine to lysine (R34K) in new *sp2-9* (Table 4.2). Apart from that in *sp2-9*, these amino acid substitutions are major changes involving the replacement of one amino acid by another with very different physicochemical properties. Such substitutions can result in changes of protein structure or function. One of the previously reported alleles, *sp2-3*, also carries a glycine substitution, similar to new *sp2-6*, though in this case it is replaced with arginine and it is located at a different position (G291R) in the amino acid sequence (Ling et al., 2019). The arginine to lysine replacement in new *sp2-9* is a conservative replacement as the amino acid is exchanged for one with similar biochemical properties: both arginine and lysine are amino acids with positively charged side chains. A similar substitution exists in the previously reported *sp2-2* allele, where an arginine is replaced by a histidine (R261H). Though such conservative substitutions rarely cause severe dysfunction in the corresponding protein, arginine has been shown to play special roles in protein interfacial binding and membrane perturbation, relative to other charged amino acids (Li et al., 2013b). Given that SP2 forms a protein retrotranslocation channel in the chloroplast OEM, these properties may be especially important for its role. Both *sp2* alleles with an arginine substitution (i.e., *sp2-2* and new *sp2-9*) display strong suppression of the chlorotic phenotype of *ppi1*, indicating that the relevant arginine residues (261 and 34, respectively) are crucial for the function of SP2.

The mapping-by-sequencing analysis for *sp3* narrowed down the analysis to eight genes on *Arabidopsis* chromosome 1, each one containing a SNP (Table 4.3). Three of the candidate genes, *At1g20360*, *At1g20430* and *At1g20890*, have mutations in either the 5' or 3' UTR region. For *At1g20360*, double-mutant plants resulting from crosses between a T-DNA insertion mutant and *ppi1* displayed no phenotypic suppression, indicating that *At1g20360* is unlikely to be the causative gene (Figure 4.6). For *At1g20430* and *At1g20890*, no homozygous double mutants

could be identified in the F2 populations resulting from crosses between T-DNA insertion mutants and *ppi1*, indicating that null mutations of these two genes are likely embryonically lethal. However, the heterozygous double-mutant plants displayed no phenotypic suppression compared to *ppi1* plants, indicating that *At1g20430* and *At1g20890* are also unlikely to be responsible for the *sp3* phenotype.

In other candidate genes, the relevant mutation caused a non-conservative amino acid substitution, as follows: proline to leucine in *At1g18740* (P283L), arginine to serine in *At1g19600* (R122S), and glycine to glutamine acid in *At1g25400* (G138E). For *At1g18740* and *At1g19600*, homozygous double-mutant plants resulting from crosses between T-DNA insertion mutants and *ppi1* showed no phenotypic differences compared to *ppi1* plants, indicating that these two genes are unlikely to be causative for *sp3* (Figure 4.6). For At1g25400, however, the T-DNA insertion mutant obtained from NASC was found to have no T-DNA insertion according to PCR-based genotyping. Thus, it is very likely that the wrong seeds had been sent by the stock center. While it would have been possible to request a new batch of mutant seeds, this ultimately seemed unnecessary when conclusive results were obtained for one of the other candidates (see below).

In the final two candidates, *At1g20540* and At1g22770, a splice site mutation was present. Such mutations can seriously affect gene function. Precursor messenger RNA (pre-mRNA) splicing is a regulated process in eukaryotic gene expression in which introns are removed from primary RNA transcripts and exons are spliced together to form the mature mRNA which subsequently migrates to the cytoplasm for translation. To carry out the splicing reaction, specific sequences around the exon-intron boundaries in the pre-mRNA must be correctly recognized by the spliceosome. The first and last two positions of each intron are the most highly conserved positions, and mutating these nucleotides can disrupt RNA splicing resulting in the loss of exons or the inclusion of introns and an aberrant protein-coding sequence (Yeo & Burge, 2004). Nonetheless, the *At1g20540* splice site mutation allele (as well as two T-DNA insertion alleles)

did not display any obvious phenotypic suppression of *ppi1*, clearly indicating that *At1g20540* is unlikely to be causative for *sp3* (Figure 4.7).

The second candidate with a splice site mutation, At1g22770, encodes the GI protein which is a key regulator of photoperiodic flowering in *Arabidopsis*. The typical phenotype of *gi* mutants includes greatly delayed flowering and numerous rosette leaves; and, significantly, such phenotypes were observed in the *sp3* mutant, which possesses the *At1g22770* splice site mutation. Moreover, this splice site allele, along with two additional alleles of *gi* mutant obtained from stock center, showed phenotypic suppression to the *ppi1* mutation, albeit to varying extents (Figure 4.8 and 4.10). Therefore, it was concluded that *At1g22770* is the casual *sp3* locus, and three mutant alleles were termed as *gi-1*, *gi-12*, and *gi-13*.

The different levels of *ppi1* suppression mediated by the different *sp3* mutant alleles is very likely related to differences in the properties of the mutations. The *gi-1* contains a five-nucleotide deletion in exon 11 of the *GI* coding sequence, resulting in a truncated protein C-terminus (the loss of 171 amino acids from a total of 1173 residues). A possible explanation for the effect of *gi-1* is that the mutation causes decreased stability of the *GI* transcript or protein because of truncation. On the other hand, *gi-12* and *gi-13*, which bear a T-DNA insertion in the ninth exon and a splice site mutation in the last nucleotide of the fourth intron, respectively, most likely produce more aberrant proteins (Figure 4.8 and 4.10). The differing nature of the mutations was also reflected in the different growth habits of the mutants. The new *gi-13* plants, containing the splice site mutation, displayed the most significant delay in flowering time, relative to wild-type plants, with the *gi-12* and *gi-1* mutants displaying intermediate and weak flowing delays, respectively (data not shown). The *gi-1* mutant also showed weaker suppression of *ppi1*, compared to *gi-12* and *gi-13*. It is worth noting that none of the three *gi* mutant alleles abolished flowering, indicating that *GI* promotes flowering but is not essential for its occurrence.

GI is a unique plant protein, first identified in 1962 as a late flowering mutant (*gi)* in *Arabidopsis* (Redei, 1962). Expression of *GI* is ubiquitously detected throughout plant development (Fowler

et al., 1999; Park et al., 1999). GI has pleiotropic functions in diverse plant developmental processes including photoperiodic flowering, light signaling, regulation of circadian rhythms, and response to stress (Brandoli et al., 2020b). Using an *Arabidopsis* protoplast transient expression system, a GI-YFP fusion protein localized in the nucleus and the nuclear bodies were observed (Figure 4.12). As described in previous reports, the formation of GI nuclear bodies is a light-dependent event in which EARLY FLOWERING 4 (ELF4), which dynamically oscillates in abundance under diurnal conditions, physically sequesters GI from the nucleoplasm to prevent GI from binding to the *CONSTANS* (*CO*) promoter, leading to the inhibition of *CO* transcription (Kim et al., 2013a). Such a subnuclear compartmentalization of GI by ELF4 plays a crucial role in the regulation of photoperiodic flowering. Interestingly, the cytosol-localized F-box protein ZEITLUPE (ZTL) was found to sequester GI to the cytosol where it acts as the cochaperone of Hsp90 to stabilize the ZTL, a circadian photoreceptor, under blue light (Cha et al., 2017). Both *in vitro* interaction analysis and *in vivo* transient coexpression in *Nicotiana benthamiana* indicated that ZTL directly interacts with GI through its N-terminal LOV (light, oxygen or voltage sensing) domain (Kim et al., 2013b; Kim et al., 2007). This potentially places GI in a position to interact with the chloroplast surface, or with cytosolic factors that regulate chloroplast protein import or homeostasis. Therefore, similar *in vitro* and *in vivo* protein interaction analysis can be employed to address such a hypothesis.

Here, the analysis of different *Arabidopsis gi* mutants revealed the functions of GI in chloroplast biogenesis. Previously, the analysis of different *gi* mutants suggested a novel role of GI in chlorophyll accumulation and chloroplast biogenesis. The *Arabidopsis gi-2* mutant was reported to show reduced sensitivity to lincomycin, a chloroplast biogenesis (translation) inhibitor, and maintaining high levels of photosynthetic proteins and chlorophyll content, whereas *GI* overexpressing plants responded in the opposite way (Cha et al., 2019). The authors interpreted this to indicate that GI inhibits chloroplast biogenesis by regulating photosynthetic protein accumulation. Moreover, *gi* mutants in *Arabidopsis* L*er* background (*gi-3*, *gi-4* and *gi-5*) showed an increased tolerance to paraquat toxicity and a significantly higher chlorophyll content in

seedlings compared to wild-type seedlings (Kurepa et al., 1998). In addition, silencing of one *GI* paralogue, *Petunia hybrida GI1* (*PhGI1*), in Petunia led to leaves with a greener appearance in the apical region with increased chlorophyll content compared to wild-type plants (Brandoli et al., 2020a). Surprisingly, no further analyses were conducted in these two studies to uncover the relationship between GI and chloroplast biogenesis even though the significantly increased level of chlorophyll content in *gi* plants was observed. Nevertheless, these results point to a general role of GI in chlorophyll homeostasis. Similarly, the data presented in this chapter showed that double-mutant *gi ppi1* plants were greener than *ppi1* plants, though there was no obvious difference in leaf size between *gi ppi1* and *ppi1* plants as observed in the *sp1 ppi1* plants (Figure 4.9 and 4.10). This greening phenotype was reflected in the chloroplast ultrastructural organization (Figure 4.11): although chloroplasts of *gi ppi1* plants were not larger than those in *ppi1*, they did have more developed thylakoids than *ppi1* chloroplasts.

Although many thylakoid proteins are encoded by the chloroplast genome, about half of them are nuclear-encoded and synthesized in the cytosol as precursors before being imported via the TOC-TIC complexes (Zhu et al., 2022). Given that GI is a plant-specific nuclear protein and a transcriptional regulator, it would be interesting to compare transcript abundances for several nuclear photosynthetic genes in the leaves of wild-type, *ppi1* and *gi ppi1* plants. This might give an indication as to whether the effect of GI on chloroplast biogenesis is mediated through transcriptional regulation of photosynthesis genes, for example by countering the effects of golden2-like (Glk) transcription factors that promote the expression of photosynthesis genes (Waters et al., 2009; Yeh et al., 2022). Moreover, immunoblotting analysis would elucidate whether any detected transcript changes are reflected in the abundance of photosynthetic proteins.

It would also be worthwhile to examine whether the expression of TOC genes is modulated by GI. A role in controlling the expression of translocon genes was previously revealed for chloroplast import apparatus 2 (CIA2), a transcription factor that increases chloroplast protein

import by up regulating the expression of the *TOC33* and *TOC75* genes in *Arabidopsis* (Sun et al., 2009). It would be interesting to explore whether GI acts as a negative regulator of TOC genes during chloroplast biogenesis. Of course, immunoblotting would be needed to assess whether TOC protein abundancies are also affected. If they are, chloroplast protein import assays could be conducted to determine if GI affects protein import, by comparing protein import efficiencies between wild-type, *ppi1*, and *gi ppi1* plants. All these analyses would help us to understand whether and how *GI* participates in the regulation of chloroplast protein import and plastid biogenesis. Although my subcellular localization analysis indicated that GI is a nuclear-localized protein, previous results indicated that GI is present in both the nucleus and the cytosol, and that it associates with different partners (Huq et al., 2000; Kim et al., 2007). Therefore, it will also be necessary to examine whether GI can physically interact with the CHLORAD components and TOC proteins at the chloroplast surface.

Taken together, the preliminary data presented in this chapter imply a role for GI, a well-studied plant-specific protein that regulates flowing time, in plastid biogenesis, probably through the regulation of chloroplast protein import. There was no time to further investigate this interesting hypothesis during the course of this project, but in the future, a series of molecular, biochemical and genetic experiments should be conducted to pursue these ideas.

4.5 Tables and figures

Table 4.1 A list of M3 lines that were secondarily screened for greener *ppi1* suppressor phenotypes

Group A						Group B			
1A-5	6A-2	12A-8	26A-6	34A-5	44A-3	1B	28B-3	37B-6	41B-2
1A-5b	6A-3	13A-1	27A-4	35A-1	44A-5	3B	28B-4	37B-7	42B
1A-6	6A-5	13A-3	27A-5	35A-2	44A-6	4B-1	28B-5	37B-8	43B-3
1A-7	7A-1	13A-5	27A-6	35A-3	45A-1	4B-2	30B-1	37B-9	44B-3
1A-11	7A-3	13A-7	27A-8	36A-4	45A-3	14B-1	30B-2	38B-1	44B-4
2A-1	7A-4	14A-2	28A-1	37A-1	45A-4	14B-2	30B-3	38B-2	44B-5
2A-2	7A-5	15A-6	28A-2	37A-2	45A-5	14B-3	30B-4	38B-6	44B-6
2A-3	8A-1	15A-8	28A-3	37A-4		15B	34B-1	38B-7	45B-1
2A-4	8A-2	16A-2	28A-4	37A-5		18B	34B-2	38B-8	46B-1
2A-7	8A-3	17A-1	29A-2	38A-1		21B-1	34B-3	38B-9	46B-2
2A-8	8A-4	17A-4	29A-3	39A-4		24B-1	34B-4	38B-10	46B-3
2A-9	9A-3	17A-6	32A-2	39A-6		24B-2	34B-5	38B-11	46B-4
2A-10	10A-1	17A-7	32A-3	40A-1		24B-3	34B-6	38B-12	46B-6
3A-1a	10A-2	18A-1	32A-4	40A-2		24B-4	34B-7	38B-13	47B-1
3A-1b	10A-3	20A-1	32A-5	40A-3		26B	34B-8	39B-2	47B-3
3A-2	10A-4	20A-4	32A-6	40A-4		27B-2	34B-9	39B-3	47B-4
3A-3	11A-1	20A-6	33A-1	41A-1		27B-3	34B-10	39B-4	48B-2
4A-1a	11A-2	20A-9	33A-2	41A-2		27B-4	35B	40B-1	48B-3
4A-1b	11A-4	21A-2	33A-3	41A-5		27B-5	36B	40B-3	48B-4
5A-2	11A-6	23A-5	33A-4	44A-1		28B-1	37B-1	40B-4	48B-8
5A-4	12A-2	24A-5	34A-2	44A-2		28B-2	37B-3	41B-1	

Highlighting indicates the outcome of M3 screening: Red - no germination; Green – greener phenotype observed; Grey - no phenotypic difference from *ppi1* observed. The original mutant screen was conducted by Alistair Haslam and Dr Saumya Awasthi. This further screen was performed by Dr Binquan Huang.

Table 4.2 Screening for *sp1* and *sp2* alleles

Line	Position of mutation[1]	WT sequence around mutation position[2]	Mutation	Effect of mutation	Mutant	Contributor
sp1						
27B-3	494	CTTGGAGT	GGA→GAA	Gly → Glu	*sp1-4**	Alistair Haslam
44B-5						
21B						
38B-12	294	TCTTGGGT	TGG→TGA	Trp → stop codon	*sp1-5**	
41B-1						
sp2						
4B-2	926	CCCCGGAAACC	G missing	truncated protein	*sp2-1* (Ling et al., 2019)	Alistair Haslam
14B-1						
20A-9						
34B-7						
30B-3						
7A-5	29-34	CTGGTAGAGCC	GTAGAG missing	two aa missing	*sp2-5**	Sabri Ali
3A-3	314	CACGGCACC	GGC→GAC	Gly → Asp	*sp2-6**	Sabri Ali
17A-4	886	TTCTTGGAT	GAT→AAT	Asp → Asn	*sp2-7**	Sabri Ali
35B						Alistair Haslam
2A-4	442	GAGCATG	CAT→TAT	His → Tyr	*sp2-8**	Sabri Ali
9A-3	101	TTCAGGGA	AGG→AAG	Arg → Lys	*sp2-9**	Sabri Ali
26B						Alistair Haslam
47B-3						Alistair Haslam
28B-2						

[1] Relative to start codon in genomic sequence.

[2] Underling indicates the nucleotides mutated in EMS.

* New alleles. Data shown in this table was produced by Dr Sabri Ali.

Table 4.3 Summary of the candidate mutations for *sp3* as identified by SHOREmap analysis

Genomic position (Ch.1)	Genetic locus	Frequency of SNP	Reference base	Mutant base	Nature of mutation	Amino acid substitution	Description	Putative subcellular localization
6464972	AT1G18740.1	0.85	C	T	Missense	P>L	ROH1, putative (DUF793)	chloroplast, integral component of membrane
6779606	AT1G19600.1	0.87	G	C	Missense	R>S	pfkB-like carbohydrate kinase family protein	cytoplasm
7046629	AT1G20360.1	0.9	G	A	3' UTR		F-box family protein	mitochondrion
7083344	AT1G20430.1	0.84	G	A	3' UTR		hypothetical protein	chloroplast, mitochondrion
7113307	AT1G20540.1	0.9	G	A	Splice site		transducin/WD40 repeat-like superfamily protein	Cul4-RING E3 ubiquitin ligase complex, nucleus
7267236	AT1G20890.1	0.94	G	A	5' UTR		caveolin-1 protein	integral component of membrane
8063420	AT1G22770.1	0.94	G	A	Splice site		GIGANTEA	cytoplasm, nucleoplasm, nucleus
8911917	AT1G25400.1	0.93	C	T	Missense	G>E	transmembrane protein	integral component of membrane, nucleus

Table 4.4 Summary of the obtained mutant lines for the eight candidate genes

Genetic locus	Mutant line	Mutation type	Insertion site	Genotyping outcome	Double mutant identification (after crossing to *ppi1*)	Analysis group
AT1G18740.1	SALK_020993	Insertion	Exon	Homozygous	Homozygous *At1g18740 ppi1*	1st group
	SALK_019913	Insertion	Exon	Homozygous	Not crossed	
AT1G19600.1	SALK_003847	Insertion	Intron	Homozygous	Homozygous: *At1g19600 ppi1*	1st group
	SAIL_1211_G03	Insertion	Exon	Heterozygous	Not crossed	
AT1G20360.1	SALK_047784	Insertion	Exon	Homozygous	Not crossed	
	SALK_110612	Insertion	Exon	Homozygous	Homozygous *At1g20360 ppi1*	1st group
AT1G20430.1	SALK_051176	Insertion	Exon	Heterozygous	Heterozygous *At1g20430/+ ppi1*	
	SALK_103090	Insertion	Exon	No insertion	Not crossed	
	SALK_107587	Insertion	Exon	No insertion	Not crossed	
AT1G20540.1	SALK_026098	Insertion	Exon	Homozygous	Homozygous *At1g20540-1 ppi1*	2nd group
	SAIL_1158_D07	Insertion	Intron	Homozygous	Homozygous *At1g20540-2 ppi1*	2nd group
AT1G20890.1	SALK_043518	Insertion	Intron	Heterozygous	Heterozygous *At1g20890/+ ppi1*	
AT1G22770.1	*gi-1*	Deletion	Exon	Homozygous	Homozygous *At1g22770-1 ppi1*	2nd group
	GABI_829D10	Insertion	Exon	Homozygous	Homozygous *At1g22770-2 ppi1*	2nd group
AT1G25400.1	SALK_093560	Insertion	Exon	No insertion	Not crossed	

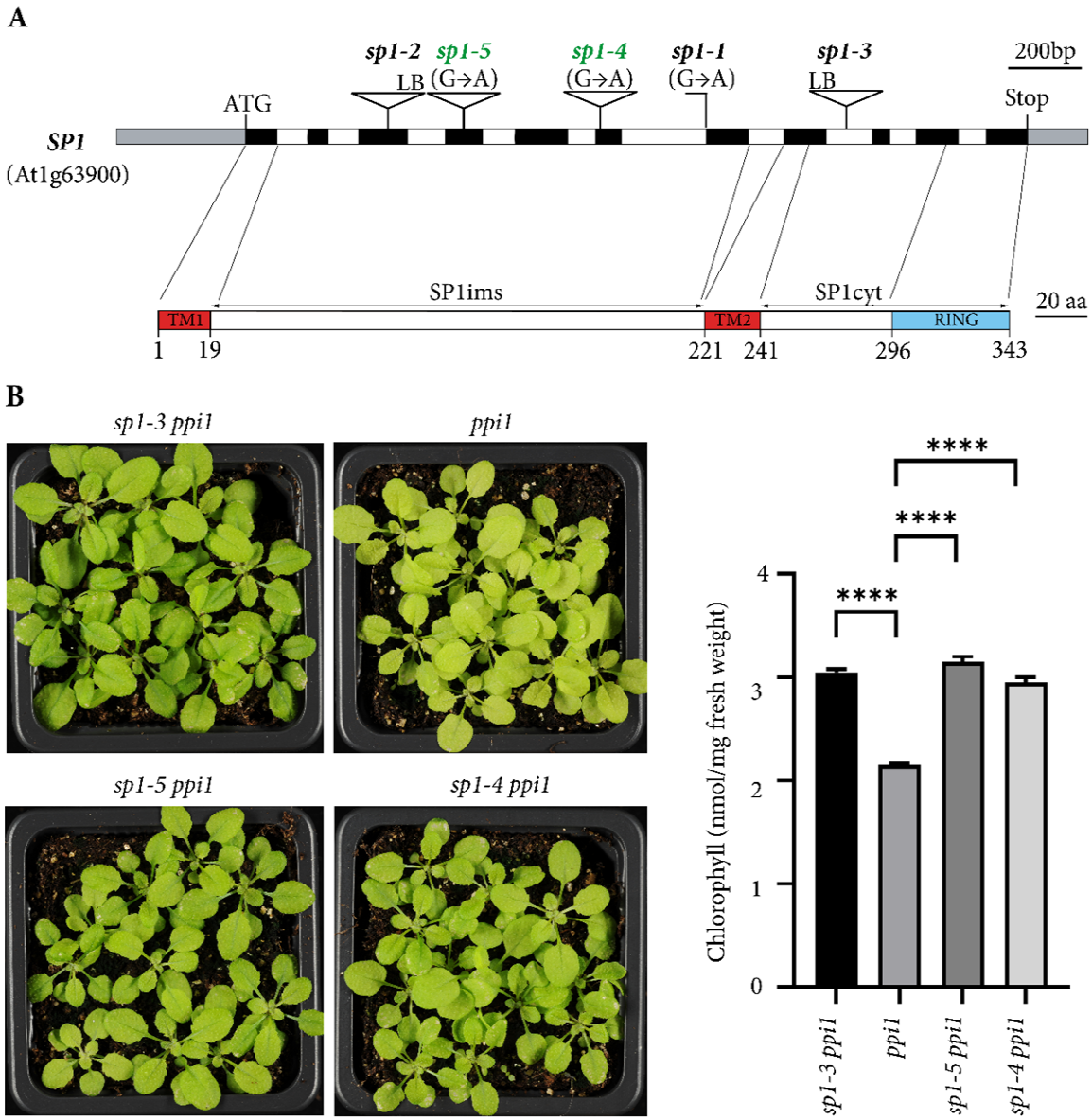


Figure 4.1. New alleles of *sp1* identified in the genetic screen that produced *sp3*. **(A)** Schematic diagram showing the new and previously identified alleles of *sp1* in the context of the *SP1* gene (top) and SP1 protein (bottom) (Ling et al., 2012). In the *SP1* gene model, the positions of the three previously characterized *sp1* alleles (*sp1-1*, *sp1-2* and *sp1-3*), and the two new *sp1* alleles from this study (*sp1-4* and *sp1-5* highlighted in green) are indicated. The *sp1-1* allele and the two new alleles possess single nucleotide substitutions (indicated), whereas *sp1-2* and *sp1-3* are T-DNA insertion alleles. Black boxes = exons; interconnecting white boxes = introns; grey boxes =

untranslated regions; LB = left border sequences of the T-DNA insertions; ATG = translation initiation codon; Stop = translation termination codon. In the corresponding protein model below, the domain architecture of SP1 is shown: TM domains are shown in red, RING domain is shown in blue, and the regions of the intermembrane space (SP1ims) and cytosolic domain (SP1cyt) are shown with arrows. **(B)** Phenotypic analysis of the two new *sp1* alleles in *ppi1* background. **Left:** Visible appearance of the *sp1-4 ppi1* and *sp1-5 ppi1* mutants. The plants were grown under standard conditions on soil for 26 days before photography, and representative plants are shown. Similar camera settings were employed to record all images. All of the images are at the same magnification. **Right:** Quantification of chlorophyll concentration in the new *sp1* mutants in the *ppi1* background, and in control plants. Measurements were taken on the day of photography. Chlorophyll in similar amounts of leaf tissue for each genotype was extracted in organic solvent and quantified using a spectrophotometer, and the data were converted to chlorophyll per fresh weight values using a published equation. Values shown are means (n=5) with error bars indicating SEM. Asterisks above the columns indicate the significance of differences (Student's *t*-test: $^{****}P < 0.0001$).

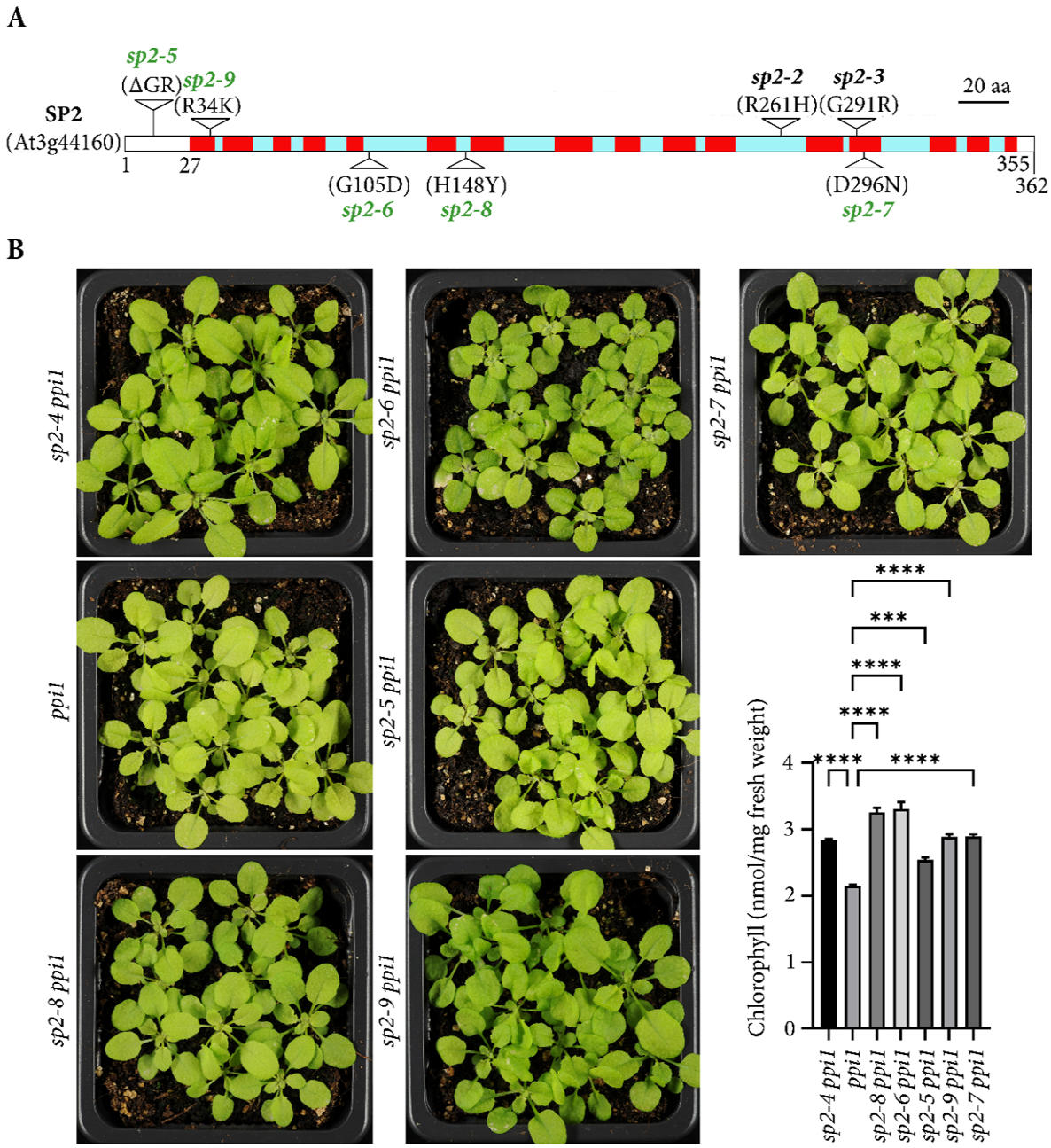


Figure 4.2. New alleles of *sp2* identified in the genetic screen that produced *sp3*. (A) Schematic diagram showing the new and previously identified alleles of *sp2* in the context of the SP2 protein. The positions of two of the four previously characterized *sp2* alleles (*sp2-2* and *sp2-3*), and the five new *sp2* alleles from this study (*sp2-5* to *sp2-9* highlighted in green), are indicated. All of indicated alleles cause an amino acid substitution or deletion, as indicated in parentheses; for the substitutions, the numbers show the position of the affected residue. G, glycine; D,

aspartic acid; N, asparagine; H, histidine; Y, tyrosine; R, arginine; K, lysine. Red boxes = predicted transmembrane β-strands, blue boxes = connecting loop between the β-strands. The transmembrane β-strands were predicted with Phyre2 (Kelley et al., 2015). **(B)** Phenotypic analysis of five new *sp2* alleles in the *ppi1* background. **Left:** Visible appearance of *sp2-5 ppi1*, *sp2-6 ppi1*, *sp2-7 ppi1*, *sp2-8 ppi1* and *sp2-9 ppi1* mutants. The plants were grown under standard conditions on soil for 26 days before photography, and representative plants are shown. Similar camera settings were employed to record all images. All of the images are at the same magnification. **Bottom right:** Quantification of chlorophyll concentration in the new *sp2* mutants in the *ppi1* background, and in control plants. Measurements were taken on the day of photography. Chlorophyll in similar amounts of leaf tissue for each genotype was extracted in organic solvent and quantified using a spectrophotometer, and the data were converted to chlorophyll per fresh weight values using a published equation. Values shown are means (n=5) with error bars indicating SEM. Asterisks above the columns indicate the significance of differences (Student's *t*-test: $^{****}P < 0.0001$).

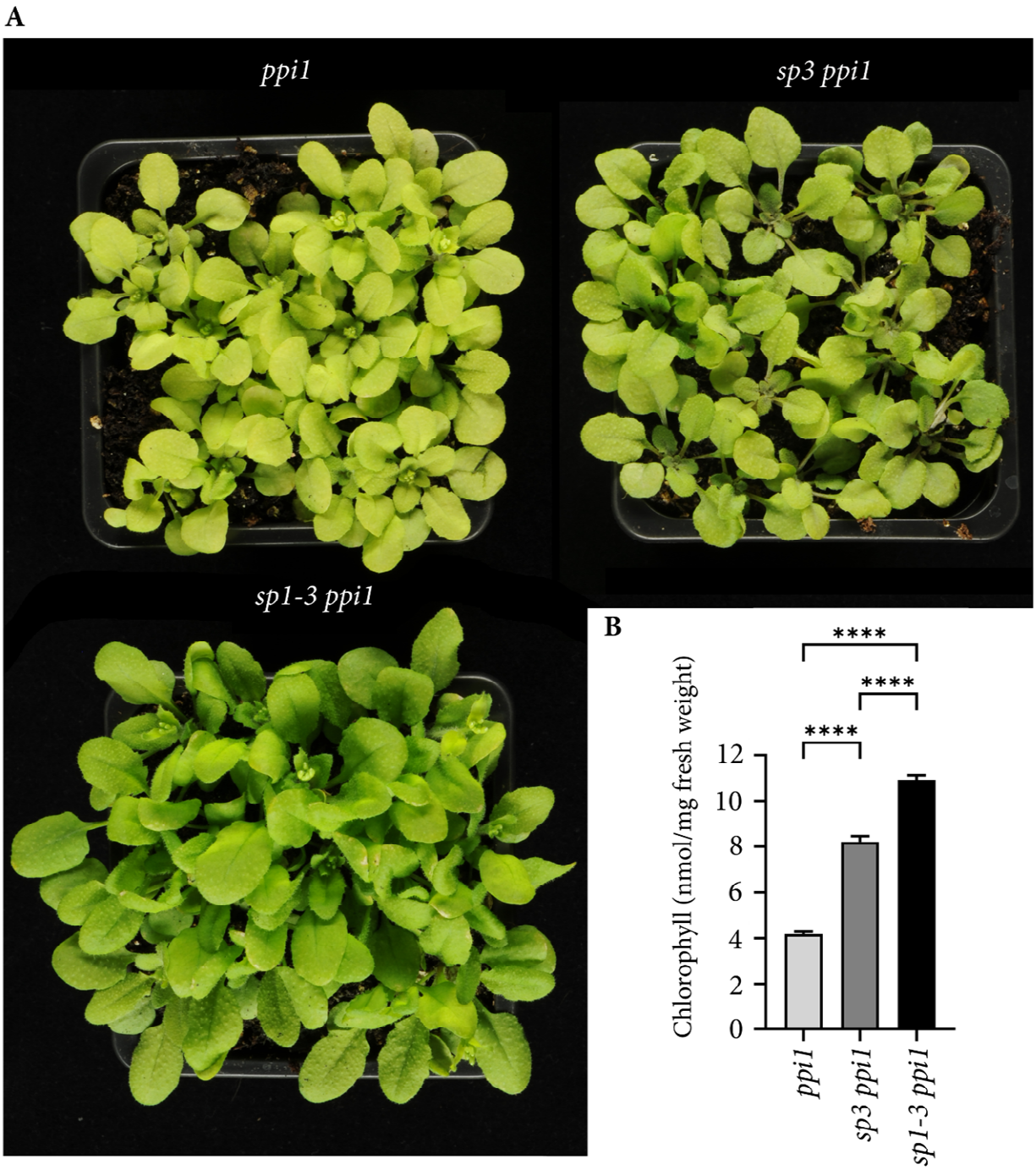


Figure 4.3. Phenotypic analysis of the *sp3* mutant in the *ppi1* background. (A) Visible appearance of the *sp3 ppi1* (47B-3) double-mutant. Plants were grown under standard conditions on soil for 32 days before photography, and representative plants are shown. Similar camera settings were employed to record all images. All of the images are at the same magnification. The *sp3 ppi1* (47B-3) double mutant was greener than ppi1 plants, but paler than

sp1 ppi1 plants. **(B)** Quantification of chlorophyll concentration in the *sp3 ppi1* double mutant, and in control plants. Measurements were taken on the day of photography. Leaves were analysed using a Konica-Minolta SPAD-502 meter, and the meter values were converted to chlorophyll per fresh weight values using a verified calibration equation. Values shown are means (n=15) with error bars indicating SEM. Asterisks above the columns indicate the significance of differences (Student's *t*-test: $^{****}P < 0.0001$).

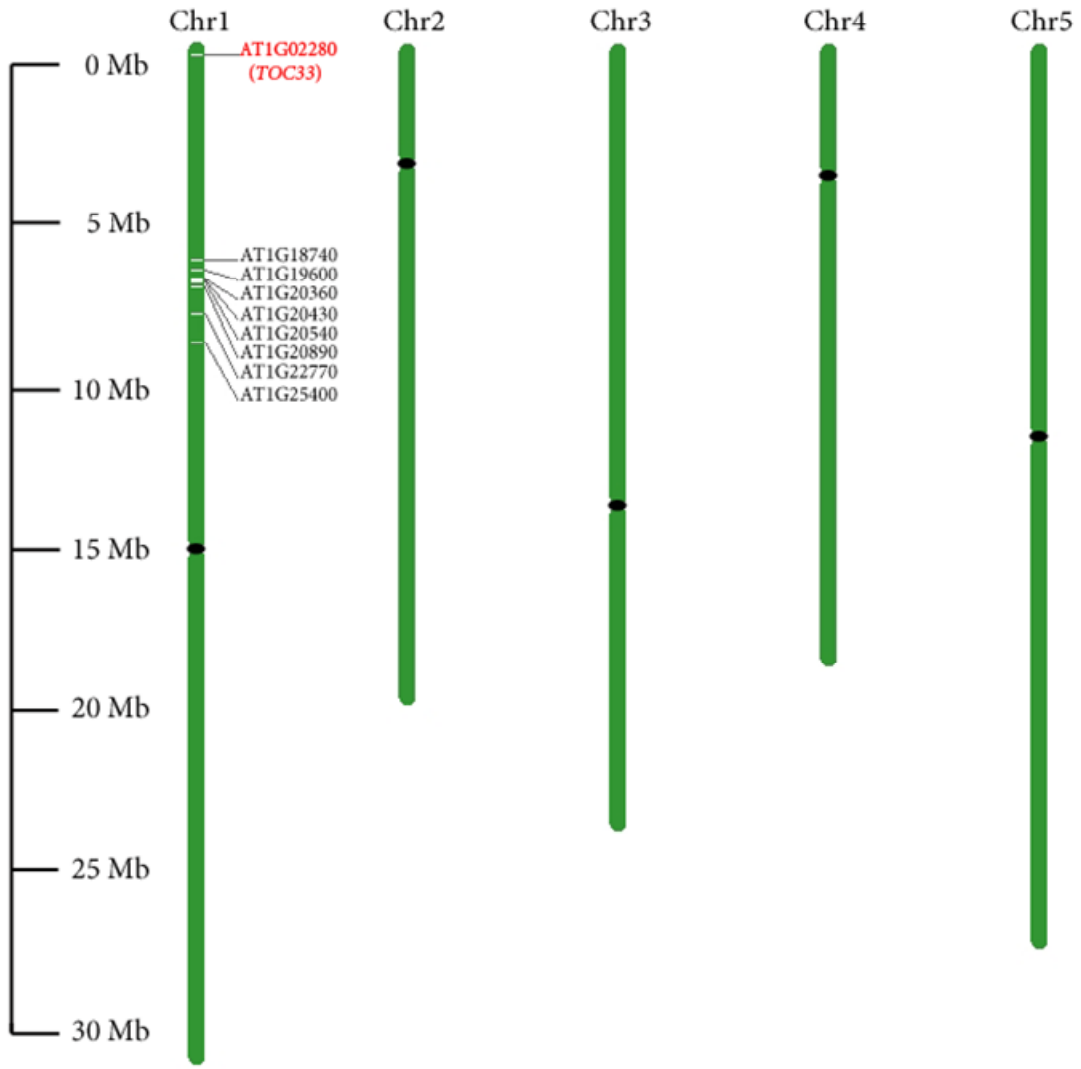


Figure 4.4. Distribution of the eight *SP3* candidate genes on the chromosomes of *Arabidopsis thaliana*. The chromosomes are drawn to scale. Each candidate gene is indicated by its locus name. The position of the *ppi1* locus is shown in red. The black ovals represent the positions of the centromeres on the chromosomes.

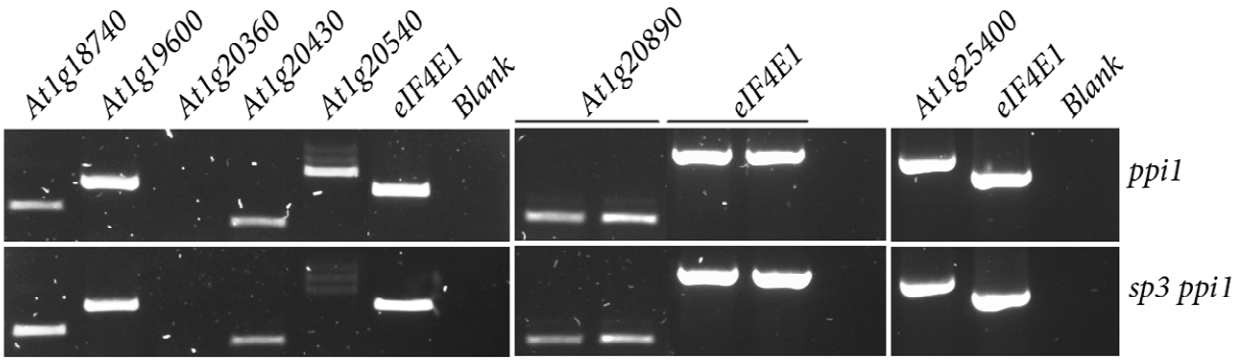


Figure 4.5. Analysis by RT-PCR of the expression of *SP3* candidate genes in the *sp3 ppi1* (47B-3) mutant plants. Total RNA samples isolated from 32-day-old plants of the *sp3 ppi1* and *ppi1* genotypes, were analysed by RT-PCR using gene-specific primers for *At1g18740*, *At1g19600*, *At1g20360*, *At1g20430, At1g20540*, *At1g20890* and *At1g25400*, and for the reference gene *eIF4E1*. Amplifications employed a limited number of cycles to avoid saturation, and products were analysed by agarose gel electrophoresis.

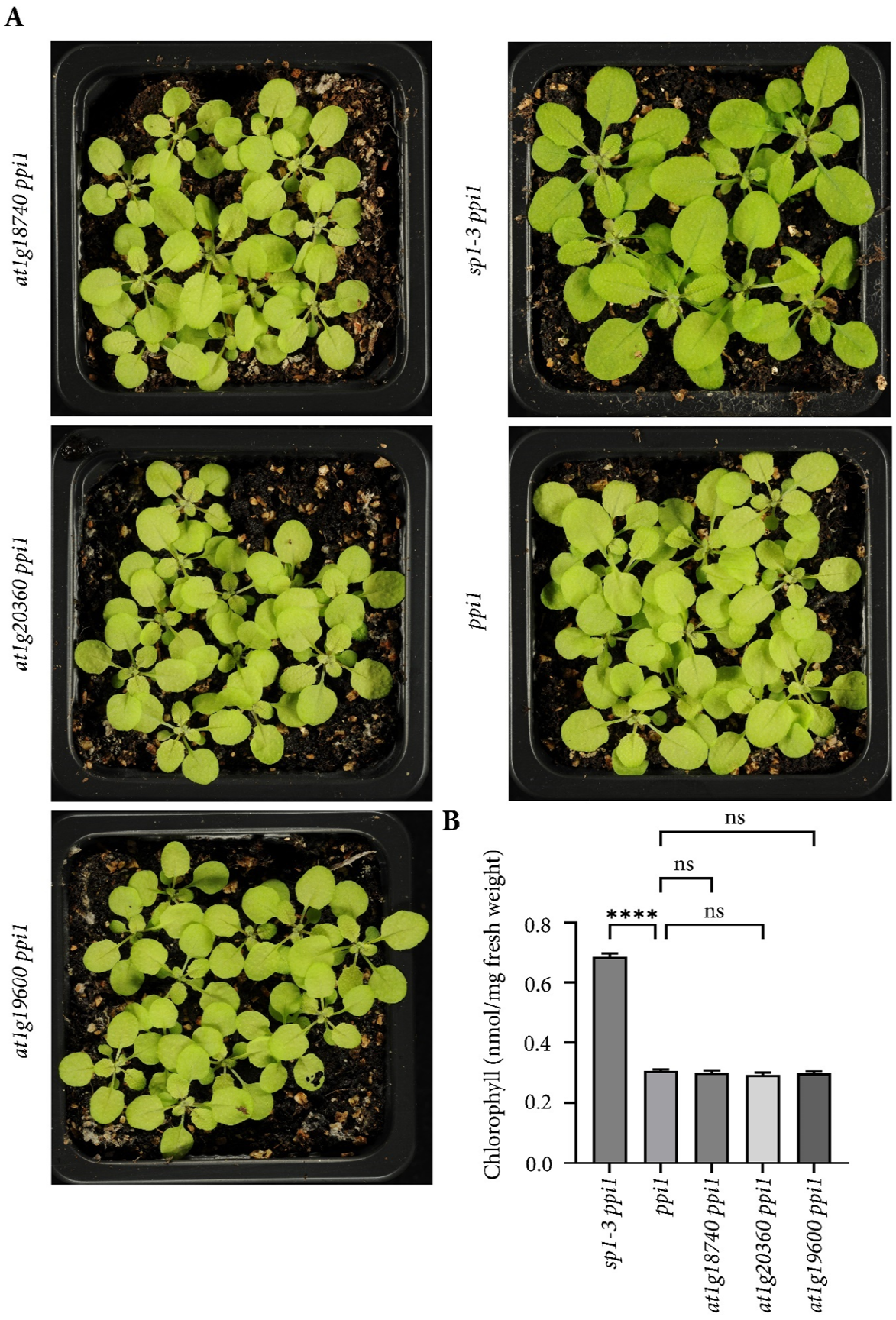

A
at1g18740 ppi1
sp1-3 ppi1
at1g20360 ppi1
ppi1
at1g19600 ppi1
B
Chlorophyll (nmol/mg fresh weight)
0.0
0.2
0.4
0.6
0.8
****
ns
ns
ns
sp1-3 ppi1
ppi1
at1g18740 ppi1
at1g20360 ppi1
at1g19600 ppi1

Figure 4.6. Phenotypic analysis of the homozygous *at1g18740*, *at1g20360* and *at1g19600* T-DNA mutants in the *ppi1* background. (A) Visible appearance of *at1g18740 ppi1*, *at1g20360 ppi1* and *at1g19600 ppi1* mutants. The plants were grown under standard conditions on soil for 23 days before photography, and representative plants are shown. Similar camera settings were employed to record all images. All of the images are at the same magnification. **(B)** Quantification of chlorophyll concentration in the *at1g18740 ppi1*, *at1g20360 ppi1* and *at1g19600 ppi1* mutants, and in control plants. Measurements were taken on the day of photography. The leaves were analysed using a Konica-Minolta SPAD-502 meter, and the meter values were converted to chlorophyll per fresh weight values using a verified calibration equation. Values shown are means (n=16) with error bars indicating SEM. Asterisks above the columns indicate the significance of differences (Student's *t*-test: $^{****}P < 0.0001$).

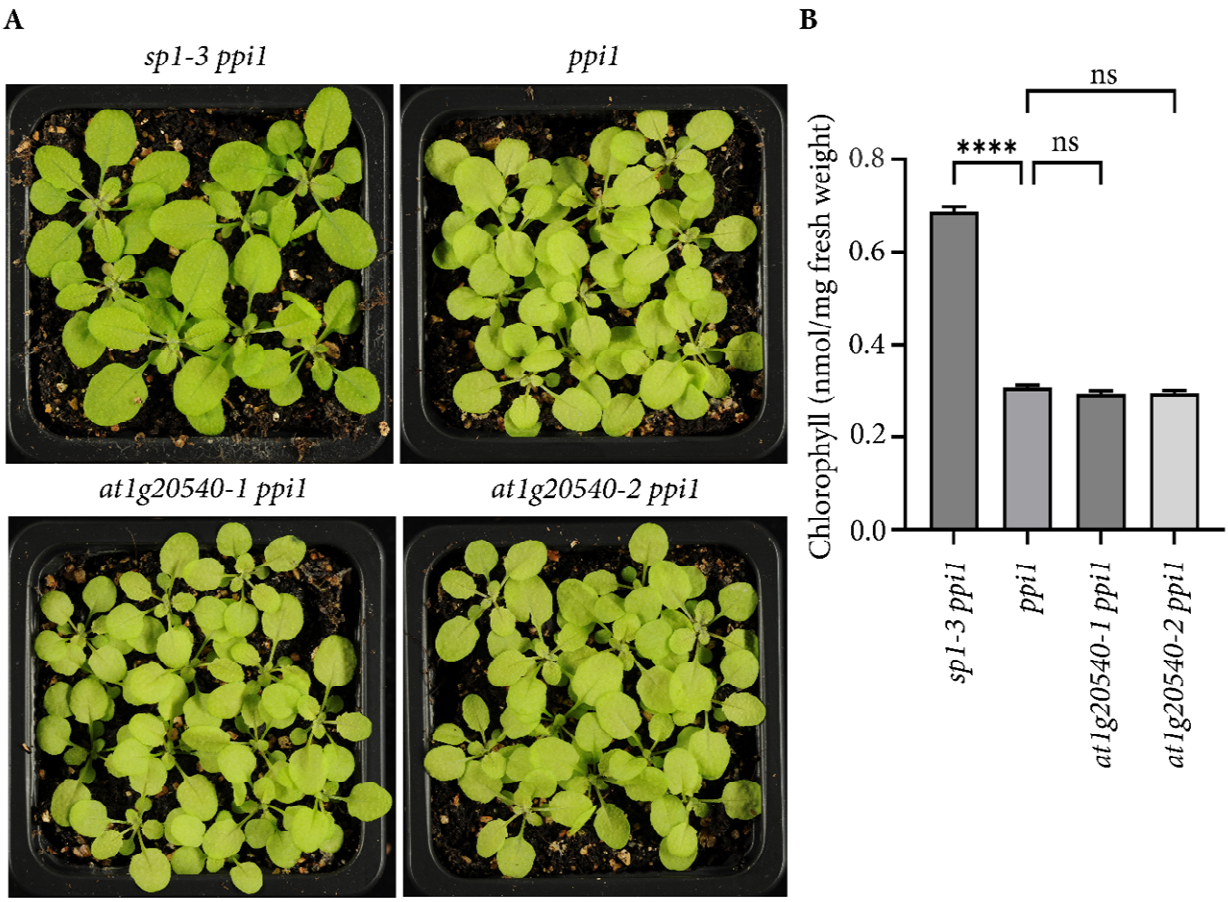


Figure 4.7. Phenotypic analysis of the homozygous *At1g20540* T-DNA mutants in the *ppi1* background. (A) Visible appearance of *at1g20540-1 ppi1* and *at1g20540-2 ppi1* mutants. The plants were grown under standard conditions on soil for 23 days before photography, and representative plants are shown. Similar camera settings were employed to record all images. All of the images are at the same magnification. **(B)** Quantification of chlorophyll concentration in the *at1g20540-1 ppi1* and *at1g20540-2 ppi1* mutants, and in control plants. Measurements were taken on the day of photography. The leaves were analysed using a Konica-Minolta SPAD-502 meter, and the meter values were converted to chlorophyll per fresh weight values using a verified calibration equation. Values shown are means (n=16) with error bars indicating SEM. Asterisks above the columns indicate the significance of differences (Student's *t*-test: $^{****}P <$ 0.0001).

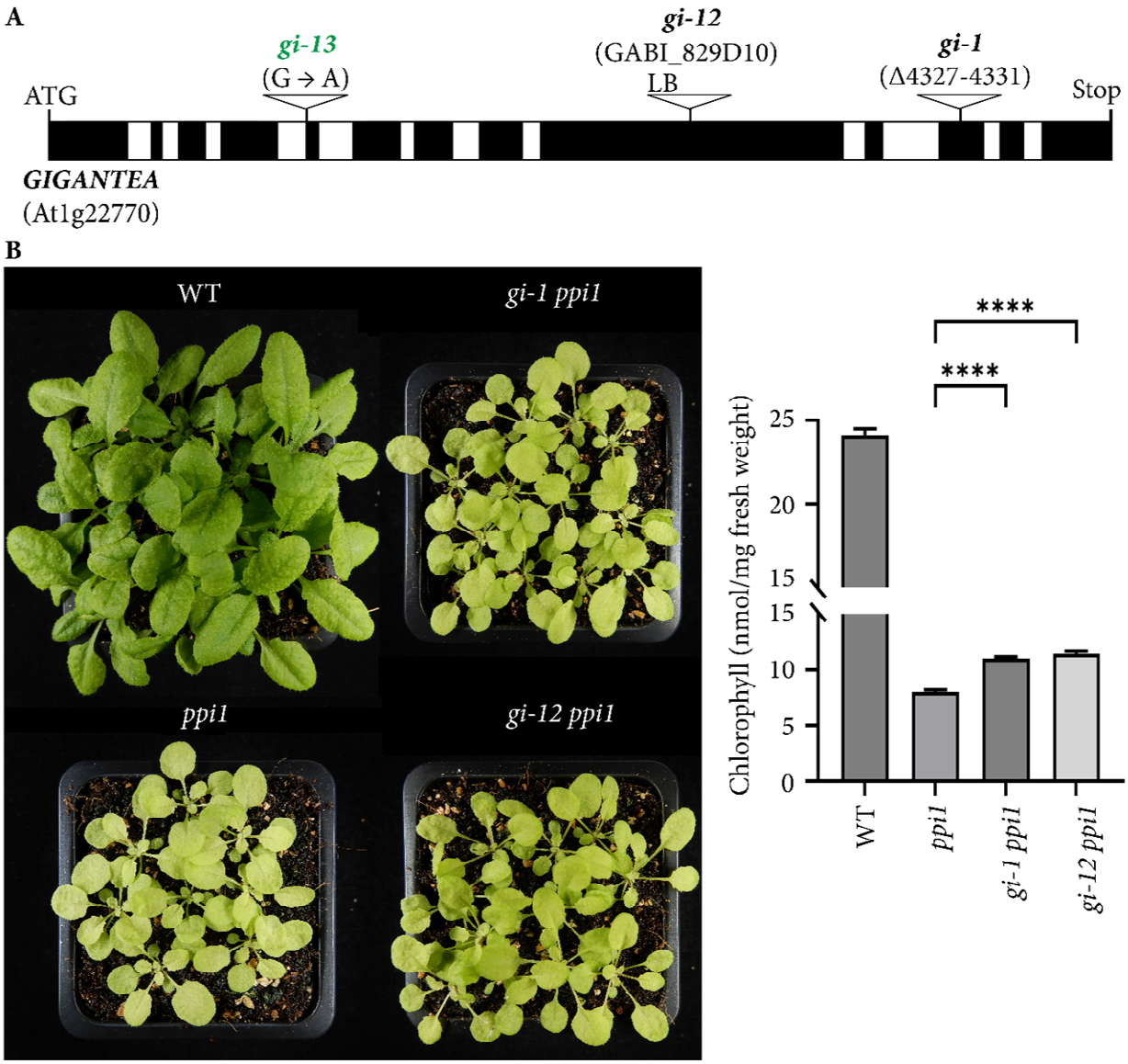


Figure 4.8. Phenotypic analysis of the homozygous *gi* (*At1g22770)* mutants in the *ppi1* background. (A) Schematic diagram showing the new and previously identified alleles of *gi* in the context of the *GI* gene. The positions of two previously characterized *gi* alleles (*gi-1* and *gi-12*), and the new *gi* allele from this study (*gi-13* highlighted in green), are indicated. The *gi-1* allele possesses a five nucleotides deletion (indicated), *gi-12* possesses a T-DNA insertion, and *gi-13* possesses a single nucleotide substitution (indicated). Black boxes = exons; interconnecting white boxes = introns; LB = left border sequences of the T-DNA insertions; ATG = translation initiation codon; Stop = translation termination codon. (**B**) Visible appearance of *gi-1 ppi1* and

gi-12 ppi1 mutants. **Left:** The plants were grown under standard conditions on soil for 28 days before photography, and representative plants are shown. Similar camera settings were employed to record all images. All of the images are at the same magnification. **Right:** Quantification of chlorophyll concentration in the *gi-1 ppi1* and *gi-12 ppi1* mutants, and in control plants. Measurements were taken on the day of photography. The leaves were analysed using a Konica-Minolta SPAD-502 meter, and the meter values were converted to chlorophyll per fresh weight values using a verified calibration equation. Values shown are means (n=15) with error bars indicating SEM. Asterisks above the columns indicate the significance of differences (Student's *t*-test: $^{****}P < 0.0001$).

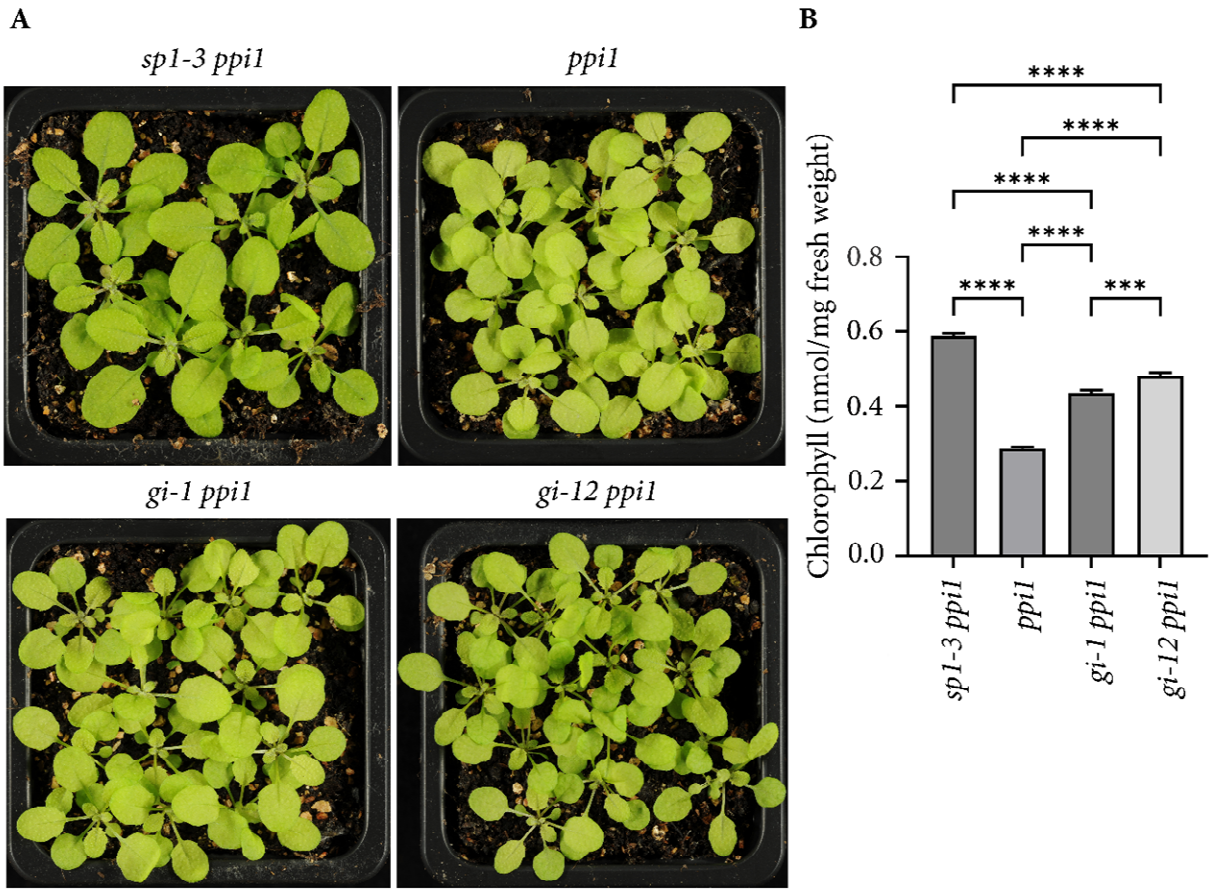


Figure 4.9. Phenotypic comparison between the *gi ppi1* and *sp1-3 ppi1* mutant plants. (A) Visible appearance of *gi-1 ppi1*, *gi-12 ppi1* and *sp1-3 ppi1* mutants. The plants were grown under standard conditions on soil for 23 days before photography, and representative plants are shown. Similar camera settings were employed to record all images. All of the images are at the same magnification. **(B)** Quantification of chlorophyll concentration in the *gi-1 ppi1* and *gi-12 ppi1* mutants, and in control plants. Measurements were taken on the day of photography. The leaves were analysed using a Konica-Minolta SPAD-502 meter, and the meter values were converted to chlorophyll per fresh weight values using a verified calibration equation. Values shown are means (n=16) with error bars indicating SEM. Asterisks above the columns indicate the significance of differences (Student's *t*-test: $^{****}P < 0.0001$).

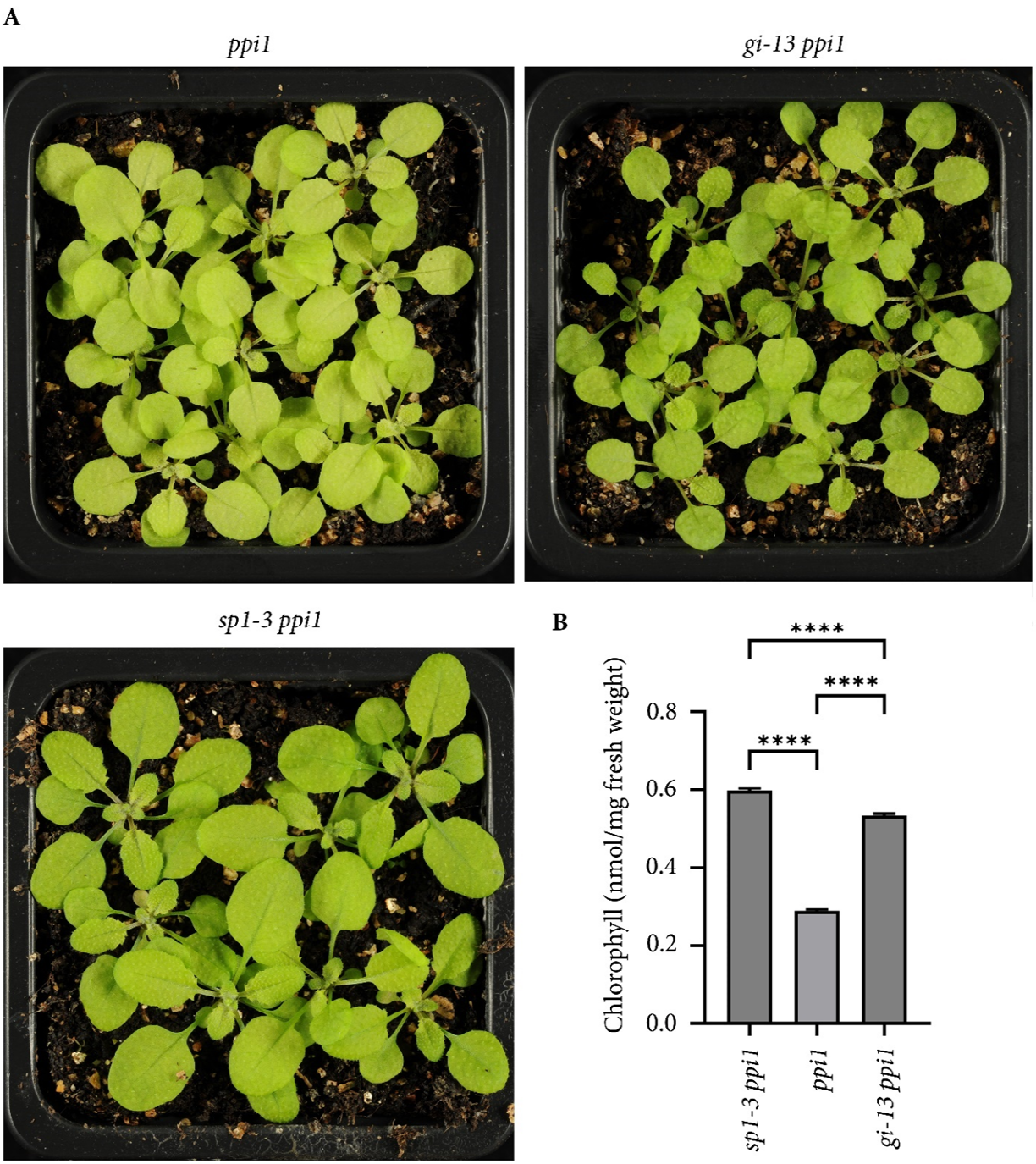


Figure 4.10. Phenotypic analysis of the homozygous *gi-13* mutant in the *ppi1* background. (A) Visible appearance of *gi-13 ppi1* and *sp1-3 ppi1* mutants. The plants were grown under standard conditions on soil for 23 days before photography, and representative plants are shown. Similar camera settings were employed to record all images. All of the images are at the same

magnification. **(B)** Quantification of chlorophyll concentration in the *gi-13 ppi1* mutant, and in control plants. Measurements were taken on the day of photography. The leaves were analysed using a Konica-Minolta SPAD-502 meter, and the meter values were converted to chlorophyll per fresh weight values using a verified calibration equation. Values shown are means (n=16) with error bars indicating SEM. Asterisks above the columns indicate the significance of differences (Student's *t*-test: $^{****}P < 0.0001$).

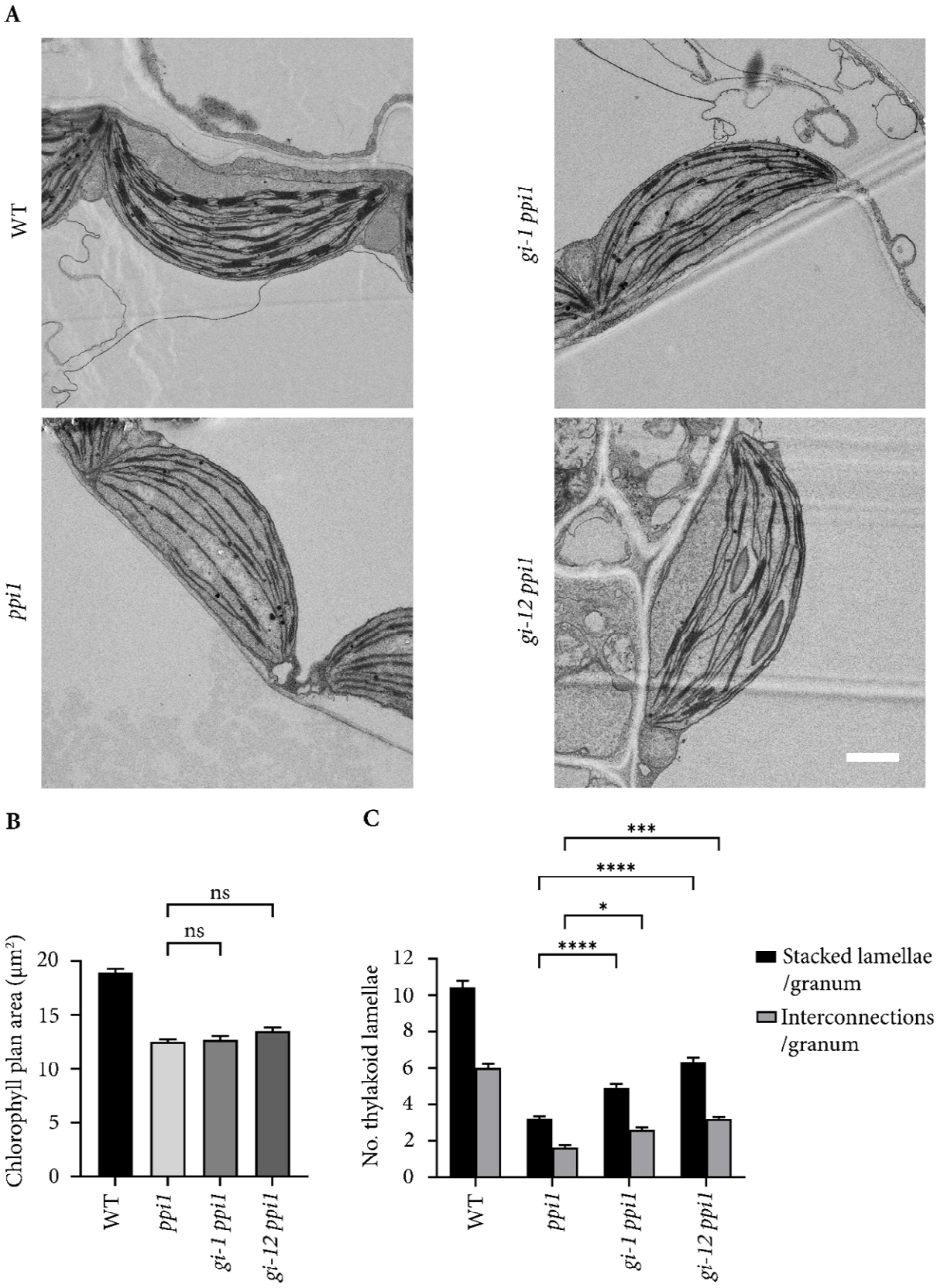

A
WT
ppi1
gi-1 ppi1
gi-12 ppi1
B
Chlorophyll plan area (µm²)
ns
ns
WT
ppi1
gi-1 ppi1
gi-12 ppi1
C
No. thylakoid lamellae
***
****
*
****
Stacked lamellae /granum
Interconnections /granum
WT
ppi1
gi-1 ppi1
gi-12 ppi1

Figure 4.11. Chloroplast ultrastructure in the *gi ppi1* mutants. (**A**) Ultrastructure of rosette leaf chloroplasts in 3-week-old plants of the indicated genotypes. Samples were analysed by transmission electron microscopy, and typical organelles are shown. Scale bar = 1 μm. Quantitative analysis of the presented electron micrographs, and of other similar micrographs, is shown in (**B**) and (**C**). (**B**) Quantification of chloroplast cross-sectional area. The data are based on measurements of 120 chloroplasts from wild type, 100 chloroplasts from *ppi1* and 80 chloroplasts from each *gi ppi1* double mutant. Values shown are means with error bars indicating SEM. (**C**) Quantification of thylakoid development. The number of lamellae per granal stack, and the number of membrane interconnections per granal stack, was determined for each genotype. The data are based on the measurements of 60 chloroplasts (for lamellae per granum), or 40 chloroplasts (for interconnection per granum) per genotype. Values shown are means with error bars indicating SEM. Asterisks above the columns indicate the significance of differences (Student's *t*-test: $^{****}P < 0.0001$, $^{*}P < 0.05$).

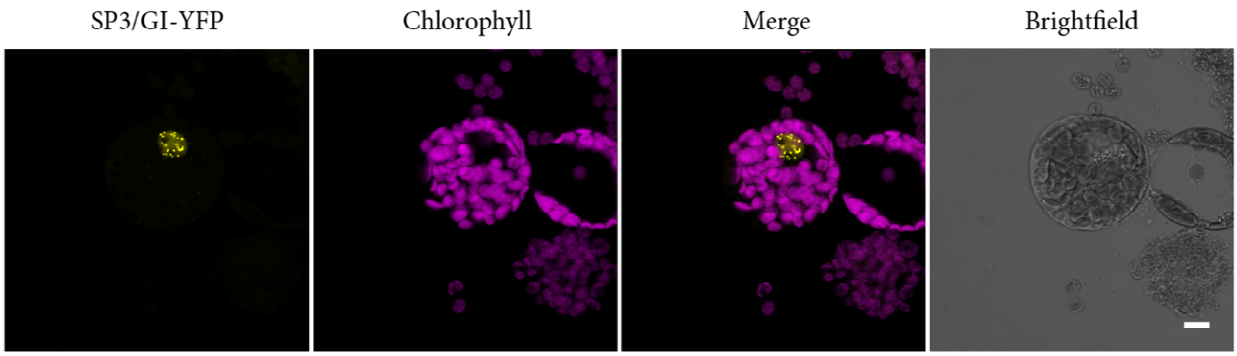


Figure 4.12. Subcellular localization analysis of SP3/GI proteins by confocal microscopy. *Arabidopsis* protoplasts transiently expressing the YFP fused SP3/GI proteins under 35S promoter were analysed by confocal microscopy. The punctate spots of GI-YFP fluorescence indicates nuclear bodies (Kim et al., 2013a). Representative protoplasts are shown. In each case, YFP fluorescence, chlorophyll autofluorescence, merged YFP and chlorophyll fluorescence, and bright field images are shown. Bar = 10 μm.

Chapter 5

General discussion

5 General discussion

5.1 Summary of key findings

The first aim of this thesis was to characterize the role of PUX10, a cofactor of Cdc48, in *Arabidopsis*. I was particularly willing to investigate the potential involvement of PUX10 in the regulation of chloroplast protein import and plastid biogenesis. The homologues of PUX10 in yeast and mammalian cells have been well studied for playing important roles in the ER, mitochondria, and lipid droplet (LD) associated protein degradations (Martensson et al., 2019; Neuber et al., 2005; Schuberth & Buchberger, 2005; Schuberth et al., 2004; Wang & Lee, 2012; Zheng et al., 2022). Although previous studies suggested that PUX10 is involved in LD-associated protein degradation (LDAD) in pollen tubes and during seed germination by recruiting Cdc48 to LDs (Deruyffelaere et al., 2018; Kretzschmar et al., 2018), no cofactor of Cdc48 has been reported to play roles in chloroplast-associated protein degradation (CHLORAD).

To achieve this aim, the subcellular localization of PUX proteins was first screened by confocal microscopy and PUX10 was then identified as the only PUX protein showing distinct localization in chloroplast. Further protein topology analysis revealed that PUX10 is indeed an integral chloroplast envelope protein with both the N-terminal UBA and C-terminal UBX domains projecting into the cytosol. The subsequent protein interaction analyses clearly indicated that PUX10 can effectively interact with ubiquitinated TOC proteins and Cdc48 via its UBA and UBX domains, respectively. PUX10 therefore controls the partitioning of Cdc48 to the chloroplasts. Moreover, PUX10 was also proved to interact with SP1 and SP2, other two key components of CHLORAD pathway. Genetic analyses showed that the *pux10-1* mutation suppressed the *ppi1* phenotype, and such a phenotypic suppression was attributable to the substantial recovery of TOC proteins in *pux10-1 ppi1* plants relative to *ppi1* plants. Intriguingly, when the *pux10* mutation was introduced into SP1-OX *ppi1* background, the resulting *pux10-1*

SP1-OX *ppi1* plants appeared larger and greener than the SP1-OX *ppi1* progenitor plants; and this effect of the *pux10* mutation was linked to obviously increased leaf chlorophyll content, improved chloroplast ultrastructural organization, and restored accumulation of TOC proteins. Additionally, previous studies showed that *SP1* overexpression accelerated the leaf senescence in *Arabidopsis*, while the *sp1* mutation delivered an opposite impact (Ling et al., 2012). Interestingly, *pux10-1* SP1-OX plants exhibited attenuated leaf senescence compared to SP1-OX plants, indicating that PUX10 is required for SP-dependent physiological processes. It is worth noting that in both cases, *pux10* mutation only partially blocked the phenotypes caused by *SP1* overexpression. Moreover, the phenotypic suppression of *pux10* mutation in *ppi1* was also not as strong as the effect of *sp1* or *sp2* single mutation in *ppi1*. These results led to the hypothesis that unknown proteins functionally redundant to PUX10 also involved in the degradation of ubiquitinated TOC proteins.

Taken together, the data presented in chapter 2 and chapter 3 demonstrated that PUX10 is a part of CHLORAD complex for the degradation of chloroplast TOC proteins by the UPS. PUX10 can physically interact with both CHLORAD components and ubiquitinated TOC proteins to recruits cytosolic Cdc48 to chloroplast surface to be adjacent to its substrates. However, such a bridging role of PUX10 seems not to be indispensable during chloroplast development. Furthermore, the suppression of *pux10* mutation in SP1-OX suggests that PUX10 improves the efficiency of CHLORAD by coordinating the ubiquitination and retrotranslocation activities necessary for the rapid turnover of TOC proteins.

The second aim of this thesis was to discover the new suppressor of *ppi1* locus. Given the importance and complexity of regulatory mechanisms of TOC complexes, the identification of new regulators of plastid protein import will enrich our knowledge regarding the molecular mechanisms underpinning plastid biogenesis.

To achieve this aim, a forward genetic screen was conducted in the group, in a similar manner to the identification of SP1 and SP2. The pale *TOC33* knockout mutant *ppi1* was mutagenized with

EMS and plants displaying synthetic recovery phenotypes were isolated and characterized to be the suppressors of *ppi1*. Around 20,000 *ppi1* seeds were subjected to EMS mutagenesis, and 64 mutant lines which displayed greener phenotype than the *ppi1* progenitor plants were isolated. Of these, a total of 19 variable mutants were selected and subjected to secondary screening for potential mutations in either *SP1* or *SP2*. This led to the identification of two new *sp1* alleles (*sp1-4* and *sp1-5*) and five new *sp2* alleles (*sp2-5* to 9), and the discovery of *suppressor of ppi1 locus 3* (*sp3*), which contained no mutations in either *SP1* or *SP2*. Next generation sequencing (NGS) was then applied to map the causative genetic lesions in the genome of *sp3* plants. The following SHOREmap analysis identified eight candidate genes on *Arabidopsis* chromosome 1 bearing various types of mutation. Based on the gene expression and genetic complementary analysis, *SP3* was identified as the gene encoding GIGANTEA (GI).

GI is a key regulator of photoperiodic flowering in *Arabidopsis*. In this study, *gi ppi1* plants exhibited increased chlorophyll content and improved chloroplast ultrastructure relative to *ppi1* plants. Moreover, previous studies of different *gi* mutants suggested a function of GI in chlorophyll accumulation and chloroplast biogenesis (Brandoli et al., 2020a; Cha et al., 2019; Kurepa et al., 1998). Although GI is predominantly localized in the nucleus, the cytosolic F-box protein ZEITLUPE (ZTL) was found to sequester it to the cytosol where it acts as the cochaperone of Hsp90 to stabilize the ZTL, a circadian photoreceptor, under blue light (Cha et al., 2017). Therefore, it is plausible that GI can interact with the chloroplast surface, or with cytosolic factors that regulate chloroplast protein import. Additionally, as a transcriptional factor, GI might also regulate the expression of TOC genes.

Taken together, the preliminary data presented in chapter 4 imply a role for GI in plastid biogenesis, probably through the regulation of chloroplast protein import. There was not enough time to further investigate this interesting hypothesis during the course of this doctoral study, but in the future a series of molecular, biochemical and genetic experiments should be conducted to pursue these ideas.

5.2 Critical appraisal of the role of PUX10 in CHLORAD pathway

5.2.1 PUX10 is a chloroplast-localized scaffold protein that recruits Cdc48 to ubiquitinated TOC proteins

Previous studies demonstrated the PUX proteins were involved in the recruitment of Cdc48 to specific cellular compartments, or in regulating the activity of Cdc48 in *Arabidopsis thaliana* (Deruyffelaere et al., 2018; Gallois et al., 2013; Huang et al., 2020; Kretzschmar et al., 2018; Marshall et al., 2019; Park et al., 2007; Rancour et al., 2004). PUX10 was recently identified as an LD-localized Cdc48 adaptor protein that regulates the degradation of LD proteins during seed germination. Intriguingly, the subcellular localization of PUX10 was swiftly changed from LDs to chloroplasts during seed maturation, suggesting that PUX10 delivers multifunctional roles in a phase-specific manner during plant development (Deruyffelaere et al., 2018).

After conducting a general subcellular localization screening of PUX proteins in *Arabidopsis*, PUX10 was found to be the only PUX protein showing distinct association with chloroplasts (Figure 2.1). The subsequent topology analysis revealed that PUX10 was anchored to the chloroplast envelope membrane via a highly hydrophobic transmembrane region. Moreover, a minor association of PUX10 with the ER was observed in this study, as well as the previous studies (Deruyffelaere et al., 2018). These observations indicated a specific partitioning of PUX10 between organelles during plant development. Such partitioning between organelles was also observed for Ubx2 and FAS-Associated Factor 2 (FAF2, also known as Ubxd8), the homologues of PUX10 in yeast and mammals, respectively. Ubx2 was shown to be a very dynamic protein, and the employment of Ubx2 in multiple subcellular compartments for quality control purposes suggested that such protein-processing pathways may require coregulation. (Martensson et al., 2019; Schuberth & Buchberger, 2005; Wang & Lee, 2012). The FAF2 protein, a close homologue of Ubx2 in mammals, is similarly involved in regulation of protein degradation in multiple compartments (the ER, LDs, and mitochondria), implying a functional conservation of this property (Mueller et al., 2008; Wang & Lee, 2012; Zheng et al., 2022). 0Although PUX10 did not

localize to mitochondria, its association with LDs, ER, and chloroplasts – an organelle specific to photosynthetic organisms - further supported the notion that this multilocation property is conserved for this group of proteins (Figure 2.2 and 2.3).

A transmembrane protein always has a specific orientation in the membrane which reflects the different functions of its cytosolic and non-cytosolic domains. Consequently, proteins within chloroplast envelope membranes must adopt appropriate orientations to interact with their respective partners. The PUX10 protein has a hydrophobic transmembrane region, an N-terminal UBA domain, and a C-terminal UBX domain. The 'dual protease' protection assay using thermolysin and trypsin in this study clearly indicated that both UBA and UBX domains are projecting into the cytosol (Figure 2.5 B to D). The cytosolic orientation of both domains of PUX10 ensures the interactions with its functional partners.

Such a notion was subsequently proved through a series of protein interaction analyses. Both BiFC and Co-IP experiments indicated that the PUX10 protein could recruit cytosolic Cdc48 efficiently to the chloroplast envelope through its UBX domain (Figure 2.7 and 2.8). Moreover, the Co-IP assays indicated that PUX10 can interact with ubiquitin and ubiquitinated TOC proteins via its UBA domain (Figure 2.9 and 3.4). Therefore, such a UBA–UBX structure of PUX10 functions in post-ubiquitination steps by tethering both ubiquitinated TOC proteins and Cdc48 to promote the dislocation of TOC components and their subsequent degradation.

Taken together, PUX10, a plant UBX domain-containing protein, is a cofactor of Cdc48 in *Arabidopsis*. The characteristic protein domain structure of PUX10 defines its role as a chloroplast membrane-bound scaffold protein for recruiting Cdc48 to ubiquitinated substrates of the CHLORAD pathway. Therefore, it is reasonable to propose that PUX10 is a new component of the CHLORAD complex and involved in the regulation of the turnover of TOC components.

5.2.2 PUX10 promotes the rapid turnover of TOC components.

The three key components of the CHLORAD pathway, SP1, SP2 and Cdc48, act cooperatively to regulate the turnover of TOC complex in *Arabidopsis*. Besides Cdc48, PUX10 was also proved to physically interact with SP1 and SP2 and TOC proteins through a series of protein interaction assays, suggesting a potential role of PUX10 in the regulation of the turnover of TOC machinery.

Arabidopsis pux10 null mutants displayed no obvious phenotypic differences from wild-type plants (Figure 2.6). However, the *pux10* mutation was found to suppress the *ppi1* phenotype since *pux10 ppi1* double mutant plants were larger and greener than *ppi1* plants and exhibited increased chlorophyll content (Figure 3.5). Such a phenotypic suppression was linked to the substantial recovery of TOC protein abundance in *pux10 ppi1* plants relative to *ppi1* plants (Figure 3.5).

Moreover, when the *pux10* mutation was introduced into the SP1-OX *ppi1* background, and the resulting *pux10-1* SP1-OX *ppi1* plants appeared larger and greener than the SP1-OX *ppi1* plants and showed increased chlorophyll content and abundance of TOC proteins, and improved chloroplast ultrastructural organization (Figures 3.7 and 3.8). In addition, *pux10-1* SP1-OX plants exhibited attenuated leaf senescence compared to SP1-OX plants, indicating that PUX10 is required for the reorganization of TOC complexes mediated by SP1 during important developmental transition (Figure 3.9).

Collectively, these results displayed that as part of CHLORAD complex, PUX10 improves the efficiency of CHLORAD by coordinating the ubiquitination and retrotranslocation activities necessary for the rapid turnover of TOC proteins. Such a coordinating role of PUX10 is important for the SP1 mediated reorganization of TOC machinery during critical developmental phases.

5.2.3 Functionally redundant cofactors of Cdc48 in CHLORAD

The *pux10* null mutants displayed no obvious phenotypic differences from wild-type plants (Figure 2.6). This was unsurprising since neither *sp1* nor *sp2* mutants display any obvious visible defects under normal conditions (Ling et al., 2019; Ling et al., 2012). Moreover, the single homozygous mutants of characterized *PUX* genes were fertile and phenotypically indistinguishable from the wild type under normal growth conditions (Gallois et al., 2013; Marshall et al., 2019; Rancour et al., 2004). Intriguingly, previous studies revealed that multiple PUX proteins act together in regulating protein degradation. Such combined action was observed in the PUX7/PUX8/PUX9/PUX13 subgroup which recruits non-functional Cdc48 for autophagic clearance, and in the PUX3/4/5 subgroup which regulates inner nuclear membrane protein degradation (Huang et al., 2020; Marshall et al., 2019). Moreover, in LD-associated protein degradation (LDAD), the *pux10* mutation considerably reduced but did not completely abrogate the degradation of structural LD proteins, indicating that PUX10 plays an important but not indispensable role in the LDAD pathway (Deruyffelaere et al., 2018; Kretzschmar et al., 2018). These observations implied that other uncharacterized cofactors of Cdc48 function redundantly to PUX10.

The genetic analyses in this study indeed suggested the possibility of such a functional redundancy. The *pux10* mutation was found to suppress the pale phenotype of *ppi1*, However, the suppression effect of *pux10* was much weaker than that of *sp1* or *sp2* mutation (Ling et al., 2019; Ling et al., 2012). Additionally, the *pux10* mutation was found to only partially block the phenotypes caused by *SP1* overexpression. All these observations implied that there are unknown proteins functionally redundant to PUX10 that also involved in the degradation of ubiquitinated TOC proteins.

The functional redundancy is a rather conserved phenomenon for the cofactors recruiting Cdc48 to organelle membrane. For example, Shp1 (also known as Ubx1) and Ubx2 possess important but overlapping functions in the degradation of a Cdc48-dependent model substrates in yeast

(Schuberth et al., 2004). Moreover, Dfm1, a Der1-like ER membrane protein, was found to be capable of recruiting Cdc48 to ER membrane in the absence of Ubx2 (Stolz et al., 2010). Interestingly, AtDerlin-1 (AtDer1), the homologue of Dfm1 in *Arabidopsis*, may be active in chloroplasts based on the prediction by ARAMEMNON (http://aramemnon.uni-koeln.de/), though the significance of this prediction has not been confirmed experimentally. Though Derlin proteins are well-known for their function in ERAD in eukaryotes (Schekman, 2004), the multi-localization of Derlin-1 protein was indeed found in *Caenorhabditis elegans* and mouse macrophages (Schaheen et al., 2009). Therefore, AtDer1 might also have multi-localization in plant cell.

Additionally, besides the putative Ubx2 orthologue, other UBX and non-UBX proteins were found also to contribute to the recruitment of p97/Cdc48 to the ER membrane in ERAD in the mammalian system (Liang et al., 2006; McNeill et al., 2004; Ye et al., 2004). It is therefore very likely that some other PUX proteins can function redundantly to PUX10 during the regulation of degradation of TOC proteins. For instance, the cytosolic PUX proteins containing both UBA and UBX domain, such as PUX5, PUX8, PUX9 or PUX13, can possibly bridge Cdc48 and ubiquitinated TOC components through the UBX and UBA domains, respectively. In principle, this function would not require the bridge to be an integral membrane protein.

Besides, zinc finger (ZnF) domain is another ubiquitin binding domain (Alam et al., 2004; Lee et al., 2006; Reyes-Turcu et al., 2006). Unlike Npl4 in yeast, the homologues of NPL4 in *Arabidopsis* contain no ZnF domains. Instead, Ufd1C, one variant of Ufd1 homologues in *Arabidopsis* (At4g15420) contains a C-terminal ZnF domain. The preliminary data from protein interaction analyses indicated that Ufd1C interacts with Npl4, Cdc48, CHLORAD components and TOC proteins (unpublished data from Simon Thomson). Therefore, it is plausible that Ufd1C can recruit Cdc48-Npl4-Ufd1 complex to chloroplast surface by interacting with ubiquitinated TOC proteins via its ZnF domain. Additionally, PUX2 is predicted to have a ZnF domain, though such a prediction has not been confirmed experimentally (Zhang et al., 2022b).

Additionally, PUX11 is another PUX protein containing a putative membrane-anchoring hydrophobic patch (Zhang et al., 2022b). Although PUX11 possesses no UBA domain, the ubiquitin-associating (UAS) domain in PUX11 might help to recruit ubiquitinated substrates indirectly (Lim et al., 2009).

Taken together, as a new component of CHLORAD complex, PUX10 ensures a robust and accurate orientation of ubiquitinated TOC proteins to CDC48 and the subsequent retrotranslocation and cytosolic degradation, though it is not indispensable for such a process. Other functionally redundant cofactors of CDC48 might also be involved in CHLORAD pathway. Further biochemical and genetic analyses will help to address such a hypothesis.

5.2.4 A working model of PUX10 in CHLORAD Pathway

Thousands of chloroplast destined proteins encoded by nuclear genes are imported via the TOC-TIC complexes in the chloroplast envelope membrane. Protein import is hence vital for chloroplast biogenesis and functioning. The CHLORAD pathway influences plastid development by regulating the turnover of TOC proteins to manipulate protein import. Three key components of CHLORAD assembly, SP1, SP2 and Cdc48, are proved to work cooperatively in the ubiquitination, retrotranslocation and degradation of TOC proteins (Ling et al., 2019; Ling et al., 2012). The data from this doctoral study unveiled the role of PUX10, a new component of CHLORAD, in plastid biogenesis. PUX10 is a chloroplast membrane-bound scaffolding protein. The UBA domain of PUX10 recognizes SP1 ubiquitinated TOC proteins, while its UBX domain is essential for the recruitment of cytosolic Cdc48 to chloroplast surface to be adjacent to its substrates. Such a bridging role of PUX10 ensures the rapid reorganization of TOC components to respond to environment and developmental cues (Figure 5.1). In addition, a series of genetic analyses indicated that alternative proteins functionally redundant to PUX10 might also be involved in the regulation of degradation of TOC proteins and plastid protein import.

In summary, I proposed a working model for the PUX10 involved degradation of TOC proteins by UPS. In this model, TOC proteins are ubiquitinated by OEM-localized SP1 E3 ligase.

Chloroplast envelope anchored PUX10 then recognizes the polyubiquitin chain on TOC protein via its UBA domain. Meanwhile, the cytosolic Cdc48 is recruited to chloroplast surface by PUX10 via its UBX domain to be adjacent to its substrates. The pulling force generated from Cdc48 through ATP hydrolysis promotes the dislocation of TOC proteins through retrotranslocaiton channel formed by the β-barrel protein SP2 into cytosol for degradation by the 26S proteasome. Moreover, the unknown membrane-bound cofactor, or cytosolic cofactor functionally redundant to PUX10 remains to be determined (Figure 5.1).

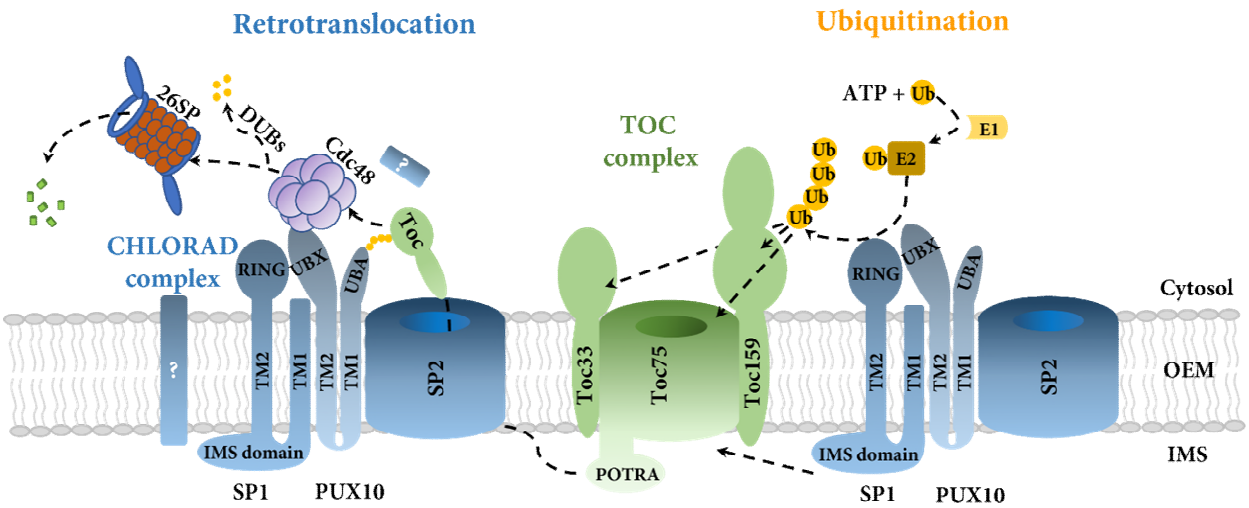


Figure 5.1. A proposed model for the role of PUX10 in the CHLORAD pathway. TOC proteins are marked with a polyubiquitin by E2 ubiquitin conjugating and SP1 E3 ligase enzyme. PUX10 is integrated into chloroplast OEM via its transmembrane domains (TMs). PUX10 bridges the ubiquitinated TOC proteins and Cdc48 through its UBA and UBX domains, respectively, to facilitate the retrotranslocation of ubiquitinated TOCs from the chloroplast OEM. Once dislocated into cytosol, ubiquitins are cleaved from TOC proteins by yet unknown deubiquitinases before TOCs are degraded by the 26S proteasome. *Arabidopsis* TOC proteins are shown and labelled by convention according to their molecular weight in kilodaltons. Putative unknown proteins (?) that share functional redundancy with PUX10 are shown. Abbreviations: POTRA domain, polypeptide transport-associated domain; RING, really interesting new gene; UBX, ubiquitin regulatory X; UBA, ubiquitin-associated; TM, transmembrane; Ub, ubiquitin;

OEM, outer envelope membrane; IMS, intermembrane space; SP1, suppressor of *ppi1* locus 1; SP2, suppressor of *ppi1* locus 2; Cdc48, cell division cycle protein 48; DUBs, deubiquitinases; 26SP, 26S proteasome; CHLORAD, chloroplast-associated protein degradation.

5.3 A new *suppressor* of the *ppi1* mutation

Following the identification of SP1 and SP2 through the *ppi1* suppressor screen, a new forward genetic screening for suppressors of *ppi1* was carried out to search for new components of SP1-dependent proteolytic pathway, or new factors that regulate chloroplast protein import. A new mutant showing phenotypic suppression of *ppi1* similar to *sp1* and *sp2* was selected and named *suppressor* of *ppi1 locus 3* (*sp3*) (Figure 4.3).

Mapping of the *sp3* mutant led to the identification of *GIGANTEA* (*GI*) gene. GI is a plant-specific protein and *GI* expression is ubiquitously detected throughout development (Fowler et al., 1999; Park et al., 1999). GI has pleiotropic functions in diverse plant developmental processes such as photoperiodic flowering, light signaling, regulation of circadian rhythm, and response to stress (Brandoli et al., 2020b). Intriguingly, previous studies indicated a novel role of GI in chlorophyll homeostasis and chloroplast biogenesis. The *Arabidopsis gi-2* mutant was reported to show reduced sensitivity to lincomycin, a chloroplast biogenesis (translation) inhibitor, and maintaining high levels of photosynthetic proteins and chlorophyll content, whereas *GI* overexpressing plants responded in the opposite way. These results indicated that GI inhibits chloroplast biogenesis by regulating photosynthetic protein accumulation (Cha et al., 2019). Moreover, *gi* mutants in *Arabidopsis* L*er* background (*gi-3*, *gi-4* and *gi-5*) showed an increased tolerance to paraquat toxicity and a significantly higher chlorophyll content in seedlings compared to wild-type seedlings (Kurepa et al., 1998). In addition, silencing of one *GI* paralogue, *Petunia hybrida GI1* (*PhGI1*), in Petunia, led to leaves with a greener appearance in the apical region with increased chlorophyll content compared to wild-type plants (Brandoli et al., 2020a). Similarly, the data presented in this thesis showed that *gi ppi1* plants were greener than *ppi1* plants, though there was no obvious difference in leaf size between *gi ppi1* and *ppi1* plants

(Figure 4.9 and 4.10). This greening phenotype was reflected in the increased chlorophyll content and improved chloroplast ultrastructural organization (Figures 4.9, 4.10 and 4.11): although chloroplasts of *gi ppi1* plants were not larger than those in *ppi1*, they did have more developed thylakoids than *ppi1* chloroplasts. Therefore, these results point to a general role of GI in chlorophyll homeostasis and chloroplast biogenesis.

Given that half of thylakoid proteins are nuclear-encoded and imported via the TOC-TIC complexes (Zhu et al., 2022), and GI is a plant-specific transcriptional regulator, it would be interesting to compare transcript abundances for several nuclear photosynthetic genes in the leaves of wild-type, *ppi1* and *gi ppi1* plants. This might give an indication as to whether the effect of GI on chloroplast biogenesis is mediated through transcriptional regulation of photosynthesis genes, for example by countering the effects of golden2-like (Glk) transcription factors that promote the expression of photosynthesis genes (Waters et al., 2009; Yeh et al., 2022). Moreover, immunoblotting analysis would elucidate whether any detected transcript changes are reflected in the abundance of photosynthetic proteins. Moreover, it is also worth testing whether the transcript level of *TOC* gene is modulated by GI.

The subcellular localization analysis of *GI* indicated that GI protein is predominantly present in the nucleus (Figure 4.12). However, the cytosol-localized F-box protein ZEITLUPE (ZTL) can sequester GI to the cytosol where it acts as the cochaperone of Hsp90 to stabilize the ZTL, a circadian photoreceptor, under blue light (Cha et al., 2017). This potentially places GI in a position to interact with the chloroplast surface, or with cytosolic factors that regulate chloroplast protein import or homeostasis.

Collectively, the preliminary data presented in this thesis imply the role of GI, a well-studied plant-specific protein for regulating flowing time, in plastid biogenesis probably through regulating chloroplast protein import. A series of molecular, biochemical, and genetic experiments will be conducted to pursue these ideas.

5.4 Concluding remarks and perspectives

Cdc48 is an essential, abundant, and highly conserved cytosolic ATPase driving the turnover of ubiquitinated proteins in eukaryotes. However, the substrate specificity of Cdc48 relies on a large number of cofactors by recruiting it to different cellular pathways. Although the essential role of Cdc48 in CHLORAD pathway has been well studied, the cofactor responsible for its association with chloroplast remains unknown. The work presented in this thesis has unveiled PUX10, a chloroplast-bound UBX domain-containing protein, recruits Cdc48 to chloroplast surface and promotes the extraction of ubiquitinated TOC proteins into cytosol for degradation by the 26S proteasome. Genetic analyses suggest that PUX10 is required for the SP1-mediated remodeling of the TOC complex during plant development by facilitating the binding of ubiquitinated TOC proteins with Cdc48 for their rapid degradation. Moreover, the characterization of the *pux10* mutation indicates that alternative proteins functionally redundant to PUX10 might also participate in the regulation of degradation of TOC complex. This is an interesting open question for the further investigation.

Given the importance and complexity of regulatory mechanisms of TOC complexes, additional work is still required to further understand the molecular mechanism underpinning plastid biogenesis. The identification of Gi protein has unlocked the possibility of studying the chloroplast protein import regulation in a novel direction. The work presented in this thesis provides a solid foundation for the future investigation of the link between Gi and the regulation of plastid protein import and, possibly, the CHLORAD pathway.

Chapter 6

Materials and methods

6 Materials and methods

6.1 Plant materials

All *Arabidopsis thaliana* plants used in this work are of the Columbia-0 (Col-0) ecotype. Two T-DNA mutant lines, *pux10-1* (SAIL_1187_B06) and *pux10-4* (WiscDsLox424B8), were obtained from the Salk Institute Genomic Analysis Laboratory (SIGnAL) (Alonso et al., 2003), via the Nottingham Arabidopsis Stock Centre (NASC). The *pux10-1* has been described previously (Deruyffelaere et al., 2018; Kretzschmar et al., 2018). The *pux10-1* and *pux10-2* T-DNA insertion lines were verified using the primers PUX10_SAIL_F/PUX10_SAIL_R and PUX10_Wisc_F/PUX10_Wisc_R, respectively (Table 6.1). DNA insertion positions within *PUX10* were confirmed by Sanger sequencing of the PCR-amplified products obtained with specific T-DNA left border sequences and primers on either side of the *PUX10* insertion site. RT-PCR analysis were further performed to analyse gene expression in homozygous mutants. The sequences of primers used for PCR amplifications are listed in Table 6.1. The *ppi1*, *tic110*/+, *sp1 ppi1* mutants, as well as the 35S promoter–driven SP1overexpressor (SP1-OX) and SP1-OX *ppi1* transgenic lines, have all been described previously (Ling et al., 2012). For making double and triple mutants, the *pux10-1* allele was used; double or triple mutants were verified by PCR based genotyping, and RT-PCR if needed.

All T-DNA mutant lines of putative genes for *sp3* mutant were also obtained from NASC. The T-DNA insertion mutants were genotyped using gene specific primers (Table 6.1). The *gi-1* has been described previously (Fowler et al., 1999). The single nucleotide substitution of *gi-13* was confirmed by dCAPS genotyping.

6.2 Plant growth conditions

In most cases, plants were grown in growth chambers (Percival Scientific, Inc.) under long-day photoperiod (16 hours light, 8 hours dark). The light intensity was approximately 100-120

μE/m^2/s, and the temperature was maintained at 20°C with ~70% relative humidity. A greenhouse with a constant temperature of 20°C were also used to grow the plants for propagation purposes under standard long-day cycle.

6.2.1 Plants grown on soil

For most experiments, such as propagating plants for seeds, floral dipping, or collecting leaf tissues for protoplast isolation, et al., seeds were geminated directly on soil (80% (v/v) compost, 20% (v/v) vermiculite and 0.3g/L Imidasect). Plants were grown in module tray holding 15 individual pots and watered regularly. In most of cases, dry seeds were soaked into water for at least 10min before resuspending into 0.1% top agar and then directly sown onto prewetted soil. The trays were subsequently kept in cold room for 3-4 days for vernalization before transferred to a percival or greenhouse. All trays were covered with a plastic dome to maintain high humidity till cotyledons were fully opened, then the dome was removed, and the plants were watered regularly.

For transgenic plants screen, seedlings were transferred from MS agar media plates containing specific antibiotics to soil after approximately 10-14 days of growth. Roots should remain intact during transferring, and deeply plated into soil to prevent dehydration. The trays were kept in a percival under standard growth condition.

6.2.2 Plants grown on medium

For the *in vitro* growth, seeds were aliquoted in microfuge tubes and surface-sterilized for at least 10 minutes with 70% (v/v) ethanol and 0.05% (v/v) Triton X-100 on an orbital shaker, followed by an additional 5-minute incubation with 100% (v/v) ethanol with shaking. After sterilization, each aliquot of seeds was transferred to an ethanol-sterilized Whatman filter paper (70 mm diameter) in a laminar flow hood till completely dry (~20 mins, depending on the quantity of seeds). The dry seeds were then sown directly onto Murashige-Skoog (MS) agar medium (4.3 g/L MS basal salt mixture; 0.5% (w/v) sucrose; 0.05% (w/v) 2-(N-morpholino)ethanesulfonic acid

(MES); pH adjusted to 5.7 with potassium hydroxide (KOH); phyto-agar was added to a concentration of 0.65% (w/v) before sterilization via autoclaving at 110°C for 15 minutes) in petri plates to a density of approximately 100-150 seeds per plates. The plates were then sealed with Micropore tape (3M), cold-treated at 4°C for 3-4 days, and thereafter kept in a percival for 10-14 days before used for the downstream experiments. For the induction of Cdc48-DN or Cdc48-WT expression in the corresponding transgenic lines, 8-day-old seedlings were transferred from MS agar media plates into MS liquid medium supplemented with 4 μM Estradiol (Sigma) and incubated for an additional two days with gentle shaking on an orbital shaker under standard growth condition.

6.3 Plant physiological studies

6.3.1 Crossing of *Arabidopsis* plants

Plants were grown on the soil as described above. For an efficient crossing, choose mother plant at a stage when they have developed 5-6 inflorescences, and father plants that have started to form siliques. Usually, a genotype with clear, recessive phenotype was designated as female acceptors. For the projects presented here, the *ppi1*, *tic110*/+ and SP1-OX *ppi1* mutants were used as mother plants, and the absence of the pale phenotype in the F1 generation could be therefore used as the indication of successful crossings.

Before crossing, the mature siliques as well as opened flowers and buds that already have a white tip from the inflorescence of the mother plants were removed using fine forceps. The meristem with those buds that were too small were also removed and 2-3 larger flower buds were remained. For emasculation, the flower bud was opened by inserting the tip of fine forceps between petals and sepals, and all sepals, petals and immature anthers were subsequently removed with care not to damage the carpel. An opened and mature flower from the father plant was taken with one pair of fine forceps (Jewelers forceps, Dumont No. 5, Sigma) and used to pollinate the already emasculated mother flower by gently tapping the anther on the stigma to cover it with pollen grains as much as possible. The whole pollination procedure was conducted under a dissecting

microscope to ensure that the mother flower was originally free from contamination of pollen grains, and that the stigma was covered with the desired pollen grains. The pollinated inflorescence was marked with a small thin tape labeled with crossing information such as mother, father, and date.

Siliques with hybrid seeds would mature after 15-25 days depending on growth conditions. They were harvested by cutting them directly into a 1.5 ml Eppendorf tube when siliques were a bit yellow, but prior to opening. A couple of small holes were then poked through the lid of Eppendorf tube and seeds were kept at room temperature for further maturation and drying.

6.3.2 Floral dipping transformation of *Arabidopsis* plants

Floral dipping transformation of *Arabidopsis* was adapted from a method described previously (Zhang et al., 2006). Plants of desired genotypes were grown on soil as described in section 6.2.1 until aged between 4-5 weeks. The primary bolts were clipped to encourage the growth of secondary stems, and thus more flowers per plants. The plants would then be ready for transformation within a week after clipping.

For preparing the *Agrobacterium* culture needed, *Agrobacterium tumefaciens* GV3101 colonies were picked from antibiotic selection LB plates incubated at 28°C for 3 days. Single colony was propagated in 5ml of LB medium containing the relevant antibiotic for overnight at 28°C with shaking at 200rpm. 250 µl of the overnight culture was then diluted into 500 ml conical flask containing 250 ml of LB medium and antibiotic and incubated at 28°C for 24 hrs with shaking at 200 rpm.

On the day of transformation, a solution containing 5% sucrose (no autoclave needed) were freshly prepared, and roughly 500 ml of solution was needed for each transformation. The cultured *Agrobacterium* cells were centrifuged at 5000 rpm for 10min, and pellet was resuspended in ~300ml of 5% sucrose solution. The cell density was measured, and the volume

of the solution might be adjusted to achieve the OD_{600} reading of 0.8. The Silwet L-77 surfactant was added to the cell suspension at a final concentration of 0.3% right before the dipping.

The open flowers and siliques of the plants were removed before the transformation to reduce the number of non-transformed seeds. The above-ground parts of plants were dipped into the *Agrobacterium* suspension for 20-30 seconds with gentle swirling. The dipped plants were laid flat in the tray covered with plastic dome for one day to retain high humidity. The plants were then restored upright and watered as usual after a couple of days until full maturity.

The mature T1 seeds were sown on MS agar medium plates containing 200 μg/ml cefotaxime (to prevent growth of *Agrobacterium*) and an additional specific antibiotic to screen for the positive transformants.

6.3.3 Chlorophyll measurements

The content of leaf chlorophyll was measured via two different methods.

6.3.3.1 DMF extraction and spectrophotometer

The chlorophyll content of young seedlings (~10 days) was measured using a spectrophotometer following the extraction with *N,N'*-dimethylformamide (DMF). Rosette leaves were collected into 2 ml Eppendorf tube from each genotype and the fresh weight was measured using fine balance (Sartorius). The material could be frozen in liquid nitrogen at this stage and stored in the -80°C freezer, or continued to the following steps. For ~50 mg of leaf material, 1 ml of DMF was added into the tube in the fume hood. All the tubes were closed tightly and placed in a rack. The rack was double wrapped with foil and left to incubate overnight at 4°C on an orbital shaker at ~50 rpm.

The absorbance of each sample was then measured in a quartz cuvette (Hellma Analytics) in the fume hood for the wavelength of 646.8 nm and 663.8 nm relative to blank (DMF) using a spectrophotometer (Ultrospec 100 Pro visible, Amersham Biosciences). The cuvette was rinsed

with DMF between the read to eliminate the cross contamination. Ideally, the absorbance reading should be between 0.01 and 0.8; if it exceeded 0.8, samples were further diluted with DMF. The absolute chlorophyll concentration in nmol/mg fresh weight or nmol/mg per plant was calculated using published equations (Porra et al., 1989), taking into account the dilution factor if available:

Chlorophyll a = [(13.43 × Abs at 663.8) – (3.47 × Abs 646.8)]/fresh weight × dilution factor

Chlorophyll b = [(22.90 × Abs at 646.8) – (5.38 × Abs 663.8)]/fresh weight × dilution factor

Chlorophyll a+b = [(19.43 × Abs at 646.8) + (8.05 × Abs 663.8)]/fresh weight × dilution factor

6.3.3.2 SPAD meter

For the mature plants, the chlorophyll content of individual leaves per genotype were measured using a SPAD-502 meter (Konica Minolta) according to the manufacturer's guidelines. The SPAD reading, x, were converted into nmol of total chlorophyll (a + b) per mg of fresh weight using the calibrated equation (Ling et al., 2011):

Chlorophyll a+b = $(0.0007x^2 + 0.023x) + 0.054$

6.3.4 Senescence

Dark treatments for the induction of senescence were conducted as previously described (Ling et al., 2012). Developmentally equivalent leaves of 28-day-old plants were wrapped in aluminium foil whilst still attached to the plant, and then left under standard growth conditions for 5-6 days. The maximum photochemical efficiency of photosystem II (F_v/F_m) was determined by measuring chlorophyll fluorescence with a CF imager (Technologica, UK) as described previously. Three experiments were performed, and approximately ten leaves (each one from a different plant) were analysed per genotype in each experiment.

6.4 Plant DNA and RNA related works

6.4.1 DNA extraction from *Arabidopsis* leaf tissue

DNA was extracted from mature rosette leaves. One or two rosette leaves were cut from the plants of interested into a 2 ml Eppendorf tube containing one or two steel balls followed by flash-frozen in liquid nitrogen immediately. The frozen samples were then ground into fine powder using a TissueLyser (Qiagen) at 25 Hz for 2-3 minutes. The tissue powder was collected at the bottom of tube by centrifuge at 1000 rpm for 1 minute before adding 300 µl of DNA extraction buffer (200 mM Tris(hydroxymethyl)aminomethane-HCl (Tris-HCl) pH 7.5, 250 mM NaCl, 25 mM (ethylenedinitrilo) tetraacetic acid (EDTA), 0.5% (w/v) sodium dodecyl sulfate (SDS)). Each sample was then vortexed for 5 seconds and centrifuged at maximum speed for 5 minute at room temperature. The supernatant of each sample was then transferred into a fresh 1.5 ml Eppendorf tube followed by adding 300 µl of isopropanol and mixing thoroughly via brief vortex. The sample was centrifuged at maximum speed for 5 minutes at room temperature. The supernatant was then discarded, and the pellet was washed with 1 ml of 70% (v/v) ethanol by centrifuge for 5min at maximum speed. The ethanol was then removed, and the tube was kept upside down to let the pellet air-dried at room temperature. Each dried pellet was resuspended in ~30 µl of dH_2O and stored in fridge for further use.

6.4.2 Polymerase Chain Reactions (PCR)

All PCRs was carried out on a Biometra T3 Thermocycler using standard reaction mixtures: 10 mM Tris-HCl pH 8.3, 50 mM KCl, 50 mM $MgCl_2$, 200 µM of deoxyribonucleoside triphosphates (dNTPs), 0.25 µM of each primer, and 0.5 units of Taq DNA Polymerase. In the case of cloning and sequencing, the Phusion Hot Star II High Fidelity DNA polymerase (Fisher Scientific) was used in PCR reaction for high accuracy during DNA amplification. In this case, PCR reactions were performed according to the manufacturer's instruction.

The primers for all PCR-based analyses in this study can be found in Table 6.1.

6.4.3 Agarose gel electrophoresis

PCR amplicons were resolved on 1% to 3% (w/v) agarose gels depending on the sizes of the DNA fragments to be separated. The appropriate mass of agarose was weighed into an Erlenmeyer flask followed by adding 0.5 x TBE running buffering (40 mM Tris-HCl pH 8.3, 45 mM boric acid, 1 mM EDTA) into the flask. The Agarose/buffer mixture was subsequently melted by heating in a microwave till the agarose has completely dissolved. After cooled down for ~5 minutes on benchtop, 4 μl of 1x SYBR Safe DNA stain was added into 100ml of the molten agarose before pouring it into a gel mold placed with an appropriate comb. When the gel was set, the comb was removed, and the gel was placed into the gel running tank containing 0.5 x TBE buffer. Alternatively, the gel can also be wrapped with a cling film and stored at 4°C until use.

PCR amplicons were loaded in 1 x Orange G loading buffer (0.1% (w/v) Orange G, 50% (v/v) glycerol) and resolved by running on prepared agarose gel with desired voltage until the loading dye had migrated to an appropriate distance. An appropriate DNA size marker should always be loaded along with experimental samples. When electrophoresis has completed, the gel was exposed to UV light for visualization using GeneFlash (Syngene) gel documentation system.

6.4.4 Genotyping of T-DNA insertion mutants

A series of *Arabidopsis* T-DNA insertion mutants were used in this study and each mutant was genotyped via PCR using gene-specific primers paired with standard left border genotyping primers that anneal to the T-DNA insert. For example, LBb1, LBb1.3 or LBa1 was used for SALK lines, while LB1, LB2 orLB3 was used for SAIL lines. In each genotyping procedure, two parallel PCR reactions were set up using genomic DNA extracted from the mutant plants, as well as a wild-type plant as negative control. The first PCR used a primer specific for the left-border of the T-DNA, and a complementary primer which was placed approximately 500 bp downstream of the putative T-DNA insertion site. This would confirm presence of the T-DNA in the sequence of interested. The second PCR used a pair of primers specific to the gene of interested, which

located on each side of T-DNA, respectively. Amplification of this product would not occur under the standard PCR conditions if a T-DNA were present. Conversely, when the T-DNA is absent, the amplicon of expected size from the interested gene would be detected. The amplicons from both PCR reactions were resolved via agarose gel electrophoresis. Amplification in both reactions indicated heterozygosity, whereas the sole amplification in the first reaction indicated homozygosity, and the amplification in second reaction only indicated wild type.

6.4.5 Genotyping by dCAPS

EMS mutagenesis often caused the single nucleotide substitution. When such a single nucleotide polymorphism (SNP) needed to be detected, a specific method called Derived Cleaved Amplified Polymorphic Sequences (dCAPS) analysis would be employed. A primer containing one or more mismatches to the template DNA was designed to create a restriction site at the polymorphic locus. The restriction site could be created either in wild type or mutant gene sequence. The dCAPS primers used in this study were designed via a simple program called dCAPS Finder 2.0. The typical length of the amplicon from the PCR using dCAPS primers was around 100 bp. After being treated with specific restriction enzyme, two different sized bands could be detected after gel electrophoresis: ~100 bp band for the non-cleaved amplicon, and ~80bp band for the cleaved amplicon. Such a 20 bp difference could be distinguished on a 3% agarose gel, and the homozygous or heterozygous genotype could be determined based on the availability of different size bands.

6.4.6 RNA extraction from *Arabidopsis* leaf tissue

20-50mg of rosette leaves from *Arabidopsis* plants were collected into a 2 ml Eppendorf tube containing 2-3 steel balls. Leaf samples were subsequently flash frozen in liquid nitrogen before homogenized into fine powders using a TissueLyser (Qiagen) at 25 Hz for 3 minutes. Total RNA was then extracted using a Spectrum Plant Total RNA Kit (Sigma) by following the manufacturer's instructions. Potential DNA contamination was eliminated from RNA samples

during the extraction by using On-Column DNase I Digestion Set (Sigma). The concentration of each RNA sample was determined using a NanoPhotometer P330 (Implen).

6.4.7 First-strand cDNA synthesis

The complementary DNA (cDNA) was synthesized using a SuperScript IV Reverse Transcriptase (Invitrogen) system in accordance with manufacturer's instructions. Each reaction was prepared to a 20 µl total volume, and a total of 1 µg of RNA was used. The cDNA samples were diluted 1:5 or 1:10 before used as the templates in the following reverse transcription polymerase chain reaction (RT-PCR).

6.4.8 Semi-quantitative RT-PCR

Semi-quantitative RT-PCR was carried out using primers specific for the target gene, and the primers for control gene which was *EUKARYOTIC TRANSLATION INITIATION FACTOR 4E-1* (*eIF4E1*) in this study. An equal amount of cDNA was used for each PCR reaction, and a low number of PCR cycles (20-25 cycles) was applied to avoid saturation of amplicons. The PCR amplicons were resolved on 1% agarose gel and imaged using gel documentation system as described in Section 6.4.3.

6.5 Bacterial work and molecular cloning

6.5.1 Preparation of lysogeny broth (LB) medium

Liquid LB medium was made from 10 g of bacto-tryptone, 5 g of yeast extract, and 5 g of NaCl in 1 L of dH_2O. 400 ml of broth was aliquoted into a 500 mL Duran bottles and autoclaved for 15 minutes at 110°C. For LB agar plates, 1% (w/v) of agar was added to the liquid LB medium prior to autoclaving. For making LB agar plates, LB agar medium was melted in the microwave and left to cool to ~ 60°C. Before poured into 9 cm diameter petri dishes in a flow hood, the relevant antibiotics were added to the LB medium for selection of bacteria containing the plasmids of interest. The final concentration of antibiotics used in this study were: 100 µg/ml of ampicillin,

50 µg/ml kanamycin, 50 µg/ml spectinomycin and 10 µg/mL gentamycin. The plates were left to dry for at least 30 minutes.

6.5.2 *E. coli* transformation and plasmid DNA extraction

The heat shock method was employed for the transformation of plasmid DNA or ligation product into *E. coli*. 25 µl of DH5α *E. coli* competent cells (α-Select Silver Efficiency Competent Cells, Bioline) aliquot for each transformation were thawed on ice. 2.5 µl of plasmid DNA or ligation product was added to the cells and incubated on ice for 30 minutes. The cells were then heat shocked for 45 seconds at 42°C in a water bath and immediately placed back on ice for 2 minutes. 450 µl of liquid LB medium was then added to the cells followed by incubation at 37°C for 1 hour with shaking at 200 rpm. After incubation, 100-150 µl of the transformed cells were spread on LB agar plates containing the appropriate antibiotics for selection using disposable plastic spreaders. The colonies grew overnight at 37°C.

Following overnight incubation, PCR was performed on several colonies growing on the selective LB agar plates to check whether the plasmid or ligation product had been inserted into *E. coli*. Individual colony was picked using a sterile pipette tip into 1.5 ml Eppendorf tube containing 20 µl of LB liquid medium and vortexed for 30 seconds. This mixture was used as the template of PCR reaction using primers specific to the cloned gene or fragment. The mixture containing the positive colony was then diluted into 5 ml of LB liquid medium containing relevant antibiotic and incubated overnight at 37°C with shaking at 200rpm.

Plasmid DNA was isolated from transformed bacterial cells using a miniprep (Qiagen Plasmid Mini Kit) or a midiprep kit (Qiagen Plasmid Midi Kit) depending on the requirement for the certain concentration of plasmid DNA. For miniprep isolation, 5 ml of overnight cell culture was sufficient, whereas 50 ml of overnight cell culture was needed for midiprep extraction. In both cases, the plasmid DNA extraction was performed according to the manufacturer's protocol. DNA concentration was determined by using a NanoPhotometer P330 (Implen).

6.5.3 Blue-white screening

Blue-white screening is a convenient way to distinguish bacterial colonies that contain a cloning vector with a proper DNA insert, from those containing empty vectors. In this study, blue-white screening was used to identify *E. coli* colonies transformed with pGEM-T Easy vector containing insertion of interested gene or DNA fragment. This was done by spreading 40 µl of 20 mg/ml 5-bromo-4-chloro-3-indolyl-beta-D-galactopyranoside (X-Gal) dissolved in DMSO, and 40 µL of 0.1 M isopropyl thiogalactoside (IPTG) onto each LB agar plate containing 100 µg/ml ampicillin prior to spreading the transformed bacterial cells on the same plate. After overnight incubation at 37°C, the bacterial colonies transformed with pGEM-T Easy, containing the insert of interest would appear white, whereas those transformed with empty pGEM-T Easy vector appeared blue. White colonies were subsequently selected and propagated.

6.5.4 Preparation of competent *Agrobacterium* cells

The *Agrobacterium* strain used in this study is GV3101 which has both resistance to Rifampicin and Gentamycin. A LB agar medium plates containing 50 µg/ml of rifampicin and 50 µg/ml of gentamycin was streaked with *Agrobacterium* GV3101 cells taken from a frozen stock of competent cells. The plate was kept at 28°C for 3-5 days till colonies grew into medium size. A single colony was picked and cultured in 5 ml of LB liquid medium containing appropriate Rifampicin and Gentamycin for overnight at 28°C with shaking at 200 rpm. 2ml of overnight culture was then diluted into 50 ml of LB liquid medium containing same antibiotics in a 250ml of flask and incubated at 28°C with shaking at 200 rpm until the cells grew to OD_{600} of 0.5-1. The cell culture was then cooled down on ice before centrifuged at 3000 g for 5 minutes at 4°C to pellet cells. The supernatant was discarded, and the cell pellet was resuspended with 1 ml of 20 mM ice-cold $CaCl_2$. Cell aliquot (50 µl) was dispensed into pre-chilled 1.5 ml Eppendorf tube and flash frozen in liquid nitrogen. *Agrobacterium* competent cells were stored at -80°C.

6.5.5 *Agrobacterium* freeze-thaw transformation

The freeze-thaw transformation of *Agrobacterium* used in this study was adapted from a method described previously (Weigel & Glazebrook, 2006). A 50 µl aliquot of *Agrobacterium* competent cells was thawed on ice. Typically, 1 µl of the binary plasmid containing the DNA sequence of interest was added to the *Agrobacterium* competent cells aliquot. The cells were then flash frozen in liquid nitrogen and subsequently thawed by incubating at 37°C in a water bath for 5 minutes. 1 ml of LB medium was added to the cells followed by incubation at 28°C for 3 hours with shaking at 200 rpm. The cells were then pelleted via centrifugation at 5000 rpm for 30 seconds and resuspended in ~100 µl of LB liquid medium. The cells were spread on LB agar medium plates containing gentamycin, rifampicin, and specific antibiotic for the selection of agrobacteria transformed with the desired binary vector. The plates were then incubated at 28°C for 3-5 days. Individual resistant colonies were picked for PCR conformation followed by propagation.

6.5.6 Cloning using Gateway system

The constructs used in all co-IP experiments and *Agrobacterium*-mediated plant transformations were generated via the Gateway cloning system (Invitrogen). All primers used for gateway cloning are listed in Table 6.1.

The specific forward and reverse primers of the interested gene were appended with Gateway *attB1* sequence 5'-GGGGACAAGTTTGTACAAAAAAGCAGGCTCC-3' and *attB2* sequence 5'-GGGGACCACTTTGTACAAGAAAGCTGGGTT-3', respectively, to generate a modified gene fragment containing the *attB1* and *attB2* sequences at 5' and 3' ends, respectively via PCR using Phusion polymerase. Where necessary, 1 M betaine was added into the PCR reaction mixture to reduce the annealing temperature since the extended primers were used. The *PUX10* fragments with various domain deletions were generated by overlapping PCR. All PCR amplicons were resolved by agarose gel electrophoresis and bands were purified using GenElute Gel Extraction Kit (Sigma).

The purified DNA fragments flanked with *attB* recombination sites were inserted into pDONR201 entry vector via incubation with BP clonase according to the manufacturer's protocol. The reaction mixtures were then used to transform *E. coli* competent cells as described in section 6.5.2. Individual resistant colonies were picked for PCR conformation followed by propagation for plasmid DNA extraction. The plasmid DNA samples were then sent for Sanger sequencing (Source Bioscience). The sequence data was analysed using SnapGene software, and the constructs containing correct insertions were used for the following LR reaction.

For LR reaction, the pDONR201 entry vector bearing accurate insertion was incubated with destination vector and LR clonase. The destination vectors used in this study included p2GWY7 used in all protoplast transfections, as well as modified pH2GW7 containing a C-terminal haemagglutinin (HA) epitope-tag and pK7YWG2 used for generating the transgenic plants. The LR reactions were set up according to the manufacturer's instructions and the reaction mixtures were then used to transform *E. coli* competent cells as described in section 6.5.2. The plasmid DNA was extracted from the cell culture of resistant bacterial colony bearing accurate insertion.

6.5.7 Cloning using restriction enzyme digest and ligation method

All the constructs used in the bimolecular fluorescence complementation (BiFC) experiments in this study were generated via restriction enzyme digest and ligation method. The primes used in these cloning procedures are listed in Table 6.1.

The coding sequence of interested gene was analysed for the presence of restriction sites, and pairs of restriction enzymes that were absent in coding sequence but present in the multiple cloning site (MCS) of BiFC vector, pSAT4A-nEYFP-N1 or pSAT4A-cEYFP-N1, were chosen. The pair of restriction sites were then added to the 5' end of the pair of primers which were used for amplifying the full-length CDS of the interested gene without stop codon, respectively. The gene insert was then flanked by the restriction sites compatible with the recipient BiFC vector's MCS via PCR using Phusion polymerase. The BiFC vector was linearized via double digestion in

the MCS using these designated restriction enzymes (NEB). Meanwhile, the same double digestion was applied to the gel purified PCR product flanked with restrictions sites to leave overhangs complementary to those of the digested vector. Alternatively, the PCR product flanked with restrictions sites could firstly be subcloned into pGEM-T Easy vector followed by *E. coli* transformation as described in section 6.5.2 and 6.5.3. The Plasmid DNA was extracted from the propagated single colony bearing accurate DNA insert and was then double digested with the designated restriction enzymes. Following double digestion, both DNA insert and linearized vector were resolved on agarose gel and purified by using the GenElute Gel Extraction Kit (Sigma). The ligation reaction was typically performed by using an approximately 3:1 molar ratio of DNA insert to vector, and incubating overnight at 4°C or room temperature for 3 hours with T4 ligase (Promega) in a 10 µl of reaction volume. Both restriction enzyme digestion and T4 ligase catalyzed DNA ligation were carried out according to the manufacturer's protocols. After incubation, 2.5 µl of ligation reaction was subsequently used to transform 25 µl of *E. coli* competent cells as described in section 6.5.2. The single colony bearing correct construct was cultured and the plasmid DNA was extracted for use in the BiFC experiments.

6.5.8 Constructs generated for this study

All constructs generated for this study are listed in Table 6.1.

6.6 Protein analysis

6.6.1 Total protein extraction from *Arabidopsis* plants

Approximately 50-60 mg of seedlings grown *in vitro* for 10 -14 days, or rosette leaves from 3-4 weeks of plants grown on soil, were collected into 2 ml of Eppendorf tubes containing 1-2 steel balls and flash frozen in liquid nitrogen. Plant samples were subsequently homogenized into a fine powder by using a TissueLyser (25 Hz for 3 minutes) and immediately suspended in ~300 µl of ice-cold protein extraction buffer (PEB) (100 mM Tris-HCl pH 6.8, 10% (v/v) glycerol, 1% (w/v) SDS, 0.1% (v/v) Triton X-100, 5 mM EDTA) containing dithiothreitol (DTT) and Protease

Inhibitor Cocktail (PIC; Sigma). Typically, 10 µl of 1M DTT and 10 µl of PIC were added to every 1ml of PEB right before the suspension of homogenized tissues. The samples were then vortexed and incubated on ice for 30 minutes. The samples were then centrifuged at maximum speed for 10 minutes at 4°C in a microcentrifuge. ~250 µl of the supernatant from each sample was transferred into a fresh 1.5 ml of Eppendorf tube and store at -20°C for short term or -80°C for long term, or used for the downstream experiments immediately.

6.6.2 Protein quantification by Bradford assay

Where necessary, the concentration of each protein sample was determined via a Bradford assay. Before analysis, 10 µg/µl bovine serum albumin (BSA) stock was diluted 1:10 in dH_2O to 1 µg/µl. A series of BSA standards were then made by adding 0, 1, 2, 4, 8 and 10 µl of 1 µg/µl BSA to 6 Eppendorf tubes containing dH_2O, respectively, to reach a total volume of 799 µl each. 1µl of protein extraction buffer used in section 6.6.1 was added to each tube. For each protein sample, 1 µl of protein was added to 799 µl of dH_2O. Afterwards 200 µl of Bio-Rad Protein Assay (Bio-Rad) was added to each tube containing either BSA standard or extracted protein sample to reach a total volume of 1ml. The samples were vortexed briefly and applied for Absorbance readings (OD_{595}) using a NanoPhotometer P330 (Implen). The absorbance values were plotted against the concentration of BSA standards in Microsoft Excel, and the equation of a linear approximation was used to calculate the concentration of extracted protein samples.

6.6.3 Preparation of SDS-PAGE gel

All the SDS-PAGE gels used in this study were manually cast using glass plates and a compatible casting assembly (Mini Protean III, Bio-Rad). Two essential solutions, 4 × resolving buffer and 4 × stacking buffer, were prepared beforehand, and stored at room temperature. 4 × resolving buffer contains 1.5 M Tris at pH8.8 and 0.4% SDS. 4 × stacking buffer contained 0.5 M Tris at pH6.8 and 0.4% SDS. 12% SDS-PAGE gel were used in all the western blotting experiment throughout this study. For preparing 12% SDS-PAGE gels, 4ml of 30% (w/v) acrylamide stock

containing 0.8% (w/v) bis-acrylamide (ProtoGel) was mixed with 2.5 ml of 4 × resolving solution and the mixture was then topped up to 10 ml using dH_2O. Before pouring, 50 µl of 10% (w/v) ammonium persulfate (APS) and 5 µl of tetramethylethylenediamine (TEMED) were added to 10ml of resolving gel solution in order to polymerize the acrylamide. ~3.5 ml of resolving gel solution was then loaded into an SDS-PAGE casting assembly (Mini Protean III, Bio-Rad), and isobutanol was immediately added to the top to level the surface and aid polymerization by excluding air. The gel was left at room temperature for ~45 minutes for solidify. The overlaid isobutanol was subsequently poured off and the gel surface was raised with running tap water to remove residuals. The 5% stacking gel solution was prepared by adding 0.67 ml of 30% (w/v) acrylamide stock into 1ml of 4 × stacking buffer and topped up to 4 ml with dH_2O. 50 µl of 10% (w/v) ammonium persulfate (APS) and 5 µl of tetramethylethylenediamine (TEMED) were then added to 4 ml of stacking gel solution. ~1ml of stacking gel solution was carefully loaded on the top of the resolving gel to avoid bubbles and a comb was inserted to form the wells. The gel was left at room temperature for ~15-30 minutes to set.

6.6.4 SDS-PAGE

Prior to loading to SDS-PAGE gel, the protein samples were denatured by mixing with equal volume of 2 × protein loading buffer (0.1 M Tris-HCl, pH 6.8, 2% (w/v) SDS, 20% (v/v) glycerol, 0.02% (w/v) bromophenol blue) supplemented with 0.1 M DTT and boiled at 95°C for 5 minutes. Denatured protein samples were centrifuged at maximum speed for 3 minutes to precipitate debris and an appropriate volume of supernatant (typically 10 µl) from each sample was taken for loading into SDS-PAGE gel.

Each gel was fitted into the Mini-PROTEAN gel chamber (Bio-Rad) which was then filled with enough 1 × Tris-Glycine-SDS running buffer (TGS; 25 mM Tris, 192 mM glycine, 0.1% (w/v) SDS) to cover both electrodes. 10 µl of each denatured protein sample was loaded into each well. Importantly, a pre-stained protein ladder (Precision Plus Protein Dual Color Standards, Bio-Rad)

was loaded in the first and last wells in each gel. The gel was then run at 180V at room temperature for 60 minutes.

6.6.5 Coomassie staining

Where needed, the SDS-PAGE gel was incubated in InstantBlue Protein Stain (Expedeon) for at least 10 minutes at room temperature with gentle shaking. The stained gel was then photographed using LAS-4000 imager (Fujifilm).

6.6.6 Western blotting

In most cases, proteins separated in SDS-PAGE gel were directly transferred out of the gel to the surface of a nitrocellulose blotting membrane (Amersham Protran 0.2μm NC nitrocellulose blotting membrane, GE Healthcare). This was done by first creating a "transfer sandwich" in a transfer cassette in the ice-cold transfer buffer (25 mM Tris, 192 mM glycine, 20% methanol) in such orders: sponge, 3 filter papers, gel, NC membrane, 3 filter papers and sponge. It was crucial to ensure that there were no air bubbles between the gel and NC membrane. The cassette was closed and then placed in the Mini Trans-Blot Cell system (Bio-Rad), with the gel facing the negative electrode, and NC membrane facing the positive electrode. The ice-cold transfer buffer was added to the tank till the "transfer sandwich" completely submerged in buffer. An ice pack was also inserted into the transfer tank to keep the assembly cool. The transfer was done at 100V for 60 minutes with gentle stirring.

Once the transfer was completed, the membranes were removed from the cassettes and blocked in blotto (5-8% (w/v) skimmed milk in TBS-T solution (10 mM Tris-HCl pH 8, 150 mM NaCl, 0.05% (v/v) Tween 20)) for 30 minutes at room temperature with gentle shaking. After blocking, each membrane was cut into 2-3 sections according to the sizes of proteins to be analysed, and each membrane section was then incubated with specific primary antibody diluted in blotto overnight at 4°C with gentle shaking. The dilution ratio of primary antibodies depended on the properties of the individual antibodies.

On the next day, the membrane strips were removed from primary antibody solutions and briefly rinsed with TBS-T separately before combined into a single tray and further washed three times at room temperature with gentle shaking, for 5 minutes each time with 20 ml TBS-T. After washing, the membrane sections were incubated with a secondary antibody for 1 hour at room temperature with gentle shaking. The secondary antibody was selected according to the organism in which the primary antibody was raised. The secondary antibodies used in this study were polyclonal goat anti-rabbit IgG conjugated with horseradish peroxidase (Sigma, 12-348), or, in the case of immunoprecipitations, monoclonal mouse anti-rabbit IgG light-chain-specific conjugated with peroxidase (Jackson ImmunoResearch, 211-032-171). The secondary antibody was diluted in Blotto (1:5000 – 1:10000). The membrane sections were then rinsed with TBS-T and further washed three times at room temperature with gentle shaking, 5 minutes each time in 20 ml TBS-T. Chemiluminescence was detected using EZ-ECL Chemiluminescence Detection Kit (Biological Industries, Sartorius), and an LAS-4000 imager (Fujifilm). Band intensities were quantified using AIDA software (Raytek). Quantification data were based on results from at least three experiments all showing a similar trend.

6.7 Chloroplast-related assays

6.7.1 Chloroplast isolation

Chloroplast isolation was carried out as described previously (Ling & Jarvis, 2016).

All the solutions, devices, equipment, and rotors were kept in the old room one day before isolation. The whole process was performed in a cold room and the plant materials were kept on ice throughout the isolation. All the centrifugations were carried out at 4 °C in the Avanti JXN-26 high-speed centrifuge (Beckman Coulter).

For the induction of Cdc48-DN or Cdc48-WT expression in the corresponding transgenic lines, 8-day-old seedlings were transferred from MS agar media plates, by gently scraping them off with a gloved hand, into a sterilized flask of MS liquid medium supplemented with 4 μM

Estradiol (Sigma) and incubated for an additional two days with gentle shaking (~100 rpm) under standard growth condition.

Prior to plant homogenization, a continuous density gradient was prepared by mixing 13 ml of Percoll, 13 ml of 2 × CIB buffer (0.6 M sorbitol, 10 mM magnesium chloride ($MgCl_2$), 10 mM Ethylene Glycol Tetraacetic Acid (EGTA), 10 mM ethylenediaminetetraacetic acid (EDTA), 20 mM sodium bicarbonate ($NaHCO_3$), 40 mM 4-(2-hydroxyethyl)piperazine-1-ethanesulfonic acid (HEPES); pH 8.0 with KOH), and ~5 mg of glutathione into a 50 ml centrifuge tube and centrifuging the mixture at 43,000 × g for 30 minutes with the brake off by setting "acceleration" to "maximum" and "deceleration" to "9" in the centrifuge to avoid disturbing the gradient. The tube was then removed from the centrifuge carefully not disturbing the gradient and kept on ice for the later use.

After estradiol induction, the young seedlings were removed from the liquid MS medium by tipping them into a sieve and transferred into a beaker containing 100 ml of 1 × CIB (diluted 2 × CIB 1:1 with pre-chilled distilled water) for rinsing off any residual liquid MS medium. Seedlings were then transferred to another beaker containing 100 ml of fresh 1 × CIB.

For the homogenization, a total of 100 ml of 1 × CIB per sample was used in five consecutive rounds of 20 ml of 1 × CIB. Most of the seedlings were placed into a 50 ml beaker containing 20 ml of fresh pre-chilled 1 × CIB and placed under the rotor of Polytron (Kinematica PT10-35) and homogenized with two pulses of 1 - 2s each for the first round of homogenization. The homogenate was filtered through the double layer of Miracloth into a 250 ml of centrifuge tube kept on ice by gentle squeezing the Miracloth around the tissues. The tissues left on the Miracloth and any remaining tissue not used in the first round of homogenization were placed back into the 50 ml beaker containing the second 20 ml of 1 × CIB, and the homogenization and filtration steps were repeated until the 100 mL 1 × CIB has been used up. The homogenates from all five rounds of homogenization were pooled and centrifuged at 1000 × g for 5 minutes with braking on by setting both "acceleration" and "deceleration" to "maximum" in the centrifuge.

The supernatant was poured off immediately and the pellet was resuspended in the residual supernatant left in the tube (500 µl-1 ml) by gently agitating the tube on ice.

The resuspended homogenate was slowly transferred onto the top of the premade continuous Percoll gradient by using a Pasteur pipette to add it via the wall of the tube to avoid disturbing the gradient. The tube was then subjected to centrifugation in a swinging-bucket rotor at 7800 × g for 10 min with the brake off by setting "acceleration" to "maximum" and "deceleration" to "9" in the centrifuge to avoid disturbing the gradient. Once centrifugation was completed, two green bands were seen in the gradient: the lower band contains intact chloroplasts, whereas the upper band contains broken chloroplasts. To recover the intact chloroplasts, the top band was disposed by pipetting using a Pasteur pipette, and the lower band was transferred carefully via a Pasteur pipette into a fresh ice-cold 50 ml centrifuge tube. The volume of recovered intact chloroplasts ranged from 3 to 8 mL per gradient.

~25 ml of pre-chilled 1 x HMS buffer (50 mM HEPES, 3 mM magnesium sulphate, 0.3 M sorbitol; pH 8.0 with sodium hydroxide) was added to the tube containing intact chloroplasts followed by inverting tube twice to rinse off the Percoll from the chloroplasts. The tube was then placed back into the swinging-bucket rotor and centrifuged at 1000 × *g* for 5 min with the brake on by setting both "acceleration" and "deceleration" to "maximum" in the centrifuge. The supernatant was discarded, and the pellet of intact chloroplasts was resuspended in the remaining HMS buffer left in the tube by gently agitating the tube on ice. Where necessary, an additional 100-300 µl of fresh ice-cold 1 × HMS buffer was added. The chloroplasts were then transferred into a 2 ml microcentrifuge tube using a cut 1 ml pipette tip and kept on ice.

The integrity and yield of the isolated chloroplasts were assessed under a phase-contrast microscope (Nikon Eclipse 80i). A 1:100 dilution of isolated chloroplasts was firstly prepared by adding 5 µl of chloroplasts to 495 µl of 1 × HMS using a cut tip in a 1.5 ml microfuge tube and mixed by flicking the tube gently. The counting chamber of the haemocytometer (Improved Neubauer BS748 chamber, Hawksley Technology) was covered by a cover glass, and ~40 µl of

diluted chloroplasts was slowing added into the gap between the cover glass and the counting chamber. The haemocytometer was then placed under the phase-contrast microscope and the counting grid area was focused with a 10 × or 20 × objective. The intact chloroplast is round and bright green and surrounded by a halo of light under phase contrast. The number of chloroplasts per large square was ideally between 10 to 20. If too few or too many chloroplasts were observed, the dilution factor was adjusted and diluted sample was counted again. The number of chloroplasts per ml was calculated as follows: n (the average number of chloroplasts per large square) × 25 (total number of large squares in the grid) × 100 (dilution factor of chloroplast suspension) × 10^4 (scaling factor to express data per 1 ml, since the volume above the 25 squares is 0.1 mm^3). The yield of chloroplasts could be estimated by multiplying the concentration by the volume of chloroplasts suspension obtained. The chloroplasts were then aliquoted and used for the following assays.

6.7.2 Alkaline treatment of chloroplasts

The alkaline treatment to determine the membrane localization and integration of PUX10 was performed using chloroplasts isolated from 10-day-old seedlings of *35S: FLAG-PUX10-YFP* transgenic line grown on MS agar media as described previously (Chu & Li, 2011). 1 × 10^7 chloroplasts were used per sample for the alkaline treatment. All the centrifugations were performed at 4°C in this section.

When the chloroplasts isolation was completed, two aliquots of 100 µl of the chloroplasts were added to two fresh 1.5 ml microfuge tubes as the "Total sample" and "Extraction sample", respectively. Both samples were subjected to centrifugation at 3000 × g for 3 minutes and the supernatants were discarded. The chloroplasts pellet from the "Total sample" was resuspended in 30 µl of protein extraction buffer as described in section 6.6.1 and kept on ice as the "Total fraction".

Meanwhile, 200 µl of the alkaline solution (100 mM Na_2CO_3, pH 11.5) was added to the "extraction sample" tube to resuspend the chloroplasts pellet, and the resuspension was

incubated on ice for 30 minutes. After incubation, the resuspension was centrifuged at 100,000 × g for 45 minutes, and the supernatant was then transferred into a fresh 1.5 ml microcentrifuge tube as "The soluble fraction". The pellet was resuspended with 500 µl of the Alkaline solution before subjected to further centrifugation at 100,000 × g for 15 minutes. The supernatant was disposed, and the pellet was resuspended with 30 µl of the protein extraction buffer and kept on ice as the "The membrane fraction".

"The soluble fraction" was precipitated by adding an equal volume of 20% (w/v) trichloroacetic acid (TCA) solution and incubated on ice for 30 minutes. The precipitate was collected via centrifugation at 14,000 rpm for 30 minutes and then washed with 500 µl of ice-cold 100% acetone followed by the centrifugation at 14,000 rpm for 5 minutes. The supernatant was discarded, and the residual acetone was dried out in a fume hood. The precipitate was then resuspended with 30 µl of the protein extraction buffer and kept on ice.

For all three fractions (Total, soluble and membrane), 30 µl of 2 × protein loading buffer (0.1 M Tris-HCl, pH 6.8, 2% (w/v) SDS, 20% (v/v) glycerol, 0.02% (w/v) bromophenol blue) supplemented with 0.1 M DTT was added to each fraction and incubated at 95 °C for 5 minutes for protein denaturation. After incubation, the samples were centrifuged at maximum speed for 5 minutes, and 10 µl of supernatants of all three fractions were resolved on 12% SDS-PAGE followed by western blotting as described in section 6.6. Meanwhile, 5 µl of supernatants of all three fractions were resolved on 12 % SDS-PAGE followed by coomassie staining as descried in 6.6.5 as a loading control.

6.7.3 Chloroplast "dual protease" protection assay

The "dual protease" protection assay was conducted on chloroplasts isolated from 10-day-old seedlings of *35S: FLAG-PUX10-YFP* transgenic line grown on MS agar media, according to previously published method (Froehlich, 2011) with modifications. In this assay, 2×10^7 chloroplasts were used for each sample.

150 µl aliquots of isolated chloroplasts were sequentially added to four fresh 1.5 ml microfuge tubes. The four separate aliquots were treated as follows: Tube #1 (Mock [-] protease treatment control): 150 µl of chloroplasts and 100 µl of 1 × HMS are added, to give a final volume of 250 µl; Tube #2 (Thermolysin treatment): 150 µl of chloroplasts, 12.5 µl of thermolysin stock solution (10 mg/ml, freshly prepared in 5 mM $CaCl_2$/1 × HMS), and 87.5 µl of 1 × HMS are added, to give a final volume of 250 µl; Tube #3 (Trypsin treatment): 150 µl of chloroplasts, 25 µl of trypsin stock solution (1mg/ml, freshly prepared in 1 × HMS), and 75 µl of 1 × HMS are added, to give a final volume of 250 µl; and Tube #4 (Thermolysin + 1% Triton X-100 treatment): 150 µl of chloroplasts, 12.5 µl of thermolysin stock solution (10 mg/ml, freshly prepared in 5 mM $CaCl_2$/1 × HMS), 25 µl of 10% Triton X-100, and 62.5 µl of 1 × HMS are added, to give a final volume of 250 µl. All four tubes of reactions were incubated on ice for 30 minutes.

After incubation, the protease reactions were quenched on ice for 5 minutes as follows: Tube #1: add 50 µl of 1 × HMS (mock quench); Tube #2: add 50 µl of thermolysin quench solution (60 mM EDTA prepared in 1 × HMS); Tube #3: add 50 µl of trypsin inhibition solution (1 mg/ml in 1 × HMS); and Tube #4: add 50 µl of thermolysin quench solution (60 mM EDTA prepared in 1 × HMS).

After quenching, the chloroplasts of each reaction were pelleted via centrifugation at 2000 rpm for 5 minutes at 4°C and the pellets were then resuspended in 200 µl of lysis buffer (25 mM HEPES-KOH, pH 8.0, and 4 mM $MgCl_2$) and incubated on ice for 20 minutes. The lysed chloroplasts were centrifuged at 14000 × g for 30 minutes at 4°C and the supernatants were transferred into fresh 1.5 ml microfuge tubes (~200 µl for each reaction). The supernatants were precipitated by adding 800 µl of reagent grade acetone to each tube and keeping all the tubes on ice for 30 minutes. After incubation, the precipitates were recovered by centrifugation at 14000 × g for 5 minutes at 4°C. The supernatants were discarded, and the pellets were resuspended in 60 µl of 2 × protein loading buffer containing 0.1 M DTT and boiled at 95°C for 5 minutes. All the samples were ready for analyses via SDS-PAGE and western blotting as described in section 6.6.

6.8 Protoplast transient expression and immunoprecipitation

All centrifuge steps were performed at 4°C using 6441 swinging buckets in a Sorvall Legend RT centrifuge unless stated.

6.8.1 Protoplasts isolation from *Arabidopsis* plants

All the solutions used in this section were prepared in advance.

Protoplasts were isolated from the rosette leaves of 3-5-week-old plants using a modified "Tape-*Arabidopsis* Sandwich" method (Wu et al., 2009). Leaves were collected from wild type plants or specific transgenic plants and were stabilized to a strip of Time tape (3M) via their upper epidermal surfaces, while a Magic tap (Scotch) was fixed to the lower epidermal surfaces. The midvein of each leaf was crushed using a pair of curved-tip tweezers and gentle pressures were then applied to the leaves to promote the adherence of leaves to the magic tap. Approximately 18-30 leaves were used for each extraction depending on the properties of assays. The Magic tape was then carefully pulled away to peel off the lower epidermal cell layers. While still adhering to the Time tape, the peeled leaves were then incubated in ~25 ml of enzyme solution (1% (w/v) cellulase Onozuka R-10 (Duchefa), 0.25% (w/v) macerozyme R-10 (Duchefa), 0.4 M mannitol, 10 mM $CaCl_2$, 20 mM KCl, 0.1% (w/v) BSA, 20 mM MES; pH 5.7) in a petri dish on a platform shaker at 40 rpm for 2-3 hours at room temperature.

After incubation, the Time tape with digested leaves was removed, and the protoplast suspension was transferred to a 50 ml Falcon tube (Corning). The protoplasts were then subjected to centrifugation at 60 × g for 5 minutes. The enzyme solution was discarded, and the protoplast pellet was washed twice with ice-cold W5 solution (154 mM NaCl, 125 mM $CaCl_2$, 5 mM KCl, 5 mM glucose, 2 mM MES; pH 5.7), 25 ml each time. After the second wash, the protoplasts were suspended in 25 ml of fresh ice-cold W5 solution and incubated on ice for at least 30 minutes. After incubation, the protoplasts were pelleted by centrifugation at 40 × g for 4 minutes,

resuspended in 2 - 4 ml ice-cold MMg solution (0.4 M mannitol, 15 mM $MgCl_2$, 4 mM MES; pH 5.7) and kept on ice till use.

6.8.2 Protoplast transfection

All protoplast transfection procedures in this section were carried out at room temperature. 1M mannitol solution and 1M $Ca(NO_3)_2$ used in this section were prepared in advance.

Protoplasts were transfected via an established method with a modification (Wu et al., 2009). Before starting, a polyethylene glycol 4000 (PEG4000) solution was freshly prepared (40% (w/v) PEG 4000, 0.1 M $Ca(NO_3)_2$, 0.2 M mannitol) and kept at room temperature. Typically, 100 µl of ice-cold protoplast MMg suspension and 5 µg of plasmid DNA in no more than 10 µl were mixed in a 2 mL microcentrifuge tube by gentle pipetting 2-3 times. An aliquot of room temperature PEG4000 solution (110 µL) was immediately added to the tube and mixed by gently inverting tube. The tube was then kept at room temperature for 5 minutes. After incubation, the following series of room temperature W5 solution volumes was added sequentially to the tube after every 5 minutes of incubation and mixed by gentle inversion: 200 µl, 400µl and 800µl. After the final incubation, the transformed protoplasts were harvested by centrifuge at 40 × g for 3 minutes, and the protoplast pellet was then washed twice with 1.5 ml of W5 solution each time. After the second wash, the pellet was resuspended in 600 µl of W5 solution and transferred to the well of a 24-well culture plate (Corning). The culture plates were wrapped in aluminium foil and placed in a Percival growth chamber for incubation overnight at 20°C in the dark.

6.8.3 co-immunoprecipitation (co-IP)

For co-IP, the protoplasts were co-transfected with two constructs of interest following the procedures described in section 6.8.2. However, 50 µg of plasmid DNA from each construct was used to co-transfect 600 µl of the protoplast suspension in each case.

On the next day, 5 μM bortezomib (a proteasome inhibitor) was added to the overnight cultured transfected protoplast suspension which was then left on a worktop at room temperature for 4 hours. The protoplast suspension was then transferred into a 50 ml Falcon tube and centrifuged at 100 × g for 2 minutes to pellet the cells. The pelleted protoplasts were resuspended in 500 μl of lysis buffer (25 mM Tris-HCl pH 7.5, 150 mM NaCl, 10% (v/v) glycerol, 1 mM EDTA, 1% (v/v) Triton X-100, 5 μM bortezomib, 0.5% (v/v) PIC) and incubated for 30 minutes at 4°C on a rotating mixer. The lysate was then centrifuged at maximum speed for 10 minutes at 4°C and the supernatant was collected into a fresh 2 ml Eppendorf tube. A 30 μl aliquot of the supernatant was taken out as a 'total lysate' (TL) control.

For the following immunoprecipitation, the GFP-Trap MA magnetic beads (Chromotek) and Pierce™ Anti-c-Myc Agarose beads (ThermoFisher Scientific) were used in this study. A 25 μl aliquot of beads was equilibrated with 500 μl of ice-cold IP buffer (same as lysis but without bortezomib) in a 1.5 ml Eppendorf tube. After vortexed for 10 seconds, the beads were either pelleted via centrifugation (applied to agarose beads), or magnetically separated from IP buffer by using a MagJET Separation Rack (Thermo Fisher). The IP buffer was discarded, and the equilibration was repeated two more times. After the final equilibration, the IP buffer was disposed, and the cleared lysates was then added to the equilibrated beads and incubated at 4°C for overnight with rotating.

After overnight incubation, the beads were then pelleted via centrifugation or magnetically separated. Where necessary, a 30 μL aliquot of the supernatant was retained as a 'flow through' (FT) sample; these samples were taken to determine the binding efficiency of the target protein to the beads. The rest of supernatant was discarded, and the beads were washed for five times with ice-cold wash buffer (same as lysis but without bortezomib and PIC); in each wash, 500 μl of wash buffer was used to resuspend the beads and incubate at 4°C for 10 minutes with rotating.

After the final wash, the wash buffer was disposed, and the beads bound target protein was eluted from beads as "IP" sample by adding 60 μl of 2 × protein loading buffer containing 0.1 M DTT

and boiled at 95°C for 5 minutes (see section 6.6.4). Meanwhile, the retained 30 µl of TL and FT samples were diluted 1:1 in the same loading buffer and boiled at 95°C for 5 minutes for denaturation. The TL, FT and IP samples were resolved simultaneously by western blotting.

6.8.4 Subcellular localization and BiFC experiments

The constructs of *YFP* fused full-length *PUX* genes and *GI* gene, or truncated *PUX10* CDS were used for subcellular localization analysis via protoplast transient expression system. Additionally, a series of pairs of complementary BiFC vector were also co-transfected into protoplasts for transiently expression. All the constructs used in this section were made as described section 6.5.6 and 6.5.7 and listed in Table 6.1.

Protoplasts used for transfection in this section were extracted from either 4-week-old wild-type plants, or the genetically encoded reporter lines of ER, mitochondria, or Golgi, as described in section 6.8.1. The protoplast transfection was then carried out as described in section 6.8.2. 1µg of single plasmid DNA in 10 µl was used for the subcellular localization assay, while 1 µg of plasmid DNA for each contract in a total volume of 10 µl was used for BiFC assay.

Following the overnight incubation, the transformed protoplasts were collected and the YFP fluorescence was visualized under confocal microscopy (Leica TCS SP5). The images were analysed by using the LAS AF Lite software. If fluorescence quantification was required, Image J was employed for the analysis.

6.9 Microscopy

6.9.1 Confocal microscopy

A Leica TCS SP5 confocal microscope was used for all fluorescence imaging in this study. A Leica HC Plan Apochromat CS2 63.0 x UV water immersion lens was employed for visualizing the cells. All images were captured using the same setting to enable comparisons.

For visualizing the YFP fluorescence for the transgenic plants expressing YFP fusion protein, a small leave tissue (~ 0.5 cm × 0.5 cm) taken from each plant was mounted in perfluorodecalin (PFD), as it can easily infiltrate leaf tissue and fill the intercellular air spaces of mesophyll to enable high-resolution confocal images of the mesophyll (Littlejohn et al., 2010). The mounted leaf samples were then placed on a microscopy slide and covered with a cover slide. The cover slide was immobilized by fixing both ends with tape (3M). The slide was then visualized under confocal microscopy. Samples were excited with an argon laser to collect YFP and chlorophyll fluorescence at 514 nm and 650 nm- 750 nm, respectively.

Following protoplast transfection as described in section 6.8.2, 5 μM bortezomib (a proteasome inhibitor) was added to the overnight cultured transfected protoplast suspension which was then left on a worktop at room temperature for 4 hours before fluorescence imaging. After incubation, protoplasts were concentrated by centrifugation at 100 × g for 2 minutes. Supernatant was disposed and protoplasts were resuspended in the remaining solution (~100 μl). 20 μl of protoplast suspension was then pipetted onto a microscopy slide and gently covered with a cover slide. The cover slide was immobilized by fixing both ends with tape (3M). The slide was then visualized under confocal microscopy. Samples were excited with an argon laser to collect YFP, GFP, RFP and chlorophyll fluorescence at 514 nm, 488 nm, 543nm and 650 nm- 750 nm, respectively.

6.9.2 Transmission electron microscopy

The TEM samples were processed by Dr Errin Johnson at the Sir William Dunn School of Pathology, University of Oxford, using an establishes protocol (Hyman & Jarvis, 2011) with modifications.

6.9.2.1 Leaf sample fixation

3 or 4 -week-old rosette leaves were collected from plants of different genotypes that had been grown simultaneously under standard growth condition in a percival. Small leave discs (2 mm in

diameter) were dissected from the region of the leaf lamina using a biopsy punch. For primary fixation, each disc was immediately immersed in a drop of fixative solution (2.5% (v/v) glutaraldehyde, 4% (v/v) paraformaldehyde (PFA) in 0.1 M sodium cacodylate buffer (SCB), pH 6.9) and cut in half using a single-edged razor blade. This was swiftly done for 5 leaves from individual plants for each genotype. Leaf samples were then placed into individual plastic baskets and transferred to microwave for processing fixation. The samples were fixed at 37°C for 10 minutes, then subjected to five alternating 2-minute cycles of 20 W and 0 W power. Samples were then transferred to glass vials over-filled with fixative solution to make sure no air was kept in the vial when capped, and the vials were shaken vigorously till the leaf samples fell to the bottom of each vial. The vials were kept at room temperature for roughly five hours before moved to the refrigerator overnight.

On the next day, the leaf samples were washed twice with 0.1 M SCB pH 6.9 for 5 minutes with rotation before transferred to fresh 2 ml centrifuge tubes. They were then washed sequentially for two more times in SCB (45 minutes, then 30 minutes), one time in 50 mM glycine in SCB for 30 minutes, and one time in SCB again for 20 minutes with rotation throughout the steps.

Leaf samples were then subjected to secondary fixation. 1 ml of secondary fixative solution (1% (v/v) osmium tetroxide and 1.5% (w/v) potassium ferrocyanide in SCB) was added to each sample followed by incubation for 2 hours at 4°C with vigorous shaking, and subsequently 50 minutes at room temperature with rotation. Samples were then washed with distilled water at room temperature with rotation once for 5 minutes, once for 1.5 hours, and three times for 15 minutes each time.

For tertiary fixation, each sample was immersed in 1 ml of tertiary fixative solution (2% (w/v) uranyl acetate) and incubated for 2 hours in the dark at room temperature with rotation. Samples were then washed with distilled water three times with rotation for 5 minutes each time.

6.9.2.2 Leaf sample dehydration

After removing the final wash, the fixed leaf samples were dehydrated via a series of ethanol solutions.

Firstly, the leaf samples were consecutively incubated with 10%, 20%, 30% and 40% (v/v) ethanol with rotation at room temperature for 10 minutes each time. The samples were then incubated sequentially at room temperature with 50% (v/v) ethanol for 20 minutes, 60% (v/v) ethanol for 10 minutes, and then 70% (v/v) for 5 minutes. The samples were then resuspended with 1 m of fresh 70% ethanol and transferred to a refrigerator overnight. Rotation was applied to each step.

On the next day, samples were incubated sequentially with ice-cold 80%, 90%, 100% (v/v) ethanol and 100% (v/v) anhydrous ethanol, for 30 minutes each time at 4°C with rotation. Finally, the samples were immersed in 1 ml of ice-cold acetone for 30 minutes at 4°C with rotation.

6.9.2.3 Epoxy resin infiltration

TAAB Hard Plus epoxy resin was used. All steps in this section were carried out at room temperature with rotation in a fume hood. Samples were centrifuged at 4000 × g for 1 minute after each solution change to promote resin infiltration.

Samples were incubated with a graded resin/acetone (v/v) series as follows (in order of increasing resin concentration): 25% for 2 hours, 50% for 3 hours, 75% for 1 hour and 100% resin overnight.

On the next day, 100% resin was replaced with fresh resins twice: one at 12 pm, and another one at 5 pm. The samples were left to incubate overnight.

On the following day, the final resin change was conducted at 10:30 am with centrifugation, followed by embedding in the afternoon.

6.9.2.4 Leaf sample embedding, sectioning and staining

The embedding moulds were prepared by polymerizing a thin layer of resin on the base of each mould via incubation in a pre-heated oven at 60°C for approximately 2 hours. Each mould must be labelled with the name of the sample. Each sample was then placed in the embedding mould labeled with the sample name and overlaid with fresh resin. The blocks were then polymerized in a pre-heated oven for 48 hours at 60°C.

The sample block was trimmed to remove excess resin from around the tissue, and the semi-thick sections (~0.5 μm) were firstly carried out. The thick sections were observed using a light microscope to determine the exact location within the sample that has been reached, and to further locate the area to be used for electronic microscopy. Once the information was confirmed, the ultra-thin sections (60-90 nm) were then cut using an ultramicrotome and collected on the surface of grid with a diameter of 3.05 mm. Usually, 3-4 sections were collected on a single grid.

The sections collected on the grids were then contrasted using heavy metal stains as descried previously (Hyman & Jarvis, 2011). After staining, the grids were washed by immersion in freshly boiled distilled water. Following the first wash with boiled distilled water containing 1-2 drops of 1M NaOH to reduce the lead carbonate precipitation, the grids were further passed through three successive boiled distilled waters to remove all traces of stains. The grids were air-dried and stored in a grid storage box prior to observation under TEM.

6.9.2.5 Imaging

The leaf sample sections were imaged using a FEI Tecnai T12 TEM. Three grids with leaf tissue sections were generated for each genotype, representing three biological replicates. At least 50 different chloroplast images were taken for each grid. All images were captured at the same magnification level. The images were analysed using Images J (Schindelin et al., 2012). The analysis of chloroplast ultrastructural organization was performed as described previously

(Huang et al., 2011). Chloroplast cross-sectional area was estimated as described (Kovacheva et al., 2005), using the equation: $\pi \times 0.25 \times \text{length} \times \text{width}$.

6.10 Forward genetic screen

6.10.1 Mutagenesis

Mutagenesis was conducted using chemical mutagen ethyl methanesulphonate (EMS) in a Atmos bag (Sigma) within a fume hood, according to the published protocol (Salinas & Sánchez-Serrano, 2006).

An estimated 20,000 *ppi1-1* seeds were placed in two modified 50 ml syringes. The front end of the syringe was cut off and covered with a circle of fine nylon mesh. The plungers were pulled to draw the appropriate solutions through the nylon mesh onto the seeds in the following steps.

The seeds were first pre-imbibed overnight in a 0.1% (w/v) potassium chloride solution at room temperature followed by soaked in an EMS solution (0.1 M sodium phosphate, 5% (v/v) dimethyl sulphoxide (DMSO), 50-100 mM EMS, pH 5.0) for three hours with a mixing every hour.

After mutagenesis, the seeds were washed twice in 50 ml of 100 mM sodium thiosulphate for 15 minutes each time to destroy the EMS, and then twice in 50 ml of distilled water for 15 minutes each time. All the waste solution produced in the above steps were discarded into a beaker containing solid sodium thiosulphate placed in the "Atmos" bag. The sodium thiosulphate deactivated waste was poured into the sink and washed down with running tap water. The contaminated beaker was washed under running tap water for at least half an hour. The seeds were then removed from the Atmos bag and transferred to filter paper (Waterman) for drying out overnight.

The next day, the EMS-mutagenized M1 seeds were sown out onto soil in 100 separate batches and each batch contained approximately 200 seeds. Each Batch of seeds were sown on a half tray

(15.5 × 21 × 5.5 cm (length/width/height)), with the plants on each half of the tray named A and B. Therefore, a total of 100 pools of M1 plants were generated, termed as 1A-50A and 1B-50B. The pooled M2 seed of each batch was separately harvested and in total 100 pools M2 seeds were obtained.

6.10.2 M2 screening

The M2 seeds were subjected to the screen for plants which displayed a greener phenotype than the *ppi1* progenitor. The M2 seeds and control *ppi1* seeds were sown on MS agar medium in large petri dishes (120 × 120 mm) and grown in a percival under standard growth condition for 14 days prior to phenotypic screen. The seedlings carrying greener phenotype than *ppi1* were transferred to soil and allowed to grow to maturity for M3 seeds harvesting.

All M3 putative suppressor mutants, as well as wild-type and *ppi1* control plants were grown on soil for 3-4 weeks for further phenotypic confirmation by measuring the leaf size and the content of chlorophyll in each mutant. The mutants with distinct greener and/ or bigger leaves were allowed to grow to maturity for collecting M4 seeds.

The selected M4 mutants displaying significant suppressor phenotype were sown on soil and grown for 3-4 weeks. The CDSs of both *SP1* and *SP2* were amplified by PCR from each mutant line for sequencing to assess the potential mutation in *SP1* or *SP2* which would contribute to the suppressor phenotype. The mutant lines containing no mutation in both *SP1* and *SP2* were grown to maturity and M5 seeds were harvested.

The M5 seeds of the novel suppressor mutants, as well as *ppi1* seeds, were sown on soil and grown until they were ready for backcrossing. The novel suppressor mutants were backcrossed with *ppi1* progenitor and then selfed to obtain the F2 segregating population.

Then, individuals with suppressor phenotype from the F2 population were selected, pooled, and subjected to NGS.

6.10.3 Genomic DNA preparation for NGS

More than 200 plants from the F2 population which clearly showed the *ppi1* suppressor phenotype were selected and pooled for genomic DNA extraction using a DNeasy Plant Mini Kit (Qiagen). Meanwhile, the genomic DNA of *ppi1* was also extracted using the same protocol. The quality and quantity of DNA samples were determined as follows: running the DNA samples on a 1% agarose gel to check the degradation; A NanoPhotometer P330 (Implen) and a Qubit 2.0 Fluorometer (Invitrogen) were employed to measure the DNA concentration and quality of extraction.

Approximately 1-5 μg of genomic DNA per genotype at a minimum concentration of 29.4 ng/ μl was used for preparing a sequencing library. The DNA samples of the novel suppressor mutant and *ppi1* were then sent to the Oxford Genomics Centre at the Wellcome Centre for Human Genetics and sequenced on one lane of Illumina HiSeq 4000 with 150 base pair-end reads.

6.10.4 Mapping by sequencing

The sequenced genomes from the pooled backcrossed F2 population of the novel suppressor mutant and *ppi1* progenitor were analysed using SHOREmap (Schneeberger et al., 2009). A list of candidate loci bearing single-nucleotide polymorphisms (SNPs) between the mutant mapping populations and the progenitor were identified and used for further analysis via genetics and molecular biology.

6.11 Tables

Table 6.1 Primers used during the course of the study

(A). Primers used to generate various constructs			
Primer name	**Primer sequence (5' to 3') ***	**Used to generate…**	**Comments**
PUX10-BglII-F	AAAGATCTATGGTTGAT ACTGTTGACAAATTAGG	pSAT4(A)-nEYFP-PUX10/ pSAT4(A)-cEYFP-PUX10	PUX10-nY/ PUX10-cY In Figure 2.8, 3.1, 3.3
PUX10-SalI-ns-R	AAGTCGACAGTTGATCT CGATGAAGAGACTTGC		
ΔUBX-XhoI-F	AACTCGAGATGGTTGAT ACTGTTGACAAATTAGG	pSAT4(A)-cEYFP- ΔUBX	UBX-cY In Figure 2.8
ΔUBX-EcoRI-R	AAGAATTCAGGTTCTTC TCCAAGAGCAAGAG		
SP1-Xhol1-F	AACTCGAGATGATTCCT TGGGGTGGAG	pSAT4(A)-nEYFP-SP1	SP1-nY In Figure 3.1
SP1-Kpn-ns-R	GGTACCTGTGACGATAT GTCTTAACC		
Toc34-HindIII-F	AGAAGCTTCGATGGCAG CTTTGCAAACG	pSAT4-cEYFP-Toc34	Toc34-cY In Figure 3.3
Toc34-XbaI-R	AATCTAGATCAAGACCT TCGACTTGC		
Toc33-HindIII-F	AGAAGCTTCGATGGGGT CTCTCGTTCGT	pSAT4-cEYFP-Toc33	Toc33-cY In Figure 3.3
Toc33-XbaI-R	AATCTAGATTAAAGTGG CTTTCCACT		
Toc132-Xhol-F	AACTCGAGCTATGGGAG ATGGGACTGAG	pSAT4-cEYFP-Toc132	Toc132-cY In Figure 3.3
Toc132-SmaI-R	AACCCGGGTCATTGTCC ATATTGCGT		
Cdc48-KpnI-F	AAGGTACCATGTCTACC CCAGCTGAATC	pSAT4-nEYFP-Cdc48	Cdc48-nY In Figure 2.8
Cdc48-XmaI-ns-R	AACCCGGGATTGTAGAG ATCATCATCGTCC		
Toc159-EcoRI-F	AAGAATTCAATGGACTC AAAGTCGGTT	pSAT4-cEYFP-Toc159	Toc159-cY In Figure 3.3
Toc159-SalI-R	AAGTCGACTTAGTACAT GCTGTACTT		
SFR2-Kpn-F	GGTACCAACTAGAAAGATCCGGTG	pSAT4(A)-nEYFP-SFR2	SFR2-nY In Figure 3.1
SFR2-XmaI-ns-R	CCCGGGGTCAAAGGGTGAGGCTAA		
CDKA1-Xho-F	CTCGAGATGGATCAGTA CGAGAAAG	pSAT4(A)-nEYFP-CDKA1/pSAT4(A)-cEYFP-CDKA1	CDKA1nY/ CDKA1-cY In Figure 3.1, 3.3
CDKA1-EcoR-ns-R	GAATTCAGGCATGCCTC CAAGATC		

Cdc48-attB1-F	AAAAAGCAGGCTCCATG TCTACCCCAGCTGAAT	p2GWY7-Cdc48/p2GW7-Cdc48-HA	Cdc48-YFP/ Cdc48-HA In Figure 2.8
Cdc48-attB2-ns-R	AGAAAGCTGGGTTATTG TAGAGATCATCATCGTCC		
ΔUBA-attB1-F	GGGGACAAGTTTGTACA AAAAAGCAGGCTCCATG TCTTCTGATCAAGACGCT TCG	p2GWY7-ΔUBA/ pK7YWG2-ΔUBA	ΔUBA-YFP In Figure 2.7, 2.9,3.4
ΔUBA-attB2-ns-R	GGGGACCACTTTGTAC AAGAAAGCTGGGTTGT TGATCTCGATGAAGAG ACTTGC		
ΔUBX-attB1-F	GGGGACAAGTTTGTAC AAAAAAGCAGGCTCCA TGGTTGATACTGTTGA CAAATTAGG	p2GWY7-ΔUBX/ pK7YWG2-ΔUBX	ΔUBX-YFP In Figure 2.7, 2.8
ΔUBX-attB2-ns-R	GGGGACCACTTTGTAC AAGAAAGCTGGGTTAG GTTCTTCTCCAAGAGC AAGAG		
ΔTM-attB1-1F	GGGGACAAGTTTGTAC AAAAAAGCAGGCTCCA TGGTTGATACTGTTGAC AAATTAGG	p2GWY7-ΔTM1/2/ pK7YWG2-Δ TM1/2	ΔTM1/2-YFP In Figure 2.4, 2.7
ΔTM-1R	GAGAATACGACGGTAA AGTAATAATCCT		
ΔTM-2F	TACTTTACCGTCGTATT CTCTTGGTATG		
ΔTM-attB2-ns-2R	GGGGACCACTTTGTAC AAGAAAGCTGGGTTGT TGATCTCGATGAAGAG ACTTGC		
PUX10-FLAG-F	TACAAAGACGATGACGA CAAAATGGTTGATACTG TTGACAAATTAGG	pK7YWG2-FLAG-PUX10	FLAG-PUX10-YFP In Figure 2.5
attB1-FLAG	GGGGACAAGTTTGTACA AAAAAGCAGGCTCCATG GACTACAAAGACGATGA CGAC		
PUX10-Pro-HindIII-F	AAAAGCTTACATCGTCC TGCATTTTTCGATG	*pPUX10*-K7YWG2-PUX10	*pPUX10*-PUX10-YFP In Figure 2.2
PUX10-Pro-SpeI-R	AAACTAGTTTTCAGAAA ACCCTAATTCGATTTTCCC		
PUX1-attB1-F	AAAAAGCAGGCTCCATG TTTGTTGATGACCCTTCTC	p2GWY7-PUX1	PUX1-YFP In Figure 2.1
PUX1-attB2-ns-R	AGAAAGCTGGGTTCATT TTAAACCACTTAGGCTT TGTGG		

PUX2-attB1-F	AAAAAGCAGGCTCCATG GATGACGTTAAAGATAA GC	p2GWY7-PUX2	PUX2-YFP In Figure 2.1
PUX2-attB2-ns-R	AGAAAGCTGGGTTCGAG AGTGGTTCACTGATC		
PUX3-attB1-F	AAAAAGCAGGCTCCATG CTAGTTTTGTTTCTGGC TAAGC	p2GWY7-PUX3	PUX3-YFP In Figure 2.1
PUX3-attB2-ns-R	AGAAAGCTGGGTTGAAT TTCTGAATGACTACAGA ACTTG		
PUX4-attB1-F	AAAAAGCAGGCTCCATGT CTTCGAAAGACAAGAAACC	p2GWY7-PUX4	PUX4-YFP In Figure 2.1
PUX4-attB2-ns-R	AGAAAGCTGGGTTGAAT TTCTGAAGAACAACAGAGTTG		
PUX5-attB1-F	AAAAAGCAGGCTCCAT GGCGACGGAGACGAACGAGAA	p2GWY7-PUX5	PUX5-YFP In Figure 2.1
PUX5-attB2-ns-R	AGAAAGCTGGGTTGAA TTTCTGGATGACGACG		
PUX6-attB1-F	AAAAAGCAGGCTCCAT GGACGTTAACTCGCCGGAGA	p2GWY7-PUX6	PUX6-YFP In Figure 2.1
PUX6-attB2-ns-R	AGAAAGCTGGGTTGAA TTTTTGGACGAGGACAGAG		
PUX7-attB1-F	AAAAAGCAGGCTCCATG GAAGGAATGTTGTCGTC	p2GWY7-PUX7	PUX7-YFP In Figure 2.1
PUX7-attB2-ns-R	AGAAAGCTGGGTTTTCC CACGTAGCAGAGATC		
PUX8-attB1-F	AAAAAGCAGGCTCCATG GCGACACCGAATCAG	p2GWY7-PUX8	PUX8-YFP In Figure 2.1
PUX8-attB2-ns-R	AGAAAGCTGGGTTGATA AGCTCAAGGAACAATGC		
PUX9-attB1-F	AAAAAGCAGGCTCCATG GTGAGTCCGACGAGAG	p2GWY7-PUX9	PUX9-YFP In Figure 2.1
PUX9-attB2-ns-R	AGAAAGCTGGGTTCACC AGCAGTTCCAGAAAC		
PUX10-attB1-F	AAAAAGCAGGCTCCATGGT TGATACTGTTGACAA ATTAG	p2GWY7-PUX10/ pK7YWG2-PUX10	PUX10-YFP In Figure 2.1, 2.2, 2.3, 2.4, 2.7, 2.8, 2.9, 3.2, 3.4
PUX10-attB2-ns-R	AGAAAGCTGGGTTGTTG ATCTCGATGAAGAGAC		
PUX11-attB1-F	AAAAAGCAGGCTCCATG GAAGCTCTGTCTTCTC	p2GWY7-PUX11	PUX11-YFP In Figure 2.1
PUX11-attB2-ns-R	AGAAAGCTGGGTTTCGT CTATCATTACTGTCTC		
PUX12-attB1-F	AAAAAGCAGGCTCCATG CTCGAGTGTCAATCAATG	p2GWY7-PUX12	PUX12-YFP In Figure 2.1
PUX12-attB2-ns-R	AGAAAGCTGGGTTGAG CCAAGTAACAGAAACC		

PUX13-attB1-F	AAAAAGCAGGCTCCATGGCGACACCTACTCAG	p2GWY7-PUX13	PUX13-YFP In Figure 2.1
PUX13-attB2-ns-R	AGAAAGCTGGGTTGATCAGCTCCAAGAACAATG		
attB1	GGGGACAAGTTTGTACAAAAAGCAGGCT	complete Gateway recombination sites for cloning into pDONR201	Constructs In Figure 2.1
attB2	GGGGACCACTTTGTACAAGAAAGCTGGGT		
Gi-attB1-F	GGGGACAAGTTTGTACAAAAAAGCAGGCTCCATGGCTAGTTCATCTTCATCTGAG	p2GWY7-Gi	Gi-YFP In Figure 4.13
Gi-attB2-nsR	GGGGACCACTTTGTACAAGAAAGCTGGGTTTTGGGACAAGGATATAGTACAGC		

*Nucleotides shown in red do not corresponding to the target gene, but instead correspond to linker sequences. Restriction sequences are underlined.

(B). Primers used in RT-PCR experiments

Primer name	Primer sequence (5' to 3')	Comments
PUX10-RT-1F	GTTTCTGGTAGCTTAGGGTTAGT	Figure 2.6
PUX10-RT-1R	TGATCGGCTTCAAGAGCAG	
PUX10-RT-2F	GTGGTGGAACGCTTTGTA	Figure 2.6
PUX10-RT-2R	AAGTCGACAGTTGATCTCGATGAAGAGACTTGC	
Toc159-F	TGTTGTAGGAGACGCAGAGG	Figure 3.5
Toc159-R	ACTTATTATGCACATCAGGGATGT	
Toc132-F	GATGGGACTGAGTTTGTGGTTAG	Figure 3.5
Toc132-R	CCTCTTGTTCTGTCTGTATGCC	
Toc75-F	GTTGGGTTAATGGTACAGTCG	Figure 3.5
Toc75-R	ATCTCAACAATAATGCCCCCT	
Toc34-F	TTGTCGGTGCTATAACTGATGC	Figure 3.5
Toc34-R	CTTGCTAAACCGGAGTCTCG	
Tic110-F	CACAACAAAGAGAGACGATTCAG	Figure 3.5
Tic110-R	CAAATCATTCAGCGACAAGAC	
Tic40-F	TCTCGTCGGACTCCTAATATTGT	Figure 3.5
Tic40-R	CTTTCTTCTCTTTGCTTGCCT	
SP1-F	GGTACAAGATAGTGCGTTGATG	Figure 3.6
SP1-R	CTGCAGTCAGTGACGATATGTCTTAAC	
At1g18740-F	ACGCCTCGACCAAACGATGTC	Figure 4.6
At1g18740-R	CATCATATTCAGACAAACATGTGC	
At1g19600-F	AGTTCGAGGCTTGAGTGTTGGG	Figure 4.6
At1g19600-R	CCGAGAGCACGGATGACAGA	
At1g20360-F	ATGAACAGCTTACCTTTGCATC	Figure 4.6

At1g20360-R	ACGCTTGCCATCGTACAC	
At1g20430-F	CCTCGTTGACTCAAACCAATC	Figure 4.6
At1g20430-R	TCTAGCTCTCACTCTCAGCTTG	
At1g20540-F	CTAGATGTATATCGGATGTGA	Figure 4.6
At1g20540-R	CATAGACACTGTCTTCATAGTC	
At1g20890-F	AGAAGCTGGGTATGATATCTTG	Figure 4.6
At1g20890-R	ATCGATTTACGCTATAAAGAATG	
At1g25400-F	GGGGACAAGTTTGTACAAAAAAGCAGGC TCCATGGAGGTCCCGATTATAAACAG	Figure 4.6
At1g25400-R	GGGGACCACTTTGTACAAGAAAGCTG GGTTTCAATGACGGCGTCTGCGTCTTCTCA	
eIF4E1-F	AAACAATGGCGGTAGAAGACACTC	
eIF4E1-R	AAGATTTGAGAGGTTTCAAGCGGTGTAAG	
(C). Primers used to genotype T-DNA mutants		
Primer name	**Primer sequence (5' to 3')**	**Comments**
PUX10-SAIL-F	GTTTCTGGTAGCTTAGGGTTAGT	
PUX10-SAIL-R	TGATCGGCTTCAAGAGCAG	
LBb1	GCGTGGACCGCTTGCTGCAACT	
LBb1.3	ATTTTGCCGATTTCGGAAC	
LBa1	TGGTTCACGTAGTGGGCCATCG	
LB1	GCCTTTTCAGAAATGGATAAATAGCCTTGCTTCC	
PUX10-Wisc-F	GAGAGATACTAAACTTGGTGCC	
PUX10-Wisc-R	ACATCTAGTATGTATGAATGTGAGG	
WiscDsLoxLB	AACGTCCGCAATGTGTTATTAAGTTGTC	
SALK_020993_F	GCCACCACGAGCCAAGCACCATGG	
SALK_020993_R	GTCTTTGACTCTTCCGAATGAACGGTTAC	
SALK_019913_F	ACGCCTCGACCAAACGATGTC	
SALK_019913_R	CATCATATTCAGACAAACATGTGC	
SALK_003847_F	AGTTCGAGGCTTGAGTGTTGGG	
SALK_003847_R	CCGAGAGCACGGATGACAGA	
SAIL_1211G03_F	TGGTCAGGAATTCTAAATCAGAG	
SAIL_1211G03_R	CCGAGAGCACGGATGACAGA	
SALK_047784_F	ATGAACAGCTTACCTTTGCATC	
SALK_047784_R	ACGCTTGCCATCGTACAC	
SALK_110612_F	ATGAACAGCTTACCTTTGCATC	
SALK_110612_R	ACGCTTGCCATCGTACAC	
SALK_051176_F	CCTCGTTGACTCAAACCAATC	
SALK_051176_R	TCTAGCTCTCACTCTCAGCTTG	
SALK_103090_F	CCTCGTTGACTCAAACCAATC	
SALK_103090_R	TCTAGCTCTCACTCTCAGCTTG	
SALK_107587_F	CCTCGTTGACTCAAACCAATC	
SALK_107587_R	TCTAGCTCTCACTCTCAGCTTG	

SALK_026098_F	CTAGATGTATATCGGATGTGA	
SALK_026098_R	CATAGACACTGTCTTCATAGTC	
SAIL_1158D07_F	GTAACTGCAGAGGATGAATCTG	
SAIL_1158D07_R	CATAGACACTGTCTTCATAGTC	
SALK_043518_F	AGAAGCTGGGTATGATATCTTG	
SALK_043518_R	ATCGATTTACGCTATAAAGAATG	
SALK_093560_F	GGGGACAAGTTTGTACAAAAAAG CAGGCTCCATGGAGGTCCCGATTATAAACAG	
SALK_093560_R	GGGGACCACTTTGTACAAGAAAG CTGGGTTTCAATGACGGCGTCTGCGTCTTCTCA	

(C). Primers used to genotype mutant plants by dCAPS (derived Cleaved Amplified Polymorphic Sequence) †

Primer name	**Primer sequence (5' to 3') ***	**Mutant**	**Restriction enzyme**
dCAPS-TaqI-F	CTTGATGCTCATGTTGGTAAGATTAATCG	*At1g20540*	TaqI
dCAPS-TaqI-R	GATTAACTTGTCACATCTTCCAGA		

* Nucleotides shown in red do not correspond to the target gene, but instead correspond to linker sequences or mutation sites.

† The PCR products amplified using dCAPS primers were digested with restriction enzyme, and thereafter resolved on 3% agarose gels. Genotypes were determined by comparing the sizes of the bands with controls corresponding to wild type and the homozygous mutant.

Table 6.2 Plasmid vectors used during the course of the study

Name	**Comments**
pGEM-T EASY	A1360, Promega
p2GWY7	https://gatewayvectors.vib.be/collection/p2gwy7 (Ling et al., 2019; Ling et al., 2012)
pK7YWG2	https://gatewayvectors.vib.be/collection/pk7ywg2 (Ling et al., 2019; Ling et al., 2012)
pSAT4-nEYFP-N1	(Citovsky et al., 2006; Ling et al., 2019)
pSAT4-cEYFP-N1	(Citovsky et al., 2006; Ling et al., 2019)
pSAT4(A)-nEYFP-N1	(Citovsky et al., 2006; Ling et al., 2019)
pSAT4(A)-cEYFP-N1	(Citovsky et al., 2006; Ling et al., 2019)

Bibliography

Accossato, S., Kessler, F., & Shanmugabalaji, V. (2020). SUMOylation contributes to proteostasis of the chloroplast protein import receptor TOC159 during early development. *Elife*, *9*. https://doi.org/10.7554/eLife.60968

Adam, Z., & Clarke, A. K. (2002). Cutting edge of chloroplast proteolysis. *Trends in Plant Science*, *7*(10), 451-456. https://doi.org/10.1016/S1360-1385(02)02326-9

Agne, B., Andres, C., Montandon, C., Christ, B., Ertan, A., Jung, F., Infanger, S., Bischof, S., Baginsky, S., & Kessler, F. (2010). The Acidic A-Domain of Arabidopsis Toc159 Occurs as a Hyperphosphorylated Protein. *Plant Physiology*, *153*(3), 1016-1030. https://doi.org/10.1104/pp.110.158048

Agne, B., Infanger, S., Wang, F., Hofstetter, V., Rahim, G., Martin, M., Lee, D. W., Hwang, I., Schnell, D., & Kessler, F. (2009). A Toc159 Import Receptor Mutant, Defective in Hydrolysis of GTP, Supports Preprotein Import into Chloroplasts. *Journal of Biological Chemistry*, *284*(13), 8661-8670. https://doi.org/10.1074/jbc.M804235200

Alam, S. L., Sun, J., Payne, M., Welch, B. D., Blake, B. K., Davis, D. R., Meyer, H. H., Emr, S. D., & Sundquist, W. I. (2004). Ubiquitin interactions of NZF zinc fingers. *Embo Journal*, *23*(7), 1411-1421. https://doi.org/10.1038/sj.emboj.7600114

Allen, J. F. (2015). Why chloroplasts and mitochondria retain their own genomes and genetic systems: Colocation for redox regulation of gene expression. *Proceedings of the National Academy of Sciences of the United States of America*, *112*(33), 10231-10238. https://doi.org/10.1073/pnas.1500012112

Allen, M. D., Buchberger, A., & Bycroft, M. (2006). The PUB domain functions as a p97 binding module in human peptide N-glycanase. *Journal of Biological Chemistry*, *281*(35), 25502-25508. https://doi.org/10.1074/jbc.M601173200

Amerik, A. Y., & Hochstrasser, M. (2004). Mechanism and function of deubiquitinating enzymes. *Biochimica Et Biophysica Acta-Molecular Cell Research*, *1695*(1-3), 189-207. https://doi.org/10.1016/j.bbamcr.2004.10.003

Anstis, P. J. P., & Northcot, D. H. (1973). Development of Chloroplasts from Amyloplasts in Potato-Tuber Disks. *New Phytologist*, *72*(3), 449-464. https://doi.org/10.1111/j.1469-8137.1973.tb04394.x

Aronsson, H., Boij, P., Patel, R., Wardle, A., Topel, M., & Jarvis, P. (2007). Toc64/OEP64 is not essential for the efficient import of proteins into chloroplasts in Arabidopsis thaliana. *Plant Journal*, *52*(1), 53-68. https://doi.org/10.1111/j.1365-313X.2007.03207.x

Asano, T., Yoshioka, Y., Kurei, S., Sakamoto, W., & Machida, Y. (2004). A mutation of the CRUMPLED LEAF gene that encodes a protein localized in the outer envelope membrane of plastids affects the pattern of cell division, cell differentiation, and plastid division in Arabidopsis. *Plant Journal*, *38*(3), 448-459. https://doi.org/10.1111/j.1365-313X.2004.02057.x

Azevedo, C., Santos-Rosa, M. J., & Shirasu, K. (2001). The U-box protein family in plants. *Trends in Plant Science*, *6*(8), 354-358. https://doi.org/10.1016/s1360-1385(01)01960-4

Baek, G. H., Cheng, H., Choe, V., Bao, X., Shao, J., Luo, S., & Rao, H. (2013). Cdc48: a swiss army knife of cell biology. *J Amino Acids*, *2013*, 183421. https://doi.org/10.1155/2013/183421

Baldwin, A., Wardle, A., Patel, R., Dudley, P., Park, S. K., Twell, D., Inoue, K., & Jarvis, P. (2005). A molecular-genetic study of the Arabidopsis Toc75 gene family. *Plant Physiology*, *138*(2), 715-733. https://doi.org/10.1104/pp.105.063289

Baldwin, A. J., & Inoue, K. (2006). The most C-terminal tri-glycine segment within the polyglycine stretch of the pea Toc75 transit peptide plays a critical role for targeting the protein to the chloroplast outer envelope membrane. *FEBS J*, *273*(7), 1547-1555. https://doi.org/10.1111/j.1742-4658.2006.05175.x

Ballar, P., Shen, Y. X., Yang, H., & Fang, S. Y. (2006). The role of a novel p97/valosin-containing protein-interacting motif of gp78 in endoplasmic reticulum-associated degradation. *Journal of Biological Chemistry*, *281*(46), 35359-35368. https://doi.org/10.1074/jbc.M603355200

Ballar, P., Zhong, Y., Nagahama, M., Tagaya, M., Shen, Y., & Fang, S. (2007). Identification of SVIP as an endogenous inhibitor of endoplasmic reticulum-associated degradation. *Journal of Biological Chemistry*, *282*(47), 33908-33914. https://doi.org/10.1074/jbc.M704446200

Banchenko, S., Arumughan, A., Petrovic, S., Schwefel, D., Wanker, E. E., Roske, Y., & Heinemann, U. (2019). Common Mode of Remodeling AAA ATPases p97/CDC48 by Their Disassembling Cofactors ASPL/PUX1. *Structure*, *27*(12), 1830-1841. https://doi.org/10.1016/j.str.2019.10.001

Barbrook, A. C., Howe, C. J., & Purton, S. (2006). Why are plastid genomes retained in non-photosynthetic organisms? *Trends in Plant Science*, *11*(2), 101-108. https://doi.org/10.1016/j.tplants.2005.12.004

Barsan, C., Zouine, M., Maza, E., Bian, W., Egea, I., Rossignol, M., Bouyssie, D., Pichereaux, C., Purgatto, E., Bouzayen, M., Latche, A., & Pech, J. C. (2012). Proteomic analysis of chloroplast-to-chromoplast transition in tomato reveals metabolic shifts coupled with disrupted thylakoid biogenesis machinery and elevated energy-production components. *Plant Physiology*, *160*(2), 708-725. https://doi.org/10.1104/pp.112.203679

Baslam, M., Oikawa, K., Kitajima-Koga, A., Kaneko, K., & Mitsui, T. (2016). Golgi-to-plastid trafficking of proteins through secretory pathway: Insights into vesicle-mediated import toward the plastids. *Plant Signaling & Behavior*, *11*(9). https://doi.org/10.1080/15592324.2016.1221558

Bauer, J., Chen, K. H., Hiltbunner, A., Wehrli, E., Eugster, M., Schnell, D., & Kessler, F. (2000). The major protein import receptor of plastids is essential for chloroplast biogenesis. *Nature*, *403*(6766), 203-207. https://doi.org/10.1038/35003214

Bedard, J., Kubis, S., Bimanadham, S., & Jarvis, P. (2007). Functional similarity between the chloroplast translocon component, Tic40, and the human co-chaperone, Hsp70-interacting protein (Hip). *Journal of Biological Chemistry*, *282*(29), 21404-21414. https://doi.org/10.1074/jbc.M611545200

Begue, H., Jeandroz, S., Blanchard, C., Wendehenne, D., & Rosnoblet, C. (2017). Structure and functions of the chaperone-like p97/CDC48 in plants. *Biochimica Et Biophysica Acta-General Subjects*, *1861*(1), 3053-3060. https://doi.org/10.1016/j.bbagen.2016.10.001

Benlloch, R., & Lois, L. M. (2018). Sumoylation in plants: mechanistic insights and its role in drought stress. *Journal of Experimental Botany*, *69*(19), 4539-4554. https://doi.org/10.1093/jxb/ery233

Bergink, S., & Jentsch, S. (2009). Principles of ubiquitin and SUMO modifications in DNA repair. *Nature*, *458*(7237), 461-467. https://doi.org/10.1038/nature07963

Bergler, J., & Hoth, S. (2011). Plant U-box armadillo repeat proteins AtPUB18 and AtPUB19 are involved in salt inhibition of germination in Arabidopsis. *Plant Biol (Stuttg)*, *13*(5), 725-730. https://doi.org/10.1111/j.1438-8677.2010.00431.x

Bertolaet, B. L., Clarke, D. J., Wolff, M., Watson, M. H., Henze, M., Divita, G., & Reed, S. I. (2001). UBA domains mediate protein-protein interactions between two DNA damage-inducible proteins. *Journal of Molecular Biology*, *313*(5), 955-963. https://doi.org/10.1006/jmbi.2001.5105

Biedermann, S., & Hellmann, H. (2011). WD40 and CUL4-based E3 ligases: lubricating all aspects of life. *Trends in Plant Science*, *16*(1), 38-46. https://doi.org/10.1016/j.tplants.2010.09.007

Biswal, B., Mohapatra, P. K., Biswal, U. C., & Ravel, M. K. (2012). Leaf Senescence and Transformation of Chloroplasts to Gerontoplasts. *Photosynthesis: Plastid Biology, Energy Conversion and Carbon Assimilation*, *34*, 217-230. https://doi.org/10.1007/978-94-007-1579-0_10

Blair, G. E., & Ellis, R. J. (1973). Protein-Synthesis in Chloroplasts .1. Light-Driven Synthesis of Large Subunit of Fraction I Protein by Isolated Pea Chloroplasts. *Biochimica Et Biophysica Acta*, *319*(2), 223-234. https://doi.org/10.1016/0005-2787(73)90013-0

Bodnar, N. O., Kim, K. H., Ji, Z. J., Wales, T. E., Svetlov, V., Nudler, E., Engen, J. R., Walz, T., & Rapoport, T. A. (2018). Structure of the Cdc48 ATPase with its ubiquitin-binding cofactor Ufdl-Npl4. *Nature Structural & Molecular Biology*, *25*(7), 616-622. https://doi.org/10.1038/s41594-018-0085-x

Bodnar, N. O., & Rapoport, T. A. (2017). Molecular Mechanism of Substrate Processing by the Cdc48 ATPase Complex. *Cell*, *169*(4), 722-735. https://doi.org/10.1016/j.cell.2017.04.020

Bolter, B., May, T., & Soll, J. (1998). A protein import receptor in pea chloroplasts, Toc86, is only a proteolytic fragment of a larger polypeptide. *Febs Letters*, *441*(1), 59-62. https://doi.org/10.1016/S0014-5793(98)01525-7

Bolter, B., & Soll, J. (2017). Ycf1/Tic214 Is Not Essential for the Accumulation of Plastid Proteins. *Molecular Plant*, *10*(1), 219-221. https://doi.org/10.1016/j.molp.2016.10.012

Borden, K. L. (2000). RING domains: master builders of molecular scaffolds? *Journal of Molecular Biology*, *295*(5), 1103-1112. https://doi.org/10.1006/jmbi.1999.3429

Branden, C., & Tooze, J. (1999). Introduction to Protein Structure, Second Edition (New York: Garland Publishing, Taylor and Francis Group).

Brandoli, C., Petri, C., Egea-Cortines, M., & Weiss, J. (2020a). The clock gene Gigantea 1 from Petunia hybrida coordinates vegetative growth and inflorescence architecture. *Scientific Reports*, *10*(1). https://doi.org/10.1038/s41598-019-57145-9

Brandoli, C., Petri, C., Egea-Cortines, M., & Weiss, J. (2020b). Gigantea: Uncovering New Functions in Flower Development. *Genes*, *11*(10). https://doi.org/10.3390/genes11101142

Braun, S., Matuschewski, K., Rape, M., Thoms, S., & Jentsch, S. (2002). Role of the ubiquitin-selective CDC48(UFD1/NPL4) chaperone (segregase) in ERAD of OLE1 and other substrates. *Embo Journal*, *21*(4), 615-621. https://doi.org/10.1093/emboj/21.4.615

Bruce, B. D. (1998). The role of lipids in plastid protein transport. *Plant Molecular Biology*, *38*(1-2), 223-246. https://doi.org/10.1023/A:1006094308805

Bruce, B. D. (2001). The paradox of plastid transit peptides: conservation of function despite divergence in primary structure. *Biochimica Et Biophysica Acta-Molecular Cell Research*, *1541*(1-2), 2-21. https://doi.org/10.1016/S0167-4889(01)00149-5

Bruderer, R. M., Brasseur, C., & Meyer, H. H. (2004). The AAA ATPase p97/VCP interacts with its alternative co-factors, Ufd1-Npl4 and p47, through a common bipartite binding mechanism. *Journal of Biological Chemistry*, *279*(48), 49609-49616. https://doi.org/10.1074/jbc.M408695200

Buchberger, A., Schindelin, H., & Hanzelmann, P. (2015). Control of p97 function by cofactor binding. *Febs Letters*, *589*(19), 2578-2589. https://doi.org/10.1016/j.febslet.2015.08.028

Cha, J. Y., Kim, J., Kim, T. S., Zeng, Q., Wang, L., Lee, S. Y., Kim, W. Y., & Somers, D. E. (2017). GIGANTEA is a co-chaperone which facilitates maturation of ZEITLUPE in the Arabidopsis circadian clock. *Nature Communications*, *8*. https://doi.org/10.1038/s41467-016-0014-9

Cha, J. Y., Lee, D. Y., Ali, I., Jeong, S. Y., Shin, B., Ji, H., Kim, J. S., Kim, M. G., & Kim, W. Y. (2019). Arabidopsis GIGANTEA negatively regulates chloroplast biogenesis and resistance to herbicide butafenacil. *Plant Cell Reports*, *38*(7), 793-801. https://doi.org/10.1007/s00299-019-02409-x

Chapman, K. D., Dyer, J. M., & Mullen, R. T. (2012). Biogenesis and functions of lipid droplets in plants. *Journal of Lipid Research*, *53*(2), 215-226. https://doi.org/10.1194/jlr.R021436

Chen, K. H., Chen, X. J., & Schnell, D. J. (2000). Initial binding of preproteins involving the Toc159 receptor can be bypassed during protein import into chloroplasts. *Plant Physiology*, *122*(3), 813-822. https://doi.org/10.1104/pp.122.3.813

Chen, L. Y., & Hellmann, H. (2013). Plant E3 Ligases: Flexible Enzymes in a Sessile World. *Molecular Plant*, *6*(5), 1388-1404. https://doi.org/10.1093/mp/sst005

Chen, M., Ji, M. L., Wen, B. B., Liu, L., Li, S. X., Chen, X. D., Gao, D. S., & Li, L. (2016). GOLDEN 2-LIKE Transcription Factors of Plants. *Frontiers in Plant Science*, *7*. https://doi.org/10.3389/fpls.2016.01509

Chen, Q., Yu, F. F., & Xie, Q. (2020). Insights into endoplasmic reticulum-associated degradation in plants. *New Phytologist*, *226*(2), 345-350. https://doi.org/10.1111/nph.16369

Chen, X. J., Smith, M. D., Fitzpatrick, L., & Schnell, D. J. (2002). In vivo analysis of the role of atTic20 in protein import into chloroplasts. *Plant Cell*, *14*(3), 641-654. https://doi.org/10.1105/tpc.010336

Chen, Y. L., Chen, L. J., Chu, C. C., Huang, P. K., Wen, J. R., & Li, H. M. (2018). TIC236 links the outer and inner membrane translocons of the chloroplast. *Nature*, *564*(7734), 125-129. https://doi.org/10.1038/s41586-018-0713-y

Chou, M. L., Fitzpatrick, L. M., Tu, S. L., Budziszewski, G., Potter-Lewis, S., Akita, M., Levin, J. Z., Keegstra, K., & Li, H. M. (2003). Tic40, a membrane-anchored co-chaperone homolog in the chloroplast protein translocon. *Embo Journal*, *22*(12), 2970-2980. https://doi.org/10.1093/emboj/cdg281

Christianson, J. C., Olzmann, J. A., Shaler, T. A., Sowa, M. E., Bennett, E. J., Richter, C. M., Tyler, R. E., Greenblatt, E. J., Harper, J. W., & Kopito, R. R. (2012). Defining human ERAD networks through an integrative mapping strategy. *Nature Cell Biology*, *14*(1), 93-105. https://doi.org/10.1038/ncb2383

Chu, C. C., & Li, H. M. (2011). Determining the Location of an Arabidopsis Chloroplast Protein Using In Vitro Import Followed by Fractionation and Alkaline Extraction. *Chloroplast Research in Arabidopsis: Methods and Protocols*, *774*, 339-350. https://doi.org/10.1007/978-1-61779-234-2_20

Chua, N. H., & Schmidt, G. W. (1978). Post-Translational Transport into Intact Chloroplasts of a Precursor to the Small Subunit of Ribulose-1,5-Bisphosphate Carboxylase. *Proceedings*

of the National Academy of Sciences of the United States of America, *75*(12), 6110-6114. https://doi.org/10.1073/pnas.75.12.6110

Citovsky, V., Lee, L. Y., Vyas, S., Glick, E., Chen, M. H., Vainstein, A., Gafni, Y., Gelvin, S. B., & Tzfira, T. (2006). Subcellular localization of interacting proteins by bimolecular fluorescence complementation in planta. *Journal of Molecular Biology*, *362*(5), 1120-1131. https://doi.org/10.1016/j.jmb.2006.08.017

Cline, K., Wernerwashburne, M., Andrews, J., & Keegstra, K. (1984). Thermolysin Is a Suitable Protease for Probing the Surface of Intact Pea-Chloroplasts. *Plant Physiology*, *75*(3), 675-678. https://doi.org/10.1104/pp.75.3.675

Constan, D., Patel, R., Keegstra, K., & Jarvis, P. (2004). An outer envelope membrane component of the plastid protein import apparatus plays an essential role in Arabidopsis. *Plant Journal*, *38*(1), 93-106. https://doi.org/10.1111/j.1365-313X.2004.02024.x

Day, P. M., Inoue, K., & Theg, S. M. (2019). Chloroplast Outer Membrane beta-Barrel Proteins Use Components of the General Import Apparatus. *Plant Cell*, *31*(8), 1845-1855. https://doi.org/10.1105/tpc.19.00001

Day, P. M., Potter, D., & Inoue, K. (2014). Evolution and targeting of Omp85 homologs in the chloroplast outer envelope membrane. *Frontiers in Plant Science*, *5*. https://doi.org/10.3389/fpls.2014.00535

de Vries, J., Sousa, F. L., Bolter, B., Soll, J., & Gould, S. B. (2015). YCF1: A Green TIC? *Plant Cell*, *27*(7), 1827-1833. https://doi.org/10.1105/tpc.114.135541

Deruyffelaere, C., Purkrtova, Z., Bouchez, I., Collet, B., Cacas, J. L., Chardot, T., Gallois, J. L., & D'Andrea, S. (2018). PUX10 Is a CDC48A Adaptor Protein That Regulates the Extraction of Ubiquitinated Oleosins from Seed Lipid Droplets in Arabidopsis. *Plant Cell*, *30*(9), 2116-2136. https://doi.org/10.1105/tpc.18.00275

Dobberstein, B., Blobel, G., & Chua, N. H. (1977). In vitro synthesis and processing of a putative precursor for the small subunit of ribulose-1,5-bisphosphate carboxylase of

Chlamydomonas reinhardtii. *Proc Natl Acad Sci U S A*, *74*(3), 1082-1085. https://doi.org/10.1073/pnas.74.3.1082

Downes, B. P., Stupar, R. M., Gingerich, D. J., & Vierstra, R. D. (2003). The HECT ubiquitin-protein ligase (UPL) family in Arabidopsis: UPL3 has a specific role in trichome development. *Plant Journal*, *35*(6), 729-742. https://doi.org/10.1046/j.1365-313X.2003.01844.x

Drescher, A., Ruf, S., Calsa, T., Jr., Carrer, H., & Bock, R. (2000). The two largest chloroplast genome-encoded open reading frames of higher plants are essential genes. *Plant Journal*, *22*(2), 97-104. https://doi.org/10.1046/j.1365-313x.2000.00722.x

Duy, D., Wanner, G., Meda, A. R., von Wiren, N., Soll, J., & Philippar, K. (2007). PIC1, an ancient permease in Arabidopsis chloroplasts, mediates iron transport. *Plant Cell*, *19*(3), 986-1006. https://doi.org/10.1105/tpc.106.047407

Eckart, K., Eichacker, L., Sohrt, K., Schleiff, E., Heins, L., & Soll, J. (2002). A Toc75-like protein import channel is abundant in chloroplasts. *Embo Reports*, *3*(6), 557-562. https://doi.org/10.1093/embo-reports/kvf110

Elrouby, N., & Coupland, G. (2010). Proteome-wide screens for small ubiquitin-like modifier (SUMO) substrates identify Arabidopsis proteins implicated in diverse biological processes. *Proceedings of the National Academy of Sciences of the United States of America*, *107*(40), 17415-17420. https://doi.org/10.1073/pnas.1005452107

Endo, T., Kawamura, K., & Nakai, M. (1992). The chloroplast-targeting domain of plastocyanin transit peptide can form a helical structure but does not have a high affinity for lipid bilayers. *Eur J Biochem*, *207*(2), 671-675. https://doi.org/10.1111/j.1432-1033.1992.tb17094.x

Ertel, F., Mirus, O., Bredemeier, R., Moslavac, S., Becker, T., & Schleiff, E. (2005). The evolutionarily related beta-barrel polypeptide transporters from Pisum sativum and Nostoc PCC7120 contain two distinct functional domains. *Journal of Biological Chemistry*, *280*(31), 28281-28289. https://doi.org/10.1074/jbc.M503035200

Fang, J., Li, B. Q., Chen, L. J., Dogra, V., Luo, S. J., Wu, W. P., Wang, P. C., Hwang, I., Li, H. M., & Kim, C. (2022). TIC236 gain-of-function mutations unveil the link between plastid division and plastid protein import. *Proceedings of the National Academy of Sciences of the United States of America*, *119*(11). https://doi.org/10.1073/pnas.2123353119

Fellerer, C., Schweiger, R., Schongruber, K., Soll, J., & Schwenkert, S. (2011). Cytosolic HSP90 Cochaperones HOP and FKBP Interact with Freshly Synthesized Chloroplast Preproteins of Arabidopsis. *Molecular Plant*, *4*(6), 1133-1145. https://doi.org/10.1093/mp/ssr037

Flores-Perez, U., Bedard, J., Tanabe, N., Lymperopoulos, P., Clarke, A. K., & Jarvis, P. (2016). Functional Analysis of the Hsp93/ClpC Chaperone at the Chloroplast Envelope. *Plant Physiology*, *170*(1), 147-162. https://doi.org/10.1104/pp.15.01538

Flores-Perez, U., & Jarvis, P. (2013). Molecular chaperone involvement in chloroplast protein import. *Biochimica Et Biophysica Acta-Molecular Cell Research*, *1833*(2), 332-340. https://doi.org/10.1016/j.bbamcr.2012.03.019

Foresti, O., Rodriguez-Vaello, V., Funaya, C., & Carvalho, P. (2014). Quality control of inner nuclear membrane proteins by the Asi complex. *Science*, *346*(6210), 751-755. https://doi.org/10.1126/science.1255638

Fowler, S., Lee, K., Onouchi, H., Samach, A., Richardson, K., Coupland, G., & Putterill, J. (1999). GIGANTEA: a circadian clock-controlled gene that regulates photoperiodic flowering in Arabidopsis and encodes a protein with several possible membrane-spanning domains. *Embo Journal*, *18*(17), 4679-4688. https://doi.org/10.1093/emboj/18.17.4679

Franz, A., Ackermann, L., & Hoppe, T. (2016). Ring of Change: CDC48/p97 Drives Protein Dynamics at Chromatin. *Frontiers in Genetics*, *7*. https://doi.org/10.3389/fgene.2016.00073

Freemont, P. S., Hanson, I. M., & Trowsdale, J. (1991). A Novel Cysteine-Rich Sequence Motif. *Cell*, *64*(3), 483-484. https://doi.org/10.1016/0092-8674(91)90229-R

Froehlich, J. (2011). Studying Arabidopsis Envelope Protein Localization and Topology Using Thermolysin and Trypsin Proteases. *Chloroplast Research in Arabidopsis: Methods and Protocols*, *774*, 351-367. https://doi.org/10.1007/978-1-61779-234-2_21

Gallois, J. L., Drouaud, J., Lecureuil, A., Guyon-Debast, A., Bonhomme, S., & Guerche, P. (2013). Functional characterization of the plant ubiquitin regulatory X (UBX) domain-containing protein AtPUX7 in Arabidopsis thaliana. *Gene*, *526*(2), 299-308. https://doi.org/10.1016/j.gene.2013.05.056

Ganesan, I., Shi, L. X., Labs, M., & Theg, S. M. (2018). Evaluating the Functional Pore Size of Chloroplast TOC and TIC Protein Translocons: Import of Folded Proteins. *Plant Cell*, *30*(9), 2161-2173. https://doi.org/10.1105/tpc.18.00427

Ganesan, I., & Theg, S. M. (2019). Structural considerations of folded protein import through the chloroplast TOC/TIC translocons. *Febs Letters*, *593*(6), 565-572. https://doi.org/10.1002/1873-3468.13342

Gao, W., Liu, W., Zhao, M., & Li, W. X. (2015). NERF encodes a RING E3 ligase important for drought resistance and enhances the expression of its antisense gene NFYA5 in Arabidopsis. *Nucleic Acids Res*, *43*(1), 607-617. https://doi.org/10.1093/nar/gku1325

Gentle, I. E., Burri, L., & Lithgow, T. (2005). Molecular architecture and function of the Omp85 family of proteins. *Molecular Microbiology*, *58*(5), 1216-1225. https://doi.org/10.1111/j.1365-2958.2005.04906.x

Geoffroy, M. C., & Hay, R. T. (2009). An additional role for SUMO in ubiquitin-mediated proteolysis. *Nat Rev Mol Cell Biol*, *10*(8), 564-568. https://doi.org/10.1038/nrm2707

Glaser, S., van Dooren, G. G., Agrawal, S., Brooks, C. F., McFadden, G. I., Striepen, B., & Higgins, M. K. (2012). Tic22 Is an Essential Chaperone Required for Protein Import into the Apicoplast. *Journal of Biological Chemistry*, *287*(47). https://doi.org/10.1074/jbc.M112.405100

Gross, L. E., Klinger, A., Spies, N., Ernst, T., Flinner, N., Simm, S., Ladig, R., Bodensohn, U., & Schleiff, E. (2021). Insertion of plastidic beta-barrel proteins into the outer envelopes

of plastids involves an intermembrane space intermediate formed with Toc75-V/OEP80. *Plant Cell*, *33*(5), 1657-1681. https://doi.org/10.1093/plcell/koab052

Gutensohn, M., Schulz, B., Nicolay, P., & Flugge, U. I. (2000). Functional analysis of the two Arabidopsis homologues of Toc34, a component of the chloroplast protein import apparatus. *Plant Journal*, *23*(6), 771-783. https://doi.org/10.1046/j.1365-313x.2000.00849.x

Han, D. L., Lai, J. B., & Yang, C. W. (2021). SUMOylation: A critical transcription modulator in plant cells. *Plant Science*, *310*. https://doi.org/10.1016/j.plantsci.2021.110987

Hanzelmann, P., & Schindelin, H. (2017). The Interplay of Cofactor Interactions and Post-translational Modifications in the Regulation of the AAA+ ATPase p97. *Frontiers in Molecular Biosciences*, *4*. https://doi.org/10.3389/fmolb.2017.00021

Heins, L., Mehrle, A., Hemmler, R., Wagner, R., Kuchler, M., Hormann, F., Sveshnikov, D., & Soll, J. (2002). The preprotein conducting channel at the inner envelope membrane of plastids. *Embo Journal*, *21*(11), 2616-2625. https://doi.org/10.1093/emboj/21.11.2616

Heo, J. M., Livnat-Levanon, N., Taylor, E. B., Jones, K. T., Dephoure, N., Ring, J., Xie, J. X., Brodsky, J. L., Madeo, F., Gygi, S. P., Ashrafi, K., Glickman, M. H., & Rutter, J. (2010). A Stress-Responsive System for Mitochondrial Protein Degradation. *Molecular Cell*, *40*(3), 465-480. https://doi.org/10.1016/j.molcel.2010.10.021

Heo, J. M., Nielson, J. R., Dephoure, N., Gygi, S. P., & Rutter, J. (2013). Intramolecular interactions control Vms1 translocation to damaged mitochondria. *Molecular Biology of the Cell*, *24*(9), 1263-1273. https://doi.org/10.1091/mbc.E13-02-0072

Hiltbrunner, A., Grunig, K., Alvarez-Huerta, M., Infanger, S., Bauer, J., & Kessler, F. (2004). AtToc90, a new GTP-binding component of the Arabidopsis chloroplast protein import machinery. *Plant Molecular Biology*, *54*(3), 427-440. https://doi.org/10.1023/B:Plan.0000036374.92546.51

Hinnah, S. C., Hill, K., Wagner, R., Schlicher, T., & Soll, J. (1997). Reconstitution of a chloroplast protein import channel. *Embo Journal*, *16*(24), 7351-7360. https://doi.org/10.1093/emboj/16.24.7351

Hinnah, S. C., Wagner, R., Sveshnikova, N., Harrer, R., & Soll, J. (2002). The chloroplast protein import channel Toc75: Pore properties and interaction with transit peptides. *Biophysical Journal*, *83*(2), 899-911. https://doi.org/10.1016/S0006-3495(02)75216-8

Hirabayashi, Y., Kikuchi, S., Oishi, M., & Nakai, M. (2011). In Vivo Studies on the Roles of Two Closely Related Arabidopsis Tic20 Proteins, AtTic20-I and AtTic20-IV. *Plant and Cell Physiology*, *52*(3), 469-478. https://doi.org/10.1093/pcp/pcr010

Hirsch, S., Muckel, E., Heemeyer, F., von Heijne, G., & Soll, J. (1994). A receptor component of the chloroplast protein translocation machinery. *Science*, *266*(5193), 1989-1992. https://doi.org/10.1126/science.7801125

Hofmann, N. R., & Theg, S. M. (2005). Toc64 is not required for import of proteins into chloroplasts in the moss Physcomitrella patens. *Plant Journal*, *43*(5), 675-687. https://doi.org/10.1111/j.1365-313X.2005.02483.x

Hoppe, T. (2005). Multiubiquitylation by E4 enzymes: 'one size' doesn't fit all. *Trends in Biochemical Sciences*, *30*(4), 183-187. https://doi.org/10.1016/j.tibs.2005.02.004

Hsu, S. C., & Inoue, K. (2009). Two evolutionarily conserved essential beta-barrel proteins in the chloroplast outer envelope membrane. *Biosci Trends*, *3*(5), 168-178. https://www.ncbi.nlm.nih.gov/pubmed/20103843

Hsu, S. C., Patel, R., Bedard, J., Jarvis, P., & Inoue, K. (2008). Two distinct Omp85 paralogs in the chloroplast outer envelope membrane are essential for embryogenesis in Arabidopsis thaliana. *Plant Signal Behav*, *3*(12), 1134-1135. https://doi.org/10.4161/psb.3.12.7095

Hsueh, Y. C., Flinner, N., Gross, L. E., Haarmann, R., Mirus, O., Sommer, M. S., & Schleiff, E. (2017). Chloroplast outer envelope protein P39 in Arabidopsis thaliana belongs to the Omp85 protein family. *Proteins-Structure Function and Bioinformatics*, *85*(8), 1391-1401. https://doi.org/10.1002/prot.24725

Hua, Z. H., & Vierstra, R. D. (2011). The Cullin-RING Ubiquitin-Protein Ligases. *Annual Review of Plant Biology*, *62*, 299-334. https://doi.org/10.1146/annurev-arplant-042809-112256

Huang, A. B., Tang, Y., Shi, X. T., Jia, M., Zhu, J. H., Yan, X. H., Chen, H. Q., & Gu, Y. N. (2020). Proximity labeling proteomics reveals critical regulators for inner nuclear membrane protein degradation in plants. *Nature Communications*, *11*(1). https://doi.org/10.1038/s41467-020-16744-1

Huang, W. H., Ling, Q. H., Bedard, J., Lilley, K., & Jarvis, P. (2011). In Vivo Analyses of the Roles of Essential Omp85-Related Proteins in the Chloroplast Outer Envelope Membrane. *Plant Physiology*, *157*(1), 147-159. https://doi.org/10.1104/pp.111.181891

Huibregtse, J. M., Scheffner, M., Beaudenon, S., & Howley, P. M. (1995). A Family of Proteins Structurally and Functionally Related to the E6-Ap Ubiquitin-Protein Ligase. *Proceedings of the National Academy of Sciences of the United States of America*, *92*(11), 5249-5249. https://doi.org/10.1073/pnas.92.11.5249-a

Huq, E., Tepperman, J. M., & Quail, P. H. (2000). GIGANTEA is a nuclear protein involved in phytochrome signaling in Arabidopsis. *Proceedings of the National Academy of Sciences of the United States of America*, *97*(17), 9789-9794. https://doi.org/10.1073/pnas.170283997

Husnjak, K., & Dikic, I. (2012). Ubiquitin-Binding Proteins: Decoders of Ubiquitin-Mediated Cellular Functions. *Annual Review of Biochemistry*, *81*, 291-322. https://doi.org/10.1146/annurev-biochem-051810-094654

Hust, B., & Gutensohn, M. (2006). Deletion of core components of the plastid protein import machinery causes differential arrest of embryo development in Arabidopsis thaliana. *Plant Biology*, *8*(1), 18-30. https://doi.org/10.1055/s-2005-873044

Hyman, S., & Jarvis, R. P. (2011). Studying Arabidopsis Chloroplast Structural Organisation Using Transmission Electron Microscopy. *Chloroplast Research in Arabidopsis: Methods and Protocols*, *774*, 113-132. https://doi.org/10.1007/978-1-61779-234-2_8

Inaba, T., Alvarez-Huerta, M., Li, M., Bauer, J., Ewers, C., Kessler, F., & Schnell, D. J. (2005). Arabidopsis Tic110 is essential for the assembly and function of the protein import machinery of plastids. *Plant Cell*, *17*(5), 1482-1496. https://doi.org/10.1105/tpc.105.030700

Inaba, T., Li, M., Alvarez-Huerta, M., Kessler, F., & Schnell, D. J. (2003). AtTic110 functions as a scaffold for coordinating the stromal events of protein import into chloroplasts. *Journal of Biological Chemistry*, *278*(40), 38617-38627. https://doi.org/10.1074/jbc.M306367200

Infanger, S., Bischof, S., Hiltbrunner, A., Agne, B., Baginsky, S., & Kessler, F. (2011). The Chloroplast Import Receptor Toc90 Partially Restores the Accumulation of Toc159 Client Proteins in the Arabidopsis thaliana ppi2 Mutant. *Molecular Plant*, *4*(2), 252-263. https://doi.org/10.1093/mp/ssq071

Inoue, H., Li, M., & Schnell, D. J. (2013). An essential role for chloroplast heat shock protein 90 (Hsp90C) in protein import into chloroplasts. *Proceedings of the National Academy of Sciences of the United States of America*, *110*(8), 3173-3178. https://doi.org/10.1073/pnas.1219229110

Inoue, H., Rounds, C., & Schnell, D. J. (2010). The Molecular Basis for Distinct Pathways for Protein Import into Arabidopsis Chloroplasts. *Plant Cell*, *22*(6), 1947-1960. https://doi.org/10.1105/tpc.110.074328

Inoue, K., & Potter, D. (2004). The chloroplastic protein translocation channel Toc75 and its paralog OEP80 represent two distinct protein families and are targeted to the chloroplastic outer envelope by different mechanisms. *Plant Journal*, *39*(3), 354-365. https://doi.org/10.1111/j.1365-313X.2004.02135.x

Ivanova, Y., Smith, M. D., Chen, K. H., & Schnell, D. J. (2004). Members of the Toc159 import receptor family represent distinct pathways for protein targeting to plastids. *Molecular Biology of the Cell*, *15*(7), 3379-3392. https://doi.org/10.1091/mbc.E03-12-0923

Jackson, D. T., Froehlich, J. E., & Keegstra, K. (1998). The hydrophilic domain of Tic110, an inner envelope membrane component of the chloroplastic protein translocation apparatus, faces the stromal compartment. *Journal of Biological Chemistry*, *273*(26), 16583-16588. https://doi.org/10.1074/jbc.273.26.16583

Jarvis, P. (2004). Organellar proteomics: Chloroplasts in the spotlight. *Current biology*, *14*(8), R317-R319. https://doi.org/10.1016/j.cub.2004.03.054

Jarvis, P. (2008). Targeting of nucleus-encoded proteins to chloroplasts in plants. *New Phytologist*, *179*(2), 257-285. https://doi.org/10.1111/j.1469-8137.2008.02452.x

Jarvis, P., Chen, L. J., Li, H. M., Pete, C. A., Fankhauser, C., & Chory, J. (1998). An Arabidopsis mutant defective in the plastid general protein import apparatus. *Science*, *282*(5386), 100-103. https://doi.org/10.1126/science.282.5386.100

Jarvis, P., & Lopez-Juez, E. (2013). Biogenesis and homeostasis of chloroplasts and other plastids. *Nature Reviews Molecular Cell Biology*, *14*(12), 787-802. https://doi.org/10.1038/nrm3702

Jin, Z. Y., Wan, L., Zhang, Y. Q., Li, X. C., Cao, Y., Liu, H. B., Fan, S. Y., Cao, D., Wang, Z. M., Li, X. B., Pan, J. M., Dong, M. Q., Wu, J. P., & Yan, Z. (2022). Structure of a TOC-TIC supercomplex spanning two chloroplast envelope membranes. *Cell*, *185*(25), 4788-4800. https://doi.org/10.1016/j.cell.2022.10.030

Jumper, J., Evans, R., Pritzel, A., Green, T., Figurnov, M., Ronneberger, O., Tunyasuvunakool, K., Bates, R., Zidek, A., Potapenko, A., Bridgland, A., Meyer, C., Kohl, S. A. A., Ballard, A. J., Cowie, A., Romera-Paredes, B., Nikolov, S., Jain, R., Adler, J., Back, T., Petersen, S., Reiman, D., Clancy, E., Zielinski, M., Steinegger, M., Pacholska, M., Berghammer, T., Bodenstein, S., Silver, D., Vinyals, O., Senior, A. W., Kavukcuoglu, K., Kohli, P., & Hassabis, D. (2021). Highly accurate protein structure prediction with AlphaFold. *Nature*, *596*(7873), 583-589. https://doi.org/10.1038/s41586-021-03819-2

Kakizaki, T., Matsumura, H., Nakayama, K., Che, F. S., Terauchi, R., & Inaba, T. (2009). Coordination of Plastid Protein Import and Nuclear Gene Expression by Plastid-to-Nucleus Retrograde Signaling. *Plant Physiology*, *151*(3), 1339-1353. https://doi.org/10.1104/pp.109.145987

Kasmati, A. R., Topel, M., Khan, N. Z., Patel, R., Ling, Q. H., Karim, S., Aronsson, H., & Jarvis, P. (2013). Evolutionary, Molecular and Genetic Analyses of Tic22 Homologues in Arabidopsis thaliana Chloroplasts. *Plos One*, *8*(5). https://doi.org/10.1371/journal.pone.0063863

Kasmati, A. R., Topel, M., Patel, R., Murtaza, G., & Jarvis, P. (2011). Molecular and genetic analyses of Tic20 homologues in Arabidopsis thaliana chloroplasts. *Plant Journal*, *66*(5), 877-889. https://doi.org/10.1111/j.1365-313X.2011.04551.x

Keeling, P. J. (2010). The endosymbiotic origin, diversification and fate of plastids. *Philos Trans R Soc Lond B Biol Sci*, *365*(1541), 729-748. https://doi.org/10.1098/rstb.2009.0103

Kelley, L. A., Mezulis, S., Yates, C. M., Wass, M. N., & Sternberg, M. J. E. (2015). The Phyre2 web portal for protein modeling, prediction and analysis. *Nature Protocols*, *10*(6), 845-858. https://doi.org/10.1038/nprot.2015.053

Kerppola, T. K. (2008). Bimolecular fluorescence complementation: visualization of molecular interactions in living cells. *Methods Cell Biol*, *85*, 431-470. https://doi.org/10.1016/S0091-679X(08)85019-4

Kessler, F., Blobel, G., Patel, H. A., & Schnell, D. J. (1994). Identification of 2 Gtp-Binding Proteins in the Chloroplast Protein Import Machinery. *Science*, *266*(5187), 1035-1039. https://doi.org/10.1126/science.7973656

Kessler, F., & Schnell, D. (2009). Chloroplast biogenesis: diversity and regulation of the protein import apparatus. *Current Opinion in Cell Biology*, *21*(4), 494-500. https://doi.org/10.1016/j.ceb.2009.03.004

Kikuchi, S., Bedard, J., Hirano, M., Hirabayashi, Y., Oishi, M., Imai, M., Takase, M., Ide, T., & Nakai, M. (2013). Uncovering the Protein Translocon at the Chloroplast Inner

Envelope Membrane. *Science*, *339*(6119), 571-574. https://doi.org/10.1126/science.1229262

Kikuchi, S., Hirohashi, T., & Nakai, M. (2006). Characterization of the preprotein translocon at the outer envelope membrane of chloroplasts by blue native PAGE. *Plant and Cell Physiology*, *47*(3), 363-371. https://doi.org/10.1093/pcp/pcj002

Kikuchi, S., Oishi, M., Hirabayashi, Y., Lee, D. W., Hwang, I., & Nakai, M. (2009). A 1-Megadalton Translocation Complex Containing Tic20 and Tic21 Mediates Chloroplast Protein Import at the Inner Envelope Membrane. *Plant Cell*, *21*(6), 1781-1797. https://doi.org/10.1105/tpc.108.063552

Kim, J., Geng, R. S., Gallenstein, R. A., & Somers, D. E. (2013b). The F-box protein ZEITLUPE controls stability and nucleocytoplasmic partitioning of GIGANTEA. *Development*, *140*(19), 4060-4069. https://doi.org/10.1242/dev.096651

Kim, J. H., Cho, S. K., Oh, T. R., Ryu, M. Y., Yang, S. W., & Kim, W. T. (2017). MPSR1 is a cytoplasmic PQC E3 ligase for eliminating emergent misfolded proteins in Arabidopsis thaliana. *Proceedings of the National Academy of Sciences of the United States of America*, *114*(46), E10009-E10017. https://doi.org/10.1073/pnas.1713574114

Kim, S. J., Cho, J., Song, E. J., Kim, S. J., Kim, H. M., Lee, K. E., Suh, S. W., & Kim, E. E. (2014). Structural Basis for Ovarian Tumor Domain-containing Protein 1 (OTU1) Binding to p97/Valosin-containing Protein (VCP). *Journal of Biological Chemistry*, *289*(18), 12264-12274. https://doi.org/10.1074/jbc.M113.523936

Kim, W. Y., Fujiwara, S., Suh, S. S., Kim, J., Kim, Y., Han, L. Q., David, K., Putterill, J., Nam, H. G., & Somers, D. E. (2007). ZEITLUPE is a circadian photoreceptor stabilized by GIGANTEA in blue light. *Nature*, *449*(7160), 356-+. https://doi.org/10.1038/nature06132

Kim, Y., Lim, J., Yeom, M., Kim, H., Kim, J., Wang, L., Kim, W. Y., Somers, D. E., & Nam, H. G. (2013a). ELF4 Regulates GIGANTEA Chromatin Access through Subnuclear Sequestration. *Cell Reports*, *3*(3), 671-677. https://doi.org/10.1016/j.celrep.2013.02.021

Kim, Y., Yeom, M., Kim, H., Lim, J., Koo, H. J., Hwang, D., Somers, D., & Nam, H. G. (2012). GIGANTEA and EARLY FLOWERING 4 in Arabidopsis Exhibit Differential Phase-Specific Genetic Influences over a Diurnal Cycle. *Molecular Plant*, *5*(3), 678-687. https://doi.org/10.1093/mp/sss005

Kloppsteck, P., Ewens, C. A., Forster, A., Zhang, X. D., & Freemont, P. S. (2012). Regulation of p97 in the ubiquitin-proteasome system by the UBX protein-family. *Biochimica Et Biophysica Acta-Molecular Cell Research*, *1823*(1), 125-129. https://doi.org/10.1016/j.bbamcr.2011.09.006

Kohler, D., Helm, S., Agne, B., & Baginsky, S. (2016). Importance of Translocon Subunit Tic56 for rRNA Processing and Chloroplast Ribosome Assembly. *Plant Physiology*, *172*(4), 2429-2444. https://doi.org/10.1104/pp.16.01393

Kohler, D., Montandon, C., Hause, G., Majovsky, P., Kessler, F., Baginsky, S., & Agne, B. (2015). Characterization of Chloroplast Protein Import without Tic56, a Component of the 1-Megadalton Translocon at the Inner Envelope Membrane of Chloroplasts. *Plant Physiology*, *167*(3), 972-990. https://doi.org/10.1104/pp.114.255562

Komander, D., & Rape, M. (2012). The Ubiquitin Code. *Annual Review of Biochemistry*, *81*, 203-229. https://doi.org/10.1146/annurev-biochem-060310-170328

Kouranov, A., Chen, X. J., Fuks, B., & Schnell, D. J. (1998). Tic20 and Tic22 are new components of the protein import apparatus at the chloroplast inner envelope membrane. *Journal of Cell Biology*, *143*(4), 991-1002. https://doi.org/10.1083/jcb.143.4.991

Kouranov, A., & Schnell, D. J. (1997). Analysis of the interactions of preproteins with the import machinery over the course of protein import into chloroplasts. *Journal of Cell Biology*, *139*(7), 1677-1685. https://doi.org/10.1083/jcb.139.7.1677

Kovacheva, S., Bedard, J., Patel, R., Dudley, P., Twell, D., Rios, G., Koncz, C., & Jarvis, P. (2005). In vivo studies on the roles of Tic110, Tic40 and Hsp93 during chloroplast protein import. *Plant Journal*, *41*(3), 412-428. https://doi.org/10.1111/j.1365-313X.2004.02307.x

Kovacs-Bogdan, E., Benz, J. P., Soll, J., & Bolter, B. (2011). Tic20 forms a channel independent of Tic110 in chloroplasts. *Bmc Plant Biology*, *11*. https://doi.org/10.1186/1471-2229-11-133

Kretzschmar, F. K., Mengel, L. A., Muller, A. O., Schmitt, K., Blersch, K. F., Valerius, O., Braus, G. H., & Ischebeck, T. (2018). PUX10 Is a Lipid Droplet-Localized Scaffold Protein That Interacts with CELL DIVISION CYCLE48 and Is Involved in the Degradation of Lipid Droplet Proteins. *Plant Cell*, *30*(9), 2137-2160. https://doi.org/10.1105/tpc.18.00276

Krimm, I., Gans, P., Hernandez, J. F., Arlaud, G. J., & Lancelin, J. M. (1999). A coil-helix instead of a helix-coil motif can be induced in a chloroplast transit peptide from Chlamydomonas reinhardtii. *European Journal of Biochemistry*, *265*(1), 171-180. https://doi.org/10.1046/j.1432-1327.1999.00701.x

Kubis, S., Baldwin, A., Patel, R., Razzaq, A., Dupree, P., Lilley, K., Kurth, J., Leister, D., & Jarvis, P. (2003). The Arabidopsis ppi1 mutant is specifically defective in the expression, chloroplast import, and accumulation of photosynthetic proteins. *Plant Cell*, *15*(8), 1859-1871. https://doi.org/10.1105/tpc.012955

Kubis, S., Patel, R., Combe, J., Bedard, J., Kovacheva, S., Lilley, K., Biehl, A., Leister, D., Rios, G., Koncz, C., & Jarvis, P. (2004). Functional specialization amongst the Arabidopsis Toc159 family of chloroplast protein import receptors. *Plant Cell*, *16*(8), 2059-2077. https://doi.org/10.1105/tpc.104.023309

Kurepa, J., Smalle, J., Van Montagu, M., & Inze, D. (1998). Oxidative stress tolerance and longevity in Arabidopsis: the late-flowering mutant gigantea is tolerant to paraquat. *Plant Journal*, *14*(6), 759-764. https://doi.org/10.1046/j.1365-313x.1998.00168.x

Kurepa, J., Walker, J. M., Smalle, J., Gosink, M. M., Davis, S. J., Durham, T. L., Sung, D. Y., & Vierstra, R. D. (2003). The small ubiquitin-like modifier (SUMO) protein modification system in Arabidopsis - Accumulation of SUMO1 and -2 conjugates is increased by stress.

Journal of Biological Chemistry, *278*(9), 6862-6872. https://doi.org/10.1074/jbc.M209694200

Le, L. T., Kang, W., Kim, J. Y., Le, O. T., Lee, S. Y., & Yang, J. K. (2016). Structural Details of Ufd1 Binding to p97 and Their Functional Implications in ER-Associated Degradation. *Plos One*, *11*(9), e0163394. https://doi.org/10.1371/journal.pone.0163394

Lee, D. W., Kim, S. J., Oh, Y. J., Choi, B., Lee, J., & Hwang, I. (2016). Arabidopsis BAG1 Functions as a Cofactor in Hsc70-Mediated Proteasomal Degradation of Unimported Plastid Proteins. *Molecular Plant*, *9*(10), 1428-1431. https://doi.org/10.1016/j.molp.2016.06.005

Lee, K. H., Kim, S. J., Lee, Y. J., Jin, J. B., & Hwang, I. (2003). The M domain of atToc159 plays an essential role in the import of proteins into chloroplasts and chloroplast biogenesis. *Journal of Biological Chemistry*, *278*(38), 36794-36805. https://doi.org/10.1074/jbc.M304457200

Lee, S., Lee, D. W., Lee, Y., Mayer, U., Stierhof, Y. D., Lee, S., Jurgens, G., & Hwang, I. (2009). Heat shock protein cognate 70-4 and an E3 ubiquitin ligase, CHIP, mediate plastid-destined precursor degradation through the ubiquitin-26S proteasome system in Arabidopsis. *Plant Cell*, *21*(12), 3984-4001. https://doi.org/10.1105/tpc.109.071548

Lee, S., Tsai, Y. C., Mattera, R., Smith, W. J., Kostelansky, M. S., Weissman, A. M., Bonifacino, J. S., & Hurley, J. H. (2006). Structural basis for ubiquitin recognition and autoubiquitination by Rabex-5. *Nature Structural & Molecular Biology*, *13*(3), 264-271. https://doi.org/10.1038/nsmb1064

Leipe, D. D., Wolf, Y. I., Koonin, E. V., & Aravind, L. (2002). Classification and evolution of P-loop GTPases and related ATPases. *Journal of Molecular Biology*, *317*(1), 41-72. https://doi.org/10.1006/jmbi.2001.5378

Leister, D. (2003). Chloroplast research in the genomic age. *Trends in Genetics*, *19*(1), 47-56. https://doi.org/10.1016/S0168-9525(02)00003-3

Li, F. Q., & Vierstra, R. D. (2012). Autophagy: a multifaceted intracellular system for bulk and selective recycling. *Trends in Plant Science*, *17*(9), 526-537. https://doi.org/10.1016/j.tplants.2012.05.006

Li, G. T., Zhao, G., Schindelin, H., & Lennarz, W. J. (2008). Tyrosine phosphorylation of ATPase p97 regulates its activity during ERAD. *Biochemical and Biophysical Research Communications*, *375*(2), 247-251. https://doi.org/10.1016/j.bbrc.2008.08.018

Li, H. M., & Chiu, C. C. (2010). Protein Transport into Chloroplasts. *Annual Review of Plant Biology*, *61*, 157-180. https://doi.org/10.1146/annurev-arplant-042809-112222

Li, H. M., & Teng, Y. S. (2013a). Transit peptide design and plastid import regulation. *Trends in Plant Science*, *18*(7), 360-366. https://doi.org/10.1016/j.tplants.2013.04.003

Li, J. L., Yuan, J. R., Li, Y. H., Sun, H. L., Ma, T. T., Huai, J. L., Yang, W. Q., Zhang, W. H., & Lin, R. C. (2022). The CDC48 complex mediates ubiquitin-dependent degradation of intra-chloroplast proteins in plants. *Cell Reports*, *39*(2). https://doi.org/10.1016/j.celrep.2022.110664

Li, L. B., Vorobyov, I., & Allen, T. W. (2013b). The Different Interactions of Lysine and Arginine Side Chains with Lipid Membranes. *Journal of Physical Chemistry B*, *117*(40), 11906-11920. https://doi.org/10.1021/jp405418y

Li, W., Ahn, I. P., Ning, Y. S., Park, C. H., Zeng, L. R., Whitehill, J. G. A., Lu, H. B., Zhao, Q. Z., Ding, B., Xie, Q., Zhou, J. M., Dai, L. Y., & Wang, G. L. (2012). The U-Box/ARM E3 Ligase PUB13 Regulates Cell Death, Defense, and Flowering Time in Arabidopsis. *Plant Physiology*, *159*(1), 239-250. https://doi.org/10.1104/pp.111.192617

Liang, J., Yin, C., Doong, H., Fang, S., Peterhoff, C., Nixon, R. A., & Monteiro, M. J. (2006). Characterization of erasin (UBXD2): a new ER protein that promotes ER-associated protein degradation. *Journal of Cell Science*, *119*(Pt 19), 4011-4024. https://doi.org/10.1242/jcs.03163

Lim, P. J., Danner, R., Liang, J., Doong, H., Harman, C., Srinivasan, D., Rothenberg, C., Wang, H. M., Ye, Y. H., Fang, S. Y., & Monteiro, M. J. (2009). Ubiquilin and p97/VCP

bind erasin, forming a complex involved in ERAD. *Journal of Cell Biology*, *187*(2), 201-217. https://doi.org/10.1083/jcb.200903024

Lin, J. S., & Lai, E. M. (2017). Protein-Protein Interactions: Co-Immunoprecipitation. *Methods Mol Biol*, *1615*, 211-219. https://doi.org/10.1007/978-1-4939-7033-9_17

Ling, Q. H., Broad, W., Trosch, R., Topel, M., Sert, T. D., Lymperopoulos, P., Baldwin, A., & Jarvis, R. P. (2019). Ubiquitin-dependent chloroplast-associated protein degradation in plants. *Science*, *363*(6429), 836-848. https://doi.org/10.1126/science.aav4467

Ling, Q. H., Huang, W. H., Baldwin, A., & Jarvis, P. (2012). Chloroplast Biogenesis Is Regulated by Direct Action of the Ubiquitin-Proteasome System. *Science*, *338*(6107), 655-659. https://doi.org/10.1126/science.1225053

Ling, Q. H., Huang, W. H., & Jarvis, P. (2011). Use of a SPAD-502 meter to measure leaf chlorophyll concentration in Arabidopsis thaliana. *Photosynthesis Research*, *107*(2), 209-214. https://doi.org/10.1007/s11120-010-9606-0

Ling, Q. H., & Jarvis, P. (2015a). Functions of plastid protein import and the ubiquitin-proteasome system in plastid development. *Biochimica Et Biophysica Acta-Bioenergetics*, *1847*(9), 939-948. https://doi.org/10.1016/j.bbabio.2015.02.017

Ling, Q. H., & Jarvis, P. (2015b). Regulation of Chloroplast Protein Import by the Ubiquitin E3 Ligase SP1 Is Important for Stress Tolerance in Plants. *Current biology*, *25*(19), 2527-2534. https://doi.org/10.1016/j.cub.2015.08.015

Ling, Q. H., & Jarvis, P. (2016). Analysis of Protein Import into Chloroplasts Isolated from Stressed Plants. *J Vis Exp,*(117), e54717. https://doi.org/10.3791/54717

Ling, Q. H., Li, N., & Jarvis, P. (2017). Chloroplast Ubiquitin E3 Ligase SP1: Does It Really Function in Peroxisomes? *Plant Physiology*, *175*(2), 586-588. https://doi.org/10.1104/pp.17.00948

Ling, Q. H., Sadali, N. M., Soufi, Z., Zhou, Y., Huang, B. Q., Zeng, Y. L., Rodriguez-Concepcion, M., & Jarvis, R. P. (2021). The chloroplast-associated protein degradation

pathway controls chromoplast development and fruit ripening in tomato. *Nature Plants*, *7*, 655-666. https://doi.org/10.1038/s41477-021-00916-y

Littlejohn, G. R., Gouveia, J. D., Edner, C., Smirnoff, N., & Love, J. (2010). Perfluorodecalin enhances in vivo confocal microscopy resolution of Arabidopsis thaliana mesophyll. *New Phytologist*, *186*(4), 1018-1025. https://doi.org/10.1111/j.1469-8137.2010.03244.x

Liu, H., Li, A. J., Jean-David, R., & Liu, Z. F. (2023). Architecture of chloroplast TOC-TIC translocon supercomplex. *Nature*, *615*, 349-357. https://doi.org/10.1038/s41586-023-05744-y

Liu, S., Fu, Q. S., Zhao, J., & Hu, H. Y. (2013). Structural and mechanistic insights into the arginine/lysine-rich peptide motifs that interact with P97NCP. *Biochimica Et Biophysica Acta-Proteins and Proteomics*, *1834*(12), 2672-2678. https://doi.org/10.1016/j.bbapap.2013.09.021

Liu, Y. D., & Li, J. M. (2014). Endoplasmic reticulum-mediated protein quality control in Arabidopsis. *Frontiers in Plant Science*, *5*. https://doi.org/10.3389/fpls.2014.00162

Lopez-Juez, E., Jarvis, R. P., Takeuchi, A., Page, A. M., & Chory, J. (1998). New Arabidopsis cue mutants suggest a close connection between plastid- and phytochrome regulation of nuclear gene expression. *Plant Physiology*, *118*(3), 803-815. https://doi.org/10.1104/pp.118.3.803

Lopez-Juez, E., & Pyke, K. A. (2005). Plastids unleashed: their development and their integration in plant development. *International Journal of Developmental Biology*, *49*(5-6), 557-577. https://doi.org/10.1387/ijdb.051997el

Loudya, N., Maffei, D. P. F., J, B. D., Ali, S. M., Devlin, P. F., Jarvis, R. P., & E, L. P.-J. (2022). Mutations in the chloroplast inner envelope protein TIC100 impair and repair chloroplast protein import and impact retrograde signaling. *Plant Cell*, *34*(8), 3028-3046. https://doi.org/10.1093/plcell/koac153

Lubeck, J., Soll, J., Akita, M., Nielsen, E., & Keegstra, K. (1996). Topology of IEP110, a component of the chloroplastic protein import machinery present in the inner envelope

membrane. *Embo Journal*, *15*(16), 4230-4238. https://doi.org/10.1002/j.1460-2075.1996.tb00797.x

Maple, J., & Moller, S. G. (2007). Mutagenesis in Arabidopsis. *Methods Mol Biol*, *362*, 197-206. https://doi.org/10.1007/978-1-59745-257-1_14

Marshall, R. S., Hua, Z. H., Mali, S., McLoughlin, F., & Vierstra, R. D. (2019). ATG8-Binding UIM Proteins Define a New Class of Autophagy Adaptors and Receptors. *Cell*, *177*(3), 766-781. https://doi.org/10.1016/j.cell.2019.02.009

Martensson, C. U., Priesnitz, C., Song, J., Ellenrieder, L., Doan, K. N., Boos, F., Floerchinger, A., Zufall, N., Oeljeklaus, S., Warscheid, B., & Becker, T. (2019). Mitochondrial protein translocation-associated degradation. *Nature*, *569*(7758), 679-683. https://doi.org/10.1038/s41586-019-1227-y

Martin, G., Leivar, P., Ludevid, D., Tepperman, J. M., Quail, P. H., & Monte, E. (2016). Phytochrome and retrograde signalling pathways converge to antagonistically regulate a light-induced transcriptional network. *Nature Communications*, *7*. https://doi.org/10.1038/ncomms11431

Martin, W., Roettger, M., Kloesges, T., Thiergart, T., Woehle, C., Gould, S., & Dagan, T. (2012). Modern endosymbiotic theory: Getting lateral gene transfer in-to the equation. *Journal of Endocytobiosis and Cell Research*, *23*, 1-5.

Matsushima, R., Maekawa, M., Kusano, M., Kondo, H., Fujita, N., Kawagoe, Y., & Sakamoto, W. (2014). Amyloplast-Localized SUBSTANDARD STARCH GRAIN4 Protein Influences the Size of Starch Grains in Rice Endosperm. *Plant Physiology*, *164*(2), 623-636. https://doi.org/10.1104/pp.113.229591

May, T., & Soll, J. (2000). 14-3-3 proteins form a guidance complex with chloroplast precursor proteins in plants. *Plant Cell*, *12*(1), 53-64. https://doi.org/10.1105/tpc.12.1.53

McNeill, H., Knebel, A., Arthur, J. S. C., Cuenda, A., & Cohen, P. (2004). A novel UBA and UBX domain protein that binds polyubiquitin and VCP and is a substrate for SAPKs. *Biochemical Journal*, *384*, 391-400. https://doi.org/10.1042/Bj20041498

Merai, Z., Chumak, N., Garcia-Aguilar, M., Hsieh, T. F., Nishimura, T., Schoft, V. K., Bindics, J., Slusarz, L., Arnoux, S., Opravil, S., Mechtler, K., Zilberman, D., Fischer, R. L., & Tamaru, H. (2014). The AAA-ATPase molecular chaperone Cdc48/p97 disassembles sumoylated centromeres, decondenses heterochromatin, and activates ribosomal RNA genes. *Proceedings of the National Academy of Sciences of the United States of America*, *111*(45), 16166-16171. https://doi.org/10.1073/pnas.1418564111

Miao, Y., & Zentgraf, U. (2010). A HECT E3 ubiquitin ligase negatively regulates Arabidopsis leaf senescence through degradation of the transcription factor WRKY53. *Plant Journal*, *63*(2), 179-188. https://doi.org/10.1111/j.1365-313X.2010.04233.x

Mishra, P., & Panigrahi, K. C. (2015). GIGANTEA - an emerging story. *Frontiers in Plant Science*, *6*. https://doi.org/10.3389/fpls.2015.00008

Mohd Ali, S., Li, N., Soufi, Z., Yao, J., Johnson, E., Ling, Q., & Jarvis, R. P. (2023). Multiple ubiquitin E3 ligase genes antagonistically regulate chloroplast-associated protein degradation. *Curr Biol*. https://doi.org/10.1016/j.cub.2023.01.060

Mueller, B., Klemm, E. J., Spooner, E., Claessen, J. H., & Ploegh, H. L. (2008). SEL1L nucleates a protein complex required for dislocation of misfolded glycoproteins. *Proceedings of the National Academy of Sciences of the United States of America*, *105*(34), 12325-12330. https://doi.org/10.1073/pnas.0805371105

Nahar, S., Chowdhury, A., Ogura, T., & Esaki, M. (2020). A AAA ATPase Cdc48 with a cofactor Ubx2 facilitates ubiquitylation of a mitochondrial fusion-promoting factor Fzo1 for proteasomal degradation. *Journal of Biochemistry*, *167*(3), 279-286. https://doi.org/10.1093/jb/mvz104

Nakai, M. (2018). New Perspectives on Chloroplast Protein Import. *Plant and Cell Physiology*, *59*(6), 1111-1119. https://doi.org/10.1093/pcp/pcy083

Nakrieko, K. A., Mould, R. M., & Smith, A. G. (2004). Fidelity of targeting to chloroplasts is not affected by removal of the phosphorylation site from the transit peptide. *Eur J Biochem*, *271*(3), 509-516. https://doi.org/10.1046/j.1432-1033.2003.03950.x

Neal, S., Jaeger, P. A., Duttke, S. H., Benner, C., Glass, C. K., Ideker, T., & Hampton, R. Y. (2018). The Dfm1 Derlin Is Required for ERAD Retrotranslocation of Integral Membrane Proteins. *Mol Cell*, *69*(2), 306-320. https://doi.org/10.1016/j.molcel.2017.12.012

Neff, M. M., Neff, J. D., Chory, J., & Pepper, A. E. (1998). dCAPS, a simple technique for the genetic analysis of single nucleotide polymorphisms: experimental applications in Arabidopsis thaliana genetics. *Plant Journal*, *14*(3), 387-392. https://doi.org/10.1046/j.1365-313X.1998.00124.x

Neuber, O., Jarosch, E., Volkwein, C., Walter, J., & Sommer, T. (2005). Ubx2 links the Cdc48 complex to ER-associated protein degradation. *Nature Cell Biology*, *7*(10), 993-998. https://doi.org/10.1038/ncb1298

O'Neil, P. K., Richardson, L. G. L., Paila, Y. D., Piszczek, G., Chakravarthy, S., Noinaj, N., & Schnell, D. (2017). The POTRA domains of Toc75 exhibit chaperone-like function to facilitate import into chloroplasts. *Proceedings of the National Academy of Sciences of the United States of America*, *114*(24), E4868-E4876. https://doi.org/10.1073/pnas.1621179114

Paila, Y. D., Richardson, L. G. L., Inoue, H., Parks, E. S., McMahon, J., Inoue, K., & Schnell, D. J. (2016). Multi-functional roles for the polypeptide transport associated domains of Toc75 in chloroplast protein import. *Elife*, *5*. https://doi.org/10.7554/eLife.12631

Paila, Y. D., Richardson, L. G. L., & Schnell, D. J. (2015). New Insights into the Mechanism of Chloroplast Protein Import and Its Integration with Protein Quality Control, Organelle Biogenesis and Development. *Journal of Molecular Biology*, *427*(5), 1038-1060. https://doi.org/10.1016/j.jmb.2014.08.016

Pan, R. H., Satkovich, J., Chen, C., & Hu, J. P. (2018). The E3 ubiquitin ligase SP1-like 1 plays a positive role in peroxisome biogenesis in Arabidopsis. *Plant Journal*, *94*(5), 836-846. https://doi.org/10.1111/tpj.13900

Pan, R. H., Satkovich, J., & Hu, J. P. (2016). E3 ubiquitin ligase SP1 regulates peroxisome biogenesis in Arabidopsis. *Proceedings of the National Academy of Sciences of the United States of America*, *113*(46), E7307-E7316. https://doi.org/10.1073/pnas.1613530113

Panigrahi, R., Adina-Zada, A., Whelan, J., & Vrielink, A. (2013). Ligand Recognition by the TPR Domain of the Import Factor Toc64 from Arabidopsis thaliana. *Plos One*, *8*(12). https://doi.org/10.1371/journal.pone.0083461

Park, D. H., Somers, D. E., Kim, Y. S., Choy, Y. H., Lim, H. K., Soh, M. S., Kim, H. J., Kay, S. A., & Nam, H. G. (1999). Control of circadian rhythms and photoperiodic flowering by the Arabidopsis GIGANTEA gene. *Science*, *285*(5433), 1579-1582. https://doi.org/10.1126/science.285.5433.1579

Park, S., Rancour, D. M., & Bednarek, S. Y. (2007). Protein domain-domain interactions and requirements for the negative regulation of Arabidopsis CDC48/p97 by the plant ubiquitin regulatory X (UBX) domain-containing protein, PUX1. *Journal of Biological Chemistry*, *282*(8), 5217-5224. https://doi.org/10.1074/jbc.M609042200

Park, S., Rancour, D. M., & Bednarek, S. Y. (2008). In planta analysis of the cell cycle-dependent localization of AtCDC48A and its critical roles in cell division, expansion, and differentiation. *Plant Physiology*, *148*(1), 246-258. https://doi.org/10.1104/pp.108.121897

Patel, R., Hsu, S. C., Bedard, J., Inoue, K., & Jarvis, P. (2008). The Omp85-related chloroplast outer envelope protein OEP80 is essential for viability in Arabidopsis. *Plant Physiology*, *148*(1), 235-245. https://doi.org/10.1104/pp.108.122754

Perry, J. J. P., Tainer, J. A., & Boddy, M. N. (2008). A SIM-ultaneous role for SUMO and ubiquitin. *Trends in Biochemical Sciences*, *33*(5), 201-208. https://doi.org/10.1016/j.tibs.2008.02.001

Perry, S. E., & Keegstra, K. (1994). Envelope Membrane-Proteins That Interact with Chloroplastic Precursor Proteins. *Plant Cell*, *6*(1), 93-105. https://doi.org/10.1105/tpc.6.1.93

Porra, R. J., Thompson, W. A., & Kriedemann, P. E. (1989). Determination of Accurate Extinction Coefficients and Simultaneous-Equations for Assaying Chlorophyll-a and Chlorophyll-B Extracted with 4 Different Solvents - Verification of the Concentration of Chlorophyll Standards by Atomic-Absorption Spectroscopy. *Biochimica Et Biophysica Acta*, *975*(3), 384-394. https://doi.org/10.1016/S0005-2728(89)80347-0

Qiu, L., Pashkova, N., Walker, J. R., Winistorfer, S., Allali-Hassani, A., Akutsu, M., Piper, R., & Dhe-Paganon, S. (2010). Structure and function of the PLAA/Ufd3-p97/Cdc48 complex. *Journal of Biological Chemistry*, *285*(1), 365-372. https://doi.org/10.1074/jbc.M109.044685

Raasi, S., Varadan, R., Fushman, D., & Pickart, C. M. (2005). Diverse polyubiquitin interaction properties of ubiquitin-associated domains. *Nature Structural & Molecular Biology*, *12*(8), 708-714. https://doi.org/10.1038/nsmb962

Ramachandran, H., Herfurth, K., Grosschedl, R., Schafer, T., & Walz, G. (2015). SUMOylation Blocks the Ubiquitin-Mediated Degradation of the Nephronophthisis Gene Product Glis2/NPHP7. *PLoS One*, *10*(6), e0130275. https://doi.org/10.1371/journal.pone.0130275

Ramundo, S., Asakura, Y., Salome, P. A., Strenkert, D., Boone, M., Mackinder, L. C. M., Takafuji, K., Dinc, E., Rahire, M., Crevecoeur, M., Magneschi, L., Schaad, O., Hippler, M., Jonikas, M. C., Merchant, S., Nakai, M., Rochaix, J. D., & Walter, P. (2020). Coexpressed subunits of dual genetic origin define a conserved supercomplex mediating essential protein import into chloroplasts. *Proceedings of the National Academy of Sciences of the United States of America*, *117*(51), 32739-32749. https://doi.org/10.1073/pnas.2014294117

Rancour, D. M., Park, S., Knight, S. D., & Bednarek, S. Y. (2004). Plant UBX domain-containing protein 1, PUX1, regulates the oligomeric structure and activity of Arabidopsis CDC48. *Journal of Biological Chemistry*, *279*(52), 54264-54274. https://doi.org/10.1074/jbc.M405498200

Redei, G. P. (1962). Supervital Mutants of Arabidopsis. *Genetics*, *47*(4), 443-460. https://doi.org/10.1093/genetics/47.4.443

Reiland, S., Grossmann, J., Baerenfaller, K., Gehrig, P., Nunes-Nesi, A., Fernie, A. R., Gruissem, W., & Baginsky, S. (2011). Integrated proteome and metabolite analysis of the de-etiolation process in plastids from rice (Oryza sativa L.). *Proteomics*, *11*(9), 1751-1763. https://doi.org/10.1002/pmic.201000703

Reyes-Prieto, A., Weber, A. P., & Bhattacharya, D. (2007). The origin and establishment of the plastid in algae and plants. *Annual Review of Genetics*, *41*, 147-168. https://doi.org/10.1146/annurev.genet.41.110306.130134

Reyes-Turcu, F. E., Horton, J. R., Mullally, J. E., Heroux, A., Cheng, X., & Wilkinson, K. D. (2006). The ubiquitin binding domain ZnF UBP recognizes the C-terminal diglycine motif of unanchored ubiquitin. *Cell*, *124*(6), 1197-1208. https://doi.org/10.1016/j.cell.2006.02.038

Rial, D. V., Arakaki, A. K., Almara, A. M., Orellano, E. G., & Ceccarelli, E. A. (2006). Chloroplast Hsp70s are not involved in the import of ferredoxin-NADP(+) reductase precursor. *Physiologia Plantarum*, *128*(4), 618-632. https://doi.org/10.1111/j.1399-3054.2006.00792.x

Rial, D. V., Arakaki, A. K., & Ceccarelli, E. A. (2000). Interaction of the targeting sequence of chloroplast precursors with Hsp70 molecular chaperones. *European Journal of Biochemistry*, *267*(20), 6239-6248. https://doi.org/10.1046/j.1432-1327.2000.01707.x

Rial, D. V., & Ceccarelli, E. A. (2005). Involvement of molecular chaperones in chloroplast protein import. *Febs Journal*, *272*, 357-357. https://doi.org/10.1016/j.bbamcr.2012.03.019

Rial, D. V., Ottado, J., & Ceccarelli, E. A. (2003). Precursors with altered affinity for Hsp70 in their transit peptides are efficiently imported into chloroplasts. *Journal of Biological Chemistry*, *278*(47), 46473-46481. https://doi.org/10.1074/jbc.M306684200

Richardson, L. G. L., & Schnell, D. J. (2020). Origins, function, and regulation of the TOC-TIC general protein import machinery of plastids. *Journal of Experimental Botany*, *71*(4), 1226-1238. https://doi.org/10.1093/jxb/erz517

Richter, S., & Lamppa, G. K. (1999). Stromal processing peptidase binds transit peptides and initiates their ATP-dependent turnover in chloroplasts. *Journal of Cell Biology*, *147*(1), 33-43. https://doi.org/10.1083/jcb.147.1.33

Rolland, N., Curien, G., Finazzi, G., Kuntz, M., Marechal, E., Matringe, M., Ravanel, S., & Seigneurin-Berny, D. (2012). The Biosynthetic Capacities of the Plastids and Integration Between Cytoplasmic and Chloroplast Processes. *Annual Review of Genetics*, *46*, 233-264. https://doi.org/10.1146/annurev-genet-110410-132544

Rosnoblet, C., Begue, H., Blanchard, C., Pichereaux, C., Besson-Bard, A., Aime, S., & Wendehenne, D. (2017). Functional characterization of the chaperon-like protein Cdc48 in cryptogein-induced immune response in tobacco. *Plant Cell and Environment*, *40*(4), 491-508. https://doi.org/10.1111/pce.12686

Rott, R., Szargel, R., Shani, V., Hamza, H., Savyon, M., Abd Elghani, F., Bandopadhyay, R., & Engelender, S. (2017). SUMOylation and ubiquitination reciprocally regulate alpha-synuclein degradation and pathological aggregation. *Proc Natl Acad Sci U S A*, *114*(50), 13176-13181. https://doi.org/10.1073/pnas.1704351114

Roy, D., & Sadanandom, A. (2021). SUMO mediated regulation of transcription factors as a mechanism for transducing environmental cues into cellular signaling in plants. *Cellular and Molecular Life Sciences*, *78*(6), 2641-2664. https://doi.org/10.1007/s00018-020-03723-4

Ruckle, M. E., DeMarco, S. M., & Larkin, R. M. (2007). Plastid signals remodel light signaling networks and are essential for efficient chloroplast biogenesis in Arabidopsis. *Plant Cell*, *19*(12), 3944-3960. https://doi.org/10.1105/tpc.107.054312

Rudolf, M., Machettira, A. B., Gross, L. E., Weber, K. L., Bolte, K., Bionda, T., Sommer, M. S., Maier, U. G., Weber, A. P. M., Schleiff, E., & Tripp, J. (2013). In Vivo Function of Tic22,

a Protein Import Component of the Intermembrane Space of Chloroplasts. *Molecular Plant*, *6*(3), 817-829. https://doi.org/10.1093/mp/sss114

Ruggiano, A., Foresti, O., & Carvalho, P. (2014). ER-associated degradation: Protein quality control and beyond. *Journal of Cell Biology*, *204*(6), 868-878. https://doi.org/10.1083/jcb.201312042

Rytz, T. C., Miller, M. J., McLoughlin, F., Augustine, R. C., Marshall, R. S., Juan, Y. T., Charng, Y. Y., Scalf, M., Smith, L. M., & Vierstra, R. D. (2018). SUMOylome Profiling Reveals a Diverse Array of Nuclear Targets Modified by the SUMO Ligase SIZ1 during Heat Stress. *Plant Cell*, *30*(5), 1077-1099. https://doi.org/10.1105/tpc.17.00993

Sadali, N. M., Sowden, R. G., Ling, Q. H., & Jarvis, R. P. (2019). Differentiation of chromoplasts and other plastids in plants. *Plant Cell Reports*, *38*(7), 803-818. https://doi.org/10.1007/s00299-019-02420-2

Sako, K., Yanagawa, Y., Kanai, T., Sato, T., Seki, M., Fujiwara, M., Fukao, Y., & Yamaguchi, J. (2014). Proteomic Analysis of the 26S Proteasome Reveals Its Direct Interaction with Transit Peptides of Plastid Protein Precursors for Their Degradation. *Journal of Proteome Research*, *13*(7), 3223-3230. https://doi.org/10.1021/pr401245g

Salinas, J., & Sánchez-Serrano, J. J. (2006). *Arabidopsis protocols* (2nd ed.). Humana Press. https://doi.org/10.1385/1-59745-003-0:101

Salt, J. N., Yoshioka, K., Moeder, W., & Goring, D. R. (2011). Altered germination and subcellular localization patterns for PUB44/SAUL1 in response to stress and phytohormone treatments. *PLoS One*, *6*(6), e21321. https://doi.org/10.1371/journal.pone.0021321

Sasaki, T., Funakoshi, M., Endicott, J. A., & Kobayashi, H. (2005). Budding yeast Dsk2 protein forms a homodimer via its C-terminal UBA domain. *Biochemical and Biophysical Research Communications*, *336*(2), 530-535. https://doi.org/10.1016/j.bbrc.2005.08.126

Schafer, P., Helm, S., Kohler, D., Agne, B., & Baginsky, S. (2019). Consequences of impaired 1-MDa TIC complex assembly for the abundance and composition of chloroplast high-

molecular mass protein complexes. *Plos One*, *14*(3). https://doi.org/10.1371/journal.pone.0213364

Schaheen, B., Dang, H., & Fares, H. (2009). Derlin-dependent accumulation of integral membrane proteins at cell surfaces. *Journal of Cell Science*, *122*(13), 2228-2239. https://doi.org/10.1242/jcs.048892

Schekman, R. (2004). Cell biology - A channel for protein waste. *Nature*, *429*(6994), 817-818. https://doi.org/DOI 10.1038/429817a

Schelbert, S., Aubry, S., Burla, B., Agne, B., Kessler, F., Krupinska, K., & Hortensteiner, S. (2009). Pheophytin Pheophorbide Hydrolase (Pheophytinase) Is Involved in Chlorophyll Breakdown during Leaf Senescence in Arabidopsis. *Plant Cell*, *21*(3), 767-785. https://doi.org/10.1105/tpc.108.064089

Schindelin, J., Arganda-Carreras, I., Frise, E., Kaynig, V., Longair, M., Pietzsch, T., Preibisch, S., Rueden, C., Saalfeld, S., Schmid, B., Tinevez, J. Y., White, D. J., Hartenstein, V., Eliceiri, K., Tomancak, P., & Cardona, A. (2012). Fiji: an open-source platform for biological-image analysis. *Nature Methods*, *9*(7), 676-682. https://doi.org/10.1038/Nmeth.2019

Schleiff, E., Soll, J., Kuchler, M., Kuhlbrandt, W., & Harrer, R. (2003). Characterization of the translocon of the outer envelope of chloroplasts. *Journal of Cell Biology*, *160*(4), 541-551. https://doi.org/10.1083/jcb.200210060

Schmidt, O., Weyer, Y., Baumann, V., Widerin, M. A., Eising, S., Angelova, M., Schleiffer, A., Kremser, L., Lindner, H., Peter, M., Frohlich, F., & Teis, D. (2019). Endosome and Golgi-associated degradation (EGAD) of membrane proteins regulates sphingolipid metabolism. *Embo Journal*, *38*(15). https://doi.org/10.15252/embj.2018101433

Schneeberger, K., Ossowski, S., Lanz, C., Juul, T., Petersen, A. H., Nielsen, K. L., Jorgensen, J. E., Weigel, D., & Andersen, S. U. (2009). SHOREmap: simultaneous mapping and mutation identification by deep sequencing. *Nat Methods*, *6*(8), 550-551. https://doi.org/10.1038/nmeth0809-550

Schnell, D. J., Kessler, F., & Blobel, G. (1994). Isolation of components of the chloroplast protein import machinery. *Science*, *266*(5187), 1007-1012. https://doi.org/10.1126/science.7973649

Schuberth, C., & Buchberger, A. (2005). Membrane-bound Ubx2 recruits Cdc48 to ubiquitin ligases and their substrates to ensure efficient ER-associated protein degradation. *Nature Cell Biology*, *7*(10), 999-1006. https://doi.org/10.1038/ncb1299

Schuberth, C., & Buchberger, A. (2008). UBX domain proteins: major regulators of the AAA ATPase Cdc48/p97. *Cellular and Molecular Life Sciences*, *65*(15), 2360-2371. https://doi.org/10.1007/s00018-008-8072-8

Schuberth, C., Richly, H., Rumpf, S., & Buchberger, A. (2004). Shp1 and Ubx2 are adaptors of Cdc48 involved in ubiquitin-dependent protein degradation. *Embo Reports*, *5*(8), 818-824. https://doi.org/10.1038/sj.embor.7400203

Seo, D. H., Ryu, M. Y., Jammes, F., Hwang, J. H., Turek, M., Kang, B. G., Kwak, J. M., & Kim, W. T. (2012). Roles of Four Arabidopsis U-Box E3 Ubiquitin Ligases in Negative Regulation of Abscisic Acid-Mediated Drought Stress Responses. *Plant Physiology*, *160*(1), 556-568. https://doi.org/10.1104/pp.112.202143

Shanmugabalaji, V., Chahtane, H., Accossato, S., Rahire, M., Gouzerh, G., Lopez-Molina, L., & Kessler, F. (2018). Chloroplast Biogenesis Controlled by DELLA-TOC159 Interaction in Early Plant Development. *Current biology*, *28*(16), 2616-2623. https://doi.org/10.1016/j.cub.2018.06.006

Shen, G. X., Adam, Z., & Zhang, H. (2007b). The E3 ligase AtCHIP ubiquitylates FtsH1, a component of the chloroplast FtsH protease, and affects protein degradation in chloroplasts. *Plant Journal*, *52*(2), 309-321. https://doi.org/10.1111/j.1365-313X.2007.03239.x

Shen, G. X., Yan, J. Q., Pasapula, V., Luo, J. H., He, C. X., Clarke, A. K., & Zhang, H. (2007a). The chloroplast protease subunit ClpP4 is a substrate of the E3 ligase AtCHIP and plays

an important role in chloroplast function. *Plant Journal*, *49*(2), 228-237. https://doi.org/10.1111/j.1365-313X.2006.02963.x

Shi, L. X., & Theg, S. M. (2013). The chloroplast protein import system: From algae to trees. *Biochimica Et Biophysica Acta-Molecular Cell Research*, *1833*(2), 314-331. https://doi.org/10.1016/j.bbamcr.2012.10.002

Shih, P. M., & Matzke, N. J. (2013). Primary endosymbiosis events date to the later Proterozoic with cross-calibrated phylogenetic dating of duplicated ATPase proteins. *Proc Natl Acad Sci U S A*, *110*(30), 12355-12360. https://doi.org/10.1073/pnas.1305813110

Sibbald, S. J., & Archibald, J. M. (2020). Genomic Insights into Plastid Evolution. *Genome Biology and Evolution*, *12*(7), 978-990. https://doi.org/10.1093/gbe/evaa096

Sjuts, I., Soll, J., & Bolter, B. (2017). Import of Soluble Proteins into Chloroplasts and Potential Regulatory Mechanisms. *Frontiers in Plant Science*, *8*. https://doi.org/10.3389/fpls.2017.00168

Smith, M. D., Rounds, C. M., Wang, F., Chen, K. H., Afitlhile, M., & Schnell, D. J. (2004). AtToc159 is a selective transit peptide receptor for the import of nucleus-encoded chloroplast proteins. *Journal of Cell Biology*, *165*(3), 323-334. https://doi.org/10.1083/jcb.200311074

Soll, J., & Schleiff, E. (2004). Protein import into chloroplasts. *Nature Reviews Molecular Cell Biology*, *5*(3), 198-208. https://doi.org/10.1038/nrm1333

Song, E. J., Yim, S. H., Kim, E., Kim, N. S., & Lee, K. J. (2005). Human Fas-associated factor 1, interacting with ubiquitinated proteins and valosin-containing protein, is involved in the ubiquitin-proteasome pathway. *Molecular and Cellular Biology*, *25*(6), 2511-2524. https://doi.org/10.1128/Mcb.25.6.2511-2524.2005

Stahl, T., Glockmann, C., Soll, J., & Heins, L. (1999). Tic40, a new "old" subunit of the chloroplast protein import translocon. *Journal of Biological Chemistry*, *274*(52), 37467-37472. https://doi.org/10.1074/jbc.274.52.37467

Stanga, J. P., Boonsirichai, K., Sedbrook, J. C., Otegui, M. S., & Masson, P. H. (2009). A Role for the TOC Complex in Arabidopsis Root Gravitropism. *Plant Physiology*, *149*(4), 1896-1905. https://doi.org/10.1104/pp.109.135301

Stolz, A., Schweizer, R. S., Schafer, A., & Wolf, D. H. (2010). Dfm1 Forms Distinct Complexes with Cdc48 and the ER Ubiquitin Ligases and Is Required for ERAD. *Traffic*, *11*(10), 1363-1369. https://doi.org/10.1111/j.1600-0854.2010.01093.x

Stone, S. L., Hauksdottir, H., Troy, A., Herschleb, J., Kraft, E., & Callis, J. (2005). Functional analysis of the RING-type ubiquitin ligase family of Arabidopsis. *Plant Physiology*, *137*(1), 13-30. https://doi.org/10.1104/pp.104.052423

Sun, C. W., Huang, Y. C., & Chang, H. Y. (2009). CIA2 Coordinately Up-Regulates Protein Import and Synthesis in Leaf Chloroplasts. *Plant Physiology*, *150*(2), 879-888. https://doi.org/10.1104/pp.109.137240

Sun, H. Q., & Schneeberger, K. (2015). SHOREmap v3.0: Fast and Accurate Identification of Causal Mutations from Forward Genetic Screens. *Plant Functional Genomics: Methods and Protocols, 2nd Edition*, *1284*, 381-395. https://doi.org/10.1007/978-1-4939-2444-8_19

Sun, Y., & Jarvis, R. P. (2023). Chloroplast Proteostasis: Import, Sorting, Ubiquitination, and Proteolysis. *Annu Rev Plant Biol*, *74*. https://doi.org/10.1146/annurev-arplant-070122-032532

Sun, Y., Yao, Z., Ye, Y., Fang, J., Chen, H., Lyu, Y., Broad, W., Fournier, M., Chen, G., Hu, Y., Mohammed, S., Ling, Q., & Jarvis, R. P. (2022). Ubiquitin-based pathway acts inside chloroplasts to regulate photosynthesis. *Sci Adv*, *8*(46), eabq7352. https://doi.org/10.1126/sciadv.abq7352

Sveshnikova, N., Grimm, R., Soll, J., & Schleiff, E. (2000). Topology studies of the chloroplast protein import channel Toc75. *Biological Chemistry*, *381*(8), 687-693. https://doi.org/10.1515/Bc.2000.089

Tang, X. F., Miao, M., Niu, X. L., Zhang, D. F., Cao, X. L., Jin, X. C., Zhu, Y. Y., Fan, Y. H., Wang, H. T., Liu, Y., Sui, Y., Wang, W. J., Wang, A. Q., Xiao, F. M., Giovannoni, J., &

Liu, Y. S. (2016). Ubiquitin-conjugated degradation of golden 2-like transcription factor is mediated by CUL4-DDB1-based E3 ligase complex in tomato. *New Phytologist*, *209*(3), 1028-1039. https://doi.org/10.1111/nph.13635

Taylor, E. B., & Rutter, J. (2011). Mitochondrial quality control by the ubiquitin-proteasome system. *Biochem Soc Trans*, *39*(5), 1509-1513. https://doi.org/10.1042/BST0391509

Teng, Y. S., Su, Y. S., Chen, L. J., Lee, Y. J., Hwang, I., & Li, H. M. (2006). Tic21 is an essential translocon component for protein translocation across the chloroplast inner envelope membrane. *Plant Cell*, *18*(9), 2247-2257. https://doi.org/10.1105/tpc.106.044305

Thomson, S. M., Pulido, P., & Jarvis, R. P. (2020). Protein import into chloroplasts and its regulation by the ubiquitin-proteasome system. *Biochemical Society Transactions*, *48*(1), 71-82. https://doi.org/10.1042/Bst20190274

Timmis, J. N., Ayliffe, M. A., Huang, C. Y., & Martin, W. (2004). Endosymbiotic gene transfer: Organelle genomes forge eukaryotic chromosomes. *Nature Reviews Genetics*, *5*(2), 123-135. https://doi.org/10.1038/nrg1271

Tokumaru, M., Adachi, F., Toda, M., Ito-Inaba, Y., Yazu, F., Hirosawa, Y., Sakakibara, Y., Suiko, M., Kakizaki, T., & Inaba, T. (2017). Ubiquitin-Proteasome Dependent Regulation of the GOLDEN2-LIKE 1 Transcription Factor in Response to Plastid Signals. *Plant Physiology*, *173*(1), 524-535. https://doi.org/10.1104/pp.16.01546

Topel, M., Ling, Q., & Jarvis, P. (2012). Neofunctionalization within the Omp85 protein superfamily during chloroplast evolution. *Plant Signal Behav*, *7*(2), 161-164. https://doi.org/10.4161/psb.18677

Tranel, P. J., Froehlich, J., Goyal, A., & Keegstra, K. (1995). A Component of the Chloroplastic Protein Import Apparatus Is Targeted to the Outer Envelope Membrane Via a Novel Pathway. *Embo Journal*, *14*(11), 2436-2446. https://doi.org/10.1002/j.1460-2075.1995.tb07241.x

Tranel, P. J., & Keegstra, K. (1996). A novel, bipartite transit peptide targets OEP75 to the outer membrane of the chloroplastic envelope. *Plant Cell*, *8*(11), 2093-2104. https://doi.org/10.1105/tpc.8.11.2093

Tripp, J., Hahn, A., Koenig, P., Flinner, N., Bublak, D., Brouwer, E. M., Ertel, F., Mirus, O., Sinning, I., Tews, I., & Schleiff, E. (2012). Structure and Conservation of the Periplasmic Targeting Factor Tic22 Protein from Plants and Cyanobacteria. *Journal of Biological Chemistry*, *287*(29), 24164-24173. https://doi.org/10.1074/jbc.M112.341644

Tsai, J. Y., Chu, C. C., Yeh, Y. H., Chen, L. J., Li, H. M., & Hsiao, C. D. (2013). Structural characterizations of the chloroplast translocon protein Tic110. *Plant Journal*, *75*(5), 847-857. https://doi.org/10.1111/tpj.12249

Vandervere, P. S., Bennett, T. M., Oblong, J. E., & Lamppa, G. K. (1995). A Chloroplast Processing Enzyme Involved in Precursor Maturation Shares a Zinc-Binding Motif with a Recently Recognized Family of Metalloendopeptidases. *Proceedings of the National Academy of Sciences of the United States of America*, *92*(16), 7177-7181. https://doi.org/10.1073/pnas.92.16.7177

Vierstra, R. D. (2009). The ubiquitin-26S proteasome system at the nexus of plant biology. *Nat Rev Mol Cell Biol*, *10*(6), 385-397. https://doi.org/10.1038/nrm2688

Vojta, A., Alavi, M., Becker, T., Hormann, F., Kuchler, M., Soll, J., Thomson, R., & Schleiff, E. (2004). The protein translocon of the plastid envelopes. *Journal of Biological Chemistry*, *279*(20), 21401-21405. https://doi.org/10.1074/jbc.M401968200

Vonheijne, G., & Nishikawa, K. (1991). Chloroplast Transit Peptides - the Perfect Random Coil. *Febs Letters*, *278*(1), 1-3. https://doi.org/10.1016/0014-5793(91)80069-F

Wallas, T. R., Smith, M. D., Sanchez-Nieto, S., & Schnell, D. J. (2003). The roles of Toc34 and Toc75 in targeting the Toc159 preprotein receptor to chloroplasts. *Journal of Biological Chemistry*, *278*(45), 44289-44297. https://doi.org/10.1074/jbc.M307873200

Walther, T. C., & Farese, R. V. (2012). Lipid Droplets and Cellular Lipid Metabolism. *Annual Review of Biochemistry*, *81*, 687-714. https://doi.org/10.1146/annurev-biochem-061009-102430

Wang, C. W., & Lee, S. C. (2012). The ubiquitin-like (UBX)-domain-containing protein Ubx2/Ubxd8 regulates lipid droplet homeostasis. *Journal of Cell Science*, *125*(12), 2930-2939. https://doi.org/10.1242/jcs.100230

Waters, M. T., Wang, P., Korkaric, M., Capper, R. G., Saunders, N. J., & Langdale, J. A. (2009). GLK Transcription Factors Coordinate Expression of the Photosynthetic Apparatus in Arabidopsis. *Plant Cell*, *21*(4), 1109-1128. https://doi.org/10.1105/tpc.108.065250

Watson, S. J., Li, N., Ye, Y. T., Wu, F. J., Ling, Q. H., & Jarvis, R. P. (2021). Crosstalk between the chloroplast protein import and SUMO systems revealed through genetic and molecular investigation in Arabidopsis. *Elife*, *10*. https://doi.org/10.7554/eLife.60960.sa2

Weigel, D., & Glazebrook, J. (2006). Transformation of agrobacterium using the freeze-thaw method. *CSH Protoc*, *2006*(7). https://doi.org/10.1101/pdb.prot4666

Wiborg, J., O'Shea, C., & Skriver, K. (2008). Biochemical function of typical and variant Arabidopsis thaliana U-box E3 ubiquitin-protein ligases. *Biochemical Journal*, *413*(3), 447-457. https://doi.org/10.1042/BJ20071568

Wienk, H. L., Czisch, M., & de Kruijff, B. (1999). The structural flexibility of the preferredoxin transit peptide. *Febs Letters*, *453*(3), 318-326. https://doi.org/10.1016/s0014-5793(99)00653-5

Wu, C. B., Seibert, F. S., & Ko, K. (1994). Identification of Chloroplast Envelope Proteins in Close Physical Proximity to a Partially Translocated Chimeric Precursor Protein. *Journal of Biological Chemistry*, *269*(51), 32264-32271. https://doi.org/10.1016/S0021-9258(18)31630-2

Wu, F. H., Shen, S. C., Lee, L. Y., Lee, S. H., Chan, M. T., & Lin, C. S. (2009). Tape-Arabidopsis Sandwich - a simpler Arabidopsis protoplast isolation method. *Plant Methods*, *5*(16). https://doi.org/10.1186/1746-4811-5-16

Wu, X. D., & Rapoport, T. A. (2018). Mechanistic insights into ER-associated protein degradation. *Current Opinion in Cell Biology*, *53*, 22-28. https://doi.org/10.1016/j.ceb.2018.04.004

Xia, D., Tang, W. K., & Ye, Y. H. (2016). Structure and function of the AAA + ATPase p97/Cdc48p. *Gene*, *583*(1), 64-77. https://doi.org/10.1016/j.gene.2016.02.042

Xue, H. D., Gao, X., He, P., & Xiao, G. H. (2022). Origin, evolution, and molecular function of DELLA proteins in plants. *Crop Journal*, *10*(2), 287-299. https://doi.org/10.1016/j.cj.2021.06.005

Yan, J. Q., Wang, J., Li, Q. T., Hwang, J. R., Patterson, C., & Zhang, H. (2003). AtCHIP, a U-box-containing E3 ubiquitin ligase, plays a critical role in temperature stress tolerance in Arabidopsis. *Plant Physiology*, *132*(2), 861-869. https://doi.org/10.1104/pp.103.020800

Ye, Y. H., Meyer, H. H., & Rapoport, T. A. (2001). The AAA ATPase Cdc48/p97 and its partners transport proteins from the ER into the cytosol. *Nature*, *414*(6864), 652-656. https://doi.org/10.1038/414652a

Ye, Y. H., Meyer, H. H., & Rapoport, T. A. (2003). Function of the p97-Ufd1-Npl4 complex in retrotranslocation from the ER to the cytosol: dual recognition of nonubiquitinated polypeptide segments and polyubiquitin chains. *Journal of Cell Biology*, *162*(1), 71-84. https://doi.org/10.1083/jcb.200302169

Ye, Y. H., Shibata, Y., Yun, C., Ron, D., & Rapoport, T. A. (2004). A membrane protein complex mediates retro-translocation from the ER lumen into the cytosol. *Nature*, *429*(6994), 841-847. https://doi.org/10.1038/nature02656

Yeh, S. Y., Lin, H. H., Chang, Y. M., Chang, Y. L., Chang, C. K., Huang, Y. C., Ho, Y. W., Lin, C. Y., Zheng, J. Z., Jane, W. N., Ng, C. Y., Lu, M. Y., Lai, I. L., To, K. Y., Li, W. H., & Ku, M. S. B. (2022). Maize Golden2-like transcription factors boost rice chloroplast

development, photosynthesis, and grain yield (vol 188, pg 442, 2022). *Plant Physiology*, *188*(4), 2377-2378. https://doi.org/10.1093/plphys/kiab511

Yeo, G., & Burge, C. B. (2004). Maximum entropy modeling of short sequence motifs with applications to RNA splicing signals. *Journal of Computational Biology*, *11*(2-3), 377-394. https://doi.org/10.1089/1066527041410418

Zeng, L. R., Park, C. H., Venu, R. C., Gough, J., & Wang, G. L. (2008). Classification, expression pattern, and E3 ligase activity assay of rice U-box-containing proteins. *Molecular Plant*, *1*(5), 800-815. https://doi.org/10.1093/mp/ssn044

Zhang, A. H., Lu, Q. T., Yin, Y., Ding, S. H., Wen, X. G., & Lu, C. M. (2010). Comparative proteomic analysis provides new insights into the regulation of carbon metabolism during leaf senescence of rice grown under field conditions. *Journal of Plant Physiology*, *167*(16), 1380-1389. https://doi.org/10.1016/j.jplph.2010.05.011

Zhang, H., Zhou, J. F., Kan, Y., Shan, J. X., Ye, W. W., Dong, N. Q., Guo, T., Xiang, Y. H., Yang, Y. B., Li, Y. C., Zhao, H. Y., Yu, H. X., Lu, Z. Q., Guo, S. Q., Lei, J. J., Liao, B., Mu, X. R., Cao, Y. J., Yu, J. J., Lin, Y. S., & Lin, H. X. (2022a). A genetic module at one locus in rice protects chloroplasts to enhance thermotolerance. *Science*, *376*(6599), 1293-1300. https://doi.org/10.1126/science.abo5721

Zhang, J. R., Vancea, A. I., & Arold, S. T. (2022b). Targeting plant UBX proteins: AI-enhanced lessons from distant cousins. *Trends in Plant Science*, *27*(11), 1099-1108. https://doi.org/10.1016/j.tplants.2022.05.012

Zhang, J. R., Vancea, A. I., Hameed, U. F. S., & Arold, S. T. (2021). Versatile control of the CDC48 segregase by the plant UBX-containing (PUX) proteins. *Computational and Structural Biotechnology Journal*, *19*, 3125-3132. https://doi.org/10.1016/j.csbj.2021.05.025

Zhang, J. Y., Wu, S., Boehlein, S. K., McCarty, D. R., Song, G. Y., Walley, J. W., Myers, M., & Settles, A. M. (2019a). Maize defective kernel5 is a bacterial TamB homologue required

for chloroplast envelope biogenesis. *Journal of Cell Biology*, *218*(8), 2638-2658. https://doi.org/10.1083/jcb.201807166

Zhang, N., Xu, J., Liu, X. Y., Liang, W. X., Xin, M. M., Du, J. K., Hu, Z. R., Peng, H. R., Guo, W. L., Ni, Z. F., Sun, Q. X., & Yao, Y. Y. (2019b). Identification of HSP90C as a substrate of E3 ligase TaSAP5 through ubiquitylome profiling. *Plant Science*, *287*. https://doi.org/10.1016/j.plantsci.2019.110170

Zhang, X. P., & Glaser, E. (2002). Interaction of plant mitochondrial and chloroplast signal peptides with the Hsp70 molecular chaperone. *Trends in Plant Science*, *7*(1), 14-21. https://doi.org/10.1016/S1360-1385(01)02180-X

Zhang, X. R., Henriques, R., Lin, S. S., Niu, Q. W., & Chua, N. H. (2006). Agrobacterium-mediated transformation of Arabidopsis thaliana using the floral dip method. *Nature Protocols*, *1*(2), 641-646. https://doi.org/10.1038/nprot.2006.97

Zhao, G., Zhou, X. K., Wang, L. Q., Li, G. T., Schindelin, H., & Lennarz, W. J. (2007). Studies on peptide : N-glycanase-p97 interaction suggest that p97 phosphorylation modulates endoplasmic reticulum-associated degradation. *Proceedings of the National Academy of Sciences of the United States of America*, *104*(21), 8785-8790. https://doi.org/10.1073/pnas.0702966104

Zhao, X. Y., Higa, T., & Nakai, M. (2022). Tic12, a 12-kDa essential component of the translocon at the inner envelope membrane of chloroplasts in Arabidopsis. *Plant Cell*, *34*(11), 4569-4582. https://doi.org/10.1093/plcell/koac240

Zheng, J., Cao, Y., Yang, J., & Jiang, H. (2022). UBXD8 mediates mitochondria-associated degradation to restrain apoptosis and mitophagy. *Embo Reports*, *23*(10). https://doi.org/10.15252/embr.202254859

Zheng, X. T., Wang, C. J., Lin, W. X., Lin, C. F., Han, D. L., Xie, Q., Lai, J. B., & Yang, C. W. (2022a). Importation of chloroplast proteins under heat stress is facilitated by their SUMO conjugations. *New Phytologist*, *235*(1), 173-187. https://doi.org/10.1111/nph.18121

Zhu, D., Xiong, H. B., Wu, J. H., Zheng, C. H., Lu, D. D., Zhang, L. X., & Xu, X. M. (2022). Protein Targeting Into the Thylakoid Membrane Through Different Pathways. *Frontiers in Physiology*, *12*. https://doi.org/10.3389/fphys.2021.802057

Zufferey, M., Montandon, C., Douet, V., Demarsy, E., Agne, B., Baginsky, S., & Kessler, F. (2017). The novel chloroplast outer membrane kinase KOC1 is a required component of the plastid protein import machinery. *Journal of Biological Chemistry*, *292*(17), 6952-6964. https://doi.org/10.1074/jbc.M117.776468